

Take-Off and Landing Using Ground Based Power

DSE Group 7



DESIGN SYNTHESIS EXERCISE

GROUP 7

AE3200

Take-Off and Landing Using Ground Based Power

Final Report

Authors:

Bos, *Merijn* - 4293770
Cramer, *Lucia* - 4552830
Duzijn, *Maartje* - 4486285
Heiremans, *Jan* - 4541987
Lubbers, *Olga* - 4551052
Maaskant, *Mitchel* - 4563360
Reijnders, *Roy* - 4554183
Soomers, *Joost* - 4430875
Trombetta, *Stefano* - 4531043
Vézy, *Marie-Laure* - 4451406

Supervisors:

Erik-Jan van Kampen,
Paul Roling,
Sharif Khoshmanesh

| Version | Change | Date |
|---------|--|------------|
| 1.0 | Draft report | 25/06/2019 |
| 2.0 | Implemented feedback of peer review and coaches -Changed front picture -6.1.2: Changed image and text -6.1.3: Edited equations and text -7.8.1: Added clarification table and text -7.10.3: Clarified image and text -8.2.3: Clarification and table with input parameters -8.3.7: Added sensitivity analysis -9.1.1: General update -12.1: Compliance of requirement NCL-Fun-TO9 changed -12.2: Included technical sensitivity analysis -13.1: Added end-of-life diagram and text -13.4.3: Added this section | 28/06/2019 |

Table 1: Version control

VERSION 2.0

Preface

This project would not have been possible without the elaborate and dedicated help provided by several experts.

First of all, we would like to thank our tutors for their guidance and inputs. The critical input of dr.ir. Erik-Jan van Kempen, ir. Paul Roling and msc. Sharif Khoshmanesh has given us more opportunity to strive for the best results.

Secondly, the Aircraft Noise and Climate Effects (ANCE) department at the Faculty of Aerospace Engineering has helped in many ways to learn and scientifically evaluate the noise effects of the project. For this we would like to thank prof.dr. D.G. (Dick) Simons and dr.ir. M (Mirjam) Snellen for their time and insights in how to approach noise research. Furthermore, master student Davey Hooymeijer has provided us support with his model that helped quantify the noise production.

Furthermore, several staff members have helped us with their patient answers and guidance in their professional fields respectively. Dr. F. (Fabrizio) Oliviero, dr.ir. R. (Roelof) Vos, dr.ir. A. (Alexander) in 't Veld, ir. O. (Olaf) Stroosma and dr. C. (Calvin) Rans of our faculty have kindly given us their time for guidance in their expertises respectively and necessary references. The same holds for dr.ir. H. (Henk) Polinder and dr.ir. P. (Paddy) French of Electrical Engineering. For the hexapod design, we are very thankful for the extensive explanations and interest by dr. G. (Gabriele) Bulfalari of Mechanical Engineering.

Lastly, we would like to thank the whole organisation of the DSE including the teaching assistants for their guidance, space and opportunity to develop this project.

DSE Group 7
June 28, 2019

Executive Summary

Last January, yet another attempt to reach consensus on the growth of Schiphol has failed. Schiphol, KLM and other large airlines request a growth of 10,000 extra flight movements per year, while inhabitants, governors of municipalities and province and environmental organisations request a growth stop until 2023. The main arguments are noise disturbance in the surroundings of Schiphol and the negative effects of aviation on the local and global environment ¹.

In order to stop the limitations on aviation growth, structural changes will have to be made in the industry. One of the proposed solutions is to remove the conventional landing gear and make use of a ground based powered system to perform the landing and take-off. Firstly, the intended result is a reduction in fuel emissions due to the weight reduction of the aircraft: a conventional landing gear counts for approximately 4% of the maximum take-off weight of the aircraft. Secondly, the use of a ground based powered system provides for the opportunity to reduce noise pollution during take-off and landing. These two advantages are exactly tackling the two major issues that prevents airports like Schiphol, from growing.

Project Objectives

In this report, the design of a ground based powered system for launching and recovering commercial aircraft is elaborated on. The project objective is stated below:

Provide a ground-based powered take-off and landing system for the B737/A320 that reduces environmental impact with respect to current conventional aircraft and is economically feasible.

The environmental impact is measured in terms of improvements in fuel efficiency and noise pollution reduction. However, the final design has to be economically competitive in order to ensure feasibility of implementation in the real world. Therefore, modifications to the airframe and airport structure should be minimal.

Market Analysis

A market analysis was performed to determine the added value of the system and to identify the different stakeholders and business strategy. It was found that the added value comes from a reduction in fuel, wearing components, emission costs and noise costs. With the appropriate discount rate, it is estimated that the system is worth approximately $\text{€}7.97 \cdot 10^8$ when implemented for all small to medium aircraft arriving on and departing from Schiphol. The most obvious market concept involves Schiphol as the investor and owner of the system. Schiphol will earn a profit by leasing the system to airlines on a pay-per-go basis. The airlines need to invest in the modification of their aircraft.

Context of the Design

Based on the guidelines given by the customer, the context of the design is determined. As stated before, Schiphol Airport is used as reference airport, where the length of the Zwanenburgbaan is used as an indication for the runway length (3,300 m). Furthermore, the current capacity of Schiphol (14 departures or 12 arrivals per runway every 20 min) will have to be maintained.

Next, the reference aircraft where the system is designed for is the A321neo. The reason this aircraft is chosen as a reference, is that it is one of the heaviest in its class (short/medium range commercial aircraft).

Requirements

After having defined the project objectives, the most important stakeholders and context of the design, a set of requirements has been established. Both stakeholder and system requirements have been defined, where special attention is paid to driving and potential killer requirements. These have been listed in Table 2.

¹URL: <https://www.nrc.nl/nieuws/2018/12/13/moeizaam-polderen-over-schiphol-a3060612> [retrieved on June 23, 2019]

Table 2: Killer and driving requirements.

| Identifier | Requirement |
|--------------------|---|
| Killer | |
| NCL-Shl01 | The system shall provide for at least the same capacity as when using conventional take-off and landing systems at Schiphol airport. |
| Driving | |
| NCL-Alc09u1 | The modification of the aircraft and the different take-off and landing procedures shall decrease the absolute fuel consumption of the total flight mission with at least 5% for all flights shorter than 1,5 hour. |
| NCL-Shl18 | The system shall provide for a reduction of noise pollution of 7 ± 3 SEL dBA in comparison to the current production of noise during the take-off and landing procedure at Schiphol airport. |

Functional Analysis

In order to find out what exact functions the system has to fulfil, a functional analysis is done. Both functional flow diagrams and a functional breakdown structure are made. The system's functions can be linked to the requirements and the functional analysis is used to generate concepts. Functional analysis is especially useful to see the complete picture of what tasks the system has to be able to do to be a successful system.

Concept Generation

Based on the established requirements and functions, four concepts were generated and analysed in order to select the best design which will be able to fulfil all the requirements.

The first concept consists of a platform on a magnetic track which is extended over the entire airport. On top of the platform, a hexapod configuration of hydraulic pistons is placed to line up with the aircraft during landing and support it during taxiing. The aircraft will connect to the platform using a mechanical hook system.

The second concept is composed of a cart on wheels carrying a platform where the aircraft will land on and take-off from. The carry cart is able to lower down the platform at the gate in order to go to a charging station. A connection mechanism combining suction cups and a harpoon system is used to connect the aircraft to the platform. Moreover, the platform uses hydraulic pistons to move the platform and synchronise with the aircraft.

In the third concept, rails are placed on the runway where a metallic structure slides on carrying a circular platform. The platform is able to move in lateral direction along the bars of the metallic structure while using hydraulic pistons to line up with the aircraft in yaw, pitch and roll angle. Furthermore, the concept uses a pin-through-hole connection to attach the aircraft to the platform.

Finally, the fourth concept called the drone consists of a flying wing driven by ten propellers which approaches the aircraft in air, connect to it using a railway coupling attachment, and finally land together with the aircraft. In this concept, the drone works as a powered landing gear that also provides power during take-off and climb until FL100 is reached.

Trade-Off

The four concepts as described above, are compared using seven different trade-off criteria. Each criteria is assigned a weight related to which criteria is more important compared to others. The criteria with their weight (from the highest to the lowest) are as follows: the safety (39%), the noise reduction (22%), the modifications made to the aircraft (15%), the disruptions made to the airport (10%), the cost (6%), the take-off and landing energy and power (5%) and finally the ground movement power required (3%). The scoring of each concepts for each criteria is based on how the design performs in terms of environmental, economical and social sustainability. Hence, sustainability is fully integrated in the trading process, even though it is not a direct trade-off criteria.

From the trade-off, it is concluded that the magnetic runway concept with a score of 0.288 out of 1 won, followed closely by the rails concept with a score of 0.282 due to their energy consumption and favourable safety characteristics. Next, the carry cart scored 0.254 and is followed by the drone with a score of 0.176.

For the final proposed conceptual design, it is decided to combine the magnetic runway and the rails concept as they were very close in the trade-off. There is also more confidence that the combination of the two will have more chance in complying with the requirements. Hence, the winning concept, called the REMALS,

is mainly based in the rails concept using the power (Electromagnetic Aircraft Launch System - EMALS) of the magnetic runway design and a different connection mechanism, namely, the suction cups and the harpoon.

Design Process Set-Up

The design process is started by identifying all the different components that made up the REMALS. The components from the proposed conceptual design are thought out in more detail and linked to the functional analysis. Functions that are not yet fulfilled properly by the conceptual design were further developed such that all functions were covered.

The system is divided into two big parts: the aircraft and the ground system. For the aircraft redesign the most important aspects considered are related to the new landing mechanism design and the impact of this on aircraft performance and mass and balance characteristics. The ground system is divided into 10 different components. These components are the grid, the Stewart platform, the rotation platform, the lateral movement structure, the base structure, the rails and wheels structure, the power system, the runway station, and the taxi cart.

To keep an overview of the relations between all the different components and department, two N2-charts are used. It is decided to have two N2-charts on different hierarchical levels to have sufficient detail in the design and still keep a clear overview over the different departments. The N2-charts are continuously updated once new input or output parameters are found related to a certain component or department. Finally, several iterations through the N2-charts are done to have all the output parameters converge to their final values.

A revision of the budget break down for costs, mass and energy is made. They are also related in an equation to simplify potentially necessary revisions. The sum should not exceed the net present value of the system, so $\text{€}7.97 \cdot 10^8$. Shortages in one budget might be offset by surpluses in another.

Aircraft Design

With respect to the new aircraft design, necessary modifications are investigated. The landing gear is removed and harpoons are added for connecting to a grid on the ground based system. The critical loads in these harpoons are bending moments, due to the critical landing forces. This results in two main harpoons of 709 kg and a nose gear of 282 kg, at the same locations as the conventional landing gear. This results in a reduction of 2104 kg of the operative empty weight of the aircraft.

Consequently, this weight difference is expected to have an effect on the weight and balance of the aircraft. Therefore, a loading diagram and scissor plot are made for the conventional A321NEO and the REMALS system. The result of this is that the new design does not have to change because of the weight and balance.

Ground System Design

As stated before, the ground system consists of 10 different components, which are elaborated further on below. Figure 1 shows the configuration of the ground system, including all the components.

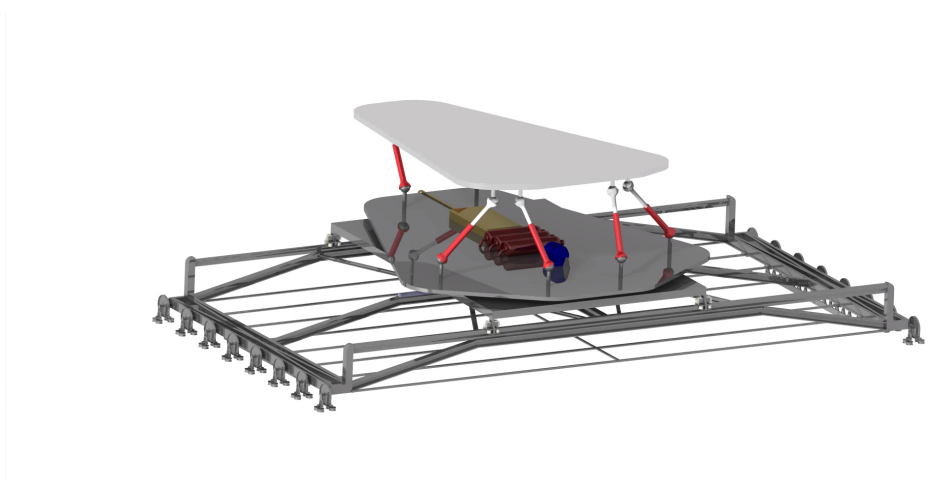


Figure 1: Visualisation of the ground based system.

Grid

A grid is designed to connect the aircraft to. This grid is on top of the ground based vehicle, and it has areas with holes that the harpoons can go through. These holes are within the accuracy of the aircraft such that it can attach to a different hole depending on where exactly it lands.

In order to connect the grid to the Stewart platform, a special connection mechanism is designed. This mechanism allows the grid to slide on top, while the bottom stays fixed to the Stewart platform. The grid on top needs to slide on top in order to move on top of the taxi cart. When the grid is in position, it can lock with a specially designed locking mechanism.

Stewart Platform

In order to accurately synchronise the platform to the aircraft, a Stewart platform is used. A Stewart platform is a platform that can be controlled in all the 6 degrees of freedom.

To be able to size the Stewart platform, the impact loads on the platform should be determined. This was done using a method that determines the maximum vertical load for conventional landing gear. From certain CS-25 regulations, this maximum vertical impact load is converted into the design drag and side loads. Additionally, the situation in which the aircraft experiences the maximum acceleration and deceleration during take-off and landing are considered.

These input forces then need to be converted into the axial forces in the actuators. To do this the joint locations on the Stewart platform were converted into vectors that represent the actuators. The obtained vectors change when the platform moves or rotates. For every possible position and rotation, the platform is assumed to be in equilibrium and using the sum of forces and sum of moments in all directions, 6 equations are found. With these 6 equations, the forces in the 6 actuators can be determined.

To find the maximum reaction forces in the actuators, the required workspace needs to be identified. The extreme platform orientations are a maximum roll angle of 5 degrees, a maximum pitch angle of 10 degrees and a maximum yaw angle of 10 degrees. Additionally, lateral and longitudinal displacements of at least 1 meter are desired. The maximum forces were found by going through these positions and orientations in combination with the different load cases. Finally, the lengths and extension ratios of the actuators are determined. It was checked whether the actuators had a feasible extension ratio and otherwise the configuration of the Stewart platform was modified. From this analysis, four actuators are required to deliver $1400kN$ and two actuators are required to deliver $1000kN$. The neutral length varies between just over 2 m and almost 4 m with all of them a extension ratio of approximately 75%.

The damping of the aircraft is also completely done by the Stewart platform. As a consequence, the dampers can be removed from the connection mechanism and the empty weight of the aircraft is further reduced. The damping is done by a controlled compression of the actuators. The servo valves and control system play a major role in the damping process.

From the required axial forces, the actuators can be sized. According to an expert in the field of actuators, a pressure of 300 bar is feasible and from that the required area can be determined. From this area and the extension rate, the required oil flow is found. Then with the assumption that all the actuators operate at this maximum extension rate for a period of 15s, the volume of the accumulators and the oil reservoir is found to be $3.8m^3$. This is a conservative value as it is not likely to occur that all actuators operate at this maximum extension rate for 15s.

The mass of the Stewart platform is estimated based on the mass of the hexapod. This machine is significantly overdesigned as it used for fatigue testing under large loads. The platform is assumed to be 5t, the base 5t as well, the actuators 2t each, the accumulators 4t, the oil 4t and the reservoir and hoses 0.5t. This all sums up to a total of 30.5t.

Lateral Movement Structure

The Stewart platform is only capable to move relatively small distances in lateral direction. Since aircraft that come in for landing are sensitive to cross-wind, it is decided to add an additional structure that can move in lateral direction. This way, an aircraft can deviate from the centre line and still land on the system. Two rails are constructed on top of the base in lateral direction. The platform will be able to slide over these rails with the help of wheels that lock onto the rails. The platform will be powered by a motor that drives a gear on a gear rack. The deviation due to cross-wind on an aircraft's lateral position can be very sudden. The platform requires a large amount of power in order to be able to move fast enough to synchronise with the aircraft. The platform is able to move 4m from its centre position within 1s and come to stand still before reaching its maximum lateral position. A peak power of 2.6MW is found. Furthermore, additional mechanical brakes are

required because the motor would not be powerful enough to slow the structure down with the aircraft on top. These brakes should be able to apply a friction force of $880kN$ on the rails.

Base Structure

To support the weight of the Stewart platform with the attached aircraft under maximum acceleration, a beam structure is designed. The structure should be $30m$ wide to have enough clearance for conventional aircraft to use the runway. The structure is analysed numerically, iterating until cross-sections are found that keep stresses in the structure under the fatigue limit. The structure is found to weigh $1.0 \cdot 10^8 kg$.

Rails and Wheels Structure

For the wheels, a significant deviation is made from conventional train wheels. A solid attachment of the wheels to a rotating axle is replaced by a stationary axle with bearings. Smaller wheels are added to provide stability in lateral movement. Stress analysis of the rails and wheels under load is performed using finite element method, again aiming to stay under the fatigue limit. Appropriate steels are selected for the rails and wheels to mitigate wear, *R350HT* and *B6*, respectively.

Power

The system that accelerates the ground based system, consists of a linear induction motor powered by the power grid in combination with flywheels. This system is based on electromagnetic propulsion currently in place on aircraft carriers.

The linear induction motor is single sided with a short secondary, meaning that a steel plate with slots is stationary in the ground, and copper windings are laid through them. This construction is called the stator and supplies an alternating magnetic field through the 3 phase current. The changing magnetic field induces eddy currents in the aluminium plate next to the stator, which is then accelerated. The stator is divided in different segments which are turned on and off depending on if the secondary is close to them, this is measured with hall effect sensors.

One time use mechanical brakes are in place in case a power shortage occur. When performing an emergency brake, the aircraft can brake more heavily as currently the $0.4g$ limit is applied for passenger comfort. Next to this, the runway is programmed such that exit velocity is at 90% of the total runway distance: the additional $330 m$ can be used if necessary.

The flywheels supply the power when the grid is not enough during procedures. They convert electrical energy into kinetic energy and this can quickly be converted back to electrical energy to power the motor. In total, 200 flywheels are used to lower the power and energy requirement of each flywheel. The flywheels are made of carbon-fibre composites as this is excellent to carry the high loads high RPMs. The energy from the flywheels goes through a cycloconverter which outputs the right voltage and frequency. This whole circle is a closed loop control system with a high accuracy and quick reaction time.

Runway Station

A loop such that the carts can drive back next to the runway is not possible to implement on every runway on the airport due to logistical problems. It is therefore decided to launch or land multiple aircraft in a row before moving all the carts that are used for for these take-offs and landings back together. This way, some time is saved because the system does not have to move back after every take-off or landing. This is required in order to meet the capacity of the runway.

The base structures that are not being are not on the runway are located outside of a safety zone where no obstructing objects are allowed. Here, the aircraft or empty grid, depending on whether a take-off or landing has been performed, is lowered and a new aircraft/empty grid is mounted on top of the structure again. These two procedures are done by two different lifts that are installed behind each other. Once these procedures have been performed, the base structure will go to a pump station that is located behind the lifts. These pumps will be used to charge the accumulators that are required for the pistons of the Stewart platform. Once all of this has been done, the system is ready to perform its next take-off or landing.

Taxi Cart

The taxi cart has a rectangular shape and has the same width and length as the grid and has a mass of $15000kg$. It has 4 pairs of wheels, one at each extremity. The size of the wheels is similar to current aircraft's wheels. The maximum power required by the taxi cart is $533kW$. Each cart is powered by an electric motor and a battery pack and can reach a velocity up to $30 km/h$. The cart is able to travel three times from the gate to the runway

and back before needing to be charged. The battery pack of each cart has a total mass of 2700 kg . Each taxi cart is able to communicate with ATC and other taxi carts and has a Collision Avoidance System such that they can operate autonomously. On top of the taxi cart there is a conveyor chain which when needed extends to grab the aircraft's grid from the top of the Stewart platform and slides it to the top of the taxi cart. The grid is able to slide using a roller coaster mechanism both mounted on top of the taxi cart and on top of the Stewart platform.

Performance Analysis of REMALS

Now that all the subsystem components have been designed, the performance of the system is analysed. Performance analysis include determining the optimal flight profile in terms of noise reduction and calculations on resulting noise and fuel reductions.

Flight Profile

In order to fulfil one of the driving requirements concerning noise, the take-off and landing procedure as we know them, will have to be changed. Since aircraft noise is commonly measured in sound exposure level (SEL, dB), which takes both intensity and duration into account, the general approach is to shorten the procedures in order to reduce noise, while not increasing the maximum peak noise.

For take-off, this is achieved by accelerating the aircraft to higher speeds than conventional aircraft reach on the runway. Using the energy height principle, the excess kinetic energy is converted into potential energy up until the point where the aircraft reaches an optimal velocity to climb. This optimal velocity to climb is determined based on Aircraft Performance Summary Tables provided by the Base of Aircraft Data. When taking off at 145 m/s (determined from noise performance analysis), the time to reach FL100 (taken as a reference) decreases with 56 seconds.

With respect to landing, the maximum allowable approach speed is determined based on power constraints to find the required flight path angle to descent at constant indicated airspeed using idle thrust. When descending at 110 m/s constant indicated airspeed, a flight path angle of 3.8 deg is found.

Noise Reduction

When doing preliminary calculations, soon it was found out that a reduction of $7 \pm 3\text{ SEL dB}$ along the entire trajectory was not feasible. The further away the aircraft from the runway, the less the difference in noise production between the A321NEO and A321REMALS became. Therefore, it is decided to look at the top 3 zip code areas from which most complaints originated in 2018, which are at the most 7.8 km located away from the runway.

Analysis showed that for take-off, the minimum take-off speed to reach the required reduction is 145 m/s . For landing, a maximum allowable approach speed of 110 m/s can be reached by the system, also resulting in compliance with the requirement for at least 7.8 km away from the runway. This results in the noise profiles as presented in Figure 2 and Figure 3.

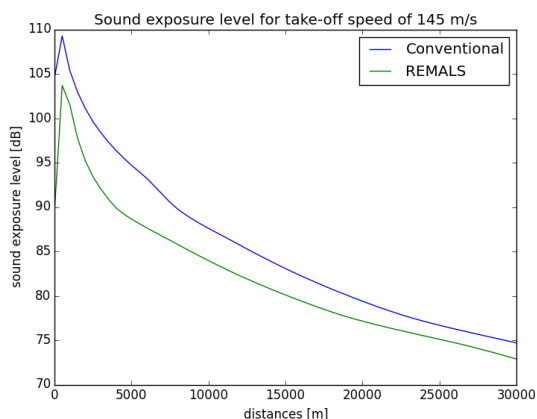


Figure 2: Noise profile for REMALS during take-off with respect to conventional A321NEO.

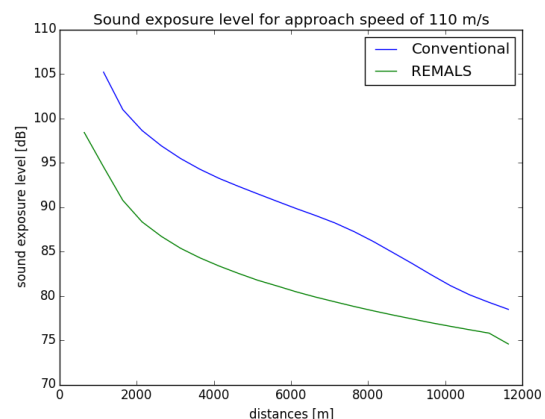


Figure 3: Noise profile for REMALS during landing with respect to conventional A321NEO.

Fuel Savings

Two requirements for the fuel reduction are set. The first requirement analyses the fuel reduction in an absolute sense, where the second does it relative to the payload and range of both aircraft. The absolute fuel reduction for all possible missions of the A321REMALS compared to the A321NEO can be found in Figure 4. As shown in the figure, fuel reduction is a function of payload and range. The fuel reduction increases for a decrease in payload and range. It can be seen that all flights with the A321REMALS will have at least 4.06% fuel reduction. For short range flights with an average flight time (1,5 hour), a fuel reduction of at least 5.2% will be reached. For A321REMALS flights with average occupancy rate (84.7%), 5% relative fuel savings is met for flights shorter 2 hour and 24 minutes. 1,5 hour flights with average occupancy will reach a 5.4% relative fuel reduction.

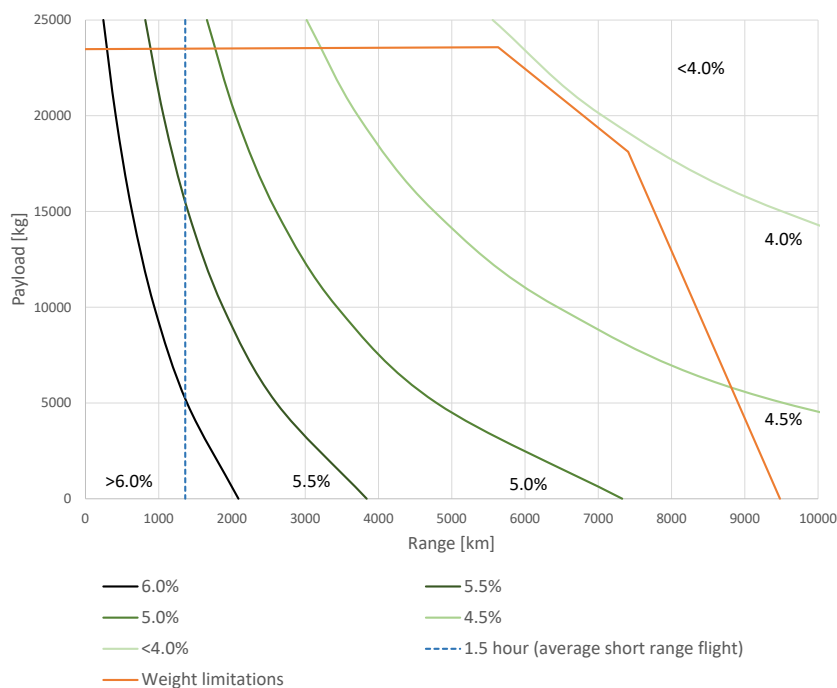


Figure 4: Fuel reduction for all flight missions.

Capacity

The capacity of the system should be the same as the capacity of a conventional runway. This means that one take-off or landing should be performed every 80s at maximum capacity. The time required to perform a landing is longer than the time required for a take-off, it takes 65s. This is less than the required 80s, but the carts have to be moved back over the runway at some point. This takes some time as well. Moving 5 carts back at once requires 75s combined with the 65s required for a landing, it takes 400s to perform 5 landings and moving all the carts back. In other words, it takes 80s on average per landing to perform 5 landings. Since the time required to perform a take-off is less, it will also take less than 80s on average to perform 5 take-offs.

Lifts will be used in order to get the aircraft or grid from the system and mounting a new one on top. Two lifts are required at both ends of the runway in order to meet the capacity of the runway. The total time required if only one lift is used is 72s which is more than the minimum interval between two consecutive take-offs or runways. By splitting the operations performed by the lift over two separate lifts, the time required is reduced such that it fits within the interval and thus the lifts do not limit the capacity of the runway.

As mentioned before, the accumulators of the Stewart platform need to be charged at the pump stations behind the lifts. They should be charged within the time they are standing still behind the runway. This can be done by 4 pumps, each having a flow rate of almost $0.4m^3/min$. There will be 4 pump stations behind the lifts on both sides of the runway. In total each runway is equipped with 32 pumps as pump stations are required at both sides of the runway.

Each aircraft on the ground will need to be supported by a taxi cart. This drives the number of carts required to operate the airport. 200 carts are required to support every aircraft and meet the airport capacity.

Operations and Functioning of REMALS

The operations of the REMALS differ from a conventional aircraft during landing, take-off and all ground operation phases. During approach, the ground vehicle needs to synchronise with the aircraft. For landing, the harpoons have to connect to the grid and lock, and the ground vehicle has to decelerate. For take-off, it is similar but in reverse order: first the "fingers" of the harpoons have to close before the decision speed and then the aircraft can take-off. On the ground, the aircraft first has to be moved to another platform for taxi. Then, the taxi cart will bring completely automated the aircraft to the gate. At the gate, normal procedures will follow and the batteries of the taxi cart will be charged. Then, for take-off, the aircraft is put on the base structure again. Similarly to conventional aircraft, in case of emergencies, a belly landing will be performed.

Modifications to the airport will mostly be performed on the runways where the rails will be added and the lift platform for the taxi cart will be implemented at each end of the runways. Also, there will be storage places on the airport for the unused taxi carts.

In order to ensure the safety of the passengers during every landing, synchronisation of the ground vehicle with the aircraft is a major aspect to look into. Multiple sensors and tracking system will be used to provide the required accuracy. The aircraft approaches the REMALS runway in a similar way as conventional aircraft and makes the ground vehicle aware of its approach using an automatic dependent surveillance-broadcast equipment (ADS-B). Once the aircraft is close enough, the ground vehicle will activate its LiDAR system to accurately synchronise with the aircraft. In clear weather, the combination of a photon LiDAR and OPAL-P1000 3D LiDAR sensor will be used. Otherwise, in case of foggy and rainy conditions, the OPAL-P1000 3D LiDAR will be replaced by a photon LiDAR sensor which performs better when the visibility is low. Finally, the Automated Weather Observing System (AWOS) already present on Siphol airport is used to inform the ground vehicle of the weather conditions. From this, the ground vehicle can determine which sensor to use.

Another aspect of the REMALS to be considered is the communication between all different components. A communication flow diagram, a hardware and software diagram and a data handling block diagram are created to provide a detailed overview of the interaction between the subsystems. For the ground system, two processing units are added: one for the EMALS part, the other one for the ground vehicle itself. Batteries and a power distribution board are added as well to distribute the power amongst the synchronisation components and the sensors. The processing units all process data received from the sensors and the aircraft. On the aircraft, a flight controller is added as an intermediate between the sensors and the processing unit of the aircraft. Finally, communication between the aircraft and the ground vehicle is mostly done via the air traffic control tower.

Risk

It is of utmost importance to identify the risks associated with the REMALS and mitigate those to ensure that a safe solution is developed. Risks in the REMALS are identified by using a failure mode effect and criticality analysis (FMECA). The failure modes are linked to the components which already had been linked to the functions before. Furthermore, combinations of events leading to failure of fulfilling a function are considered. All risks are mapped on risk maps and high and medium risks are identified. High and medium risks are mitigated to ensure a safer solution.

Before risk mitigation, 21 medium and 6 high risks are identified. These risks are mitigated by applying proper safety factors and a redundancy philosophy. The remaining risks are related to communication requirements regarding the synchronisation and the magnitude of the loads that the aircraft imposes on the ground system.

From a general risk evaluation of the system and further research on it, the solution is found to be a medium-low risk solution. Scheduled risks are medium for the system. The separate components exist, however certifying the combination of components and the hardware might impose some risks on the time schedule. The cost risks are medium for the system. It is a complex process to predict the way the economy will evolve. The system's savings with respect to current aircraft are depending on fuel prices amongst others. As the system will become profitable after more than 10 years this is a medium risk. The performance of the system cannot yet be guaranteed good enough. However, once further research on quantified requirements is conducted, the system can be straightforwardly up-scaled to meet for instance synchronisation requirements or sustain specific impact loads and performance risks are low.

RAMS

The reliability, availability, maintainability, and safety (RAMS) performance of the system should be more or less similar to that of conventional aircraft. The reliability of the REMALS has been ensured by applying safety

factors and making a redundant system which still functions if for instance a few sensors fail. The availability of the system has been ensured by always having backup ground vehicles and backup power supplies at standby. The maintainability of the system has been ensured by making the system such that components can be detached for inspection without drastically affecting the availability of the complete system. The safety of the system has been ensured by performing a technical risk analysis and risk mitigation. The safety critical functions are related to the synchronisation of the ground vehicle with the aircraft and whether it is clear to the aircraft whether the ground vehicle is synchronised or not. These safety critical functions can be ensured safe after proper analysis and modelling of aircraft pre-landing disturbances has been conducted.

Sustainability

Sustainability greatly influences the design. Sustainability is implemented and deeply embedded in the design of the system. The team designed each element of the system following the principles of the Value Sensitive Design (VSD). The VSD offers a framework that accounts for specific values throughout the design-phase of the system. A strategic approach was taken in order to tackle sustainability in a holistic way. It is described in detail in the report how sustainability influenced the design process and design choices over the past weeks and how the final design works towards achieving relevant Sustainable Development Goals. The two most important goals that this project works towards achieving are SDG 3 (Good Health and Well-being) which is strictly related to noise and SDG 13 (Climate Action) which is strictly related to the reduction in greenhouse gasses emissions.

System Verification and Validation

Each requirement that was set is verified in order to check whether it has been met. This is done by the use of compliance matrices for both the stakeholder and the system requirements. For multiple requirements, no analysis has been done yet. In these cases, the compliance matrix shows which kind of verification method can be used in order to check that specific requirement. A rationale is given for each requirement that explains why the requirement has been met or not. If the requirement has not been analysed yet, it is explained in the rationale why the selected method is applicable to requirement.

System validation was done to check if the complete system matches reality and the right solution has been developed. Since this project is conceptual and exceptionally cutting-edge, there are not many references in literature to compare it with. The outcomes of the REMALS design were compared to two similar projects found: GABRIEL and a former Design Synthesis Exercise. The results on power required by the system, required runway length, reduction in noise, reduction in fuel, costs, forces applied are compared with previous projects and roughly match the results obtained by the team therefore proving a proof of the rightness of the team's work and procedure followed. Additionally, CAD software was used to validate that the system fits together as a whole.

Project Design and Development

Regarding the post-DSE phase of the project, a development logic, a Gantt chart, a manufacturing, assembly and integration plan and a cost breakdown are made. The development logic gives an overview of the different activities that will be executed after the DSE. It starts with the technical developments that have to be improved about the design, followed by the operational issues that can be accounted. Then, an assessment is made on the potential benefits of the design. After that, the REMALS has to be built, tested and delivered.

The project Gantt chart summarises the activities mentioned in the development logic in a Gantt format. It is given in a timeline of 20 years and all activities are assigned an approximate duration.

For the manufacturing, assembly and integration plan, an overview of the production plan of the REMALS is given. It starts with manufacturing and buying the different components. Then, the parts go through sub-sub-assemblies, sub-assemblies and the final assembly. After coating, the product is tested. If the testing is successful, the REMALS can be implemented in airports and the aircraft can be delivered to airlines.

Estimates are made concerning the several costs involved in both capital and operational expenditures. The capital expenditures sum to $€6.26 \cdot 10^8$. Annual operational expenditures are $€15.4 \cdot 10^6$. Those costs, combined with the added value determined in the market analysis, $€7.97 \cdot 10^8$ are used to calculate the return on investment of the system. This is estimated to be around 9.31%, with the range due to contingencies between 3.8% and 13.9%.

Conclusion and Recommendations

In this report the main goal is to design a take-off and landing using a ground based power system. This new system is necessary as the aviation industry is currently limited in the amount of allowed movements per air-

port by the United Nations due to its lack of sustainability. Reducing fuel and noise emissions could fix this problem. This is done by removing the landing gear and launching the system with an Linear Induction Motor. In this way $\geq 5\%$ fuel is saved per short flight and the noise is reduced by at least ≥ 4 SEL dBa in a radius of 7.8 km around the airport. The concept is feasible as it meets the main requirements and stays within the cost and capacity constraints. It is an important discovery as this allows the aviation industry to keep growing.

To summarise the impact of the project, recommendations are made to improve and optimise the concept. There are technical aspects of the design that should be further evaluated, and there are aspects of the concept that should be further evaluated in order to be able to implement it. For the aircraft, the rudder could be investigated as it is designed for engine failure during take-off and this is not necessary anymore. Secondly, the thrust reversers could be decreased as deceleration can be provided by the ground based system. Lastly, for aircraft modifications, the high lift devices can be resized as the take-off speed is significantly increased.

For the ground based system, the power supply can be further investigated. The power supply can be optimised as now two take-offs and one landing are provided at the same time. For landing, the lateral landing position, the aircraft attitude and the lateral velocities of the aircraft during final approach should be better evaluated in order to optimise the design synchronisation.

Another aspect that could be investigated is the effect of different runway length. A longer length result in a lower maximum power but in a longer take-off time. The system is now designed for the shortest length used, but power can be optimised with using the different lengths of Schiphol and other airports.

Lastly, a more in depth structural analysis should be performed on the grid in order to verify the functioning of the system.

Contents

| | |
|--|-------------|
| Preface | i |
| Executive Summary | ii |
| List of Figures | xv |
| List of Tables | xvii |
| List of Symbols | xix |
| 1 Introduction | 1 |
| 2 Market Analysis | 3 |
| 2.1 Current Market | 3 |
| 2.2 Prediction of Future Market. | 3 |
| 2.2.1 Stakeholders | 4 |
| 2.3 Cost Budget | 4 |
| 2.3.1 Fuel Reduction. | 4 |
| 2.3.2 Noise. | 5 |
| 2.3.3 Reduced Wear | 5 |
| 2.3.4 Market Concepts. | 5 |
| 3 Requirements and Functional Analysis | 6 |
| 3.1 Context of the Design | 6 |
| 3.1.1 Airport: Schiphol. | 6 |
| 3.1.2 Aircraft: General Characteristics of the A321NEO | 6 |
| 3.1.3 Aircraft: Reference Flight. | 7 |
| 3.2 Stakeholder and System Requirements | 7 |
| 3.2.1 Driving Requirements | 10 |
| 3.2.2 Updates of Requirements | 11 |
| 3.3 Functional Analysis | 12 |
| 3.3.1 Functional Flow Diagram | 12 |
| 3.3.2 Functional Breakdown Structure. | 15 |
| 4 Concept Generation | 17 |
| 4.1 Concepts Overview | 17 |
| 4.1.1 Concept 1: Magnetic Runway | 17 |
| 4.1.2 Concept 2: Carry Cart | 17 |
| 4.1.3 Concept 3: Rails | 17 |
| 4.1.4 Concept 4: Drone | 18 |
| 4.2 Trade-Off Summary. | 18 |
| 4.2.1 Trade Criteria | 19 |
| 4.2.2 Criteria Weight Factor | 19 |
| 4.2.3 Trade Summary Table | 20 |
| 4.3 Winning Concept: REMALS. | 21 |
| 5 Design Process Set-Up | 22 |
| 5.1 Configuration, Component and System Identification | 22 |
| 5.1.1 Aircraft Design | 22 |
| 5.1.2 Ground System Design. | 22 |
| 5.2 N ² Chart | 23 |
| 5.3 Budget Breakdown | 25 |

| | | |
|----------|--|-----------|
| 6 | Aircraft Design | 26 |
| 6.1 | Connection Mechanism Between the Aircraft and the Grid | 26 |
| 6.1.1 | Controls of the Harpoon System | 26 |
| 6.1.2 | Architecture of the Harpoon System | 28 |
| 6.1.3 | Structural Design of the Connection Mechanism | 28 |
| 6.2 | Weight and Balance Characteristics | 31 |
| 6.2.1 | Loading diagram | 31 |
| 6.2.2 | Scissor plot | 33 |
| 6.2.3 | Sensitivity Analysis | 35 |
| 6.2.4 | Verification and Validation | 35 |
| 7 | Ground System Analysis | 36 |
| 7.1 | Grid | 36 |
| 7.2 | Connection Between Grid and Stewart Platform | 37 |
| 7.3 | Stewart Platform | 37 |
| 7.3.1 | Input Forces | 38 |
| 7.3.2 | Reaction Forces | 39 |
| 7.3.3 | Maximum Reaction Forces and Platform Configuration | 41 |
| 7.3.4 | Damping | 42 |
| 7.3.5 | Sizing the Actuators, Accumulators, and Reservoir | 43 |
| 7.3.6 | Mass | 43 |
| 7.4 | Rotation Platform | 44 |
| 7.5 | Lateral Movement Structure | 44 |
| 7.5.1 | Verification and validation | 45 |
| 7.6 | Base Structure | 46 |
| 7.7 | Rails and Wheels Structure | 47 |
| 7.8 | Power | 48 |
| 7.8.1 | EMALS | 48 |
| 7.8.2 | Electricity Grid | 55 |
| 7.8.3 | Ground Vehicle Power Supply | 55 |
| 7.9 | Runway Station | 55 |
| 7.9.1 | Accumulator Charging Station | 55 |
| 7.9.2 | Scissor lift | 55 |
| 7.10 | Taxi Cart | 56 |
| 7.10.1 | Cart General Characteristics | 57 |
| 7.10.2 | Cart Performance Sizing | 57 |
| 7.10.3 | Transfer System | 59 |
| 7.10.4 | Verification and Validation | 60 |
| 8 | REMALS Performance | 61 |
| 8.1 | Flight Profile for Take-Off and Landing | 61 |
| 8.1.1 | Take-Off Procedure | 61 |
| 8.1.2 | Landing Procedure | 65 |
| 8.1.3 | Verification and Validation | 67 |
| 8.2 | Noise Reduction | 68 |
| 8.2.1 | Aircraft Noise in General | 68 |
| 8.2.2 | Measuring Aircraft Noise | 68 |
| 8.2.3 | Noise Calculations | 69 |
| 8.2.4 | Sensitivity Analysis | 70 |
| 8.2.5 | Verification and Validation | 71 |
| 8.3 | Fuel Savings | 71 |
| 8.3.1 | Causes Fuel Reduction | 72 |
| 8.3.2 | Fuel Consumption per flight phase | 73 |
| 8.3.3 | Iteration of Fuel Weight | 76 |
| 8.3.4 | Absolute Fuel Savings | 76 |
| 8.3.5 | Relative Fuel savings | 78 |
| 8.3.6 | Justification | 78 |

| | | |
|-----------|---|------------|
| 8.3.7 | Sensitivity Analysis | 79 |
| 8.3.8 | Verification and Validation | 79 |
| 8.3.9 | Conclusion Fuel Consumption and Recommendations | 79 |
| 8.4 | Capacity | 80 |
| 9 | Operations and Functioning of REMALS | 83 |
| 9.1 | Operation and Logistics Description | 83 |
| 9.1.1 | General Description of the Operations | 83 |
| 9.1.2 | Airport Lay-Out | 85 |
| 9.2 | Synchronisation Instruments | 86 |
| 9.2.1 | Instruments | 86 |
| 9.2.2 | Procedure | 87 |
| 9.3 | Communications within the REMALS. | 87 |
| 9.3.1 | Communication Flow Diagram | 87 |
| 9.3.2 | Hardware and Software Diagram. | 88 |
| 9.3.3 | Data Handling Block Diagram | 89 |
| 10 | Risk | 91 |
| 10.1 | Risk Identification. | 91 |
| 10.2 | Risk Maps | 92 |
| 10.3 | Risk Mitigation | 94 |
| 10.4 | Risk Assessment Conclusion | 94 |
| 10.5 | RAMS | 96 |
| 11 | Sustainability | 98 |
| 11.1 | Sustainability Influence on the Design | 98 |
| 11.2 | Design Towards Achieving SDGs | 99 |
| 12 | System Verification & Validation | 101 |
| 12.1 | Requirement Compliance Matrix | 101 |
| 12.2 | Sensitivity Analysis | 107 |
| 12.2.1 | Technical Sensitivity Analysis | 107 |
| 12.2.2 | Design Sensitivity Analysis | 108 |
| 12.3 | System Validation | 108 |
| 13 | Project Design and Development | 109 |
| 13.1 | Project Design and Development Logic | 109 |
| 13.1.1 | Technical Developments. | 109 |
| 13.1.2 | Operational Issues | 110 |
| 13.1.3 | Assessment of Potential Benefit | 110 |
| 13.1.4 | End-Of-Life | 110 |
| 13.2 | Project Gantt Chart | 111 |
| 13.3 | Manufacturing, Assembly and Integration Plan | 113 |
| 13.4 | Cost Breakdown Structure | 114 |
| 13.4.1 | CAPEX | 114 |
| 13.4.2 | OPEX. | 114 |
| 13.4.3 | End-of-Life. | 115 |
| 13.5 | Return on Investment. | 115 |
| 14 | Conclusion | 116 |
| 15 | Recommendations | 117 |
| 15.1 | Design Recommendations | 117 |
| 15.2 | System Recommendations | 119 |
| | Bibliography | 123 |

List of Figures

| | | |
|------|--|------|
| 1 | Visualisation of the ground based system. | iv |
| 2 | Noise profile for REMALS during take-off with respect to conventional A321NEO. | vii |
| 3 | Noise profile for REMALS during landing with respect to conventional A321NEO. | vii |
| 4 | Fuel reduction for all flight missions. | viii |
| 2.1 | Strengths, Weaknesses, Opportunities and Threats of the system. | 3 |
| 3.1 | First level Functional Flow Diagram. | 13 |
| 3.2 | Second and third level of Functional Flow Diagram for function 1. | 13 |
| 3.3 | Second and third level of Functional Flow Diagram for function 2. | 13 |
| 3.4 | Second level of Functional Flow Diagram for function 3. | 14 |
| 3.5 | Second level of Functional Flow Diagram for function 4. | 14 |
| 3.6 | Second level of Functional Flow Diagram for function 5. | 14 |
| 3.7 | Second and third of Functional Flow Diagram for function 6. | 14 |
| 3.8 | Second level of Functional Flow Diagram for function 7. | 15 |
| 3.9 | Second level of Functional Flow Diagram for function 8. | 15 |
| 3.10 | Illustration of the Functional Breakdown Structure. | 16 |
| 4.1 | Drawing of the magnetic runway, shows hexagon hydraulic pistons and the rails. | 18 |
| 4.2 | Drawing of the carry cart with the suction pads platform and the grid. | 18 |
| 4.3 | Drawing of the rail system, the ground vehicle and the platform attaching to the runway. | 18 |
| 4.4 | Drawing of the drone, connected to the aircraft and separately. | 18 |
| 4.5 | Drawing of the final design concept. | 21 |
| 5.1 | Representation of N2-chart on the component level. | 24 |
| 5.2 | Representation of the N2-chart on the department level. | 24 |
| 6.1 | General overview of the harpoon system. | 26 |
| 6.2 | Aircraft in approach, harpoons extended. | 27 |
| 6.3 | Architecture of the electrohydraulic system of the harpoons. | 28 |
| 6.4 | Harpoon architecture when attached to the grid. | 28 |
| 6.5 | Cross-section of the strut with the parameters used for the analysis. | 29 |
| 6.6 | Loading diagrams of conventional A321NEO and REMALS concept aircraft | 32 |
| 6.7 | Scissor plot including the c.g. range at $S_h/S = 0.25$ | 35 |
| 7.1 | Visualisation of the ground based system. | 36 |
| 7.2 | Visualisation of the grid. | 36 |
| 7.3 | Connection mechanism between grid and Stewart platform. | 37 |
| 7.4 | Loads on the Stewart platform. | 39 |
| 7.5 | Connection points on the platform of the Stewart platform. | 42 |
| 7.6 | Connection points on the base of the Stewart platform. | 42 |
| 7.7 | Distance covered, velocity and power vs. time during lateral movement. | 45 |
| 7.8 | Lateral movement system used by the platform to synchronise with aircraft. | 45 |
| 7.9 | Top View of base. | 46 |
| 7.10 | Front view of base. | 47 |
| 7.11 | FEM analysis of an assisting wheel. | 48 |
| 7.12 | FEM analysis of the wheel's contact patch. | 48 |
| 7.13 | FEM analysis of the main wheel. | 48 |
| 7.14 | Electrical block diagram of the propulsion system of the ground based structure | 49 |
| 7.15 | Free Body Diagram for ground based vehicle and aircraft. | 49 |

| | | |
|------|---|-----|
| 7.16 | Acceleration and velocity profile during take-off. | 50 |
| 7.17 | Acceleration and velocity profile during landing. | 50 |
| 7.18 | Representation of a linear induction motor [34] | 51 |
| 7.19 | 3 phase windings | 51 |
| 7.20 | Power supply system used by subways. | 55 |
| 7.21 | Electrical block diagram of the ground based structure. | 55 |
| 7.22 | LSide and front view of lift platform | 56 |
| 7.23 | Velocity, acceleration and power required vs. time during the acceleration of a taxiing aircraft. | 58 |
| 7.24 | Electrical block diagram of the taxi platform | 59 |
| 7.25 | Wheel system for lateral movements on the rail. | 59 |
| 7.26 | Lateral locking mechanism. | 60 |
| 7.27 | Conveyor chain for transferring the aircraft on the lift platform. | 60 |
| | | |
| 8.1 | Height vs. time during take-off. | 64 |
| 8.2 | Height vs. velocity during take-off. | 64 |
| 8.3 | Height vs. horizontal distance covered during take-off. | 64 |
| 8.4 | Height vs. flight path angle during take-off. | 64 |
| 8.5 | Height vs. thrust during take-off. | 65 |
| 8.6 | Height vs. thrust setting during take-off. | 65 |
| 8.7 | Height vs. time during landing. | 66 |
| 8.8 | Height vs. velocity during landing. | 66 |
| 8.9 | Height vs. thrust during landing. | 66 |
| 8.10 | Height vs. thrust setting during landing. | 66 |
| 8.11 | Drag polar of REMALS. | 67 |
| 8.12 | Drag polar of A320 [71]. | 67 |
| 8.13 | Typical noise breakdown for landing and take-off procedures in terms of engine and airframe noise [19]. | 68 |
| 8.14 | Determining the sound exposure level explained [20]. | 69 |
| 8.15 | Differences in sound exposure level for different take-off speeds with respect to the conventional A321NEO. | 70 |
| 8.16 | Sound exposure level for REMALS with a take-off speed of 145 m/s with respect to conventional A321NEO. | 70 |
| 8.17 | Sound exposure level for REMALS with an approach speed of 110 m/s with respect to conventional A321NEO. | 71 |
| 8.18 | Differences in sound exposure level for different approach speeds with respect to the conventional A321NEO. | 71 |
| 8.19 | Sections of total flight mission | 72 |
| 8.20 | Fuel reduction for different flight missions | 77 |
| 8.21 | Fuel reduction per passenger per kilometer for a payload weight of 18702 kg | 78 |
| 8.22 | Sensitivity analysis for the thrust-specific constant. | 79 |
| | | |
| 9.1 | Operations diagram of the REMALS. | 84 |
| 9.2 | New airport layout of Schipol with the runways marked in red, the storage space marked in yellow, the loop addition marked in blue. | 86 |
| 9.3 | Communication flow diagram of the REMALS concept. | 88 |
| 9.4 | Hardware and software diagram of the REMALS concept. | 89 |
| 9.5 | Data handling block diagram of the REMALS concept. | 90 |
| | | |
| 11.1 | Overview of the relevant social, environmental and social SDGs goals | 99 |
| | | |
| 13.1 | Project Development & Design logic diagram. | 111 |
| 13.2 | End-of-life of the REMALS. | 111 |
| 13.3 | Post-DSE project Gantt chart. | 112 |
| 13.4 | Production plan. | 113 |
| 13.5 | Cost breakdown. | 114 |
| | | |
| 15.1 | Recommended focus areas for improving A321REMALS flight performance | 117 |

List of Tables

| | | |
|------|---|-----|
| 1 | Version control | i |
| 2 | Killer and driving requirements. | iii |
| 2.1 | Estimated annual profit of a take-off and landing system on Schiphol for flights shorter than 3 hours [in millions of euros]. | 5 |
| 3.1 | All relevant general characteristics used in this report of the A321NEO, WF072. | 7 |
| 3.2 | Requirements of stakeholder Schiphol airport, including a unique identifier. | 8 |
| 3.3 | System requirements derived from the stakeholders requirements. | 9 |
| 3.4 | System requirements linked to the functional analysis. | 10 |
| 3.5 | Driving requirements. | 11 |
| 3.6 | Reasoning for the changes in the requirements throughout the course of the project. | 11 |
| 3.7 | Changelog of stakeholder requirements throughout the course of the project | 11 |
| 4.1 | Pairwise comparison matrix with relative scores of importance and final weights of the trade criteria. | 20 |
| 4.2 | Trade summary table for the final system. | 21 |
| 6.1 | Necessary inner radius for different load cases. | 30 |
| 6.2 | Final dimensions and mass of the harpoons. | 31 |
| 6.3 | Values used for centre of gravity OEW calculation | 32 |
| 6.4 | Input values for the stability and controllability equations | 34 |
| 7.1 | Stewart platform design. | 42 |
| 7.2 | Configuration of the Stewart platform. | 42 |
| 7.3 | Mass of the Stewart platform's main components | 43 |
| 7.4 | Parameters python program | 50 |
| 7.5 | Input parameters for the flywheel sizing. | 54 |
| 7.6 | Output parameters for the flywheel sizing. | 54 |
| 8.1 | Parameters used for calculation of the flight profile during take-off for the A321NEO and A321REMAIS. | 63 |
| 8.2 | Parameters used for calculation of the flight profile during landing for the A321NEO and A321REMAIS. | 66 |
| 8.3 | Parameters used for calculation of noise produced by conventional landing gear | 70 |
| 8.4 | Top 3 zip code areas from which most complaints concerning aircraft noise originated in 2018 [9]. | 70 |
| 8.5 | All submission with corresponding fuel weight fraction and absolute fuel consumption, MTOW assumed for A321NEO | 76 |
| 8.6 | Possible combinations of payload and fuel mass | 77 |
| 8.7 | Time needed for take-offs/landings | 80 |
| 8.8 | Time required to move a certain amount of carts back. | 81 |
| 8.9 | Time needed by the lift during take-off and landing | 81 |
| 10.1 | Risk identifier categories. | 91 |
| 10.2 | List of identified risks related to the load carrying ground system. | 92 |
| 10.3 | List of identified risks related to the aircraft. | 92 |
| 10.4 | List of identified risks related to the remaining categories. | 93 |
| 10.5 | Scaling of risks used in the risk maps. | 93 |
| 10.6 | Risk map for load carrying ground system. | 93 |
| 10.7 | Risk map for aircraft categories. | 94 |
| 10.8 | Risk map for remaining categories. | 94 |

| | |
|---|-----|
| 10.9 Risk mitigation overview. | 95 |
| 10.10 Mitigated risk map for load carrying ground system. | 96 |
| 10.11 Mitigated risk map for aircraft categories. | 96 |
| 10.12 Mitigated risk map for remaining categories. | 96 |
| 12.1 Compliance matrix of the stakeholder requirements. | 102 |
| 12.2 Stakeholder requirement verification. | 102 |
| 12.3 Compliance matrix of the system requirements set 1. | 104 |
| 12.4 Compliance matrix of the system requirements set 2. | 104 |
| 12.5 System requirements verification. | 105 |
| 12.6 Sensitivity of key parameters when the system is subject to a mass change | 107 |
| 14.1 Main design parameters of the ground based system. | 116 |
| 1 Work distribution. | 120 |
| 2 Work distribution. | 121 |
| 3 Aircraft performance data provided by Base of Aircraft Data for high mass climb (83,000 kg) of A321-131. | 122 |
| 4 Aircraft performance data provided by Base of Aircraft Data for high mass descent (83,000 kg) of A321-131 | 122 |
| 5 Aircraft performance data provided by Base of Aircraft Data for high mass cruise (83,000 kg) of A321-131 | 122 |

List of symbols

| Symbol | Description | Unit |
|----------------------|--|--------------|
| A | Wing aspect ratio | [-] |
| A_i | Cross-sectional area of actuators | [m^2] |
| A_h | Horizontal tail aspect ratio | [-] |
| a | acceleration | [m/s^2] |
| B | Magnetic flux | [T] |
| b | Span | [m] |
| b_f | Width of the fuselage | [m] |
| b_n | Width of the engines | [m] |
| \bar{c} | Mean Aerodynamic Chord (MAC) | [m] |
| \vec{c} | Vector to the connection point from the centre of the coordinate system | [m] |
| c | Chord in clean configuration | [m] |
| c | Speed of sound | [m/s] |
| C | Operational costs | [€] |
| c' | Chord of the airfoil with extended flap | [m] |
| C_D | Drag Coefficient | [-] |
| C_{D0} | Zero lift drag coefficient | [-] |
| $C_{d_{gbs}}$ | Drag coefficient of the ground based structure | [-] |
| $C_{d_{ac}}$ | Drag coefficient of the ground based structure | [-] |
| c_g | Mean geometric chord ($=S/b$) | [m] |
| C_L | Lift coefficient | [-] |
| C_{L0} | Lift coefficient of the flapped wing at zero angle of attack | [-] |
| $C_{L\alpha_{A-h}}$ | Lift rate coefficient of the aircraft less tail | [1/radians] |
| $C_{L\alpha_h}$ | Lift rate coefficient of the aircraft horizontal tail | [1/radians] |
| $C_{L\alpha_w}$ | Wing lift rate coefficient | [1/radians] |
| C_{L_h} | Horizontal tail lift coefficient | [-] |
| C_{m0} | Moment coefficient at zero angle of attack | [-] |
| $C_{m_{ac}}$ | Zero lift pitching moment coefficient of the aircraft without tail | [-] |
| $\Delta C_{l_{max}}$ | Airfoil lift coefficient increase due to flap extension at landing condition | [-] |
| c_t | Thrust specific fuel consumption | [$g/kN/s$] |
| d | Wheel diameter | [m] |
| \vec{d} | Actuator vector | [m] |
| D | Drag | [N] |
| $D(\theta_d, \phi)$ | Directivity function | [-] |
| dt | Time step used for numerical integration | [s] |
| dX | Horizontal distance covered in time step | [m] |
| dH | Height covered in time step | [m] |
| E_{acc} | Energy used during acceleration | [J] |
| E_{dec} | Energy used during deceleration | [J] |
| E_{FW} | Energy stored in each flywheel | [J] |
| E_{grid} | Energy from grid per cycle | [J] |
| E_{regen} | Regenerated energy | [J] |
| E_k | Kinetic energy | [J] |
| E_{req} | Required energy | [J] |

| | | |
|-----------------------|--|---------------------|
| f | Centre frequency of subsequent 1/3 octave bands | [Hz] |
| F | Force | [N] |
| $F(S)$ | Empirical spectral function | [-] |
| F_d | Shear stress on rotor | [N/m ²] |
| $F_{friction}$ | Friction force | [N] |
| g | Gravitational acceleration | [m/s ²] |
| G | Geometry function | [-] |
| h | Height | [m] |
| H | Height | [m] |
| h_f | Fuselage height | [m] |
| I | Mass moment of inertia | [kgm ²] |
| I | Intensity of sound pressure level | [W/m ²] |
| I | Investment costs | [€] |
| I | Current | [A] |
| I_{cell} | Current of a cell | [A] |
| k | Effective length factor | [-] |
| K_c | Effect of the wing sweep angle | [-] |
| l | Length of the coil | [m] |
| l_{fn} | Distance between the nose and the beginning of the wing | [m] |
| l_h | Tail arm | [m] |
| l_n | Distance between the front of the engines and the MAC of the main wing | [m] |
| L | Length scale characteristic of airframe noise source considered | [m] |
| L | Lift generated by the aircraft | [N] |
| L_e | Effective length | [m] |
| m | Mass | [kg] |
| M | Mach number | [-] |
| \vec{M} | Moment vector | [Nm] |
| m_{FW} | Mass of flywheel | [kg] |
| M_{human} | Average human mass | [kg] |
| M_{LG} | Mass of landing gear | [kg] |
| $M_{luggage}$ | Average luggage mass | [kg] |
| m_m | Mass of motor | [kg] |
| M_x, M_y | Bending moment around the x, y axis | [N/m] |
| M_{pL} | Mass payload | [kg] |
| M_f | Mass fuel | [kg] |
| M_{ff} | Mass fuel fraction | [-] |
| δM_f | Difference in fuel consumption | [kg] |
| \dot{m} | Fuel flow | [kg/s] |
| $M_{fuel_{consumed}}$ | Consumed fuel | [kg] |
| n | Number of wheels | [-] |
| N | Normal force | [N] |
| N_{FW} | Number of flywheels | [-] |
| N_{poles} | Number of poles | [-] |
| N_{carts} | Number of carts | [-] |
| N_{rows} | Number of series in parallel | [-] |
| N_{series} | Number of cells in series | [-] |
| N_1 | Thrust setting | [%] |
| \vec{O} | Vector to the origin of a reference frame | [m] |
| p | Pressure in the actuators | [Pa] |
| P | Power function | [W] |
| P | Power | [W] |
| P_a | Power available | [W] |
| P_{acc} | Power used during acceleration | [W] |
| P_{cr} | Critical buckling load | [N] |
| P_{dec} | Power used during deceleration (recoverable) | [W] |
| $P_{FW_{max}}$ | Maximum power from flywheels | [W] |
| P_{grid} | Power required from grid | [W] |
| P_r | Power required | [W] |
| P_{req} | Power required | [W] |
| Q_i | Flow rate | [m ³ /s] |
| r | Distance from noise source to observer | [m] |
| r | Radius | [m] |

| | | |
|------------------|---|----------------------|
| R | Radius | [m] |
| R | Revenue | [€] |
| ROC | Rate of climb/descent | [m/s] |
| RC_s | Rate of climb and velocity increment | [Nm/kg s] |
| s | Distance | [m] |
| S | Strouhal number | [-] |
| S | Wing surface | [m ²] |
| S | Stroke length | [m] |
| S_h | Horizontal tail surface | [m ²] |
| S_{net} | Surface less projection of central wing part inside the fuselage | [m ²] |
| S_w | Wing surface area | [m ²] |
| S_{wf} | Flapped wing area | [m ²] |
| T | Net thrust provided | [N] |
| T_{max} | Maximum net thrust provided | [N] |
| t | time | [s] |
| t_{cycle} | time required for take-off/landing cycle | [s] |
| t_{syn} | Synchronisation and connection time | [s] |
| t_{to} | Time till take-off procedure is complete | [s] |
| t_{land} | Time till landing procedure is complete | [s] |
| V | Velocity | [m/s] |
| V | Volume | [m ³] |
| $V_{approach}$ | Approach and landing velocity | [m/s] |
| V_{cell} | Cell voltage | [V] |
| V_{dec} | Decision speed | [m/s] |
| V_{end} | Constant velocity at end of runway | [m/s] |
| V_{end} | Velocity at end of lateral acceleration | [m/s] |
| V_{FW} | Volume of the flywheel | [m ³] |
| V_h | Horizontal tail velocity | [m/s] |
| V_m | Volume of the motor | [m ³] |
| V_{min} | Minimum take-off velocity | [m/s] |
| V_{series} | Voltage of series of cells | [V] |
| V_{req} | Required voltage | [V] |
| V_{TAS} | True airspeed | [m/s] |
| V_{TO} | Take off velocity | [m/s] |
| V_y | Vertical velocity | [m/s] |
| V_{oil} | Total oil volume | [m ³] |
| V_{-1} | Velocity of previous time step | [m/s] |
| W | Aircraft weight | [kg] |
| $W_{a/c,L}$ | Aircraft landing weight | [kg] |
| $W_{a/c,TO}$ | Aircraft take-off weight | [kg] |
| x_{ac} | Longitudinal position of the aerodynamic center | [m] |
| \bar{x}_{ac} | Longitudinal position of the aerodynamic center divided by \bar{c} | [-] |
| α | Angle of attack | [deg] |
| β | Prandtl-Glauert compressibility correction factor | [-] |
| γ | Flight path angle | [deg] |
| ϵ | Downwash angle | [deg] |
| η | Airfoil efficiency factor | [-] |
| η_{LIM} | Efficiency of linear induction motor | [-] |
| η_{motor} | Efficiency of electric motor | [-] |
| θ | Angle | [deg] |
| θ_c | Angles of the connection points on the Stewart platform | [deg] |
| θ_d | Polar directivity angle | [rad] |
| $\Lambda_{0.5c}$ | Sweep angle measured at half chord length | [deg] |
| ϕ | Azimuthal directivity angle | [rad] |
| μ_1 | Effect of the camber increase associated with the deflection angle of the flaps | [-] |
| μ_2 | 2D effect lift contribution generated by the high lift devices | [-] |
| μ_3 | Effect of sweep angle | [-] |
| μ_{wheels} | Friction of the steel wheels | [-] |
| μ_0 | Bypass ratio jet engine at take-off | [-] |
| ν | Poisson ratio | [-] |
| ρ_{ke} | Density kerosine | [kg/m ³] |
| ρ | Local air density | [kg/m ³] |
| σ_z | Normal stress | [N/m ²] |
| ψ | Yaw angle | [deg] |
| ω_{FW} | Angular velocity of flywheels | [rad/s] |
| ω_m | Angular velocity of motor | [rad/s] |



Introduction

The limit on the number of air transport movements at Schiphol is a major issue, especially for the residents close to the airports due to the noise and particulate matter emissions. Consultations with stakeholders resulted in setting a maximum of 500,000 movements per year until 2020, however this ceiling was already reached in 2018 ¹. Although it is widely known that the aviation industry negatively impacts the environment, its growth does not seem to stop. IATA's forecast predicts 8.2 billion air travellers in 2037, leading to a doubling in passenger numbers from today's levels ². The aviation sector is calling for new technologies in order to cope with the future demand while lowering the environmental impact. A straightforward, yet difficult solution, would be to reduce the mass of current aircraft to significantly reduce the emissions of the air transportation industry.

This report is written in compliance with the Design Synthesis Exercise academic year 2019/2020 at Delft University of Technology, with the purpose of completing an entire design process as a group. The goal is to design a commercial aircraft that takes off and lands using a ground-based power system in order to get rid of the landing gear, hence reducing the weight of the aircraft. The reduction in aircraft's weight and in power provided by the aircraft's engines will translate in a reduction in fuel used, noise pollution and toxic gas emissions. The aim of the project is to meet these objectives therefore ensuring a more sustainable future of air transportation. The team was driven to achieve the following Mission Need Statement:

"Provide a ground-based powered take-off and landing system for the B737/A320 aircraft types that reduces environmental impact with respect to current conventional aircraft and is economically feasible."

The project is focused on designing an enhanced version of the A321NEO and the relative ground system infrastructures at Schiphol airport. This specific aircraft was chosen as a test sample because it is the heaviest in the medium range category, hence by designing for this aircraft the ground system can be easily scaled down for lighter aircraft. To truly achieve its goal, the system will eventually have to be expanded to other airports worldwide on multiple short range aircraft. This is the fourth in a series of four reports, which focuses on analysing and designing the selected concept from the previous report [23] in depth. This is done by performing the necessary technical calculations and working out the details of the design. At the end of this report the outcomes are reported, and based on the results, relevant recommendations are given to further improve the design in the post-DSE activities.

The structure of this report is the following: in chapter 2 a market analysis is performed, the current and future markets are evaluated and cost budget estimation is calculated. Moving on, in chapter 3 the stakeholders and system requirements are examined in detail. In addition, a functional analysis is discussed to identify the main functions the system has to fulfil. Then in chapter 4 the four design concepts that the team came up with to meet the requirements are displayed. From these four concepts, using specific trade criteria and assigning criteria weight factors the final design is chosen. Next, in chapter 5 an overview of the chosen design and

¹URL:<https://www.schiphol.nl/en/schiphol-as-a-neighbour/page/schiphol-and-the-future/> [Accessed 24 June 2019]

²URL:<https://www.iata.org/pressroom/pr/Pages/2018-10-24-02.aspx> [Accessed 21 June 2019]

the relative subsystems is given, including an appropriate N^2 chart to show the interaction between the subsystems. In chapter 6 all the needed modification to retrofit current A321NEO are explained and supported by calculations. Then, in chapter 7 the ground system is analysed in detail, describing all of its technical components. Furthermore, in chapter 8 an evaluation of reduction in noise pollution and fuel use is discussed. In chapter 9 the operations and logistics of the ground systems are further explained, discussing the integration and lay-out on the current airport. Then in chapter 10 a technical risk assessment is performed. Continuing, in chapter 11 the team approach to sustainability and the social relevance of the project are described. Next, in chapter 12 all the requirements are verified and validated using a compliance matrix. In chapter 13 the post-DSE activities are summarised in a Gantt chart, including all the costs faced in the future. Finally in chapter 14 and chapter 15 the results are discussed and recommendations for the future are given.

2

Market Analysis

In this chapter the competitive costs of the take-off and landing system are determined, as is the market that will purchase the product. This is done by establishing the current market and giving a prediction of the future market. Then the system is introduced with the stakeholders and the influence that the system will have on the market. This is followed by how the system would be implemented, and answers the question: who will pay for the system?

2.1. Current Market

The government has enforced a limit on the amount of movements on Schiphol, no more than 500,000 movements are allowed annually, until 2020. This limit is set to lower noise pollution in the area and to meet the EU regulations of less CO₂ emissions. When the limit is reached this will have an impact on the reachability of the Netherlands, the amount of tourist and the job opportunities. In this limitation the amount of night movements are also defined, and the amount of allowable movements is dependent on the noise emission of the aircraft. This may cause airlines to fly with less noisy airplanes which emit more green gas emissions at night. This is an example of the sub-optimal situations that are created by regulations.

Aviation is growing with 4.7% annually and it is estimated that this trend will remain steady in the years to come [38]. However, the United Nations agreed that there should be no rise in aviation emissions, from 2020 onward. If no solutions for sustainable aviation are made or implemented, other ways have to be found to offset the emissions of aviation. It is predicted that due to environmental restrictions on airports the supply and demand of flights get out of proportion, this will result in an increasing ticket prices. The annual fee paid by costumers for European flights will be increased from €2.1 · 10⁹ in 2014 to €6.3 · 10⁹ by the year 2035 [24].

2.2. Prediction of Future Market

A ground-based take-off and landing system provides opportunities for the future market. These are mainly determined by requirement NCL-Alc09 and NCL-sh118 which state that the total fuel consumption has to decrease by 5% and the noise with 7±3 SEL dBA in comparison to the current situation. With these requirements money can be saved, proportional to the amount that can be invested in the project.

To assess the system, a SWOT analysis is preformed as can be seen in Figure 2.1. It is analysed what the strengths and weaknesses of the system itself are, and what opportunities and threats the external factors provide. Some

of the strengths of the system will be expressed in terms of money that can be saved in comparison to the current market.

| | Positive | Negative |
|----------|--|--|
| Internal | <ul style="list-style-type: none"> • 7 ± 3 SEL dBA noise reduction • 5% fuel reduction on average • Capacity has not changed • No fuel emissions during taxiing <p style="text-align: right;">S</p> | <ul style="list-style-type: none"> • Redesign aircraft • High power required • (Unexpected) design costs • Insufficient funds • Limited to existing technology • Weather conditions <p style="text-align: right;">W</p> |
| External | <ul style="list-style-type: none"> • Less CO₂ emissions • Sustainable innovation grant • Increase in allowable movements on the airport <p style="text-align: right;">O</p> | <ul style="list-style-type: none"> • Implementation • Obtain certificates • Impact on conventional runway • New emergency procedures • Laws/Regulations • Passenger safety feeling <p style="text-align: right;">T</p> |

Figure 2.1: Strengths, Weaknesses, Opportunities and Threats of the system.

2.2.1. Stakeholders

To know who will benefit when implementing this system, the stakeholders have been identified, together with their main interest and constraints on the system. The stakeholders are partially the ones who will in the end pay for the system, but also the ones who will profit from it.

- **Schiphol airport:** this is the reference airport for which the system is going to be designed. It shall mainly ensure that the new system does not decrease the capacity of the airport.
- **Airline company (Airfrance - KLM):** this cooperation provides for the majority of flights arriving and departing from Schiphol airport according to the Traffic Review 2018¹. It will have an influence on the maintenance procedures, the price of the tickets or the implementation time of the system.
- **Passengers:** the customers have a large influence as stakeholders as they will be the ones using the system at the end.
- **Aircraft manufacturer (Airbus):** the reference aircraft to be designed on is the A321NEO (section 3.1). Hence, Airbus is responsible for the update of this aircraft.
- **Project team:** the final stakeholder of importance is the project team, since this is the executing party of the design.

2.3. Cost Budget

This section describes how certain costs can be impacted by implementing the developed design. This system should over time replace the competitor: the conventional landing gear. The net present values of the cost savings are calculated by using a discounted cash flow model. A discount rate of 2.5% is used, since this is the weighted average of the interest rates Schiphol pays on its five largest outstanding bonds.² Analysis is done assuming a fairly common payback period of 15 years. This is also roughly in line with Schiphol's return on equity of 7.2% [69]. Note that growth rates are neglected from the calculations, giving very conservative estimates of the benefits.

2.3.1. Fuel Reduction

Fuel costs

The annual fuel costs in 2018 were determined to be $160.7 \cdot 10^9$ euro's [38]. The average fuel reduction for flights shorter than three hours is 5%. In reality the fuel reduction per aircraft may vary as the fuel consumption depends on the type of aircraft and the take-off weight, but on average for all flights shorter than 3 hours this requirement has to be met. The fuel consumption can directly be related to the travelled distance, and short-haul flights cover 53.92% of the total distance travelled [43]. This amounts to $\text{€}85.71 \cdot 10^9$ per year and a possible saving of $\text{€}4.3 \cdot 10^9$. Schiphol holds 0.67%³ of the world's flights, which means that $\text{€}29.0 \cdot 10^6$ can be saved annually, over 15 years this gives a net present value of $\text{€}3.66 \cdot 10^8$. However, since there are always two airports involved in a flight, Schiphol can expect to only receive half of this amount, so $\text{€}1.83 \cdot 10^8$.

Emission costs

The total CO_2 emissions worldwide is 163 Tg (million tonnes) in 2017, 20% of this is produced in Europe [21]. Global aviation is growing with 4.7% a year and it is assumed that the annual CO_2 emissions grow accordingly. Schiphol holds 11.9% of the European market share and 78.88% of the flights leaving Schiphol are short flights [33]. Yearly European airlines have to pay the EU allowance for the amount of CO_2 emissions they produce, $\text{€} 24.98$ per ton⁴ is brought into account. This regulation is being introduced gradually, starting in 2020 there has to be paid for 15% of the emissions they produce, this percentage increases with 2.2% annually⁵. As the emission allowances can be traded, the price is subject to fluctuations due to supply and demand. However it is estimated that the demand will grow as currently 85% of the allowance is for free and for a conservative calculation the price per tonne CO_2 is kept constant. This amounts to an annual savings of $1.74 \cdot 10^6$ of direct gains, and $3.61 \cdot 10^6$ of indirect savings as part of the allowance is still given for free.

¹URL:<http://trafficreview2018.schiphol.tangelo.nl/movements#main-airlines> [Accessed 9 June 2019]

²URL: <https://www.schiphol.nl/en/schiphol-group/page/emtn-programme/> [Accessed 19 June 2019]

³URL: <https://www.statista.com/statistics/193533/growth-of-global-air-traffic-passenger-demand/> [Accessed 19 June 2019]

⁴URL:<https://markets.businessinsider.com/commodities/co2-european-emission-allowances> [Accessed 23 June 2019]

⁵URL: https://ec.europa.eu/clima/policies/ets/allowances/aviation_en [Accessed 23 June 2019]

2.3.2. Noise

Noise reductions around Schiphol have a direct effect on the airport charges airlines have to pay. To estimate the annual profit that can be made due to noise reductions, the 15 most common aircraft on Schiphol were analysed. Together they were responsible for 448,773 of the movements in 2018⁶. After filtering out all aircraft that are significantly bigger than the A321NEO for which the system is designed, 378,807 movements remained for analysis. Schiphol's tax rates are a function of the aircraft weight and the Effective Perceived Noise Level (EPNL)[70]. No exact mathematical relation exists between noise expressed in SEL and in EPNL. However, EPNL tends to be 3 to 5 dB higher than SEL[49]. It is therefore reasonable to assume that sound reductions in SEL give an equal dB saving in EPNL. With this data, it could be determined for every aircraft whether they would move to a better category and how much this would improve their respective tax rates. Multiplying this by their amount of movements and average weights gave total possible savings. Note that only day movements were assumed to make a conservative estimate since tax advantages due to noise reduction are less prominent during the day. It is found that a total of approximately $\text{€}5.83 \cdot 10^6$ is saved annually using 2018 data. Since flight movements are capped, it is assumed there will be no growth in those savings.

2.3.3. Reduced Wear

A conventional landing gear consists of many expendable parts. Tyres wear quickly because they still lack the rotational velocity at touch down and brakes need to dissipate so much energy that they need frequent replacement, too. Tyres are found to cost around $\text{€}4200$ per set, lasting 200 flights. This implies an average of $\text{€}21$ per flight. Similarly, maintenance of brakes costs about $\text{€}53$ per flight. With the current 500,000 annual movements, this means $\text{€}26.5 \cdot 10^6$ per year.

Summary

In Table 2.1 the money saved over 15 years is displayed, as after this period of time the system should be profitable. First the yearly savings are displayed, then the Net Present Value (NPV) over 15 year including discount rate. It should be taken into account that this system cannot be implemented on one airport, and the system will only work if multiple airports collaborate to purchase the system. However, in this project the focus will be on implementing it on Schiphol and that is why the savings are limited to aircraft taking-off and landing on Schiphol. As the fuel and emission savings have to be divided on the flight path, they are split between the landing and take-off airport.

Table 2.1: Estimated annual profit of a take-off and landing system on Schiphol for flights shorter than 3 hours (in millions of euros).

| | Direct gain [€] | NPV [€] | Indirect gain [€] |
|-------------------------|--------------------------------------|---------------------|-------------------------------------|
| Fuel | $29 \cdot 10^6$ | $362.9 \cdot 10^6$ | - |
| Emissions | $1.74 \cdot 10^6$ | $22.0 \cdot 10^6$ | $54.2 \cdot 10^6$ |
| Noise | $5.83 \cdot 10^6$ | $73.69 \cdot 10^6$ | - |
| Tyres&brakes | $26.5 \cdot 10^6$ | $334.94 \cdot 10^6$ | - |
| Total | $63.07 \cdot 10^6$ | $797.15 \cdot 10^6$ | $54.2 \cdot 10^6$ |

2.3.4. Market Concepts

To get the system implemented, a suitable business strategy is needed. This means an investor is required for the construction of the system and a clear way for this investor to recoup his investment and eventually turn a profit. Cost savings due to the system are incurred by airlines. However, due to the plethora of airlines making use of Schiphol, it is not obvious to have one or more of these finance the system at Schiphol. Additionally, the business model of airlines allows them a certain amount of freedom in planning their routes. Big investments in airports by airlines may deteriorate this inherent flexibility. The obvious choice therefore is to have Schiphol Group as the investor. Even though they do not directly participate in the profits made by the system, they can still recoup their investment and share in the profit by charging airlines for the use of the system. This way, both airlines and airports can reap some rewards from the system. Again considering the need for flexibility of airlines, it seems more logical for Schiphol to charge on a pay-per-use basis instead of periodically. This will not pose additional risk for Schiphol since the annual movements are capped by regulation, not demand.

Airlines are not completely free from the necessity to invest. If they want to leverage the system to their advantage, modifications need to be made to their aircraft.

⁶URL: <http://trafficreview2018.schiphol.tangelo.nl/movements#per-type> [Accessed 19 June 2019]

3

Requirements and Functional Analysis

In order to have a clear idea of the context in which the system eventually will be implemented, section 3.1 will elaborate on the boundary conditions imposed on the system. Based on these boundary conditions and on the various parties involved in the project as stated in chapter 2, different stakeholder needs can be defined. Originating from these needs, both stakeholder and system requirements are formulated and stated in section 3.2. In addition, a functional analysis has been performed, resulting in a functional flow diagram and functional breakdown structure as presented in section 3.3. The functional analysis will provide the basis for the concept generation in chapter 4.

3.1. Context of the Design

Based on the guidelines given by the customer, the design context of the system has been determined. In subsection 3.1.1 and subsection 3.1.2, it is elaborated on the airport where the system has to be implemented and the type of aircraft that has to be compatible with the system respectively.

3.1.1. Airport: Schiphol

Schiphol Airport is one of the largest airports in Europe. With 106 movements during arrival peak and 110 movements during departure peak (per hour), it can be considered the third airport in Europe¹. During arrival peak there are 68 arrivals and 38 departures per hour compared to 36 arrivals and 74 departures per hour during departure peak [5]. Per runway this is equal to 14 departures or 12 arrivals per 20 min.

For capacity estimations, the total ground capacity of Schiphol also has to be taken into account. The total amount of parking spots and gates is 267. It has to be noted that around 30 % of these spots are too small for commercial aircraft².

As a reference for the runway length, the Zwanenburgbaan is used. This is the second shortest runway present at Schiphol and has a length of 3,300 metres and width of 45 metres³. The shortest runway is Schiphol Oostbaan (2,014 metres), but this runway is currently mainly used for General Aviation, private jets and helicopters instead of short to medium range flights⁴. Therefore, this runway is not taken into account for implementation of a ground based powered system to launch and recover medium to short range flights.

3.1.2. Aircraft: General Characteristics of the A321NEO

The system has to be compatible with the A321NEO. Hence, all computations made are done based on the characteristics of this aircraft. As the ground based system needs to be available for all aircraft of this type, the highest weight variant of the A321NEO, WF072, is chosen. Also, it is assumed that the airline has installed 3 additional centre tanks. All relevant general characteristics used in this report are summarised in Table 3.1.

¹URL: <https://www.schiphol.nl/nl/route-development/pagina/amsterdam-airport-schiphol-airport-facts/> [Accessed 23 June 2019]

²URL: <https://www.scramble.nl/scramble/uncategorised/schiphol-aircraft-parking-spots> [Accessed on: 21:06-2019]

³URL: <https://www.schiphol.nl/en/route-development/page/amsterdam-airport-schiphol-airport-facts/> [Accessed 15 June 2019]

⁴URL: <https://www.schiphol.nl/en/schiphol-as-a-neighbour/page/flight-paths-and-runway-use/> [Accessed 15 June 2019]

| A321NEO Characteristics | | Unit | Value | Source |
|---------------------------------------|----------------|-------|--------|--------|
| Maximum take-off weight | MTOW | kg | 97,000 | [3] |
| Operational Empty weight | OEW | kg | 52,022 | [3] |
| Maximum landing weight | MLW | kg | 79,200 | [3] |
| Maximum payload weight | MPLW | kg | 23,578 | [3] |
| Max fuel weight | MFW | kg | 25,790 | [3] |
| Zero-lift drag coefficient | Cd_0 | [-] | 0.033 | [41] |
| Surface area wing | S | m^2 | 122.4 | [51] |
| Maximum thrust | F_{TAC} | kN | 286 | [3] |
| Aspect ratio | A | [-] | 9.4 | [51] |
| Oswald factor | e | [-] | 0.9244 | [41] |
| Seats | e | [-] | 240 | [3] |
| Aircraft length | l | m | 43 | [3] |
| Distance in between main landing gear | s | 7.59 | [m] | [3] |
| Mean Aerodynamic Chord | MAC, \bar{c} | m | 4.29 | [3] |

Table 3.1: All relevant general characteristics used in this report of the A321NEO, WF072.

3.1.3. Aircraft: Reference Flight

The average flight time for short haul flights is 1.5 hour [42] with an average occupancy rate of 84,7% [57]. As described in subsection 3.1.2, the number of seats in the A321NEO is 240 [3]. With an average passenger and luggage weight of 77 and 15 kg respectively[65], the total payload for this reference flight is 18702 kg.

3.2. Stakeholder and System Requirements

In subsection 2.2.1, various parties have been defined as stakeholder in the project. Based on their needs, several stakeholder requirements are formulated. The various needs of the most important stakeholders have been summarised below [10].

- **Schiphol Airport:** one of the most important needs of Schiphol Airport is the fact that the system should be able to provide for at least the same airport capacity as the conventional take-off and landing systems. In addition, the system should be profitable over its entire lifetime and should comply with all regulations that apply for these procedures at Schiphol and large commercial aircraft. Finally, the system should be as sustainable as possible to minimise environmental impact.
- **Airline company (Airfrance - KLM):** when using a ground based powered system for launching and recovering commercial aircraft, operating airliners will want the aircraft to remain easily maintainable. In addition, the system should provide for similar or even reduced operational costs, allowing for competitive ticket prices. Besides, downtime of the system should be minimised. Finally, the system should be compatible with B737/A320-like aircraft.
- **Passengers:** one of the most important needs of passengers is that the flight experience remains comfortable. This includes minimisation of the time required for take-off/landing and taxiing. Besides, perturbations during the procedures should be minimised, as well as ticket prices. Finally, safety of passengers should be ensured.
- **Aircraft manufacturer (Airbus):** with regards to the aircraft manufacturer, the most important need concerns the feasibility of production of the system, including any required aircraft modifications. In addition, enough resources should be available to provide for production of the system.
- **Project team:** for the project team, the most important need is that the project is feasible to execute with 10 people within 10 weeks.

Based on the stakeholder needs, stakeholder requirements are formulated and listed in Table 3.2. These requirements result in more technical requirements that concern the system as a whole (Table 3.3). Furthermore, several requirements are based on the functional breakdown structure as well. These are listed in Table 3.4.

Note that the "system" refers to the complete design with the updated aircraft, the ground vehicle, the connection mechanism between the aircraft and the ground vehicle, the power supply chain and the control strategy for take-off and landing.

Table 3.2: Requirements of stakeholder Schiphol airport, including a unique identifier.

| Identifier | Requirement |
|-------------------------|--|
| Schiphol Airport | |
| NCL-Shl01 | The system shall provide for at least the same capacity as when using conventional take-off and landing systems at Schiphol airport. |
| NCL-Shl06 | The construction of the system shall not disturb any present aviation traffic. |
| NCL-Shl07 | The power supply of the system shall not disturb the present electrical grid of Schiphol. |
| NCL-Shl09 | The system shall provide for at least the same rate of successful take-off and landings as conventional take-off and landing systems do. |
| NCL-Shl10 | The ground based system shall have a lifetime of at least 35 years. |
| NCL-Shl14 | The ground based system shall be implemented on existing runways. |
| NCL-Shl15 | The ground based landing and take-off system shall not interfere with current ground operations. |
| NCL-Shl16 | The ground based system shall not influence the number of landings and take-offs on Schiphol with a conventional landing gear. |
| NCL-Shl17 | The system shall be available for use at any time. |
| NCL-Shl18 | The system shall provide for a reduction of noise pollution of 7 ± 3 SEL dBA in comparison to the current production of noise during the take-off and landing procedure at Schiphol airport. |
| NCL-Shl19 | The one time investment costs for the system shall not exceed € 0.75 billion. |
| NCL-Shl20 | The implementation costs of the system into the work environment at Schiphol airport shall not exceed €50 million. |
| NCL-Shl21 | The annual fixed costs shall not exceed € 100 million. |
| Airline company | |
| NCL-Alc01 | The modified aircraft shall be used for short to medium range flights. |
| NCL-Alc03 | The costs of the modified aircraft shall not be more than 10% of current conventional aircraft. |
| NCL-Alc04 | The time between the airlines order and the fully operational aircraft delivery shall be no more than 1.5 years. |
| NCL-Alc06 | The modified aircraft shall not be reduced in its cabin capacity. |
| NCL-Alc09u1 | The modification of the aircraft and the different take-off and landing procedures shall decrease the absolute fuel consumption of the entire flight mission with at least 5% for all flights shorter than 1,5 hour. |
| NCL-Alc09u2 | The modification of the aircraft and the different take-off and landing procedures shall decrease the total fuel consumption of the entire flight mission per passenger per kilometer with at least 5% for a 1,5 hour flight with 84,7% occupancy. |
| NCL-Alc10 | The modified aircraft shall not increase the required maintenance time in comparison with the required maintenance time for aircraft's with conventional take-off and landing systems. |
| NCL-Alc11 | The additional training hours for a pilot with a A321NEO licence shall be to the utmost 6 months. |
| Passengers | |
| NCL-Pax01 | The system shall provide for a comfortable flight during all phases. |
| NCL-Pax02 | The ticket price of flights from the ground based powered system shall not be more than 120% of regular tickets. |
| Airbus | |
| NCL-Amf02 | The modified aircraft shall be able to be produced in already existing factories. |
| NCL-Amf03 | The aircraft manufacturer shall have enough resources to purchase the necessary equipment. |
| Project team | |
| NCL-Pjt01 | The final design of the system shall be completed within 10 weeks by 10 third-year BSc. students. |

Table 3.3: System requirements derived from the stakeholders requirements.

| Identifier | Requirements |
|------------------------|--|
| Schiphol | |
| NCL-Shl01-Sys03 | The system shall provide for a capacity of 756 arrivals per 24h per runway. |
| NCL-Shl01-Sys04 | The system shall provide for a capacity of 830 departures per 24h per runway. |
| NCL-Shl07-Sys01 | The system at Schiphol airport shall demand a maximum amount of electrical energy of 250 million kWh per year. |
| NCL-Shl09-Sys01 | The system shall be able to abort take-off before the decision speed has been reached. |
| NCL-Shl10-Sys01 | Non-replaceable materials used within the system shall not fail due to fatigue loadings within 35 years. |
| NCL-Shl14-Sys01 | The runway length shall not increase compared to existing runways. |
| NCL-Shl16-Sys01 | The runway shall always be available for aircraft with conventional landing gear at Schiphol airport. |
| NCL-Shl16-Sys02 | The system shall not require additional airspace that limits the use of space by other airspace users. |
| NCL-Shl17-Sys02 | The system shall be able to use back-up generators in case of a power failure in the Schiphol area. |
| NCL-Shl17-Sys03 | The system shall be able to withstand and operate normally during storms of type 9 on the scale of Beaufort. |
| NCL-Shl20-Sys01 | The total costs to incorporate the ground based system, the power supply chain and the control strategy system into the work environment at Schiphol airport shall not exceed € 650 million. |
| NCL-Shl21-Sys01 | The costs to maintain the ground based system, the power supply chain and the control strategy system at Schiphol airport shall not exceed €25 million per year. |
| Passengers | |
| NCL-Pax01-Sys01 | The landing impact shall not generate higher shocks then conventional landing. |
| NCL-Pax01-Sys02 | Seat configuration shall not be influenced by the system. |
| Airline company | |
| NCL-Alc01-Sys03 | The design of the aircraft shall be based on the A321NEO. |
| NCL-Alc03-Sys01 | The design costs shall not increase the purchase price of an aircraft by more than 10%. |
| NCL-Alc04-Sys01 | The production lead time shall not be more than 1.5 years. |
| NCL-Alc04-Sys03 | The implementation time of the system at the airport shall not exceed 2 years. |
| NCL-Alc06-Sys01 | The dimensions of the fuselage cross section of the modified aircraft shall not be changed. |
| NCL-Alc06-Sys02 | The usable cabin volume for payload of the modified aircraft shall not be adjusted. |
| NCL-Alc10-Sys01 | All the modified parts in the design shall be accessible in at least the same amount of time as before. |
| NCL-Alc10-Sys02 | All the used materials for the modifications shall have at least the same lifetime as the materials used before. |

Table 3.4: System requirements linked to the functional analysis.

| Identifier | Requirement |
|------------------------------|---|
| Ground take-off | |
| NCL-Fun-TO4 | The ground take-off system shall be able to connect to the aircraft. |
| NCL-Fun-TO8 | The ground take-off system shall disconnect from the aircraft. |
| NCL-Fun-TO9 | The ground take-off system shall be ready for next take-off in 80 s. |
| NCL-Fun-TO11 | The ground take-off system shall accelerate the aircraft no more than 1g in vertical direction. |
| NCL-Fun-TO12 | The ground take-off system shall be operational in equally as bad weather conditions as current take-off systems. |
| NCL-Fun-TO13 | The ground take-off system shall accelerate and decelerate the aircraft in less than 3300 m in case of aborted take-off. |
| NCL-Fun-TO14 | The ground system shall be able to move the aircraft to any desired location on the airport. |
| NCL-Fun-TO15 | The ground take-off system shall be able to abort take-off before the aircraft reaches the decision speed. |
| NCL-Fun-TO16 | The ground take-off system shall accelerate the aircraft no more than 1g in horizontal direction. |
| Ground landing system | |
| NCL-Fun-LA2 | The ground landing system shall decelerate the aircraft no more than 0.4g. |
| NCL-Fun-LA4 | The ground landing system shall decelerate the aircraft in less than 3300 m. |
| NCL-Fun-LA6 | The ground landing system shall be able to be re-used within 100 s after successful landing. |
| NCL-Fun-LA7 | The ground landing system shall be able to connect to the aircraft. |
| NCL-Fun-LA9 | The ground landing system shall be able to synchronize with the aircraft. |
| NCL-Fun-LA10 | The ground landing system shall be operational in equally as bad weather conditions as current take-off systems. |
| Aircraft system | |
| NCL-Fun-AC1 | The aircraft shall be able to change into climb configuration. |
| NCL-Fun-AC6 | The aircraft shall be able to connect to the gate. |
| NCL-Fun-AC8 | The aircraft shall comply with the operational means of compliance as specified in CS-25 after the design update. |
| NCL-Fun-AC9 | The aircraft structure shall be able to withstand the introduced forces introduced by the ground based powered take-off and landing system. |
| NCL-Fun-AC10 | The aircraft shall be able to provide a steady gradient of climb in landing configuration of at least 3.2% with engines at the maximum thrust. |
| NCL-Fun-AC12 | The lifetime of the aircraft shall be at least 20 years. |
| NCL-Fun-AC13 | The aircraft shall be able to change into configuration suitable for attaching to the ground landing system. |
| NCL-Fun-AC14 | In case of an engine failure during take-off, the steady gradient of climb may not be less than 1.2% at final take-off speed with the critical engine inoperative and remaining engine at available maximum thrust. |
| NCL-Fun-AC15 | The aircraft shall be able to perform an emergency landing on an airport without ground based landing system without fatalities. |

3.2.1. Driving Requirements

The driving requirements are important requirements as they drive the design during the entire process. These requirements are presented in Table 3.5.

Table 3.5: Driving requirements.

| Identifier | Requirement |
|-------------|--|
| NCL-Shl01 | The system shall provide for at least the same capacity as when using conventional take-off and landing systems at Schiphol airport. |
| NCL-Alc09u1 | The modification of the aircraft and the different take-off and landing procedures shall decrease the absolute fuel consumption with at least 5% for all flights shorter than 1.5 hour. |
| NCL-Shl18 | The system shall provide for a reduction of noise pollution of 7 ± 3 SEL dBA in comparison to the current production of noise during the take-off and landing procedure at Schiphol airport. |

3.2.2. Updates of Requirements

When taking a look at the identifiers of all requirements, it can be noted that certain requirements are deleted. The different reasons for deleting or replacing have been generally summarised in Table 3.6. In Table 3.7, the changelog for the stakeholder requirements has been visualised, where the draft of the baseline report is being used as a reference. With regards to the system requirements, a changelog has not been included in this report, since most of the changes for the system requirements result from the changes in stakeholder requirements.

Table 3.6: Reasoning for the changes in the requirements throughout the course of the project.

| Number | Reasoning |
|--------|--|
| 1 | Change of values: due to new insights in the technical performance of the design, numerical values on constraints (cost e.g.) have changed, resulting in a new requirement |
| 2 | Not relevant to determine: due to gained insight in the scope of the project, it has been determined that some requirements impose restrictions that are beyond the scope of the project |
| 3 | Rephrasing: changes on boundary conditions (type of reference aircraft e.g.) in the design lead to recasting of the requirement |
| 4 | Similarity amongst requirements: after evaluation of the complete set of requirements, similarities were found between certain requirements, leading to omittance (and rephrasing, number 3) |
| 5 | Not measurable within scope of the project: due to insights gained in literature study, it has been determined that certain requirements require a type of analysis beyond the scope of the project |
| 6 | Completion: in the process, it has been noted that certain requirements were missing, resulting in a new requirement |

Table 3.7: Changelog of stakeholder requirements throughout the course of the project

| Original identifier | Original requirement | Time of replacement/omittance | New identifier | Reasoning |
|---------------------|---|-------------------------------|----------------|-----------|
| NCL-Shl02 | The one time investment costs for the system shall not exceed €650 million. | Final report | NCL-Shl19 | 1 |
| NCL-Shl03 | The implementation costs of the system into the work environment at Schiphol airport shall not exceed €50 million. | Final report | NCL-Shl20 | 1 |
| NCL-Shl04 | The annual fixed costs shall not exceed €25 million. | Final report | NCL-Shl21 | 1 |
| NCL-Shl05 | The time between the start of the construction and the fully operational system at Schiphol airport shall not exceed <tb>years. | Final baseline report | n.a. | 2 |

| | | | | |
|------------------|--|-----------------------|--|------|
| NCL-Shl08 | The system shall be available for use at <tbid>% of the time. | Final baseline report | NCL-Shl17 | 3 |
| NCL-Shl11 | The system shall provide for a reduction of noise pollution of 20% in comparison to the current production of noise during the take-off and landing procedure at Schiphol airport. | Final baseline report | NCL-Shl18 | 1, 3 |
| NCL-Shl12 | The system shall not influence the number of landings and take-offs on Schiphol with a conventional landing gear. | Final baseline report | n.a. | 4 |
| NCL-Shl13 | The system shall not be endangered by external flying objects around Schiphol. | Final baseline report | n.a. | 2,5 |
| n.a. | n.a. | Final baseline report | NCL-Shl16 | 6 |
| NCL-Alc02 | The design of the aircraft update shall not increase the required maintenance time in comparison with the required maintenance time for aircraft's with conventional take-off and landing systems. | Final baseline report | NCL-Alc10 | 3 |
| NCL-Alc05 | The design of the aircraft update shall decrease the fuel consumption of the aircraft with at least 5% during flight. | Final baseline report | NCL-Alc09u1 NCL-Alc09u2 | 3 |
| NCL-Alc07 | The total flight time of the modified aircraft shall not be increased by <tbid>%. | Final baseline report | n.a. | 2 |
| NCL-Alc08 | The additional training hours for a pilot with a B737-800 licence shall be to the utmost <tbid>hours. | Final baseline report | NCL-Alc11 | 3 |
| NCL-Amf01 | The update of the aircraft design and the ground based system shall be able to be produced by Boeing using their current resources. | Final baseline report | NCL-Amf02/ NCL-Amf03 | 3 |

3.3. Functional Analysis

Functional analysis helps to identify the main functions a system has to fulfil. As part of the functional analysis for the posed problem both a functional flow diagram in subsection 3.3.1 and a functional breakdown structure in subsection 3.3.2 were made. The system is considered to include the aircraft, the take-off system, and the landing system. The functional analysis comes after the requirements as the system has to fulfil certain functions in order to comply with the requirements set. The functional analysis is used to generate concepts that fulfil the functions that flow from the requirements.

3.3.1. Functional Flow Diagram

The Functional Flow Diagram gives an overview of the functions performed by the system during the mission. The functions of the mission can be broken down into deeper levels to give a more precise description of the function. The blocks of the first level of the functional flow diagram have a yellow colour, the second level has red contour and the third level has a blue contour. Furthermore each step and sub-steps have their own identifying number. In the functional analysis the following speeds are referred to:

- Minimum unstick speed: Speed at which you could take off by maximum rotating the aircraft
- Decision speed: cut-off velocity below which take-off is aborted if an incident occurs
- Take-off speed: velocity at which the aircraft is detached from the ground take-off system

The top-level functions of the system are given in Figure 3.1. The system functions needed to fulfil the mission successfully are divided in 8 main parts including the procedures for non-standard conditions. Every aspect of the functional flow has its own identifier. The OR function is implemented to show that in every part of the process the system can go into an emergency mode and deal with non-standard conditions like aborted take-offs or emergency landings.

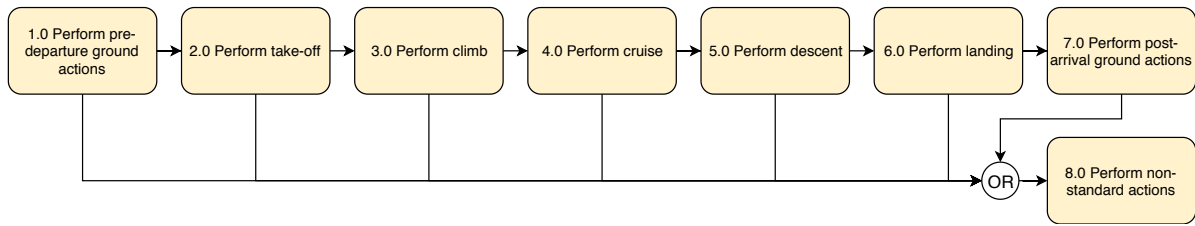


Figure 3.1: First level Functional Flow Diagram.

The functional flow diagram can be written in more detail. The most important functions are elaborated and specified in more detail until a maximum of the third level. In Figure 3.2 the functions performed as part of the pre-departure ground operations are described. Figure 3.2 links the pre-departure ground operations to the take-off. This pre-departure ground operation function is related to all functions that should be fulfilled before the aircraft arrives at the take-off ground system.

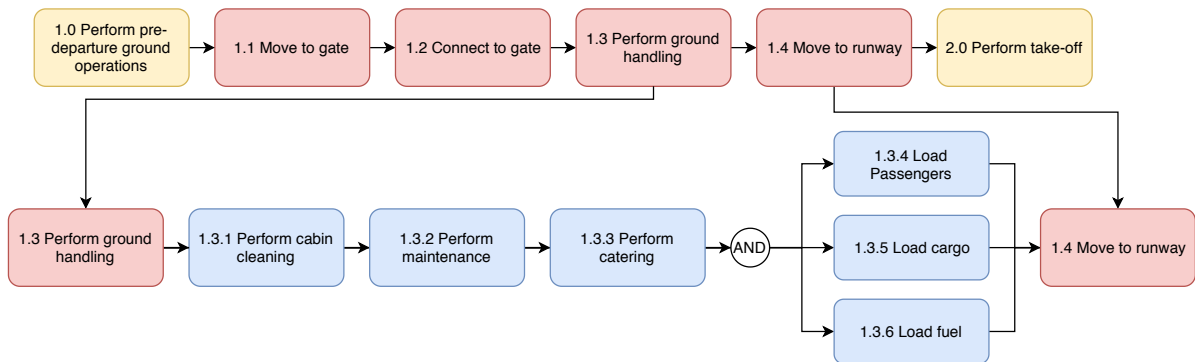


Figure 3.2: Second and third level of Functional Flow Diagram for function 1.

In Figure 3.3 the functions performed as part of the take-off are described. The take-off phase consists mainly of a connection between the aircraft system and the take-off system, an acceleration, and a disconnection between the two systems. After the aircraft has been disconnected from the take-off system, the take-off system is prepared for the next operation. Figure 3.3 links the take-off to the climb.

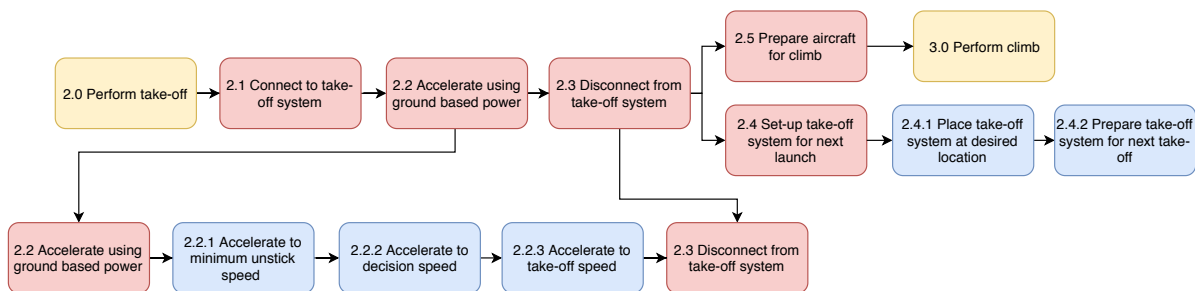


Figure 3.3: Second and third level of Functional Flow Diagram for function 2.

In Figure 3.4 the functions performed as part of the climb are described. Figure 3.4 links the climb phase to the cruise phase. The climb procedure (and flight profile) is chosen such that noise is minimised.

In Figure 3.5 the functions performed during cruise are detailed. Figure 3.5 links the cruise to the descent. The cruise conditions are chosen such that they are most economically attractive.

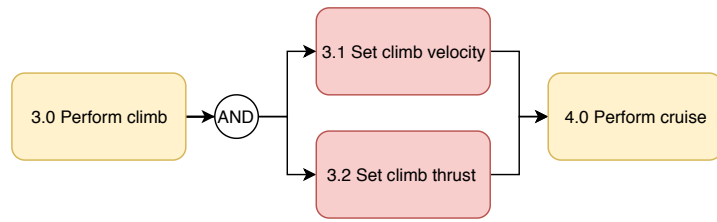


Figure 3.4: Second level of Functional Flow Diagram for function 3.

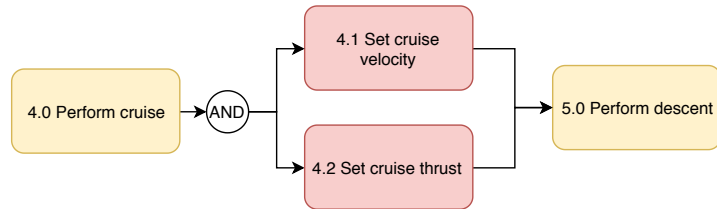


Figure 3.5: Second level of Functional Flow Diagram for function 4.

In Figure 3.6 the functions performed during descent are detailed. Figure 3.6 links the descent to the landing. The landing procedure is chosen such that noise is minimised.

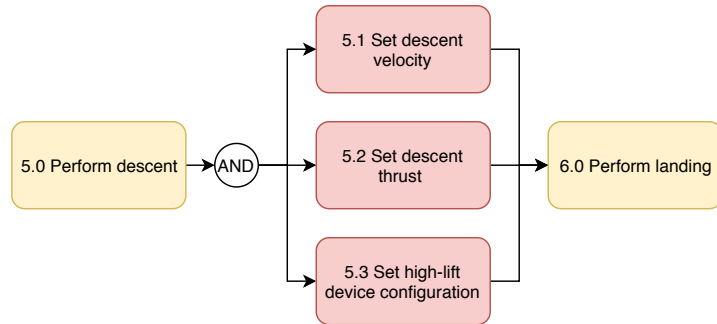


Figure 3.6: Second level of Functional Flow Diagram for function 5.

In Figure 3.7 the functions performed during landing are explained. Figure 3.7 links the landing to the post-arrival ground operations. The landing, analogous to the take-off, consists of a connection between the aircraft system and the landing system, a deceleration, and a disconnection of the two systems. Nonetheless, for the landing the ground system also has to synchronise with the aircraft and provide damping like a conventional landing gear. The landing function also includes the function where the ground system has to prepare for its next use.

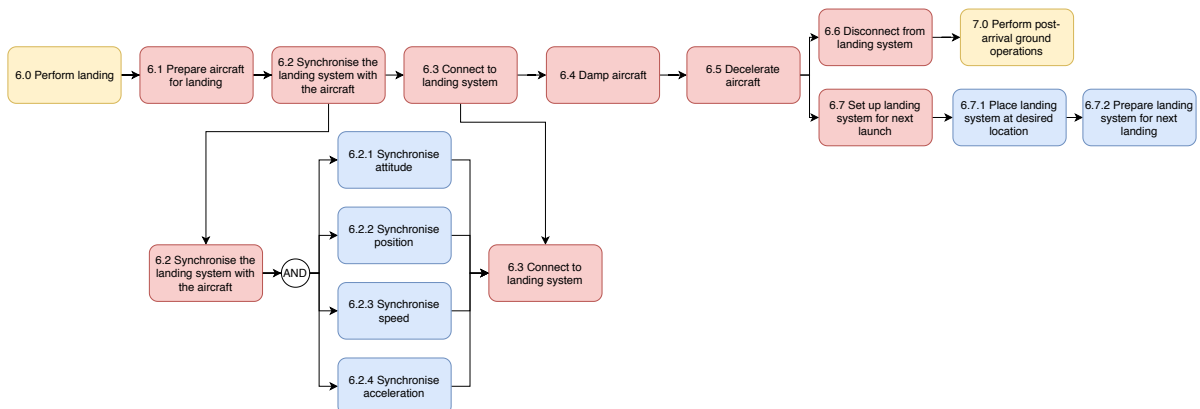


Figure 3.7: Second and third of Functional Flow Diagram for function 6.

In Figure 3.8 the functions performed during post-arrival ground operations are described. After these functions have been completed the aircraft can start the cycle again at function 1.0 as in Figure 3.1.

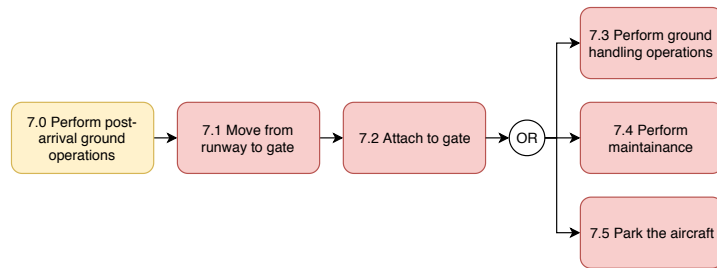


Figure 3.8: Second level of Functional Flow Diagram for function 7.

Finally, in Figure 3.9 the actions performed in case of non-standard conditions are explained. Figure 3.9 represents the function that shall be executed in case of non-standard conditions only. The tree can be entered from any function that comes before it as shown in Figure 3.2. One should also be aware of the fact that some non-standard conditions might take place at the same time. This is also accounted for in the system requirements and the risk analysis in chapter 10.

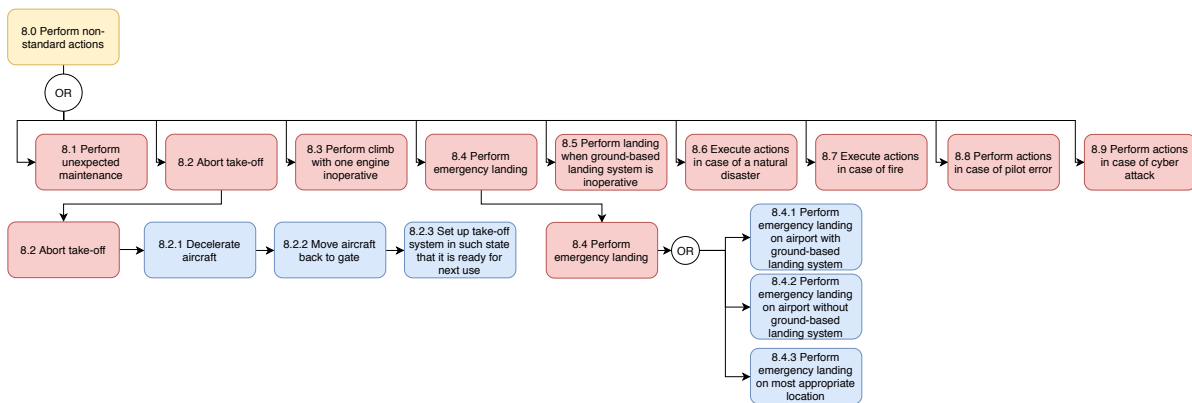


Figure 3.9: Second level of Functional Flow Diagram for function 8.

3.3.2. Functional Breakdown Structure

The Functional Breakdown Structure represents the information in the functional flow diagram in a different way. The functional breakdown structure can provide a more structured way to look at the functions in depth. It is an AND tree and the identifiers of the functions match the ones used in subsection 3.3.1. The functional breakdown structure shows in depth what separate functions are needed to be executed in order to ensure successful functionality of the complete system. The functions are specified to a maximum of five levels of depth. Do note that the Functional Breakdown does not say anything about the sequence the tasks are executed. The Functional Breakdown is shown in Figure 3.10.

The top level functions correspond to the functions in Figure 3.2. Per first level function the second level functions needed to complete the corresponding first level function are listed. The fourth and fifth level functions added are found in 1.3.6.x where the fuel loading is divided in more sub-functions. Furthermore, functions 2.4.1.x and 6.5.1.x show in a more detailed way how the ground system locations are placed at specific locations. Functions 6.1.1.x, 6.1.2.x, 6.1.3.x, and 6.1.4.x show how the synchronisation of the aircraft system and the landing system can be divided in more detailed sub-functions.

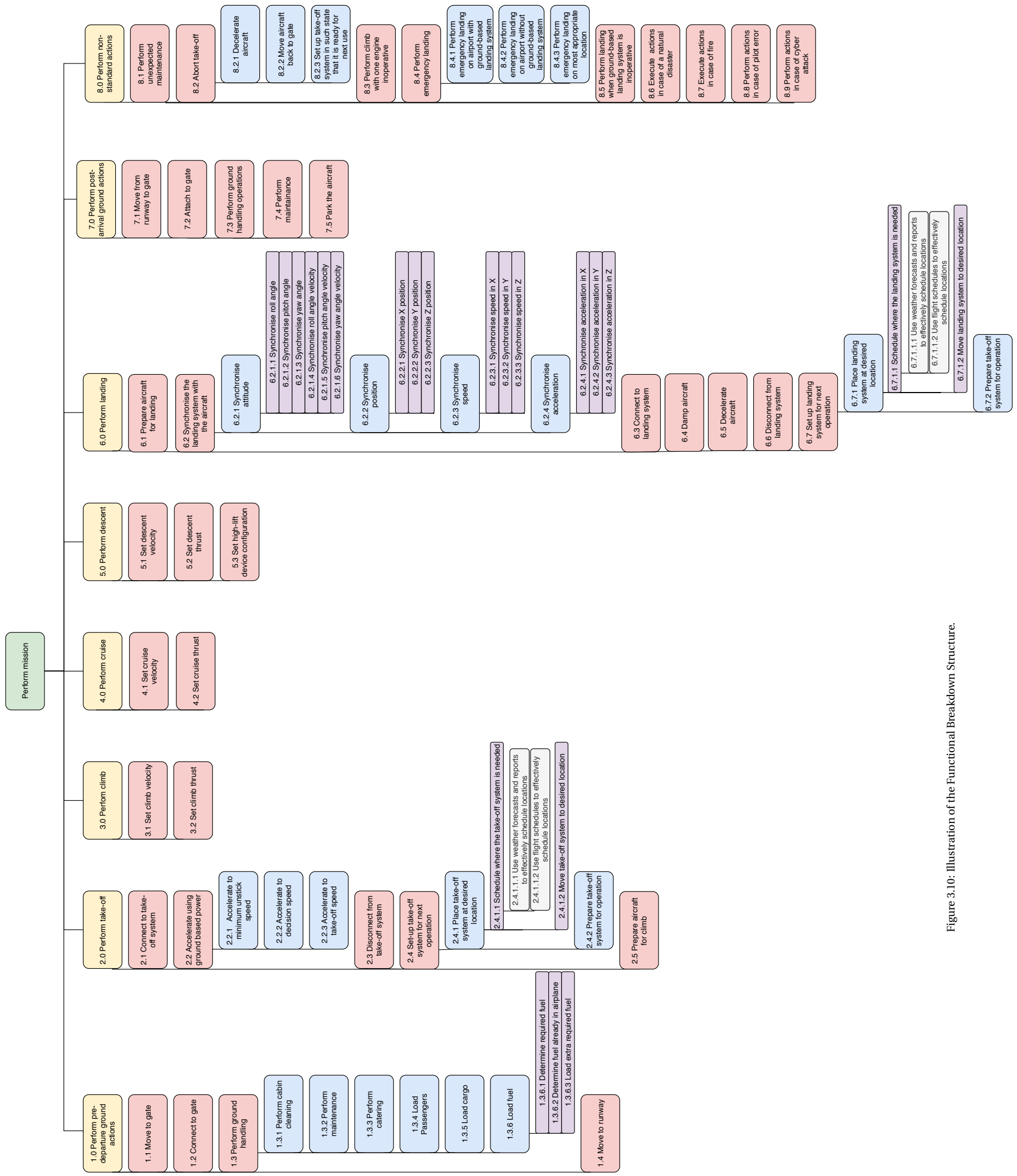


Figure 3.10: Illustration of the Functional Breakdown Structure.

4

Concept Generation

Based on the established requirements and functions as stated in chapter 3, four design concepts are generated and analysed in order to make sure that they fulfil the set of requirements. These concepts are presented in section 4.1, which is based on the analysis as reported in the midterm report [23]. In order to determine the "best" concept, a trade-off has been performed, which is reported on in section 4.2. Finally, the concept that has been decided on to proceed with during the detailed design phase is presented in section 4.3.

4.1. Concepts Overview

Based on Design Option Trees (DOTs) as presented in the midterm report [23], a complete set of design options has been generated for different aspects of the system to be designed for. After rejecting non-concepts and non-feasible options, four different concepts are generated based on the remaining design options, which are briefly explained below.

4.1.1. Concept 1: Magnetic Runway

The first concept consists of a platform on a magnetic track which is extended over the entire airport. This is shown in Figure 4.1. The platform consists of a hexapod configuration of hydraulic pistons which are used to support the aircraft and to ease the line up.

The aircraft will connect to the platform using a three point mechanical hook system with two hooks at each point. The hooks themselves will be located on the platform while the rings will be situated on the aircraft at the location where currently the landing gear is attached to the aircraft. The aircraft will land on and take-off from the platform and stays on it during the entire ground movement phase.

4.1.2. Concept 2: Carry Cart

Inspired by the robots used by Amazon, a carry cart is designed and forms the second concept as can be seen in Figure 4.2. It consist of a cart on wheels carrying a platform where the aircraft will land on and take-off from. While at the gate, the cart can put the platform down and go to a charging station.

A connection mechanism combining suction pads and a harpoon system is used to connect the aircraft to the platform. The harpoons will be located at three points on the aircraft and connect to a grid located on the platform. Also, the platform uses hydraulic pistons to synchronise with the aircraft pitch and a rotation system to compensate for the yaw.

4.1.3. Concept 3: Rails

For the third concept, at each side of the runway rails are located (underground) where two metal rods are placed on and slide along the rails. The metal rods are pulled forward using a dynamo cable, accelerated by a winch system.

A circular platform is connected to the rods with wheels and can slide along them in the lateral direction. This is presented in Figure 4.3. A rectangular frame is placed on top of the circular platform using hydraulic pistons to line up with the aircraft in pitch, yaw, and roll angle. The aircraft connects to the frame with a pin-through-hole connection mechanism. This connection requires a high accuracy, hence a converging support structure is placed in order to guide and help align the holes.

Concerning ground movement, deployable taxi wheels on the platform ensure that the system can slide off the rods. As a result, the rods can be used for the next take-off or landing while the aircraft is moved to the gate simultaneously.

4.1.4. Concept 4: Drone

The last concept consist of a flying wing driven by ten propellers which approaches an aircraft in-air, connects to it and finally lands with it as can be seen in Figure 4.4. Hence, the drone works as a powered landing gear that will also provide power during take-off and climb with the aircraft until FL100 is reached. In addition, the drone remains attached to the aircraft during all phases on the ground.

A railway coupling system used on trains nowadays is utilised to connect the drone to the aircraft. A first connection will be made in-air to make sure the aircraft is still stable. Then, two other points will connect and an airbag system will be deployed to prevent airflow between the drone and the aircraft.

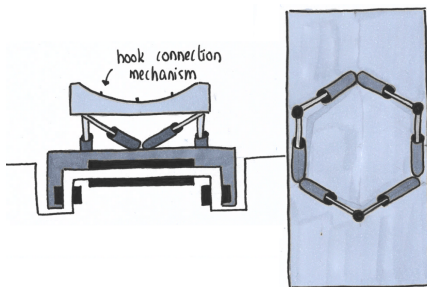


Figure 4.1: Drawing of the magnetic runway, shows hexagon hydraulic pistons and the rails.

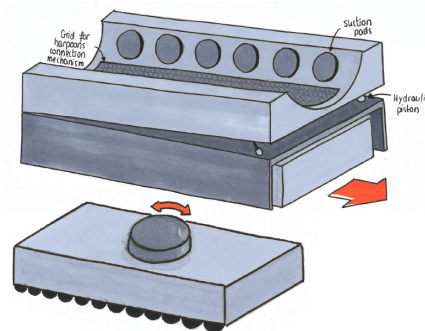


Figure 4.2: Drawing of the carry cart with the suction pads platform and the grid.

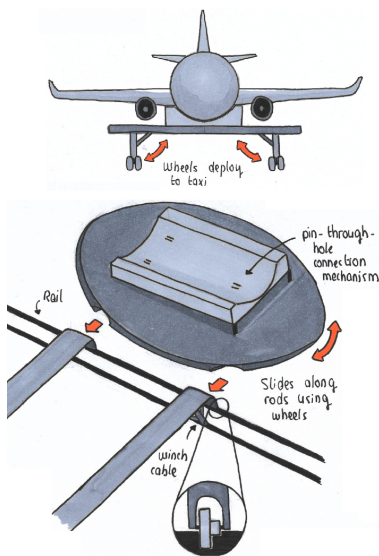


Figure 4.3: Drawing of the rail system, the ground vehicle and the platform attaching to the runway.

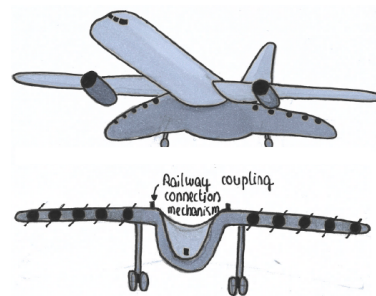


Figure 4.4: Drawing of the drone, connected to the aircraft and separately.

4.2. Trade-Off Summary

In order to be able to objectively compare the concepts with each other, trade-off criteria has been set up to evaluate the designs, which are explained in subsection 4.2.1. In addition, each criterion is given a certain weight factor, which will be elaborated on in subsection 4.2.2. Finally, the trade summary table is presented in subsection 4.2.3, which shows how each concept scores on the criteria.

4.2.1. Trade Criteria

Below, the different trade-off criteria are briefly explained. Although sustainability is not a criterion on itself, this does not mean that it has not been taken into account when performing the trade-off. On the contrary, the scoring of the concepts has been based on how the design performs in terms of environmental, economical and social sustainability for each criteria. As a result, sustainability is fully integrated in the trading process.

- **Noise reduction:** the first criterion is related to one of the driving requirements of the design: reducing the sound exposure level of a take-off and landing. Since sound exposure level takes both the intensity and the duration of the sound into account, it is assumed that noise will be reduced when the take-off or landing procedure is shortened, while not increasing the current maximum peak noise. Therefore, the ability of each concept to reduce the time for the procedures has been quantitatively reviewed. Reducing noise has a positive impact on the environment and human health surrounding the airport. Concerning economical aspects, a reduction of noise results in a possible growth of the number of allowed flight movements on airports, thus having a positive effect on the economy.
- **Aircraft modification:** the second criterion concerns the modifications that will have to be made on the aircraft as the landing gear is removed and a connection mechanism is added, resulting in a different weight of the aircraft for each concept. This is of importance to the trade-off, since the weight reduction of each concept is directly related to the possible fuel reduction, which is another driving requirement of the design. Hence, this criteria comprises a qualitative analysis regarding the modifications and a quantitative analysis for the weight reduction that follows from it.
- **Take-off/landing energy and power:** the energy efficiency was calculated for both take-off (acceleration + climb) and landing (descent + deceleration) phases. For take-off, the total energy efficiency of the system and the proportion of the energy provided by the ground based system in comparison to the total amount of energy consumed was found [23]. Both should be as high as possible to maximise the share of sustainable energy used. For landing, it was analysed if the energy could be recovered using a Kinetic Energy Recovery System (KERS).
- **Ground movement power required:** the next criterion includes a quantitative analysis of the power consumed during the movements on the ground. Power was analysed here instead of energy as it is independent of time. Furthermore, decreasing the power consumption on the ground has a positive effect on the environment.
- **Airport disruptions:** implementing a ground based powered vehicle requires some changes to the airport infrastructures. Thus, this criterion is analysed qualitatively taking into account the amount of modifications needed, if these modifications have an impact on conventional aircraft, if the management of the airport has to adapt to these changes and if this changes the capacity of the airport.
- **Cost:** the cost criterion takes into account the implementation cost, development cost, maintenance cost and energy cost per cycle. Also, the schedule and cost risks were evaluated and based on the Technology Readiness Level (TRL) of each concepts. The final design should be economically feasible and sustainable.
- **Safety:** the last criterion is evaluated based on the safety of the passengers in general and the risks that are identified for each concepts. These risks are related to the performance of the vehicle in non-nominal weather conditions and the likelihood of not performing the required functions defined in the functional flow diagrams in section 3.3.

4.2.2. Criteria Weight Factor

The weight factors are determined using an Analytic Hierarchical Process (AHP). The pairwise comparison relative importance values were chosen according to the fundamental scale of absolute numbers introduced by Saaty [68] [23]. The pairwise comparison table of the criteria and their final weights is presented in Table 4.1. The scores were given keeping in mind the sustainable approach and the main requirements stated in section 3.2.

The final weights that follow from the AHP make perfect sense. The safety criterion has the highest weight of all, thus implying that for example, cheap options are not preferred over unsafe options and a high risk system is unacceptable. If the system is unsafe, it will not have a chance of surviving the trade-off using the

current weight factors. The noise reduction criterion has the second highest weight of all criteria. This makes sense as noise reduction has been identified as a key requirement set by the stakeholders. The third most important criterion regards the aircraft modification. The aircraft modifications criterion is closely related to weight and fuel savings of the aircraft. This makes sense as it is another key requirement set by the stakeholders. The fourth and fifth most important criteria, the airport disruption criterion and the cost criterion, flow from the economic feasibility requirement and the requirement of a practical system that will not impact regular air traffic to a large extent. The least important, but still relevant criteria regard the take-off and landing energy efficiency and the ground movement energy consumption at the sixth and seventh place. These criteria together mainly come from sustainability requirements which shall not be overlooked.

Table 4.1: Pairwise comparison matrix with relative scores of importance and final weights of the trade criteria.

| | Noise reduction | Aircraft modifications | Take-off and landing energy | Ground movement power required | Airport disruptions | Cost | Safety |
|--------------------------------|-----------------|------------------------|-----------------------------|--------------------------------|---------------------|-------------|-------------|
| Noise reduction | 1 | 2 | 5 | 6 | 3 | 4 | 1/3 |
| Aircraft modifications | 1/2 | 1 | 4 | 5 | 2 | 3 | 1/4 |
| Take-off & landing energy | 1/5 | 1/4 | 1 | 2 | 1/3 | 1 | 1/6 |
| Ground movement power required | 1/6 | 1/5 | 1/2 | 1 | 1/5 | 1 | 1/7 |
| Airport disruptions | 1/3 | 1/2 | 3 | 5 | 1 | 1 | 1/4 |
| Cost | 1/4 | 1/3 | 1 | 1 | 1 | 1 | 1/6 |
| Safety | 3 | 4 | 6 | 7 | 4 | 6 | 1 |
| Weight | 0.22 | 0.15 | 0.05 | 0.03 | 0.1 | 0.06 | 0.39 |

4.2.3. Trade Summary Table

After analysing each criteria, scores are given to each concept and summarised in a trade-off table. In order to be able to compare the outcome of different criteria, all the scores are normalised by percentage of total of that specific criteria. They were then multiplied by the weight of the criteria and summed up to obtain the final scores presented in Table 4.2. The colours green, blue, yellow and red represent how well the concept performs: "excellent performance", "good performance", "satisfactory" and "unacceptable", respectively.

Table 4.2: Trade summary table for the final system.

| Criterion | Concept | | | |
|---------------------------------------|-----------------|---------------|---------------|---------------|
| | Magnetic runway | Carry cart | Rails | Drone |
| Noise reduction (0.22) | 0.47 (yellow) | 0.39 (yellow) | 0.47 (yellow) | 0.70 (green) |
| Aircraft modifications (0.15) | 0.5 (blue) | 0.4 (yellow) | 0.5 (blue) | 0.6 (blue) |
| Take-off and landing energy (0.05) | 0.8 (green) | 0.6 (blue) | 0.75 (green) | 0.3 (yellow) |
| Ground movement power required (0.03) | 0.32 (blue) | 0.22 (yellow) | 0.26 (yellow) | 0.20 (yellow) |
| Airport disruptions (0.1) | 0.3 (blue) | 0.5 (green) | 0.4 (blue) | 0.2 (yellow) |
| Cost (0.06) | 0.18 (yellow) | 0.34 (blue) | 0.31 (blue) | 0.17 (yellow) |
| Safety (0.39) | 0.8 (green) | 0.6 (blue) | 0.7 (green) | 0.1 (red) |
| Final score | 0.288 | 0.254 | 0.282 | 0.176 |

The final scores are presented in the last row of Table 4.2. From this, it could be concluded that the magnetic runway concept, with a score of 0.288 won closely followed by the rails concepts having a score of 0.282.

4.3. Winning Concept: REMALS

The final proposed conceptual design is based on the magnetic runway and the rails concept as there was more confidence that the combination of both would have more chance in complying with the requirements. This winning concept, called REMALS, is sketched in Figure 4.5. The concept is mainly based on the rails system with a different connection mechanism (harpoon + suction) and a different power source: Electro-magnetic Aircraft Launch System (EMALS) instead of the winch. The rails concept was chosen to be the base of the final design as extensive researches on a magnetic levitation system has already been done in the past. REMALS provides for a more innovative concept for solving the problem of ground-based powered take-off and landing.

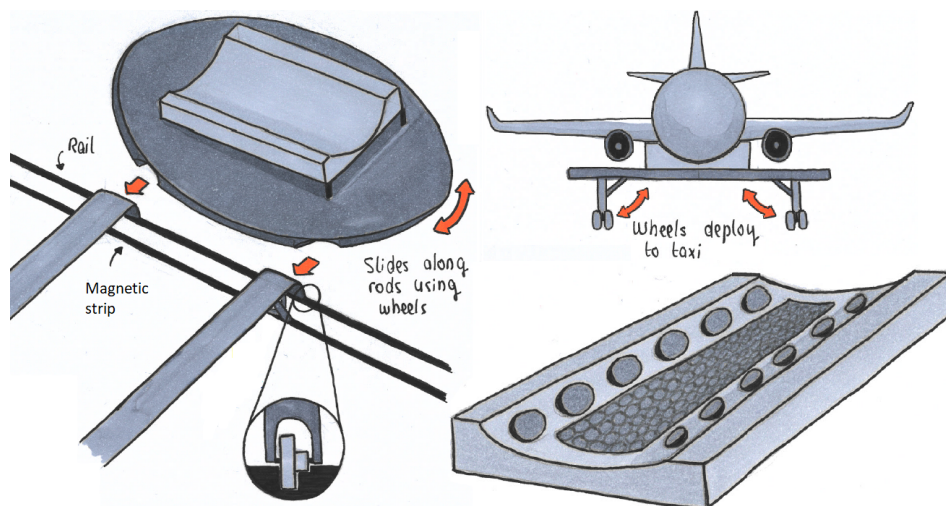


Figure 4.5: Drawing of the final design concept.

5

Design Process Set-Up

Now that the final concept has been chosen, the detailed design phase can begin. In order to have a clear idea of the build up of the system, the components of the design are explained and described in section 5.1. Next, the relation between all the different components and the engineering divisions is visualised in a N2-chart in section 5.2. Finally, a budget breakdown for the whole system is elaborated on in section 5.3.

5.1. Configuration, Component and System Identification

Before the design could be further developed the team identified the systems and sub-components of the systems that had to be considered. The aircraft design and approach is described in subsection 5.1.1. The ground system components are described in subsection 5.1.2. The systems and sub-components are closely linked to the functions presented in chapter 3.

5.1.1. Aircraft Design

The aircraft is composed of many different parts and components that affect each other. If one changes one part of the conventional aircraft design this impacts other parts of the design as well.

For the aircraft design the team investigated the main effects of replacing the conventional gear. The changes the system imposes on the aircraft are described and analysed in chapter 6. The aspects of regarding the aircraft that were investigated are the harpoon connection mechanism structure in section 6.1 and the effect of the landing gear change on the aircraft weight and balance section 6.2. The aircraft itself is closely linked to the functions 3.0 to 5.0 regarding the climb, cruise, and descent. The harpoon mechanism can mainly be linked to functions 2.1 *Connect to take-off system*, 2.3 *Disconnect from take-off system*, 6.3 *Connect to landing system*, and 6.6 *Disconnect from landing system* in section 3.3.

The suction connection mechanism, as proposed in section 4.3, is in hindsight not seen as a useful addition to the REMALS. Looking at the front view of the reference aircraft, the suction mechanism requires unnecessary high accuracy of the landing ground system in order not to damage the engines or other parts of the aircraft upon connection. Furthermore, the suction mechanism does not add much value if it is used simultaneously with the harpoon mechanism. In this case, the suction mechanism solely adds unnecessary complexity to the system, hence it is left out in the analysis.

5.1.2. Ground System Design

The ground based system is composed of 10 main different parts which interact with each other and have separate functions within the ground based system. Each of the parts are further developed and described in chapter 7. The parts are listed from top to bottom below.

- **Grid:** The harpoon mechanism connects to the grid. The grid hosts the equipment needed to connect the aircraft (the harpoons), the connection mechanism for the conveyor chain, the locking mechanism on the roller coaster track and the roller coaster wheels. The grid is the only interchangeable part of the ground based system. Further details are presented in section 7.1.
- **Grid to platform connection:** As the aircraft needs to be able to taxi around the airport and it would be expensive to have a Stewart platform for every aircraft on the ground, the grid is removable from the

ground system. On top of the Stewart platform there are two circular bars located on which the grid can slide off in lateral direction. Further details are presented in section 7.2.

- **Stewart platform:** The Stewart platform provides accurate synchronisation of the base platform to the aircraft in the 6 degrees of freedom. The Stewart platform is mainly used to synchronise the orientation of the platform to the orientation of the aircraft. The Stewart platform is a 6 degrees of freedom platform. It can move in all three directions (vertical, longitudinal and lateral) and rotate around all three axes. This platform also performs the damping function. The Stewart platform can mainly be linked to functions 6.2 *Synchronise the landing system with the aircraft* and 6.4 *Damp aircraft* in section 3.3. Further details are presented in section 7.3.
- **Rotation platform:** Once the ground based system reaches the end of the runway it needs to be able to rotate. This follows from the fact that the Stewart platform is optimised for one direction. After rotating the platform, the runway can be used in both directions and it's not limited to only one direction. In order to do so a motor spins up a pinion on a circular gear rack. The rotation platform can mainly be linked to the function 6.7.2 *Prepare landing system for next landing*. Further details are presented in section 7.4.
- **Lateral movement structure:** Ground vehicle synchronisation in lateral direction is taken care of by the lateral movement structure. Lateral movements are performed thanks to an electric motor which rotor a circular pinion against a gear rack placed on top of the base structure. Lateral movement are needed in case the aircraft does not align perfectly with the centre-line of the runway. The lateral movement structure can be linked to functions 6.2.2.2, 6.2.3.2, and 6.2.4.2 related to *synchronisation of the ground vehicle in Y*. Further details are presented in section 7.5
- **Base structure:** The base structure is the structure along which the lateral movements take place. The base structure spans the rails that are integrated along the runway. The base structure is mainly designed to transfer bending loads. Further details are presented in section 7.6
- **Rails and wheels structure:** The rails and wheels ensure smooth travel of the ground system in runway direction. The rails and wheels structure spans the runway in runway direction. Further details are presented in section 7.7.
- **Power:** The power system mainly provides power to accelerate and decelerate the ground system in runway direction. Furthermore, the power system also provides power to the components on the ground vehicle these include servo valves, LiDAR sensors, and processing units amongst others. The EMALS power system can be linked to functions 6.2.2.1, 6.2.3.1, and 6.2.4.1 related to *synchronisation of the ground vehicle in X*. Further details are presented in section 7.8.
- **Runway Station:** The runway station consists of the accumulator charging unit and a lift platform. The lift platform makes it possible to lower the grid from the height of the Stewart platform to ground level where the aircraft can start moving to the gate. The platform raises a taxi cart to the same height as the grid, such that the grid can slide onto a taxi cart. The accumulator charging unit uses pumps to charge the accumulators that shall be used in the next operation of the ground system. Further details are presented in section 7.9.
- **Taxi cart:** The taxi cart makes it possible to move the aircraft all over the airport. It is an autonomous vehicle. The taxi cart includes a conveyor belt that extends to the grid which reels in the aircraft on the grid. The aircraft slides along a lateral bar with holes in such that the aircraft's position can be fixed. The taxi cart can be related to most of the functions below 1.0 *Perform pre-departure ground actions* and 7.0 *Perform post-arrival ground actions*. Further details are presented in section 7.10.

5.2. N^2 Chart

The N^2 -chart is a system engineering tool to identify and keep track of all the relations between the different components or departments. It is decided to create two N^2 -charts on different hierarchical levels. One N^2 -chart is on the component level and one on the department level and can be found in Figure 5.1 and Figure 5.2 respectively. This is done to make sure all the relations between the different components are considered in detail while still taking the bigger picture of the complete system into account. The N^2 -charts are used by noting down all the input and output parameters of every component and department. This was done during the design process and the N^2 -charts were continuously updated. Finally, the N^2 -charts were used in iteration process. The different components are combined into one final system in this part of the design. As the input and output parameters from the different components and departments are known, a smooth iteration process was done until the output values converged to the final values.

5.3. Budget Breakdown

In order to keep the costs associated with the design process within bounds, budgets regarding energy consumption, mass and costs were established during the baseline of the project [22]. Since the design is so conceptual, only an order of magnitude estimation was performed. A revision of those budgets is now given.

To keep them comparable, all the budgets will be expressed in a monetary value. Costs, consisting of costs of subsystems and production costs, but also cost of maintenance are already expressed in euros but for the energy and mass some assumptions need to be made.

The electrical energy is assumed to be taken from the regular power grid. On average the gross energy price is approximately €181.7/MWh, or €50.47/GJ. It is expected that power suppliers will be happy to provide the energy and make the necessary reinforcements to the grid when faced with such a high fixed demand. Note that since the energy consumption is a recurring cost, it needs to be expressed in the right time frame, the payback time of 15 years. Energy prices are assumed to grow at approximately the same rate as the discount rate, therefore no corrections are made for the time value of money.

To express the system's mass in euros, it is assumed that it is completely made out of carbon steel, including the rails. This is of course not quite the case, but the majority of the structure is, so it is a good approximation. The price of carbon steel is around 680 €/tonne, or 0.68 €/kg.¹

The three budgets should add up to the total budget obtained from the market analysis. The following relation can be used if one budget is exceeded: this budget can simply be increased while reducing another one. Of course, it must be noted that the budgets are not independent, e.g. an increase in mass, *ceteris paribus*, will also lead to an increase in required power.

$$50.47 \cdot E_{req} + 0.68 \cdot m_{total} + costs \approx Total_budget \quad (5.1)$$

The initial values for the budgets are set as €1.8·10⁸ for 15 years worth of energy, €15·10⁶ worth of material and €6.02·10⁸ for all other costs.

At this stage, the project has reached the class 3 estimate class. [31] This means the required contingency for the budget has decreased to a range of –20% to +30%.

¹URL: <http://www.meps.co.uk/World%20Carbon%20Price.htm> [Accessed 23 June 2019]

6

Aircraft Design

The overall advantage of the ground based take-off and landing system is the fact that the landing gear can be removed. However, a connection mechanism needs to be added in order to connect the aircraft to the ground structure, hereby adding weight to the aircraft again. However, this extra component is not as heavy as a conventional landing gear. Section 6.1 presents the design of the harpoon connection mechanism and its implementation in the aircraft. A structural analysis is also performed to make sure it will not fail during take-off and landing and the new mass of the aircraft is determined. Then, the new mass and balance characteristics of the A321REMAIS are discussed in section 6.2.

6.1. Connection Mechanism Between the Aircraft and the Grid

In order to connect the aircraft to the grid, a harpoon system is selected as it allows to have a lower accuracy compared to other attachment mechanisms as mentioned in chapter 4. In this section, the harpoon mechanism is explained in more detail and an analysis is done to make sure it can withstand the forces applied on it during landing and take-off.

In order to fulfil requirement NCL-Alc03, stating that the cost of the new aircraft shall not be more than 10% of the current conventional aircraft, the modifications on the aircraft have to be minimal. Hence, it is decided to place three harpoons at the location of the already existing landing gear in order to be able to use the existing landing gear boxes. Furthermore, as the total fuel consumption has to decrease (requirements NCL-Alc09u1 and NCL-Alc09u2), the total weight of the three harpoons should be as low as possible. Hence, it was decided that no dampeners or shock absorbers will be present in the harpoons (this is provided by the Stewart platform explained in section 7.3).

6.1.1. Controls of the Harpoon System

To decrease the modifications and costs as much as possible, the extension and retraction systems of the harpoons are based on the same mechanisms as the conventional retractable landing gear. The entire system is composed of three main components as can be seen in Figure 6.1: the pilot interface, a digital part and a mechanical part which contains the harpoons and all physical devices used to extend and retract the harpoons.

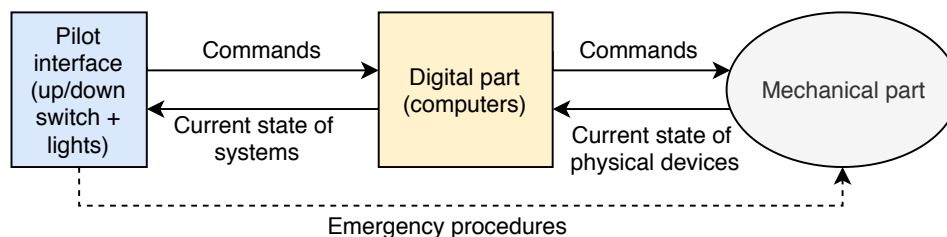


Figure 6.1: General overview of the harpoon system.

Pilot interface

With the help of a handle, the pilot commands the retraction and extension of the harpoons. When the handle is switched to "Up", the harpoons will retract and when it is switched to "Down", the sequence to extend the harpoons will be activated. The extended harpoon with the fingers still in contracted position is shown in Figure 6.2. The cockpit is also composed of a set of lights which indicate when the harpoons are correctly down and locked or retracted and locked¹. Furthermore, in case of emergencies, like conventional landing gears, a handle in the flight-deck can be activated. Through a mechanical linkage, the gears are unlocked which allows the harpoons to extend freely under their own weight¹.



Figure 6.2: Aircraft in approach, harpoons extended.

Digital system

The digital system is composed of two identical computers also used for conventional landing gears, executing the same control software. They command the movement of the harpoons and the doors, detect anomalies and inform the pilot of the current state of all systems². The state of all systems are measured with a set of discrete sensors which are also used in conventional aircraft. They provide information about:

- the harpoons being locked/not locked in extended position
- the harpoons being locked/not locked in retracted position
- the doors being open and locked/unlocked
- the doors being closed and locked/unlocked
- the hydraulic system being pressurised/not pressurised

Mechanical part

To power the harpoons, a combination of electric and hydraulic systems are used: this is called an electro-hydraulic system. Hydraulic systems are widely used today in aviation, however new aircraft tend to favour electrically controlled systems like the Boeing 787 for example, as they allow for lighter landing gears and provide higher resistance to fatigue³.

The motion of the harpoons and the doors are executed using a set of actuating cylinders². The extension of a cylinder is translated by the opening of a door or extension of a harpoon. As can be seen in Figure 6.3, each door and harpoon is controlled by a different cylinders. Hence, the system is composed of six cylinders in total.

When the handle in the flight-deck is switched to a certain position ("Up" or "Down") by the pilot, an electrical order is send to the digital system. This activates the general electro-valve which supplies each electro-valve with hydraulic power coming from the hydraulic circuit of the aircraft². Then, each electro-valve sets the pressure and provide the necessary hydraulic power to the cylinders.

¹URL:<https://www.flightliteracy.com/retractable-landing-gear-part-one/> [Accessed 23 June 2019]

²URL:https://www.irit.fr/ABZ2014/landing_system.pdf [Accessed 23 June 2019]

³URL:<https://www.safran-landing-systems.com/landing-gears/large-commercial-aircraft/boeing-787-landing-gear> [Accessed 23 June 2019]

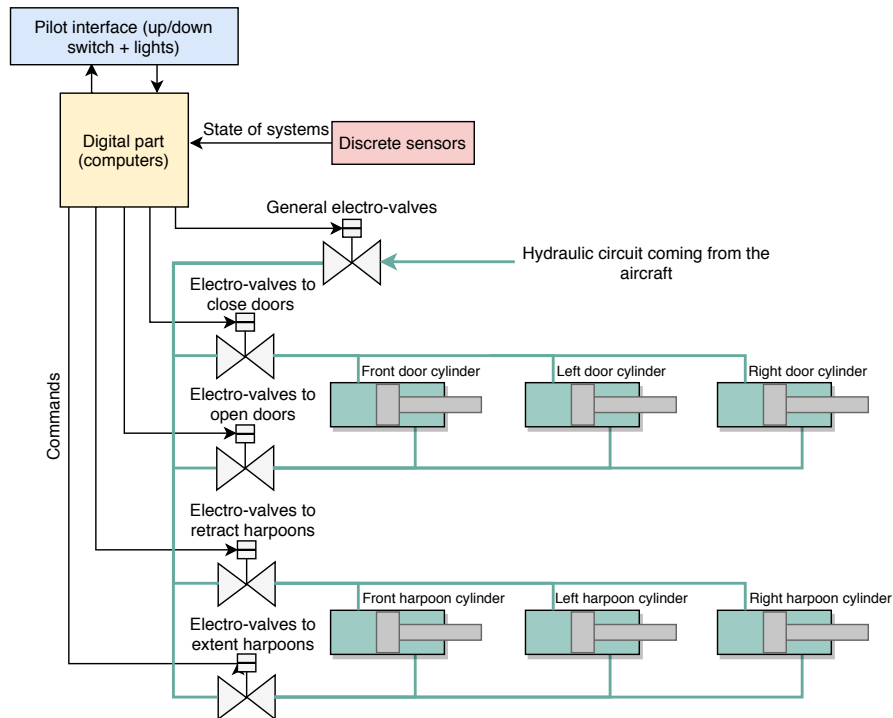


Figure 6.3: Architecture of the electrohydraulic system of the harpoons.

6.1.2. Architecture of the Harpoon System

Now that the extension and retraction processes of the harpoon system is clear, the architecture of the harpoon can be presented. The main part of the harpoon consist of a strut which has the same length as a conventional landing gear. The length could not be shortened due to engines clearance with the platform. Furthermore, five "fingers" are located at the end of the strut, which are used to lock onto the grid. The exact dimensions of the strut are given in subsection 6.1.3. Figure 6.4 presents the main harpoon when locked to the grid.



Figure 6.4: Harpoon architecture when attached to the grid.

During approach, the harpoons will deploy as explained in subsection 6.1.1.

When it is close enough to the grid (measured using a radar sensor, see section 9.2), the fingers go through the hole and open to lock in the position as shown in Figure 6.4. During the taxi phase, the harpoons stay locked to the grid at all time.

6.1.3. Structural Design of the Connection Mechanism

With this newly developed launching and landing system, the landing gear becomes unnecessary. Instead, as mentioned before, harpoons will be deployed and locked to the grid in order to keep the aircraft in place on the ground vehicle. The forces that the team needs to worry about, confirmed by dr. C. (Calvin) Rans, are with respect to what is causing the acceleration and thus the contact point of the force. In this case, the forces are transmitted to the aircraft through the harpoons. Even though the harpoons need to be as light as possible to decrease the total weight of the aircraft, they still need to be strong enough to withstand the loads of the aircraft during the most critical load scenarios.

It has been realised that due to the bigger accelerations with respect to conventional procedures, there

are also more loads applied to the wings. However, with more help of dr. C. (Calvin) Rans it is evaluated that we are accelerating in the direction where the wing is the stiffest. So a different design in the wing is not necessary.

The major inputs for the design of the connection mechanism are the forces that the aircraft exerts on the platform through the harpoons. These forces come from the Stewart platform department presented in section 7.3 where four load cases have been identified as followed:

- Case 1: Landing requirement CS25.479(d)(1) explained in section 7.3.
- Case 2: Landing requirement CS25.479(d)(2)(i) explained in section 7.3.
- Case 3: Acceleration explained in section 7.8.
- Case 4: Deceleration explained in section 7.8.

The goal of this analysis is to reduce the mass while safely designing the harpoons for each load scenario. The approach for designing the harpoons is presented in this subsection.

Original landing gear mass

The first step is to determine the original mass of the three conventional landing gears in order to have an idea on how much weight this represents. The landing gear mass is calculated using Equation 6.1⁴ where coefficient A, B, C and D are taken for retractable gears from Torenbeek. Furthermore, m_{MTO} is the take-off mass and k_{LG} equals 1 for a low wing configuration. The equation is applied separately for the main and nose landing gear and the sum of the two masses gives the total landing gear mass⁴.

$$m_{LG} = k_{LG} \cdot (A_{LG} + B_{LG} \cdot m_{MTO}^{3/4} + C_{LG} \cdot m_{MTO} + D_{LG} \cdot m_{MTO}^{3/2}) \quad (6.1)$$

This results in a total mass equal to approximately 3805 kilograms for the three landing gears together which represents a bit less than 4% of the Maximum Take-off Weight of the aircraft.

Parameters used

The harpoons are constructed and analysed as circular tubes and sized with fixed radii. In the following calculations, the thin-walled assumption can not be applied as the strut is not planned to be thin-walled.

Figure 6.5 shows the parameters used in the following calculations. The forces in x and y direction will have a maximum positive value at some location θ of the cross-section. x and y are given in polar coordinates in Equation 6.2 where r_o is the outer radius of the strut. They are expressed as a function of the outer radius because they are used in the normal stress calculations where the maximal normal stress occurs at the outer edges of the cylinder. Furthermore, the geometric properties of the tube like the area and moment of inertia are presented in Equation 6.2 as well, where r_i stands for the inner radius of the strut. I_{xy} equals 0 because the cross-section is symmetrical.

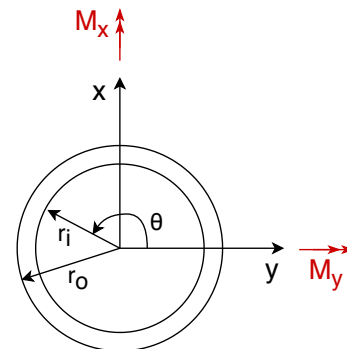


Figure 6.5: Cross-section of the strut with the parameters used for the analysis.

$$x = r_o \cos\theta \quad y = r_o \sin\theta \quad A = \pi(r_o^2 - r_i^2) \quad I_{xx} = I_{yy} = \frac{\pi}{4}(r_o^4 - r_i^4) \quad I_{xy} = 0 \quad (6.2)$$

For structural analysis, the combination of bending and axial forces is evaluated as well as the buckling characteristics of the design for each load cases. Because of the length of the struts and the thickness of the cross section, the shear is not identified as a critical load scenario, hence it is not analysed here.

Bending and axial forces

First of all, the struts are designed such that they do not fail in tension. Therefore it is undesired that the tensile stress at any point exceeds the yield stress of the material. To do so, the combination of the bending and the axial loads are evaluated. Because the axial loads act in compression, the most critical case will have a negative component of the axial load and a positive component of the bending stress. For this case, it

⁴URL: https://www.fzt.haw-hamburg.de/pers/Scholz/HOOU/AircraftDesign_10_Mass.pdf [Accessed 23 June 2019]

is assumed that for landing a single point should withhold the vertical loads of landing. Furthermore, the critical cross-section will be at either the beginning or the end of the harpoon strut, as there the highest bending moment acts depending on which side of the strut the force is applied.

As learned in AE21355-I Structural Analysis and Design, the normal bending stress is given by Equation 6.3 [52] where M is the bending moment around axis x or y and I is the moment of inertia.

$$\sigma_{z_{bending}} = \frac{(M_x I_{yy} - M_y I_{xy})y + (M_y I_{xx} - M_x I_{xy})x}{I_{xx} I_{yy} - I_{xy}^2} \quad (6.3)$$

Using the parameters defined in Equation 6.2, the normal stress in the tube could be rewritten as in Equation 6.4. It combines the axial force and the bending moments.

$$\sigma_z = -\frac{N}{A} + \frac{M_x y}{I_{xx}} + \frac{M_y x}{I_{yy}} \Rightarrow \sigma_z = -\frac{N}{A} + \frac{M_y r_o \sin\theta + M_x r_o \cos\theta}{\frac{\pi}{4}(r_o^4 - r_i^4)} \quad (6.4)$$

Here N represents the normal force, thus the net force in z -direction. The angle θ is yet to be determined depending on the moments applied. For this, Equation 6.4 is differentiated with respect to θ and set equal to zero in order to find θ_{max} . Equation 6.4 is then rewritten and the maximum normal stress in the strut is expressed as Equation 6.5 [11].

$$\sigma_{z_{max}} = -\frac{N}{\pi(r_o^2 - r_i^2)} \pm \frac{r_o \sqrt{M_x^2 + M_y^2}}{\frac{\pi}{4}(r_o^4 - r_i^4)} \quad (6.5)$$

The outer radius is at first assumed to be the same radius as for conventional landing gear. The maximum tensile stress is calculated, and it is evaluated what the maximum inner radius is with which the maximum tensile stress including safety factor does not exceed the yield strength of 1586 MPa ⁵. This corresponds to the yield strength of the 300M steel alloy which will be used for the harpoon. With the help of sensitivity analysis, it is concluded that if the outer radius is bigger, the mass decreases significantly. However, the thickness of the strut decreases.

Buckling load

With a strut as long as conventional landing gears (2500 mm long), the critical loads can lead to buckling as well. The buckling load is given in Equation 6.6 [52] where k is the effective length factor. It is equal to 2 as the strut is assumed to be modelled as a beam with one fixed and one pinned end. Furthermore, E is the Young's modulus and L_e is the effective length of the strut equal to $0.7 \cdot L$ [52].

$$P_{cr} = k \cdot \frac{\pi^2 EI}{L_e^2} \quad (6.6)$$

If this buckling load found by Equation 6.6 is lower than the load on the gear, the strut fails due to buckling, therefore it is redesigned for buckling. However, at this point in the design process, the local stress due to moments could not be taken into account for the buckling loads. The maximum buckling load is available, and the stress in the strut can be found, but further analysis has to be done to see if locally in a cylinder the critical buckling load is exceeded.

Results

With this approach, the four load cases are evaluated for an outer radius of 150mm. The results are summarised in Table 6.1.

Table 6.1: Necessary inner radius for different load cases.

| | Inner radius [mm] | | | |
|---------------|-------------------|--------|--------|--------|
| | Case 1 | Case 2 | Case 3 | Case 4 |
| Main harpoons | 105 | 133 | 125 | 135 |
| Nose harpoon | 111 | 114 | 109 | 117 |

⁵URL:<https://www.twmetals.com/products/bars/alloy-bar/300m.html>[Accessed 14 June 2019]

The lowest diameter is used in order to account for the most critical load case. The outer diameter and mass are then optimised again for each load case, and surely load case 1 is still the the most critical. The final mass of each harpoon is calculated by multiplying the density of the material used, the area and the length of the strut. The final dimensions and mass of the harpoons are summarised in Table 6.2. This leads to a final mass of 1700 kilograms saving up to 2104 kilograms.

Table 6.2: Final dimensions and mass of the harpoons.

| | Mass [kg] | Outer radius [mm] | Inner radius [mm] | Length [m] | Material |
|---------------------|-----------|-------------------|-------------------|------------|-------------------------|
| Main harpoon | 709 | 150 | 105 | 2.5 | Steel 300M ⁵ |
| Nose harpoon | 282 | 140 | 111 | 1.57 | Steel 300M ⁵ |

If the strut would fail due to buckling, an option would be to add side struts, as the effective length is reduced. However, that is not the case and the diameter is reasonable and the side struts would add to much weight. Another recommendation would be to add damping material on the surfaces that touch the grid as shown in Figure 6.4.

Verification and validation

In order to verify the program, calculations were performed by hand and other team members were consulted to check the consistencies of the units and the program itself. Furthermore, a visit to Dr. Ir. R. (Roelof) Vos has confirmed that the landing loads and load factors are commonly used in landing gear design.

6.2. Weight and Balance Characteristics

In order to limit the modifications performed on the A321 REMALS, the only major change that is make to the structure of the place is the fact that the landing gears are replaced with harpoons. As explained in section 6.1, this modification saves 2104 kg. Hence, it is expected that it might influence the stability and control of the aircraft. Therefore, a mass and balance composed of a loading diagram and a scissor plot are made to evaluate this change. It will be seen that the new concept is still in range of the scissor plot, however the most aft centre of gravity is too close to the main harpoons and thus these will have to be brought back. Furthermore, the sensitivity analysis is done to evaluate the reliability of this approach and suggest potential improvements.

6.2.1. Loading diagram

At first the loading diagram, also known as potato diagram, for the conventional A321NEO is constructed as a verification of the method. Then, the new weights of the harpoons instead of the landing gear are implemented. This results in a shift in the loading diagram.

The centre of gravity range of the Airbus A321NEO is deduced with the use of a loading diagram. First, the operational empty weight is estimated. The components of the aircraft are split up to fuselage and wing contributions. Any component not in the list are not considered to notably affect the centre of gravity. Included in the list for fuselage group are: the fuselage, the nose landing gear, the horizontal tail, and the vertical tail. Included for the wing group are: the wing structure, the main landing gear and the engines. This division is made because of the configuration of the aircraft. The tank is included in the wing group, but the fuel is added later in the loading diagram.

The location of individual centre of gravity of components is measured on the blueprints with the help of statistical data provided by the AE3211-I System Engineering and Aerospace Design course [29]. For the fuselage, the centre of gravity is between 0.42 and 0.45 of the total length of the fuselage. The centre of gravity of the wing and the tail parts are on 0.42 of their mean aerodynamic chord. Note that the values calculated with are very specific, but it is realised that there is a bigger uncertainty per value. This is described in the sensitivity analysis. The location of each component is found as a percentage of the mean aerodynamic chord (MAC), and with this the total location of the centre of gravity is found with Equation 6.7 where subscript i represents the different components. This equation is also used later for the loading diagram.

$$x_{CG} = \frac{\sum x_{CG} \cdot W_i}{\sum W_i} \quad (6.7)$$

These calculations are summarised in Table 6.3 and result in a centre of gravity located at 22% of the

MAC. As a check, again the slides of AE3211-I "System Engineering and Aerospace Design" course [29] are used. This states that the operational empty weight centre of gravity is usually at 20-25% of the MAC.

Table 6.3: Values used for centre of gravity OEW calculation

| | Item | Weight [kg] | Arm from nose [m] | % of MAC [-] |
|-----------------------|-------------------|--------------|-------------------|--------------|
| Fuselage group | Fuselage | 26974 | 10.78 | -0.04 |
| | Nose landing | 668 | 5.07 | -3.47 |
| | Horizontal tail | 1798 | 38.86 | 4.41 |
| | Vertical tail | 1199 | 40.85 | 4.87 |
| | Total | 30639 | 21.41 | 0.34 |
| Wing group | Wing | 12525 | 21.29 | 0.31 |
| | Main landing gear | 1336 | 21.97 | 0.47 |
| | Engines | 5600 | 16.87 | -0.72 |
| | Total | 19461 | 20.06 | 0.03 |
| A321NEO | Total | 50100 | 20.89 | 0.22 |

The loading diagram is then constructed making use of the "window seating rule". First, the cargo is loaded, then the passengers sitting at the window, followed by the middle seats, and at last the aisle seats are loaded. For this loading the scenario of forward to backward and backward to forward loading is considered. At the end, the fuel is loaded. There are several configurations for the A321NEO. In order to load as many passengers as possible, the single-class standard configuration is used [3]. With these positions of the passengers and a passenger weight of 80 kg including hand luggage the loading diagrams is made and represented in Figure 6.6.

For the new concept, the weight of the landing gear is drastically reduced. The nose landing gear weight is changed to 282 kilograms and each of the main landing gears weight is changed to 709 kilograms as provided by subsection 6.1.3. This weight reduction translates into extra fuel in order to take the same maximum take-off weight into account. Replacing the landing gear weight with this new weights generates the new loading diagram as can be seen in Figure 6.6. The plot shows both loading diagrams, original in grey dashed and the REMALS in purple and full line. From the plot, it is clear that decreasing the weight of the landing gears moves the centre of gravity aft with respect to the mean aerodynamic chord.

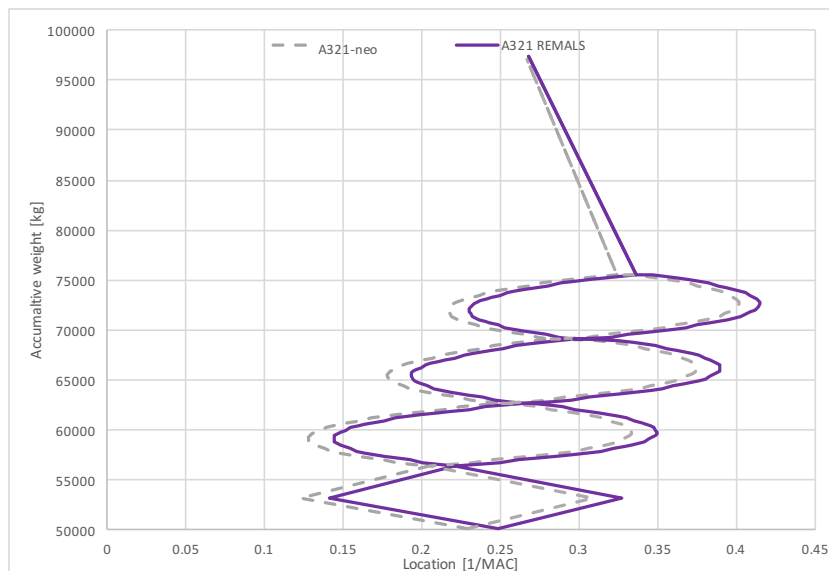


Figure 6.6: Loading diagrams of conventional A321NEO and REMALS concept aircraft

From the data accumulated, the most front and most aft centre of gravity is obtained. With a 2% margin like taught in AE3211-I, the centre of gravity range for the conventional A321neo is between 0.11 - 0.40 % of MAC. For the REMALS, the range is between 0.12-0.41 % of MAC. This range is checked below in subsec-

tion 6.2.2. Furthermore, the most aft center of gravity is not allowed to be more aft than 15% to the front of the main landing gear. Dr. F (Fabrizio) Oliviero consulted that this is usually where the most aft centre of gravity is designed in aircraft. Therefore, the most aft location due to this requirement is evaluated to be at 0.42 MAC. It is therefore concluded that both designs succeed this requirement.

6.2.2. Scissor plot

Section 6.2.1 presents the shift of the center of gravity when the landing gears are removed and the harpoons are added. The next step is to check with the scissor plot if the aircraft is still stable and controllable. Hence, this section presents how the stability and controllability curve are plotted and if the minimum and maximum c.g. established in section 6.2.1 are still in the allowable center of gravity range for a given horizontal/wing tail surface ratio (S_h/S).

Stability

Using Equation 6.8 [30], both neutral stability curve and stability curve are plotted. The stability curve uses a 5% stability margin to account for other constraints and uncertainties as the critical conditions that can occur during flight and ground operations.

$$\frac{S_h}{S} = \frac{1}{\frac{C_{L\alpha_h}}{C_{L\alpha_{A-h}}} \left(1 - \frac{d\varepsilon}{d\alpha}\right) \frac{l_h}{\bar{c}} \left(\frac{V_h}{V}\right)^2} \bar{x}_{cg} - \frac{\bar{x}_{ac} - 0.05}{\frac{C_{L\alpha_h}}{C_{L\alpha_{A-h}}} \left(1 - \frac{d\varepsilon}{d\alpha}\right) \frac{l_h}{\bar{c}} \left(\frac{V_h}{V}\right)^2} \quad (6.8)$$

In order to draw this curve, all different coefficients first have to be discussed. This is done following the empirical methods explained in [30]. All required dimensional parameters were obtained using data of the A321NEO [3] [45] or directly measured on the aircraft via CATIA and drawings.

- \bar{x}_{ac} is the aerodynamic center of the aircraft less tail calculated using Equation 6.9: it is composed of the wing aerodynamic center contribution located at a quarter chord, the contribution of the aerodynamic center of the fuselage and the nacelles.

$$\left(\frac{x_{ac}}{\bar{c}}\right)_{wf} = \left(\frac{x_{ac}}{\bar{c}}\right)_w - \frac{1.8}{C_{L\alpha_{A-h}}} \frac{b_f h_f l_{fn}}{S \bar{c}} + \frac{0.273}{1 + \lambda} \frac{b_f c_g (b - b_f)}{\bar{c}^2 (b + 2.15 b_f)} \tan \Lambda_{1/4} - 5 \frac{b_n^2 l_n}{S \cdot \bar{c} \cdot C_{L\alpha_{A-h}}} \quad (6.9)$$

- The lift rate coefficient of the aircraft less tail $C_{L\alpha_{A-h}}$ is computed according to Equation 6.10, where $C_{L\alpha_w}$ is calculated with Equation 6.11 by using data corresponding to the main wing.

$$C_{L\alpha_{A-h}} = C_{L\alpha_w} \left(1 + 2.15 \frac{b_f}{b}\right) \frac{S_{net}}{S} + \frac{\pi}{2} \frac{b_f^2}{S} \quad (6.10)$$

- $C_{L\alpha_h}$ is then calculated according to Equation 6.11 where the Mach number is taken to be equal to 0.78 and η equals 0.95 [30].

$$C_{L\alpha_h} = \frac{2\pi A_h}{2 + \sqrt{4 + \left(\frac{A_h \beta}{\eta}\right)^2 \left(1 + \frac{\tan^2 \Lambda_{0.5c_h}}{\beta^2}\right)}} \quad \beta = \sqrt{1 - M^2} \quad (6.11)$$

- Next, the downwash effect of the wing on the tail is approximated according to Equation 6.12 where the two K_ε account for the effect of the wing sweep angle and are found using Equation 6.13. r and m_{tv} are deduced from measurements done on the aircraft in CATIA.

$$\frac{d\varepsilon}{d\alpha} = \frac{K_{\varepsilon_\Lambda}}{K_{\varepsilon_\Lambda=0}} \left(\frac{r}{r^2 + m_{tv}^2} \frac{0.4876}{\sqrt{r^2 + 0.6319 + m_{tv}^2}} + \left[1 + \left(\frac{r^2}{r^2 + 0.7915 + 5.0734 m_{tv}^2} \right) \right] \left\{ 1 - \sqrt{\frac{m_{tv}^2}{1 + m_{tv}^2}} \right\} \right) \frac{C_{L\alpha_w}}{\pi A} \quad (6.12)$$

$$K_{\varepsilon_\Lambda} = \frac{0.1124 + 0.1265\Lambda + 0.1766\Lambda^2}{r^2} + \frac{0.1024}{r} + 2 \quad K_{\varepsilon_\Lambda=0} = \frac{0.1124}{r^2} + \frac{0.1024}{r} + 2 \quad (6.13)$$

- As last, the tail/wing speed ratio $\left(\frac{V_h}{V}\right)^2$ for fuselage-mounted stabiliser is equal to 0.85.

Controllability

The controllability curve is obtained applying Equation 6.14 [28]. Most of the coefficient were already calculated for the stability curve hence, only C_{L_h} and $C_{m_{ac}}$ need to be evaluated. However, all lift rate coefficient are now estimated for low speed, thus for landing conditions.

$$\frac{S_h}{S} = \frac{1}{\frac{C_{L_h}}{C_{L_{A-h}}} \frac{l_h}{\bar{c}} \left(\frac{V_h}{V}\right)^2} \bar{x}_{cg} + \frac{\frac{C_{m_{ac}}}{C_{L_{A-h}}} - \bar{x}_{ac}}{\frac{C_{L_h}}{C_{L_{A-h}}} \frac{l_h}{\bar{c}} \left(\frac{V_h}{V}\right)^2} \quad (6.14)$$

- The tail configuration (full moving tail, adjustable or fixed tail) has an effect on the controllability. Most passengers aircraft have a fixed tail corresponding to a C_{L_h} equal to $-0.35A_h^{1/3}$ where A_h is the aspect ratio of the horizontal tail.
- $C_{m_{ac}}$ is the zero lift pitching moment coefficient of the aircraft without tail which comprises the contribution of the wing, flaps, fuselage and engine nacelles respectively as follows: $C_{m_{ac}} = C_{m_{ac_w}} + \Delta_f C_{m_{ac}} + \Delta_{fus} C_{m_{ac}} + \Delta_{nac} C_{m_{ac}}$. The contribution of the nacelle is very small compared to the flaps for example, hence it is neglected in the calculations. The contribution of the wing and the flaps are presented in Equation 6.15 and 6.17 respectively. However, as Equation 6.17 is expressed with respect to a quarter chord MAC, Equation 6.16 is used to convert it with respect to the aerodynamic center.

$$C_{m_{ac_w}} \approx C_{m_{0airfoil}} \left(\frac{A \cos^2 \Lambda}{(A + 2 \cos \Lambda)} \right) \quad (6.15) \quad \Delta_f C_{m_{ac}} = C_{m_{1/4}} - C_L \left(0.25 - \frac{X_{ac}}{\bar{c}} \right) \quad (6.16)$$

$$\Delta C_{m_{1/4}} = \mu_2 \left\{ -\mu_1 \Delta C_{l_{max}} \frac{c'}{c} - \left[C_L + \Delta C_{l_{max}} \left(1 - \frac{S_{wf}}{S} \right) \right] \frac{1}{8} \frac{c'}{c} \left(\frac{c'}{c} - 1 \right) \right\} + 0.7 \frac{A}{1 + 2/A} \mu_3 \Delta C_{l_{max}} \tan \Lambda_{1/4} \quad (6.17)$$

The μ coefficients, c' and $\Delta C_{l_{max}}$ are estimated using graphs from Torenbeek [28] and the other parameters are based on measurement done on the geometry of the aircraft represented in CATIA.

Finally, the fuselage contribution is found according to Equation 6.18 where $C_{L_{\alpha_{A-h}}}$ is calculated with Equation 6.10 using landing conditions.

$$\Delta_{fus} C_{m_{ac}} = -1.8 \left(1 - \frac{2.5b_f}{l_f} \right) \frac{\pi b_f h_f l_f}{4S\bar{c}} \frac{C_{L_0}}{C_{L_{\alpha_{A-h}}}} \quad (6.18)$$

Results and Scissor Plot

All major coefficients calculated as explained before from Equation 6.8 and 6.14 are summarised in Table 6.4.

Table 6.4: Input values for the stability and controllability equations

| Stability coefficients | | | Controllability coefficients | | |
|--------------------------------|-------|-------------|--------------------------------|-------|------|
| Symbol | Value | Unit | Symbol | Value | Unit |
| $C_{L_{\alpha_h}}$ | 4.91 | [1/radians] | C_{L_h} | -0.59 | [-] |
| $C_{L_{\alpha_{A-h}}}$ | 6.06 | [1/radians] | $C_{L_{A-h}}$ | 4.85 | [-] |
| $\frac{d\bar{c}}{d\alpha}$ | 0.36 | [-] | $C_{m_{ac}}$ | -0.84 | [-] |
| \bar{x}_{ac} | 0.13 | [-] | \bar{x}_{ac} | 0.014 | [-] |
| l_h | 18 | [m] | l_h | 18 | [m] |
| $\left(\frac{V_h}{V}\right)^2$ | 0.85 | [-] | $\left(\frac{V_h}{V}\right)^2$ | 0.85 | [-] |

From this, the scissor plot is created and shown in Figure 6.7. The left curve represents the controllability curve from Equation 6.14 while the two right curves are the stability curves from Equation 6.8. Note that the dashed curve is the neutral stability while the other one includes a static stability margin of 5%.

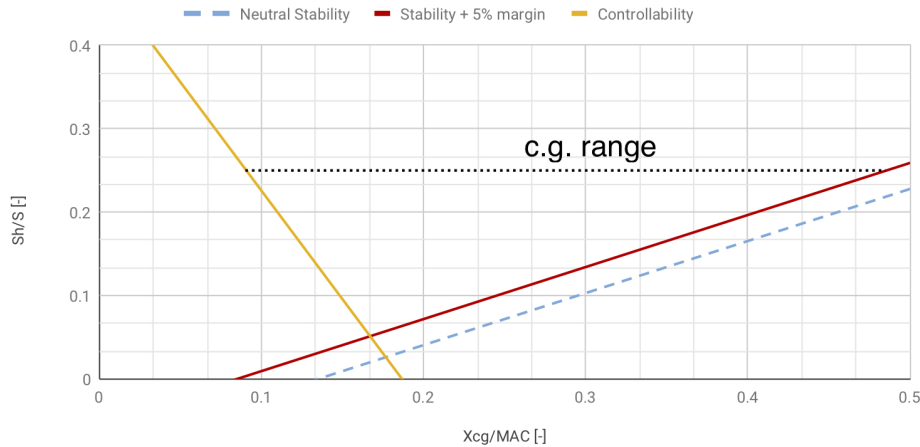


Figure 6.7: Scissor plot including the c.g. range at $S_h/S = 0.25$.

Furthermore, as no major changes are performed on the aircraft, the surfaces of the wing ($=122.4 \text{ m}^2$) and horizontal tail ($=31 \text{ m}^2$) are the same. Hence, the horizontal/wing tail surface ratio S_h/S of the A321 REMALS is equal to approximately 0.25. From this, a dotted line is drawn on the scissor plot at 0.25 on the vertical axis and between the controllability and stability curves as this is where the aircraft is stable. This gives the allowable c.g. range which is between 0.085 and 0.48 % of MAC. As mentioned in subsection 6.2.1, using a 2% margin, the center of gravity range of the A321 REMALS is found to be located between 0.16 and 0.44. The center of gravity is situated inside the allowable c.g. range, hence the A321 REMALS is concluded to stay stable when replacing the landing gears with the harpoons.

6.2.3. Sensitivity Analysis

Clearly, the nose landing gear has a big influence on the centre of gravity range of the aircraft. A solution for this would be to increase the weight of the nose landing gear, let it carry more loads. If the weight of the landing gears would be equally distributed, so not looking at equations in subsection 6.1.3 anymore, the most aft centre of gravity moves 1.5 cm to the front and the most front centre of gravity moves 1.8 cm to the front. This could be used if other airplane types investigated later are concluded to not be stable with the new harpoon weight distribution.

In the process of making the mass & balance, preliminary estimation tools including measuring on sketches are used. However, doing a sensitivity analysis, it is realised that some of these constants are very sensitive for the results. For example the distance to the leading edge of the aerodynamic chord, x_{LEMAC} , could not be found online and the values in the same family do not necessarily match. From drawing techniques, a distance of 19.95m is estimated. However, these drawing techniques are preliminary and the actual mean aerodynamic chord might be more forward or backward. Changing the distance to the leading edge of the aerodynamic chord, if it is 38 cm more aft or to the front then the aircraft still fits the landing gear requirement. Therefore, if the true location of the mean aerodynamic chord is 80 centimetres more towards the tip or towards the root of the wing, the loading diagram is still stable with respect to the location of the main landing gear requirement. Because this method worked out for the A321, it is a feasible idea of what could happen, but more research with better data of the aircraft has to be done to be sure about the stability and control.

6.2.4. Verification and Validation

Verification and validation on the mass and balance of the aircraft is difficult because there are no true data sheet to compare with other similar aircraft. Hence, professors from the faculty of Aerospace Engineering have been contacted in order to make sure that the loading diagram and scissor plot made sense for the conventional A321NEO. Then, using the same technique and only changing the weight of the landing gears, the loading diagram for the REMALS was performed. The center of gravity deduced from the loading diagram was checked with the scissor plot. The values were in the allowable c.g. range, hence it was concluded that the two programs were verified and could be further used. Furthermore, each program was verified by hand calculations to check if no mistakes were made.

Ground System Analysis

This chapter analyses the ground base system. A visualisation of the system can be found in Figure 7.1. The chapter is divided into ten ground based system section that are mentioned in subsection 5.1.2. They are structured from top to bottom.

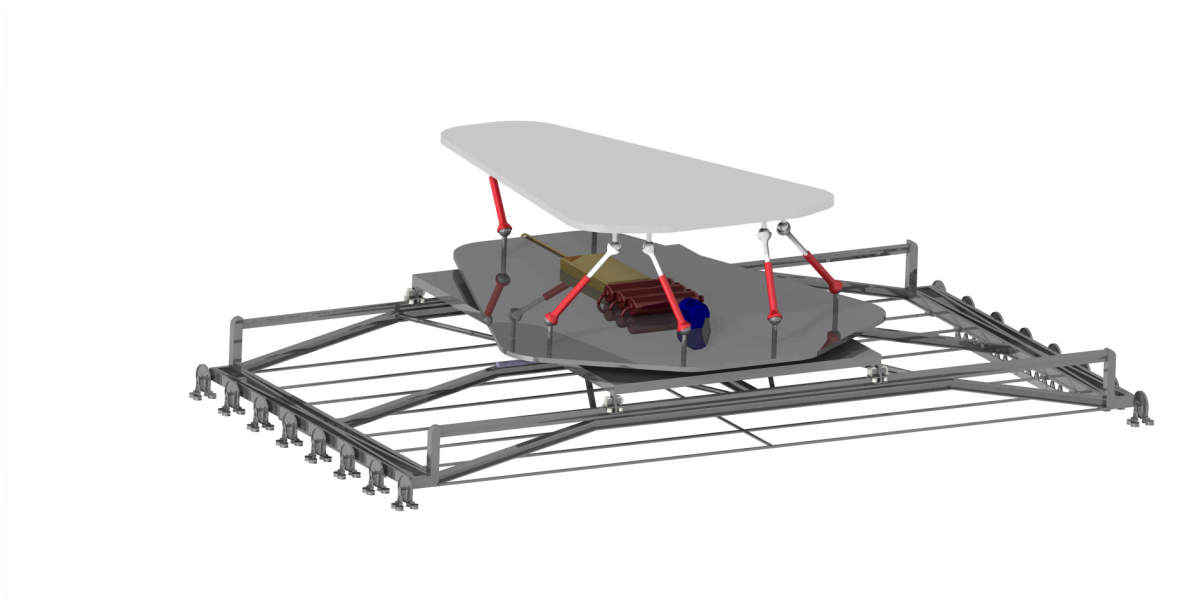


Figure 7.1: Visualisation of the ground based system.

7.1. Grid

The harpoons connect to the grid that is located on top of the Stewart platform. The grid design is based on the design of a Heligrd. The main advantages of this grid is that it is practically maintenance free and offers low costs¹. The grid allows any aircraft to land on it, as long as the matching harpoon mechanism is used. Heligrd can develop custom grids for the REMALS that meet the requirements. The dimensions of the grid have been established by looking at the landing gear positions of a conventional A321. No statistical data was found regarding pre-landing deviations of the aircraft, however it is evident that a safety margin should be included since a 100% accurate synchronisation cannot be guaranteed. Therefore, the grid is



Figure 7.2: Visualisation of the grid.

¹URL: <https://heligrd.com/> [Accessed 21 June 2019]

designed to be a circular shape around every landing gear position of the conventional aircraft that contain holes. A general rule of thumb for the deviation from the center-line of the runway landing is said to be half the main landing width, according to Dr.Ir. A.C. in 't Veld. This statement was checked by visual inspection of landing aircraft and was correct most of the time but there were extreme cases where the aircraft landed outside of this margin. Therefore, the radius of the grids are $2m$ and in combination with the lateral movement system and the Stewart platform, the freedom in the lateral landing position is considered to be sufficient at this point in time. The mass of the grid is estimated to be $5000kg$. A visualisation of the grid can be found in Figure 7.2.

7.2. Connection Between Grid and Stewart Platform

On top of the Stewart platform there is a rail structure to replace the grid. The rail structure is fixed to the Stewart platform and the grid is free to move on its wheels during the replacement process. When the grid reaches the desired position it is fixed in position thanks to a special locking mechanism. The movement mechanism is visualised in Figure 7.3. A more detailed explanation of how it works and the technical details are given in subsection 7.10.3.

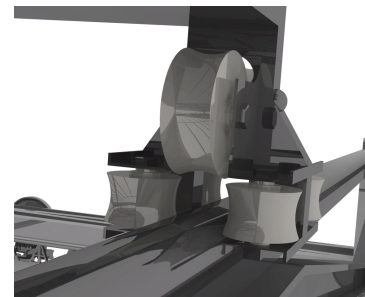


Figure 7.3: Connection mechanism between grid and Stewart platform.

7.3. Stewart Platform

In order to accurately synchronise the orientation of the platform with the orientation of the aircraft and replace the dampers in the conventional landing gear, a Stewart platform is used. The Stewart platform is highly flexible and highly adjustable to synchronise with the aircraft in a smooth way with high accuracy. The Stewart platform is a 6 degrees of freedom platform that uses 6 actuators [16]. The platform is able to move in X , Y , and Z , and is able to rotate in ϕ , θ , and ψ . Stewart platforms are currently used in flight simulators, as motion compensating platforms on sea by Ampelmann², and as Low-Impact Docking System (LIDS) by NASA³.

The Stewart platform should be able to synchronise for a certain time at a certain speed and it should be able to withstand a certain amount of forces introduced by the aircraft. As learned from Ir. O. Stroosma the Stewart platform has a restricted work space which can not be exceeded, so the actuator lengths and possible extensions need to be determined. The Stewart platform mainly ensures synchronisation of the orientation, but can synchronise its position as well if necessary.

In short, the Stewart system consists of a base, a platform, a processing unit, servo valves (which regulates the oil flow), actuators, an accumulator (which provides the oil flow), a reservoir (which stores the oil after it has been used) and connection points. The main components that ensure proper functioning of the Stewart platform with their main function and parameters are discussed below.

- **Platform and Base:** The platform is the top rigid frame of the Stewart platform. It is connected to the grid, which is removable, on which the aircraft connects using the harpoons and where the forces are initially introduced. The base is the bottom rigid frame of the Stewart platform.
- **Processing unit:** The processing unit is the heart of the Stewart platform. The processing unit converts the signals from the synchronisation instruments (the LiDAR systems) to required actuator extensions and oil flows. As the Stewart platform is a parallel manipulator one should be aware of possible singularities and avoid singularity positions. According to Ir. O. Stroosma the right control program that takes the characteristics of the system into account, is able to prevent the system from ending up in these singularities.
- **6 Electrohydraulic servo valves:** The servo valve regulates the oil flow into the actuators with great precision. The servo valve has control of the position of the actuators, the velocity of the actuators, and the hydraulic pressure resulting in a force provided by the actuators. The servo valve is used in a feedback loop, this makes it very accurate and precise.
- **6 Hydraulic double acting actuators:** The actuators extend and retract to change the position and orientation of the Stewart platform. They transfer the forces and moments introduced by the aircraft

²URL: <https://www.ampelmann.nl/systems/e8000> [Accessed 17 June 2019]

³URL: <https://technology.nasa.gov/patent/TOP9-127> [Accessed 17 June 2019]

on the platform to the base. Double acting actuators apply pressure on each side of the piston and offer more precision according to Ir. G. Bufalari.

- **Accumulators:** The accumulators are able to provide oil at the required high flow rates. As the system needs to compensate motion only for a short time it does not make sense to carry an enormous and heavy pumping system on the moving ground system. Accumulators are a better option as they are a mean of energy storage and can deliver high oil flow rates without the need of a pumping system on board.
- **Oil reservoir:** The oil reservoir stores the oil that is introduced in the circuit by the accumulators after it has passed the actuators.
- **12 Joints or connection points:** The joints connect the actuators to the platform and the base. According to Ir. O. Stroosma, these joints can be positioned freely and one can make the configuration as exotic as is desired.

It should be noted that oil pumps are not present on the Stewart platform. Oil pumps are big and heavy systems that, according to Ir. G. Bufalari, will not be able to meet the requirements regarding oil flow rates. From calculations that follow later in this section, this statement was validated and bringing oil pumps along indeed is not an option for the REMALS.

7.3.1. Input Forces

The forces that the aircraft exert on the platform need to be determined to calculate the forces in the actuators. To find the most extreme forces in the actuators, several different situations are analysed. Some are related to acceleration and deceleration of the aircraft on the runway and others are related to the impact loads during landing. First the impact loads during landing are determined for conventional landing gear according to [54]. First Equation 7.1 is used to calculate the stroke length of a conventional shock absorber. According to the CS-25 regulations, the aircraft has a limit descent velocity V of 3.05 m/s at the design landing weight [2]. The lift is equal to the weight for transport-type aircraft [54]. N is the landing gear load factor and is equal to 1.5 [54]. The shock absorber efficiency n_s is equal to 0.8 as a oleo-pneumatic shock absorber is used [40]. These values result in a stroke length of 0.40 m .

$$-\frac{WV^2}{2g} = -S n_s N W + (W - L) S \quad (7.1)$$

To obtain an impact force from this stroke length, it is assumed that all the kinetic energy in vertical direction is dissipated by the shock absorbers that exert a constant force. Using Equation 7.2, a force of approximately 950 kN is found.

$$F = \frac{\frac{1}{2} m V^2}{S} \quad (7.2)$$

This force underestimates the maximum vertical load as it assumes the minimum constant force to decelerate the aircraft and therefore a safety factor of 2 is applied to obtain a conservative value for the maximum vertical load. The CS-25 regulations specify the following severe combination of loads that is likely to arise during landing as a percentage of this maximum vertical load [2].

CS 25.479(d)(1) The landing gear and directly affected structure must be designed for the maximum vertical ground reaction combined with an aft acting drag component of not less than 25% of this maximum vertical ground reaction.

CS 25.479(d)(2)(i) A vertical load equal to 75% of the maximum ground reaction of CS 25.473(a)(2) must be considered in combination with a drag and side load of 40% and 25%, respectively, of that vertical load.

The forces obtained from the above mentioned load cases are expected to be bigger than the forces that are present in the actual situation. This follows from the fact that the ground system is able to accurately synchronise with the aircraft and de-crabbing is not required. Therefore especially the lateral forces on the aircraft will be significantly overestimated.

Additional to these load cases specified in the CS-25 regulations, the loads during acceleration and deceleration on the runway should also be taken into account. For these situations it is assumed that there are no vertical accelerations present in these situations. Therefore, the maximum vertical load is equal to 1.1 times

the weight of the aircraft to have a conservative vertical load. The acceleration and deceleration force on the platform are determined from the maximum accelerations and decelerations, the thrust and the drag in those procedures using Equation 7.3 based on Figure 7.15. The lateral forces in these situations are also minimal and therefore neglected.

$$F_{x_{platform}} = m_{aircraft} \cdot a_{x_{max}} - T_{x_{aircraft}} + D_{x_{aircraft}} \quad (7.3)$$

7.3.2. Reaction Forces

The axial reaction forces that have to be delivered by the actuators are the first step in sizing the actuators for the Stewart platform. In order to calculate the axial forces that the actuators have to deliver for an input force and moment at a certain position and orientation of the platform, a Python program was developed.

The first step in calculating the reaction forces is to define the configuration of the Stewart platform. That is to say where will the actuators connect on the base (b) and where will they connect on the platform (p). To simplify the iterative process of configuration optimisation where force requirements of the actuators was minimised, the team decided to position the 6 connection points per platform in a virtual circle. Using the dimensions of the landing gear positions of the reference aircraft from [3], basic geometry, and a safety factor the virtual radius of the platform and base were estimated. Now the location of the connection points on the two virtual circles (base and platform) could be easily modified to end up with a more optimal actuator configuration which takes less force per actuator.

In order to calculate the reaction forces at different positions and orientations of the platform relative to the base, the vectors along the actuators pointing from the platform to the base needed to be found. To calculate these vectors we need to know the coordinates of the base connection points and platform connection points in one and the same coordinate system. There is relative movement between the platform and the base. The connection points on the base are not moving with respect to the base and the connection points on the platform are not moving with respect to the platform. It was decided to express all coordinates in terms of the platform coordinate system, $(x, y, z)^p$, as in Figure 7.4 to find the actuator reaction forces. The coordinates of the connection points were found expressed in the local coordinate systems as in Figure 7.4 at a certain radius and a specific angle. The centres of the virtual circles are taken as the origin of the coordinate systems. The x and y coordinates of connection point i at angle θ_i could now be expressed as in Equation 7.4.

$$\begin{aligned} x_i &= r \times \cos(\theta_i) \\ y_i &= r \times \sin(\theta_i) \end{aligned} \quad (7.4)$$

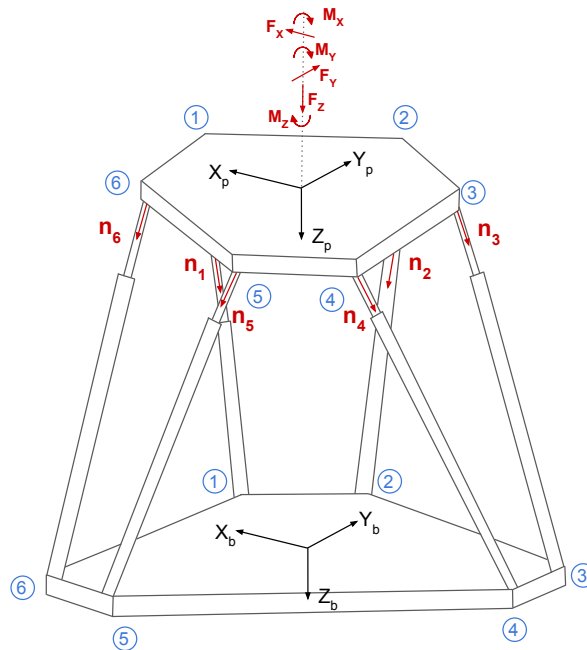


Figure 7.4: Loads on the Stewart platform.

The total transformation from the base coordinate system to the platform coordinate system consists of both a translation and a rotation. The relative position was seen as a translation. The position of the origin to the base relative to the origin of the platform was added to the original base coordinates according to Equation 7.5. Where $\vec{c}_{b_i}^{b'}$ is the vector pointing from the centre of the platform to the i th connection point on the base.

$$\vec{c}_{b_i}^{b'} = \vec{c}_{b_i}^b + \vec{O}_b^p \quad (7.5)$$

The orientation of the platform can be introduced by multiplication of three rotational transformation matrices. The orientation of the platform is expressed as a rotational transformation using the three Euler angles ϕ , θ , and ψ with respect to the orientation of the base platform. Expressing the platform's orientation as a 3-2-1 rotational transformation using the Euler angles results in Equation 7.6.

$$\begin{aligned} \mathbb{T}(\phi, \theta, \psi)_{pb} &= \left| \mathbb{T}_x(\phi) \mathbb{T}_y(\theta) \mathbb{T}_z(\psi) \right|_b \\ &= \begin{bmatrix} \cos \theta \cos \psi & \cos \theta \sin \psi & -\sin \theta \\ \sin \phi \sin \theta \cos \psi - \cos \phi \sin \psi & \sin \phi \sin \theta \sin \psi + \cos \phi \cos \psi & \sin \phi \cos \theta \\ \cos \phi \sin \theta \cos \psi + \sin \phi \sin \psi & \cos \phi \sin \theta \sin \psi - \sin \phi \cos \psi & \cos \phi \cos \theta \end{bmatrix} \end{aligned} \quad (7.6)$$

The coordinates of the base are now transformed by Equation 7.7.

$$\vec{c}_{b_i}^p = \mathbb{T}(\phi, \theta, \psi)_{pb} \cdot \vec{c}_{b_i}^{b'} \quad (7.7)$$

As the total transformation is both a translation and a rotation, both Equation 7.5 and Equation 7.7 have to be combined to find the coordinates of the connection points of the base in the coordinate system of the platform ($\vec{c}_{b_i}^p$).

Now that everything is defined in the same coordinate system, the vectors along each of the actuators can be found. These vectors are relevant as for the idealised Stewart platform the forces travel purely axially along these vectors. The vectors (\vec{d}_i^p) for every actuator from the connection point at the platform to the connection point at the base are found using Equation 7.8.

$$\vec{d}_i^p = \vec{c}_{b_i}^p - \vec{c}_{p_i}^p \quad (7.8)$$

The moments along the three axes caused by the actuators were found using the cross-product according to Equation 7.9. Where n_i is the unknown magnitude of the force in the actuator and \hat{d}_i^p is the normalised vector from Equation 7.8.

$$\vec{M}_i^p = \vec{c}_{p_i}^p \times (n_i \cdot \hat{d}_i^p) \quad (7.9)$$

Using the now known direction of the reaction forces and the moments they cause, a matrix can be constructed for the static equilibrium where Equation 7.10 holds. These are 6 equations, the 6 unknowns are the magnitude of the reaction forces along the actuators.

$$\sum F_x = \sum F_y = \sum F_z = \sum M_x = \sum M_y = \sum M_z = 0 \quad (7.10)$$

The matrix ($Ax = b$) that needs to be solved is presented in Equation 7.11 where everything is expressed in the p -frame. The rows of the A matrix are set up by taking the x , y , and z components of the directional vectors pointing to the base found by Equation 7.8 and the x , y , and z components of the moments caused per unit actuator force as a function of the magnitude of the force n_i as described by Equation 7.9. The x matrix is composed of the unknown magnitude of the forces in the actuators. The b matrix is composed of the 6 external loads introduced in the platform. Forces and moments due to gravity or accelerations in the base frame are introduced in a fixed direction in the base frame and have to be transformed to the platform coordinate system using the same logic as described before.

$$\begin{bmatrix} \hat{d}_{1_x}^p & \dots & \hat{d}_{6_x}^p \\ \hat{d}_{1_y}^p & \dots & \hat{d}_{6_y}^p \\ \hat{d}_{1_z}^p & \dots & \hat{d}_{6_z}^p \\ \vec{M}_{1_x}^p & \dots & \vec{M}_{6_x}^p \\ \vec{M}_{1_y}^p & \dots & \vec{M}_{6_y}^p \\ \vec{M}_{1_z}^p & \dots & \vec{M}_{6_z}^p \end{bmatrix} \begin{bmatrix} n_1 \\ n_2 \\ n_3 \\ n_4 \\ n_5 \\ n_6 \end{bmatrix} = - \begin{bmatrix} F_x^p \\ F_y^p \\ F_z^p \\ M_x^p \\ M_y^p \\ M_z^p \end{bmatrix} \quad (7.11)$$

If we know the 6 external loads that are introduced in the platform (F_x to M_z) and the orientation and position of the platform relative to the base the actuator forces at any platform orientation and position can be found. The magnitude of the actuator forces is found by Equation 7.12.

$$\begin{bmatrix} n_1 \\ n_2 \\ n_3 \\ n_4 \\ n_5 \\ n_6 \end{bmatrix} = - \begin{bmatrix} \hat{d}_{1,x}^p & \dots & \hat{d}_{6,x}^p \\ \hat{d}_{1,y}^p & \dots & \hat{d}_{6,y}^p \\ \hat{d}_{1,z}^p & \dots & \hat{d}_{6,z}^p \\ \vec{M}_{1,x}^p & \dots & \vec{M}_{6,x}^p \\ \vec{M}_{1,y}^p & \dots & \vec{M}_{6,y}^p \\ \vec{M}_{1,z}^p & \dots & \vec{M}_{6,z}^p \end{bmatrix}^{-1} \begin{bmatrix} F_x^p \\ F_y^p \\ F_z^p \\ M_x^p \\ M_y^p \\ M_z^p \end{bmatrix} \quad (7.12)$$

Verification and Validation

Verification and validation of the program that calculates the reaction forces was done in a few ways. The program was checked by giving inputs and checking the outputs halfway. The coordinate translations were easily checked. The coordinate rotations could be checked by performing some straightforward rotations around the axes of 180° and 360° and then checking the new coordinates. Also rotations of several other angles are verified manually. Values for which the system was known to be undetermined, such as a translation of $(0,0,0)$, were also given as inputs to see if the system was undetermined in the program as well. The sign and magnitude of the reaction forces were also checked to see they made sense. Are the actuators in tension or compression and which actuators are taking most of the load. Furthermore, the sums of forces in all directions were checked and found to be 0, according to what is expected. The verification that was done until this point was mainly focused on the model. Once the actual Stewart platform is build, tests should be performed to demonstrate that the system is able to meet the requirements.

Informal validation techniques that rely heavily on human reasoning without mathematical formalism was done [56]. Using face validation, where experts judged whether the model and its results made sense based on their intuition. This validation took place during the development of the program and the intermediate results were discussed with Ir. G. Bufalari. Furthermore, face validation was done by team members responsible of the program. Whenever a team member felt something did not make sense with the intermediate results he searched for the possible convention error or sign error. Coordinate system convention errors are easily made when working with multiple coordinate systems. Along the way of developing the force program, face validation played a substantial role in fixing errors. The program was also compared to literature articles that describe the Stewart platform in detail.

7.3.3. Maximum Reaction Forces and Platform Configuration

Now the reaction forces in the actuators can be determined for certain input forces, the maximum forces in every actuator need to be determined. The system should be able to carry the input forces identified in subsection 7.3.1 in several different platform positions. The most extreme platform conditions considered are a maximum roll angle of 5 degrees, a maximum pitch angle of 10 degrees and a maximum yaw angle of 10 degrees. A roll angle of 5 degrees follows from the minimum engine or wing tip clearance for conventional aircraft [44]. The maximum pitch angle of 10 degrees is based on the scraping angle of the A321 obtained from the technical drawings. The maximum yaw angle is found by assuming no side slip during landing in maximum crosswind conditions specified in CS-25 [2]. The regulations state a maximum 90 degrees cross wind of 37 km/h or $0.2 \cdot V_{SR0}$ whichever is greater, except that the wind velocity should not exceed 46 km/h . The maximum cross wind found is equal to 45 km/h and together with an approach speed of 300 km/h , a maximum yaw angle of 8.6 degrees is obtained. The yaw angle from the crosswind requirement is found by Equation 7.13. To have a conservative design, the system is designed for a maximum yaw angle of 10 degrees.

$$\psi = \sin^{-1} \left(\frac{V_{crosswind}}{V_{approach}} \right) \quad (7.13)$$

To find the maximum forces in every actuator, a python program was developed that loops through the possible different load case and platform position combinations. In the situation where the platform maintained a zero lateral and longitudinal position relative to the base, the maximum force in the actuators does not exceed 850 kN . Moving the platform in lateral direction significantly increases the maximum forces in the actuators

and should therefore be minimised. A lateral or longitudinal displacement of 1 *m* increases the maximum force to a value of 1369 *kN*. The design force per actuator can be found in the third column in Table 7.1.

The configuration of the Stewart Platform was optimised to obtain the lowest sum of maximum reaction forces in the actuators. The configuration can be found in Table 7.2 where the angles are taken around the positive *z* axis with 0° pointing in positive *x* direction. The radius of the circular platform and base equals 7.84 *m*.

The lengths of the actuators also needs to be determined. The magnitude of the vectors described in Equation 7.8 are used to find these values. Similar to determining the forces in the actuators, a python program was developed that loops through the different combinations of platform position and orientation with respect to the base. From these values the maximum and minimum lengths are determined and checked whether the actuator has a feasible extension ratio. If the actuator elongates more than 75% of its initial length, the extension ratio is said to be too large. If possible, the extension ratio is reduced by modifying the configuration of the Stewart platform. The maximum extension situation is a situation where a maximum lateral movement is combined with a maximum rotation and these situations should be taken into account in the control system. If the control system knows the limits of the workspace, it can for example exchange lateral displacement of the platform for lateral displacement of the cart on the base structure to reduce the required actuator elongation. The neutral lengths and stroke lengths of the actuators are shown in Table 7.1. A visualisation of the connection points on the platform and base are presented in Figure 7.5 and Figure 7.6 respectively.

Table 7.1: Stewart platform design.

| Actuator | Maximum force [kN] | Design force [kN] | Cross-sectional area [m ²] | Neutral length [m] | Stroke length [m] |
|----------|--------------------|-------------------|--|--------------------|-------------------|
| 1, 6 | 1369 | 1400 | 0.047 | 2.45 | 1.8 |
| 2, 5 | 1304 | 1400 | 0.047 | 3.94 | 2.7 |
| 3, 4 | 963 | 1000 | 0.033 | 2.11 | 1.5 |

Table 7.2: Configuration of the Stewart platform.

| Platform connection (c_{p_i}) | Angle [deg] | Base connection (c_{b_i}) | Angle [deg] |
|-----------------------------------|-------------|-------------------------------|-------------|
| 1, 6 | ± 5 | 1, 6 | ± 15 |
| 2, 5 | ± 150 | 2, 5 | ± 125 |
| 3, 4 | ± 160 | 3, 4 | ± 165 |

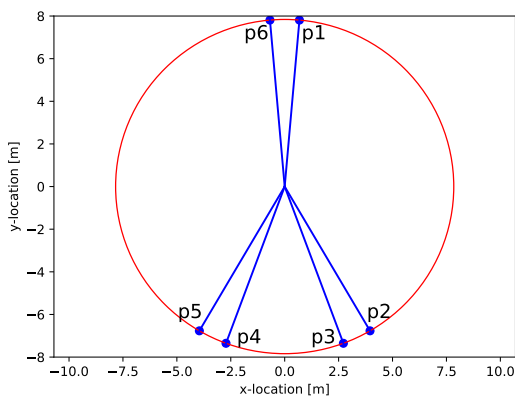


Figure 7.5: Connection points on the platform of the Stewart platform.

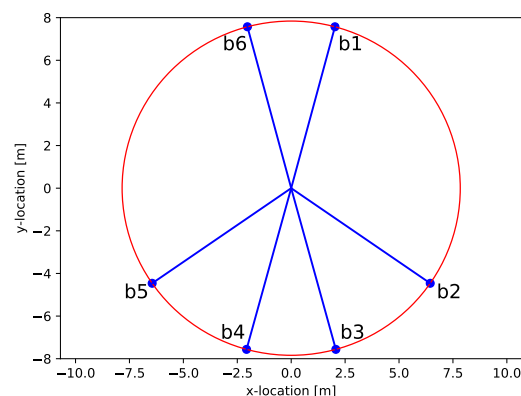


Figure 7.6: Connection points on the base of the Stewart platform.

7.3.4. Damping

The damping of the aircraft is completely done by the actuators in the Stewart platform. By removing the dampers from the landing gear of the aircraft, the weight of the landing gear is reduced and this is beneficial

for the performance of the aircraft. When the platform is positioned in the desired position for connection with the aircraft, the controls of the platform should be changed into damping controls. This means that the position of the platform is not constrained after touchdown of the aircraft. In that situation the deceleration of the aircraft has a higher priority than the position of the platform. The platform however should still be in its workspace and the maximum forces in the actuators cannot be exceeded. The damping concept is similar to damping of conventional aircraft. The actuators compress at a certain rate and eventually exert a maximum force to decelerate the aircraft. This maximum force exerted on the aircraft depends on the maximum allowable deceleration and therefore accelerometers should be installed to accurately monitor the deceleration of the aircraft. The force will be controlled by controlling the pressure inside the actuators using the servo valves.

7.3.5. Sizing the Actuators, Accumulators, and Reservoir

The next step in designing the Stewart platform is sizing the actuators, accumulators and oil reservoir. Using the design forces established in subsection 7.3.3 and the amount of bars the hydraulic system can deliver, the actuators can be sized.

From the design forces (F_{des}) for each actuator (i) as in Table 7.1 and the pressure (p) at which the oil can be pumped through the actuator, the minimal cross-section area of the actuator (A_i) can be determined according to Equation 7.14. According to Ir. G. Bufalari a pressure of 300 bar is a good starting value. The resulting cross-sectional areas are found in Table 7.1.

$$A_i = \frac{F_{des_i}}{p} \quad (7.14)$$

Now that the actuators are sized, the accumulators and oil reservoir can be sized. The speed at which the actuators move (v_a) determines the required oil flow rate per actuator (Q_i) according to Equation 7.15. According to Koekebakker, an actuator speed (v_a) of 1 ms^{-1} is a good starting value [67]. The resulting flow rates are relatively high and companies like MOOG could provide custom servo valves that are able to meet the high needs regarding flow rates at this pressure. The sum of the flow rates equals the total maximum flow rate that should be provided by the accumulators. According to Ir. G. Bufalari accumulators can provide very high flow rates and the flow rates are not the limiting factor in the design.

$$Q_i = A_i \cdot v_a \quad (7.15)$$

Using the required oil flow rate per actuator and the time that the actuators have to be active, the accumulators and oil reservoir can be sized. The total oil reservoir size and necessary accumulator oil volume (V_{oil}) required is determined by the maximum time (t) all the actuators need to move at a specific speed according to Equation 7.16. The time all actuators need to move at maximum velocity is estimated to be maximal 15 s. This estimate was made by looking at observations of aircraft landings in non-nominal conditions. Specifically looking at the stability of aircraft before de-crabbing, the team did not see any instance where the platform would have needed to synchronise for longer than 15 s. The resulting oil volume is a conservative value as in reality not all of the actuators will be moving continuously at the specified maximum speed for the full maximum time.

$$V_{oil} = \left(\sum_{i=1}^6 Q_i \right) \cdot t \quad (7.16)$$

The total required volume to be stored in the accumulators and the oil reservoir was found to be 3.8 m^3 each. This oil volume requires accumulators that can carry this amount of oil under pressure and an oil reservoir to store the oil after it has passed the actuators. The accumulators and the oil reservoir will be positioned in the middle of the Stewart platform where there is sufficient space. This space is not part of the workspace of the Stewart platform as the actuators do have a minimal extension above this space. The accumulators will be charged at the runway station which is further explained in section 7.9.

7.3.6. Mass

Now that all main parts of the Stewart platform have been sized the team can make a mass estimate of the Stewart system. The mass of

Table 7.3: Mass of the Stewart platform's main components

| Component | Mass [t] |
|---------------------|-------------|
| Platform | 5 |
| Base | 5 |
| 6 Actuators | 12 |
| Accumulators | 4 |
| Oil | 4 |
| Reservoir and hoses | 0.5 |
| Total | 30.5 |

the main components can be found in Table 7.3. The platform and base mass are estimated to be 5 tonnes each. According to Ir. G. Bufalari, Delft's Hexapod has a top platform with a mass of 13t. This platform is significantly oversized as the Hexapod is used for fatigue testing under large loads, in the REMALS the platform can be downsized to approximately 5t. The same train of logic can be followed for the base. The actuators of the Hexapod have a mass of 1750 kg each, but could have been 500 kg each had they not been designed for fatigue testing. Actuators for the REMALS can be estimated to weigh around 2t each or 12t in total. The accumulator weight is estimated from the maximum oil volume that needs to be stored. From Hydac's product catalogue the regular oil volume:accumulator weight ratio of a piston accumulator is 1:5, but this can be increased to 1:1 if the right material is used ⁴. Weight reduced hydraulic accumulators can be provided by Hydac on request. These accumulators weigh over 80 % less than equivalent carbon steel accumulators. The mass of the oil follows from the combination of the density of the hydraulic oil according to fluids by Bosch Rexroth ⁵ and the volume specified in subsection 7.3.5, a safety factor of 20 % is added for unforeseen circumstances. The mass of the reservoir needed to store the oil after it has passed the actuators and the hoses that carry the oil are estimated to weigh approximately 0.5 t.

7.4. Rotation Platform

As the runway can be used in two directions and the Stewart platform is optimised to be used in one direction, the Stewart platform itself should be 180° rotatable. The Stewart platform can not resist the same forces in all directions, thus it is made 180° rotatable by use of a slewing drive. This mechanism supports the rotating structure using a slewing bearing. A slewing bearing has characteristics that are very beneficial for the rotating structure. For example it is able to deal with high loads, has a low friction and can integrate power transmission for rotation ⁶.

Mass

The rotation platform does not have substantial mass as it is integrated into the base of the Stewart platform and the lateral movement structure. Nonetheless, it is assumed that the lateral movement platform and the rotation platform have a combined mass of 5000kg.

7.5. Lateral Movement Structure

During landing, an aircraft can experience a crosswind gust that blows the aircraft from the centre of the runway. Based on real life observations in non-nominal conditions, it was found that the system should be able to travel 4m from the centre in 1s and come to a halt before reaching the side of the rails. Further statistical research should be performed in order to support this. First of all it was assumed that the platform would travel this distance at constant acceleration. Equation 7.17 and Equation 7.18 can be used in order to find the required acceleration in order to travel 4m in 1s at constant acceleration.

$$V_{end} = \frac{2 \cdot distance}{t} \quad (7.17)$$

$$a = \frac{V_{end}}{t} \quad (7.18)$$

The mass that has to be accelerated by the lateral movement system is simply the sum of the rotation platform, the hexapod and the grid. The mass of the hexapod is 30500kg as is explained in section 7.3. The mass of the grid and the rotation platform combined with the lateral movement platform were assumed to be 5000kg each as in section 7.4. this results in a total mass of 40500kg. Next, a Python script was used to numerically integrate the acceleration to find the the velocity which was then integrated again to find the position. the following equations can be used for this integration. where V_{-1} and $distance_{-1}$ are the velocity and distance respectively of the previous time interval. Furthermore dt is the length of the time interval and a is simply the constant acceleration.

$$V = V_{-1} + a \cdot dt \quad (7.19)$$

$$distance = distance_{-1} + V \cdot dt \quad (7.20)$$

⁴URL: <https://m.hydac.com/fileadmin/pdb/pdf/PRO000000000000000000000030000050011.pdf> [Accessed 17 June 2019]

⁵URL: <https://www.boschrexroth.com/en/xc/products/product-support/hydraulic-fluids/index> [Accessed 17 June 2019]

⁶URL: <https://www.skf.com/group/products/bearings-units-housings/slewing-bearings/index.html> [Accessed 17 June 2019]

Since there is a constant acceleration and mass, there is a constant acceleration, there is a constant force since $F = m \cdot a$. Based on this force and velocity at every instance, the power required can be calculated at every instance since $P = F \cdot V$. All of this was repeated in a loop until the cart travelled the required $4m$.

Once, the cart has reached this distance, it needs to slow down again with the aircraft attached to it before reaching the maximum lateral distance. Since the aircraft is attached, the mass that needs to be decelerated is equal to the mass before combined with the aircraft mass of $97000kg$. This results in a total mass of $137500kg$. The width of the lateral movement platform is $12m$ and the width of the rail is $30m$. based on these values the remaining distance to slow down can be calculated using the following equation.

$$distance_{rem} = \frac{width_{rails} - width_{platform}}{2} - distance_{covered} \quad (7.21)$$

This resulted in a remaining distance of $5m$ to slow down. It is decided that the platform slows down with constant deceleration. Based on this the average velocity and thus the time required could easily be found. The average velocity is simply half the end velocity of the acceleration since the final velocity will be zero. the time required then simply follows from $t = \frac{distance_{rem}}{V_{avg}}$. Next, the required acceleration can be calculated since $a = \frac{\Delta V}{t}$ where ΔV is simply the end velocity of the acceleration. Based on these values, numerical integration could be performed again similar to the acceleration part until the the lateral velocity is equal to zero. The power was calculated at every instance again with the constant force due to the constant acceleration. The results were plotted against the time. Figure 7.7 shows the distance the platform has travelled, the velocity and the power required versus the time. From this it is clear that the required power from the motor is equal to $2.6MW$. Nevertheless, the motor by itself is not strong enough to slow the system down since the energy would have to be regenerated at $7MW$.

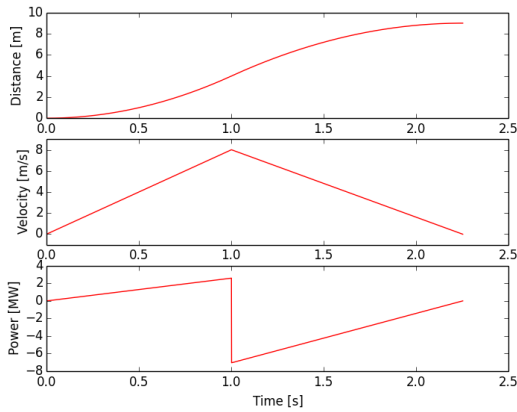


Figure 7.7: Distance covered, velocity and power vs. time during lateral movement.

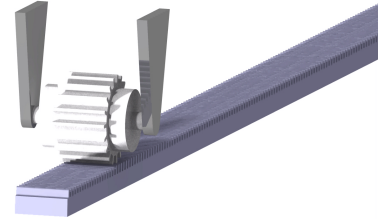


Figure 7.8: Lateral movement system used by the platform to synchronise with aircraft.

In order to slow the the structure down, mechanical friction brakes will have to be used in addition to the motor. It is decided that these brakes should be able to slow the structure down by them selves in case the motor fails. This means that they should be able to deliver a braking force of $880kN$ which is required since $F = m \cdot a$.

The platform will move in lateral direction by a gear that is connected to platform and powered by a motor that rolls over a gear rack on the base structure as can be seen in Figure 7.8. The $2.6MW$ motor was sized using the same method as in Equation 7.8.1. A 2 pole motor was chosen, the shear stress on the rotor is $44000kN/m^2$ and a grid frequency of $50Hz$ as is usual in Europe. The material of the rotor is decided to be copper; This resulted in a rotor mass of almost $1700kg$.

7.5.1. Verification and validation

The lateral movement system was verified by changing the input variables of the algorithm. These include the time required, the distance travelled, the masses and the width of the rails and the platform. All these

parameters are changed one by one and the outcome is checked. Every time, the expected outcome was found. For example, increasing the time limit to move the desired distance lowered the power required as did lowering the desired distance and lowering the masses. Furthermore, increasing the width of the rail decreases the power required to brake as is expected.

7.6. Base Structure

In order to support the actuator system with the platform and the aircraft under acceleration, a sufficiently strong structure needs to be designed. Besides the obvious goal of distributing stresses in a manner that prevents failing of the structure, the necessity of moving the platform limits the amount of bending that can take place. Therefore, it was decided that a maximum of 15cm of displacement is allowed over the structure. Finally, since this structure is accelerated along with the aircraft, the mass should be kept within bounds.

As a starting point, a preliminary design of the structure is made. A slight arch is chosen, since this enables the axles to carry some of the loads in tension, instead of having beams under pure bending. This structure was modelled in MatrixFrame, software that uses systems of basic beam deflection equations to analyse a frame. Naturally, the software was verified by checking the load distributions of simple loaded beams with manual calculations. The Von Mises stresses were also checked.

Both the weight and the inertial forces are modeled as evenly distributed over the three parallel bars, as can be seen in Figure 7.9 and 7.10. It was found that the inertia and weight forces are so large that forces due to crosswind have a negligible influence on this structure. The electric propulsion was modeled as two reaction forces in longitudinal direction. This gives the benefit of an extra verification step: the reaction forces should be equal in case of equal loading and they should add up to the total inertial forces.

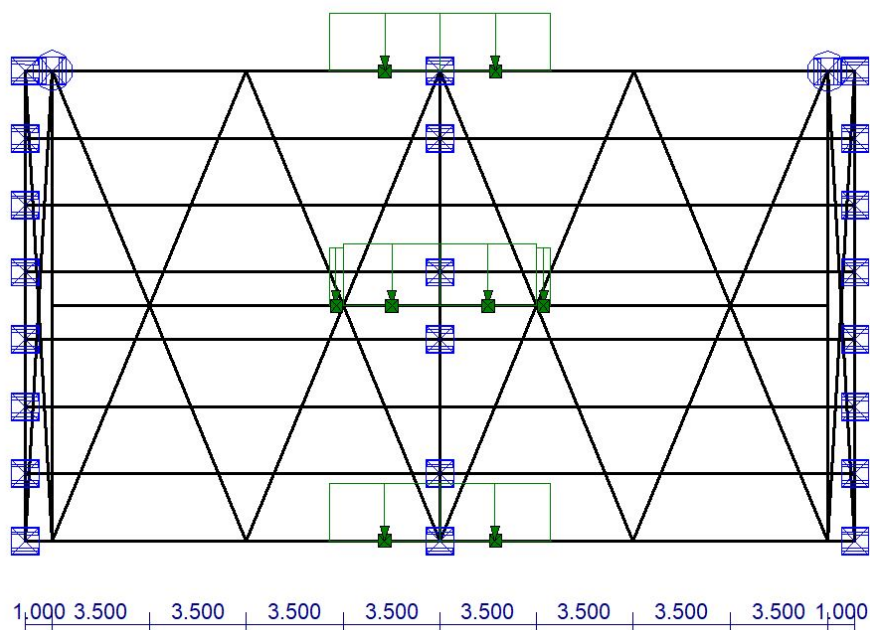


Figure 7.9: Top View of base.

Using this MatrixFrame model, the cross-sections of the various beams can easily be changed until a satisfactory result is obtained for the relevant forces. The mass of the structure is then found using

$$m = \Sigma A \cdot L \cdot \rho \quad (7.22)$$

The main driver for the cross-section designs is the deflection in bending. To keep the deflection within the previously set bounds, it is found that a mass upward of $3.6 \times 10^5 \text{ kg}$ would be needed. It was then tested what the effect of placing wheels in the middle is. Since airport modifications in the middle of the runway would interfere with conventional aircraft too much, these middle wheels will not have a rail but only give a reaction force in vertical direction. This addition to the concept shifted the design driver from deflection to

stress. In order to comply with requirement NCL-Sh110-Sys01, stating that the system should not fail due to fatigue within 35 years, the stress should be kept under the fatigue limit. For this reason, steel was chosen as a material for the structure since steel, in contrast with aluminium, has a clear fatigue limit, typically around 50% of the ultimate strength [12]. Since AISI 1090 Carbon Steel, with an ultimate strength of 696 MPa⁷, will be used for the structure for its high specific strength, stresses should be kept below roughly 350 MPa. It was found that this requirement is met with a structure of approximately 1.0×10^5 kg.

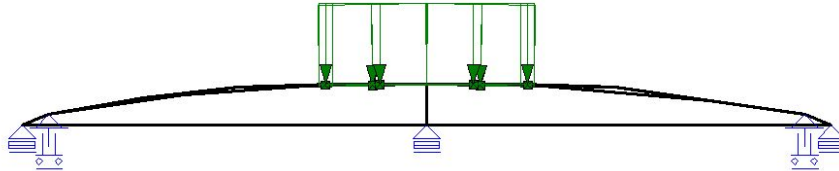


Figure 7.10: Front view of base.

7.7. Rails and Wheels Structure

In order to design a rail and wheels combination for this system, first an investigation was done into train rails and wheels. However, it was found that the design drivers for trains are quite different from a rail system that supports an aircraft on a runway. Conventional trains use solid axles, making the wheels on both sides turn at the same velocity. This is a cheap solution when power and braking need to be applied to the wheels. Turns and lateral stability are accommodated by the fact that the wheels have a conical shape. [64]

The rails required for supporting an aircraft, on the other hand, require significantly higher lateral reaction forces and stability. The system is also pulled forward by the linear induction motors; no torque is applied to the axle. Additionally, by not having the axles rotate, they can be used to carry some shear loads, which is very useful with a cart of 30m wide. A final small advantage of stationary axles that is worth mentioning is the fact that rotating eight 30m long axles would require quite some energy. The decision is therefore made to deviate from regular train concepts to a system with a stationary axle and bearings that is more similar to a roller coaster design, in that it has additional wheels for better support in lateral direction.

In normal railways, sleepers are used to distribute loads underneath the rail and simplify keeping the spacing between the rails even. They do however introduce new bending stresses and vibrations when the wheel load is between two sleepers. The rail spacing of 30m, in conjunction with the short distance that has to be covered (so less difficulty keeping the spacing right) led to the decision to leave the sleepers out. Due to the lack of the previously mentioned bending stresses, the axle load is set equal to the axle load of the Fortescue railway, which features the heaviest axle load in the world. ⁸ This assumed axle load of 40 tonnes implies a configuration with 8 axles, also assuming a dynamic load factor of 3. A diameter of 1.1m is chosen since this is the largest diameter in use in train wheels[64], providing the largest contact patch for a given wheel width, thus minimising contact stresses.

Since the contact area of the wheels with the rail is very hard to predict analytically, the system is analysed by the finite element method using Comsol MultiPhysics. A piece of concrete with embedded rail and a single main wheel with corresponding small wheels for lateral stability is modeled and meshed using a fine free tetrahedral mesh. Dirichlet boundary conditions are set on the outer boundaries of the concrete. Appropriate contact conditions are also set for elements that touch under load. The vertical load in combination with the 25% side load mentioned in CS25.479(d)(2)(i), evenly distributed over all wheels and with an applied safety factor of 50%, are applied to the axle. The system is then analysed using Equation 7.23.

$$-\nabla \cdot \sigma = F \cdot v \quad (7.23)$$

Since the loading frequency of the rails and wheels is very high, longevity of the components is a big concern in the design. Therefore, just as for the base structure, the design goal is to keep stresses under the fatigue

⁷URL: <https://www.azom.com/article.aspx?ArticleID=6560> [Accessed 18 May 2019]

⁸URL: <https://web.archive.org/web/20100628060821/http://www.fmgil.com.au/IRM/ShowStaticCategory.aspx?CategoryID=213&HideTopLine=True> [Accessed 23 June 2019]

limit. The results can be seen in Figure 7.11, 7.13 and 7.12. As can be seen, the stresses are significantly below the fatigue limit of steel, at around 27% of the yield stress of B6 steel of 585MPa

Since the rail is partially cast in concrete, this is the most labour-intensive and expensive component to replace. To minimise wear, a combination of R350HT steel for the rails and B6 wheel steel is chosen.[50] Both steels are hard. This increases their resistance to abrasive wear. To achieve minimum wear on the rail, wheel wear should also be minimised, as deterioration of the tire profile causes additional damage to the rails.

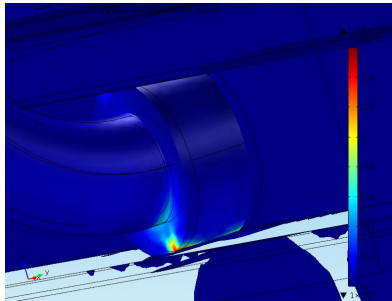


Figure 7.11: FEM analysis of an assisting wheel.

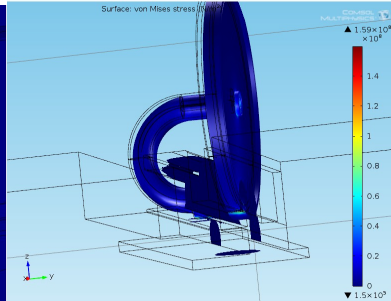


Figure 7.12: FEM analysis of the wheel's contact patch.

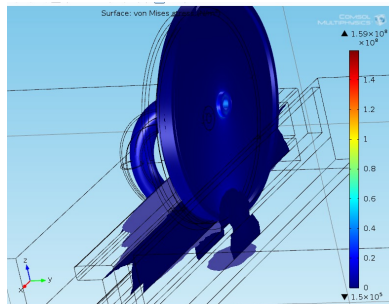


Figure 7.13: FEM analysis of the main wheel.

7.8. Power

In this section the power systems of the REMALS will be discussed. In subsection 7.8.1 the electromagnetic launch system will be analysed. In subsection 7.8.2 the power supply from the electricity grid is described. And finally, in subsection 7.8.3 the power supply to the ground vehicle is discussed.

7.8.1. EMALS

To propel the aircraft along the rails a similar power source is utilised as for the Electromagnetic launch system on aircraft carrier (EMALS). First the general characteristics of this power system were researched: It consists of a Linear induction motor, flywheel and cycloconverter, the electrical block diagram of this system is shown in Figure 7.14. The system is designed such that it can power three runways at the same time, to optimise the use of the kinetic recovery system that becomes activated during deceleration. This is the maximum amount of runways that is in use at Schiphol at the same time. Often a runway is only used for take-off or landing and thus making the power system for multiple runways can combine the the gain from one system and usage of the other. Then the system was designed for two runways being used for take-off and one for landing during peak hours as this results in the highest energy requirement.

Linear motors are known for the fact that they can produce a constant tow force, and the maximum force current linear induction motors deliver is approximately 1 MN. To have an estimation of the amount of energy that was necessary to power the system a preliminary python program was written that estimated the obtainable accelerations given a constant force and mass of the aircraft and mass of the ground based system. The obtainable accelerations determined the time and energy necessary for the procedures, Equation 7.24 till Equation 7.31 were used, together with Figure 7.15. Loops were implemented in the program such that the

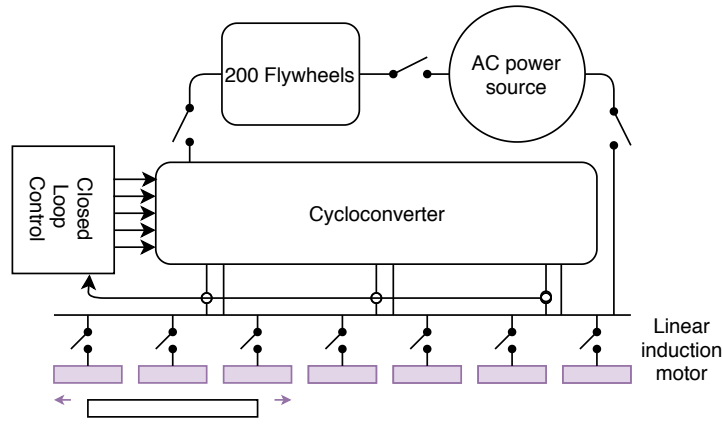


Figure 7.14: Electrical block diagram of the propulsion system of the ground based structure

force delivered by the motor during take-off was reduced until the procedure finished within the 3300 m with a safety margin of 10% with a take-off velocity as required by the noise. During landing the approach speed was calculated with this force such that the acceleration of the cart, connection phase and deceleration of the aircraft and cart fit within the 3300 m including safety factor. To calculate the acceleration, it had to be taken into account that the drag increases with the increasing velocity. This phenomena can clearly be seen in Figure 7.18 and Figure 7.19.

$$D_{fric} = m \cdot C_{d_{wheels}} \quad (7.24) \quad D_{ac} = \frac{1}{2} \rho V^2 S C_{d_{ac}} \quad (7.25) \quad D_{gbs} = \frac{1}{2} \rho V^2 A C_{d_{gbs}} \quad (7.26)$$

$$a = \frac{T + F_{emals} - D_{fric} - D_{ac} - D_{gbs}}{m_{tot}} \quad (7.27)$$

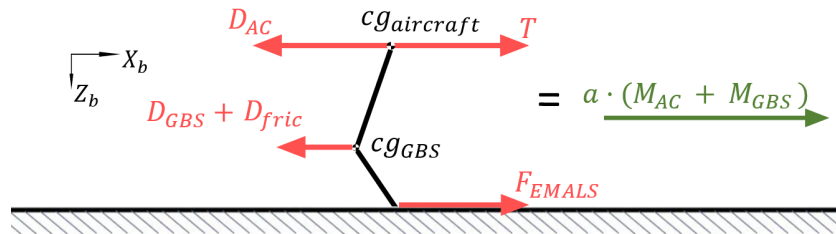


Figure 7.15: Free Body Diagram for ground based vehicle and aircraft.

The maximum acceleration and deceleration of the ground based system is limited and determined by $F = m \cdot a$. Additionally, there are limitations on the maximum acceleration and deceleration that human are able to deal with comfortably. The maximum acceleration is 1 g in longitudinal direction. Deceleration is limited to 0.4g as the seat belts are currently not designed to keep people pushed against there back of their seat. It is an unwanted effect that people fall against the seat in front of them, and as the changes to conventional aircraft are preferably limited, not the whole seat will be redesigned to implement a different seat belt. To give people time to brace against accelerations and deceleration, a gradient of one second is implemented for all changes in accelerations.

One time use mechanical brakes are in place in case of an emergency. However there is also a generator placed on the airport in case there is a power cut. When performing an emergency brake, the aircraft can brake more heavily as currently the 0.4g limit is applied for passenger comfort, not due to limitations of the system itself. Next to this, the runway is programmed such that exit velocity is reached at 90% of the total runway distance, this means that there is an additional 330 m is available to brake till the acceptable velocity. All these factors mean that the aircraft will come to a stand still in time.

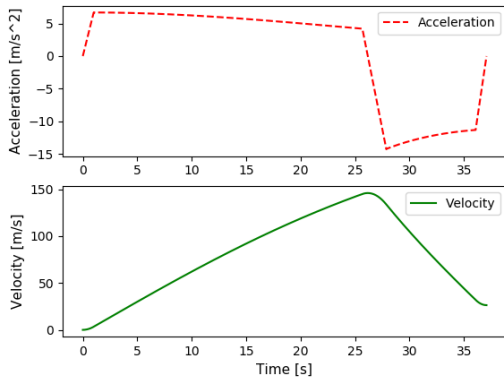


Figure 7.16: Acceleration and velocity profile during take-off.

$$dv = a \cdot dt \quad (7.28)$$

$$P = F \cdot V \quad (7.30)$$

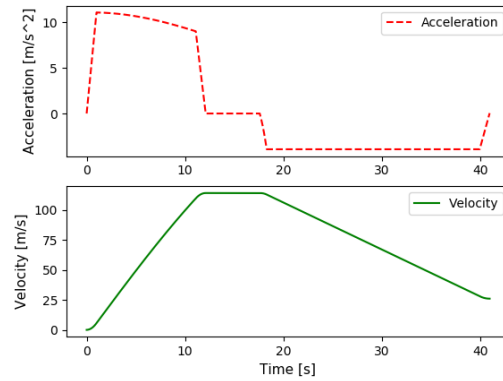


Figure 7.17: Acceleration and velocity profile during landing.

$$ds = v \cdot dt \quad (7.29)$$

$$E = P \cdot t \quad (7.31)$$

Table 7.4: Parameters python program

| Input parameters | Quantity | Unit |
|--|--------------------|---------|
| V_{to} | 145 | m/s |
| Max allowable acceleration a/c | 9.81 (1g) | m/s^2 |
| Max allowable deceleration a/c | $0.4 \cdot g$ | m/s^2 |
| Force LIM | 1000000 | N |
| Mass aircraft | 97000 | kg |
| Mass ground-based system (bars, platform, secondary) | 128000 | kg |
| μ_{wheels} | 0.02 ^a | - |
| Cd_{gbs} | 1.2 [37] | - |
| Cd_{ac} | 0.062 [41] | - |
| S_{ac} | 122.4 [3] | m^2 |
| A_{gbs} | 30 [37] | m^2 |
| t_{syn} | 6.5 [23] | s |
| Thrust | $2 \cdot 43420.91$ | N |
| Runway length | $3300 \cdot 0.9$ | m |
| N_{carts} | 5 | - |

^aURL: https://www.engineeringtoolbox.com/rolling-friction-resistance-d_1303.html [Accessed 12 June 2019]

| Output parameter | Quantity | Unit |
|-----------------------|----------|---------|
| $V_{approach}$ | 110 | m/s |
| $V_{decision}$ | 117.9 | m/s |
| V_{min} | 83.2 | m/s |
| $P_{acc_{alc}}$ (max) | 207.96 | MW |
| $P_{acc_{gbs}}$ (max) | 162.00 | MW |
| $P_{dec_{alc}}$ (max) | 162.00 | MW |
| $P_{dec_{gbs}}$ (max) | 207.96 | MW |
| $E_{acc_{alc}}$ | 2900.51 | MJ |
| $E_{acc_{gbs}}$ | 1905.22 | MJ |
| $E_{dec_{alc}}$ | 2313.01 | MJ |
| $E_{dec_{gbs}}$ | 1330.16 | MJ |
| $E_{acc_{carts}}$ | 2504.61 | MJ |
| $E_{dec_{carts}}$ | 2192.43 | MJ |
| $F_{X_{connection}}$ | 562519.4 | N |
| t_{to} | 37.1 | s |
| t_{land} | 40.9 | s |
| v_{end} | 26 | m/s |
| acc_{max} | 6.69 | m/s^2 |
| dec_{max} | -3.87 | m/s^2 |
| Force LIM | 711000 | N |

Based on these values the flywheels and linear induction motor could be sized. It was taken into account that the power from the grid should be limited and preferably constant. To size the power necessary from the grid three factors had to be taken into account: The charging time of the flywheels, the maximum power necessary during the take-off procedure and the thrust generated by the aircraft itself. The engines of the aircraft need approximately 10 seconds till full throttle is achieved, this should be the case at the minimum take off velocity in case something goes wrong with the ground-based system. From the program, it was concluded that the minimum take-off speed is reached within the first 10 seconds of the procedure, thus the engines are turned on at the start. For this Equation 7.32 was used.

$$V_{min} = 1.3 \cdot \sqrt{\frac{W \cdot 2}{S \cdot \rho \cdot C_{Lmax}}} \quad (7.32)$$

Then the remaining power requirement has to be fulfilled by combining the flywheel power, and the direct

power provided from the grid. This was an iteration as the flywheel has to be charged during a certain period of time, and then the combination of the grid power plus the charged flywheel has to amount to the total energy requirement of the system.

Linear Induction Motor

Linear Induction Motors were chosen as they have little moving parts and thus little maintenance is needed. They are applied in systems where high velocities have to be obtained, such as the EMALS systems on aircraft carriers. These systems have a high accuracy due to the closed control loop with hall effect sensors. The system is capable of operating at a 1.05 peak-to-mean acceleration [66], due to the drag the acceleration varies more than that during the take off. It does mean however that the applied force can be precisely modified to achieve this accuracy. And in case of unforeseen circumstances during launch the system can account for this.

Working principle The single sided linear induction motor consists of two parts, a stator (primary) and rotor (secondary) as can be seen in Figure 7.18 and 7.19⁹. The short secondary will be the moving part in this configuration and pull the cart forward, as the primary has to be powered to create a magnetic field. Moving the primary would create the problem of having to energise coils that are being accelerated up to almost 2g's [7].

The primary of a LIM is a steel plate with slots, through these slots 3-phase copper windings are laid that produce a linearly moving magnetic field. The secondary in this configuration is an aluminium sheet, this sheet completes the magnetic circuit and induces magnetic flux. This aluminium plate is backed by iron to create a return path for the magnetic flux. Because the aluminium plate is placed into a varying magnetic field an eddy current will be induced. These two magnetic fields repel each other and create a motion as the magnetic field moves through the aluminium plate.

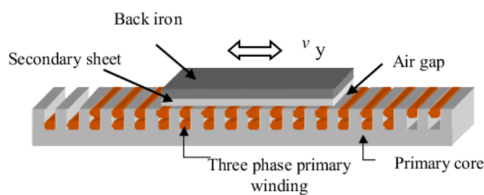


Figure 7.18: Representation of a linear induction motor [34]

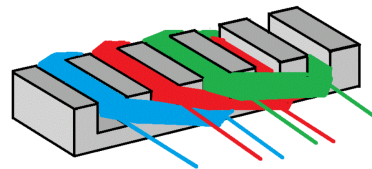


Figure 7.19: 3 phase windings

Design The secondary dimensions have to be calculated, this can be done based on the shear stress that is exerted by the linear induction. The shear stress induced in the aluminium plate is around the $100\text{ kN}/\text{m}^2$, as a force of 711 kN is applied this results in a plate area of 7.11 m^2 . The stator height is estimated to be around 1 meter as with the EMALS system [63], then the length of the secondary plate becomes 7.11 meter with the combined weight of aluminium and back iron.

As a rule of thumb these types of machines function with a magnetic flux density (B) of 0.9 to 1 Tesla. As the force that has to be induced is relatively high, a flux density of 1 T is chosen. Using Equation 7.33 this results in an current of 15 kA [63].

$$F = B \cdot l \cdot i \quad (7.33)$$

To be able to supply this current at a certain frequency at a certain voltage the stator is split up into sections. The stator sections will be longer at the outer ends of the tracks as there the velocity is lower, in the middle the stators will have to be shorter as the vehicle moving past them is faster and the frequency will have to alternate faster [63].

The thickness of the sheet determines the thermal conductivity, however if it gets thicker the efficiency of the motor decreases. The secondary is designed to be wider than the primary next to it, such that the current closes its path outside the active region. For this purpose the back iron is placed on the aluminium. It should also be longer than the pole pitch to minimise the end effect which occurs due to the fact that the magnetic field will reach its end [6]. The current densities vary between 30 and $50\text{ A}/\text{mm}^2$ in the coils for the general systems.

The stator is positioned with an offset to the slit through which the aircraft is connected to the secondary such that no contamination or rain can influence the coils. A drainage system is implemented, as to not hinder the secondary sliding through water [66].

⁹URL: https://en.wikipedia.org/wiki/Linear_induction_motor[Accessed 16 June 2019]

For designing the LIM in more detail, three professionals were contacted who all concluded that it was outside the scope of this project as it is an advanced electrical engineering problem. The weight of the secondary was estimated with the help of these people to be 2000 kg.

Control system

Hall effect sensors are used as positioning sensors in the system. A hall effect sensor consists of a thin strip of metal through which a current runs. When held perpendicular to a magnetic field, the electrons move to one side of the strip, this produces a measurable voltage gradient across the plate [39]. In the Electrical block diagram, Figure 7.14, they are presented as circles that give input to the control unit.

Flywheels

The system requires a significant amount of power, 578 MW to operate two take-off runways and one landing runway. In order to reduce the power required from the grid, flywheels will be installed. These flywheels can be 'loaded' with kinetic energy over a bigger time span and thus reducing the power requirements of the grid. Furthermore, energy from a landing aircraft that usually would be lost can be stored in the flywheels again to be used for the next take-off. As mentioned before, the limiting situation is when two take-offs and one landing are performed during one cycle. The interval between two consecutive take-offs or landings is usually 80 seconds. First, the total energy required per cycle can be calculated. This can be done by using the following formula.

$$E_{req} = \frac{2 \cdot E_{acc_{alc}} + E_{acc_{gbs}} + 3 \cdot E_{acc_{cart}} / N_{carts}}{\eta_{LIM} \cdot \eta_{motor}} \quad (7.34)$$

Here E_{req} is the required energy per cycle. The generator efficiency of the motor of the flywheel should actually be used here since that motor is used as a generator when the flywheel is providing energy, but the generator efficiency of a motor is approximately the same as its normal efficiency. These efficiencies are 0.5 [46] and 0.97¹⁰ respectively. It is normal that the efficiency of a linear motor is lower than the efficiency of a normal electric motor. Here E_{req} is the required energy per cycle and this results in an energy requirement 19 GJ per cycle when using the values for the energy required for acceleration from Table 7.4. The amount of carts that will be used in the system is explained in chapter 9. The regenerated energy per cycle from either the base structure braking after a take-off or the aircraft and the base structure braking after a landing can be calculated in a similar way.

$$E_{regen} = (2 \cdot E_{dec_{alc}} + E_{dec_{gbs}} + 3 \cdot E_{dec_{cart}} / N_{carts}) \cdot \eta_{LIM} \cdot \eta_{motor} \quad (7.35)$$

Using the same efficiencies as before, although the linear induction motor is used as a generator, results in 3 GJ of recovered energy per cycle. This means that a total of 16 GJ is required from the grid per cycle since this is simply the difference between the two. By making use of Equation 7.36 a power required from the grid of 200 MW can be found. This power is continuously supplied to the airport, and divided between charging the flywheels and powering the runways. When looking at the average power consumption of the Netherlands¹¹, 200 MW is 0.016% of this consumption and thus seems like a reasonable demand.

$$P_{grid} = \frac{E_{grid}}{t_{cycle}} \quad (7.36)$$

The maximum power from the flywheels can be calculated using the the following equation.

$$P_{FW_{max}} = \frac{2 \cdot P_{acc_{alc}} + P_{acc_{gbs}}}{\eta_{LIM}} - P_{grid} \quad (7.37)$$

This results in a maximum power required of 956 MW from the flywheels. In order to reduce the power requirement of the flywheels, it was decided to have 200 flywheels such that each flywheel only needs to provide 4.8 MW. In a similar way the energy that each flywheel has to contain is determined. It is decided that all the energy that is necessary for one cycle can be stored within the flywheels. This resulted in Equation 7.38 where N_{FW} is the number of flywheels. This resulted in an energy requirement of 95 MJ.

¹⁰ URL: https://library.e.abb.com/public/3e32bd0135a5443694abd2c64ffba74b/ABB_General_purpose_motors_catalog_LR.pdf?x-sign=jNRELDYSrO0ah9hAAobVtEqBsBwjAVXs4/jbgtGVK3Hss/u+V7NI70vyvUL8VaLr [Accessed 17 June 2019]

¹¹ URL: <https://www.worlddata.info/europe/netherlands/energy-consumption.php> [Accessed 28 June 2019]

$$E_{FW} = \frac{E_{req}}{N_{FW}} \quad (7.38)$$

The next step is to find the required mass moment of Inertia of the flywheel. This was done based on the energy requirement and a maximum angular velocity of a flywheel which was found to be around 3000 rad/s ¹². The following equation can be used to find the mass moment of Inertia.

$$I = \frac{2 \cdot E_{FW}}{\omega_{FW}} \quad (7.39)$$

It was decided that the flywheel will have the shape of a solid cylinder with a radius of 1.5 m . Based on this, the mass could be calculated based on Equation 7.40. Next the volume of the flywheel was determined. In order to do this, the material of the flywheel has to be selected. It is decided to use a carbon-fiber composite, which has a density of approximately 1550 kg/m^3 ¹³, since it can deal very well with the high angular velocities. Finally, the height of the flywheel can be determined using Equation 7.41. This results in a height of 5.15 m for the flywheel.

$$I = \frac{1}{2} \cdot m \cdot r^2 \quad (7.40) \quad V_{FW} = h \cdot r^2 \cdot \pi \quad (7.41)$$

Now that the flywheel itself has been sized, the motor/generator of the flywheel can be sized. Since the mass of a motor is mainly determined by the mass of its rotor, only the mass of the rotor is calculated. The motor of the flywheel needs to provide/generate 4.8 MW . Furthermore a grid frequency of 50 Hz is assumed since this is what is used in Europe and it is assumed that the motor has two poles. A shear stress of 44 kN/m^2 on the rotor is assumed [35]. The angular velocity of the motor can be found by using the following formula.

$$\omega_m [RPM] = \frac{60 \cdot f}{N_{poles}} \quad (7.42)$$

This results in a angular velocity of 1500 RPM which is equal to 157 rad/s . The volume of the rotor can be calculated with Equation 7.43 [35].

$$V = \frac{P_{FW_{max}}}{2 \cdot \omega_m \cdot F_d} \quad (7.43)$$

This results in a volume of 0.346 m^3 . Finally, in order to find the mass of the rotor, this volume can be multiplied by the density of copper which is the material rotors are typically made of. The density of copper is 8941 kg/m^3 ¹⁴. This results in a mass of 3090 kg for the rotor. The input variables with their values are summarised in Table 7.5. These input variables result in the outputs that are summarised in Table 7.6.

¹²URL: <https://sciencewriter.org/flywheels-spinning-into-control/> [Accessed 23 June 2019]

¹³URL: <https://www.clearwatercomposites.com/resources/properties-of-carbon-fiber/> [Accessed 23 June 2019]

¹⁴URL: https://www.amesweb.info/Materials/Density_of_Copper.aspx [Accessed 23 June 2019]

Table 7.5: Input parameters for the flywheel sizing.

| Input parameters | Quantity | Units |
|------------------|----------|----------|
| P_{max} | 578 | MW |
| t_{cycle} | 80 | s |
| $E_{acc_{alc}}$ | 2900.51 | MJ |
| $E_{acc_{gbs}}$ | 1905.22 | MJ |
| $E_{acc_{cart}}$ | 2500 | MJ |
| N_{carts} | 5 | - |
| η_{LIM} | 0.5 | - |
| η_{motor} | 0.97 | - |
| $E_{dec_{gbs}}$ | 1330.16 | MJ |
| $E_{dec_{alc}}$ | 2313.16 | MJ |
| $E_{dec_{cart}}$ | 2200 | MJ |
| $P_{acc_{alc}}$ | 207.96 | MW |
| $P_{acc_{gbs}}$ | 162 | MW |
| N_{FW} | 200 | - |
| ω_{FW} | 3000 | rad/s |
| r | 1.5 | m |
| N_{poles} | 2 | - |
| f | 50 | Hz |
| F_d | 44 | kN/m^2 |

Table 7.6: Output parameters for the flywheel sizing.

| Output parameters | Quantity | Units |
|-------------------|----------|---------|
| E_{req} | 19000 | MJ |
| E_{regen} | 3000 | MJ |
| E_{grid} | 16000 | MJ |
| P_{grid} | 200 | MW |
| $P_{FW_{max}}$ | 4.8 | MW |
| E_{FW} | 95 | MJ |
| I | 52000 | kgm^2 |
| m_{FW} | 56400 | kg |
| V_{FW} | 36.4 | m^3 |
| h | 5.15 | m |
| ω_m | 157 | rad/s |
| V_m | 0.346 | m^3 |
| m_m | 3090 | kg |

Cycloconverter

The cycloconverter links the flywheels to the Linear Induction motor, and converts a DC to DC with the correct frequency, voltage and ampere.

Verification and Validation

For this section several programs were written, first the general power program will be checked, next the flywheel sizing is looked at.

As a unit check it was tested that the acceleration would stay zero if the thrust and force delivered by the motor remains zero, this gave the expected results. As a subsystem check graphs were produced, in this way it could be verified that the program worked as expected. For example there are acceleration limitations set, these could clearly be viewed in the graph. The power and velocity graph over time also matched, which is as expected as constant force is applied by the motor and only the velocity is variable. Another check that was conducted is the influence on the drag force, the drag is supposed to increase with velocity, with the effect that less acceleration can be obtained. Thus is the drag coefficients or area's are increased, the slope of the acceleration would be more prominent. This was also visualised in a graph.

In order to verify the sizing of the flywheels, inputs were changed and outcomes were checked both half way and at the end. The first input variables that were changed are all the required and regenerated energy values, all of them were set equal to zero. This resulted in a power required from the grid of $0W$ and a mass and height of the flywheel of zero as is expected. Next, both efficiencies were changed to 1. as expected, A lot less energy was required and more energy could be regenerated. This decreased the power required from the grid drastically to $35MW$. If the efficiencies are changed to 0, no outcomes were found as this would divide by 0. Next, the take-off and landing interval was changed. As expected, when the interval is increased, the power required from the grid increased and vice versa. The maximum power required was changed as well. This only changed the size of the motor, but not from the flywheels as is expected from the equations. Finally the characteristics of the flywheels themselves were changed. These include the radius, maximum RPM and the density of the material. All of these influenced the results as expected. If the RPM is increased the flywheels become smaller. If the density is increased as well. The radius influences the mass moment of Inertia of the flywheels which influences the required mass as well.

As part of validation it was checked of the minimum take-off speed was comparable to that of the real aircraft. As this was around $80 m/s$ this made sense.

In order to validate the flywheels, it was checked how much energy large flywheels can typically store. These values vary between $3kWh$ and $133kWh$ [15]. Each flywheel used by the system would be storing $95MJ$ which is equal to $26.4kWh$ and is thus within a realistic range.

7.8.2. Electricity Grid

The flywheels require a set amount of power from the grid to charge within the given time period. This amounts to a total power requirement from the grid of 200 MW, this requirement is given to an energy supplier. A contract is in place which requires that all power delivered to Schiphol must be green¹⁵, the contracted supplier can see this as a opportunity to built more windmills in the North sea. To meet the power requirement about 50 new windmills are necessary, based on the current power that the windmills produce. This 200 MW does only have to be supplied during peak hours, thus when it is more quiet on the airport the power can be redirected a city. Another option is to store it in the generator that is present on Schiphol in case of emergency, and fully charge the flywheels for when full capacity is necessary.

7.8.3. Ground Vehicle Power Supply

There are multiple system on the base structure that require some power. In order to power these systems without using a battery, a similar system as in subways will be used. An additional rail will be installed on one side next to the wheels and a brush will be installed on the base structure that is in contact with the additional rail. The rail will be connected to the power grid and the different systems can be powered through the brush as can be seen in Figure 7.21. Figure 7.20 shows how the system works in more detail¹⁶. Additionally, a cable festoon system will be installed on the base structure to provide electricity to the moving lateral movement system.

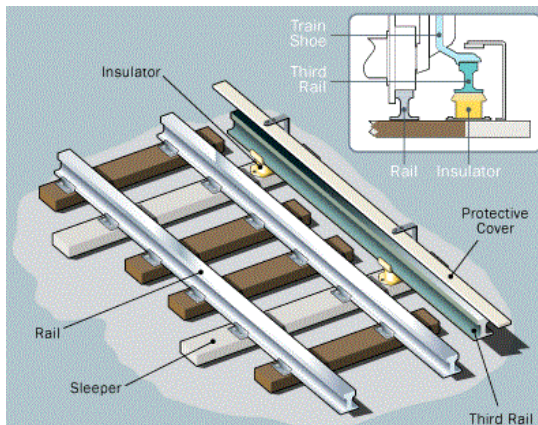


Figure 7.20: Power supply system used by subways.

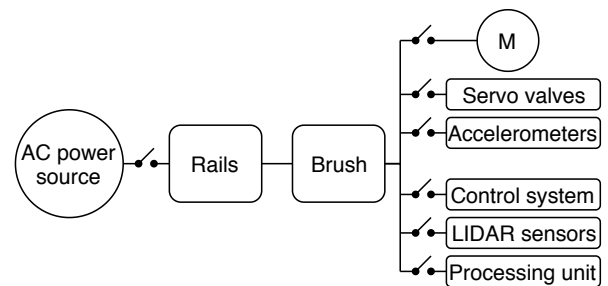


Figure 7.21: Electrical block diagram of the ground based structure.

7.9. Runway Station

At the end of each runway there is a runway station equipped with accumulator charging station to recharge the Stewart platform and scissor lift to lower the grid down. In the next subsections these elements will be explained in further detail.

7.9.1. Accumulator Charging Station

The pistons of the Stewart platform require accumulators instead of pumps since they can have a much higher flow rate and thus increase the movability of the Stewart platform. Unfortunately, these accumulators need to be charged by pumps. The accumulator charging station is the unit where the accumulators are charged. Each ground vehicle is charged by 4 pumps when it is standing still. There will be 4 pump stations, each with 4 pumps, at each side of the runway. A more detailed description of this charging station can be found in section 8.4.

7.9.2. Scissor lift

Since the Stewart platform is relatively high, the grid will have to be lowered to taxi to the gate. This is done by the use of a lift. The lift platform is dug into the ground and lifts the taxi-cart to the same level as the aircraft's grid and is briefly shown in Figure 7.22. The lift platform is equipped with 6 pistons, 3 on each side and in

¹⁵<https://www.schiphol.nl/en/schiphol-group/page/100-percent-dutch-wind-power/> [Accessed 20 June 2019]

¹⁶URL: <https://s.hswstatic.com/gif/subway-track.gif> [Accessed 23 June 2019]

total can lift the mass of the aircraft and the mass of the grid. The lift platform has four levels and in order to lift the aircraft and the cart the force delivered by the pistons is equivalent to 4600000 N .

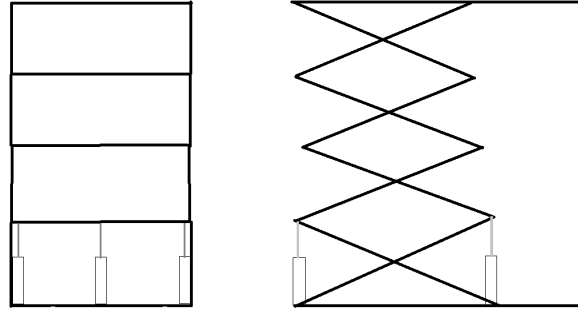


Figure 7.22: LSide and front view of lift platform

By knowing the number of pistons, the weight supported and reasonable working pressure of hydraulic cylinders (250 bar), the radius, the area and the volume of the pistons can be sized. The area is found from Equation 7.14

The total area needed is 0.22 m^2 therefore each piston has an area of 0.04 m^2 and a radius of 12 centimetres. Moreover, the platform need to reach an height of 6 meters, therefore after it has been decided that the lift platform needs 4 levels. The maximum extension of each piston is 1.5 meters using Equation 7.44.

$$l_{ext_{max}} = \frac{h_{max}}{\#levels} \quad (7.44)$$

The minimum extension of each piston is 0.85 meters assuming a piston elongation of factor e_p of 0.75 using Equation 7.45

$$l_{ext_{min}} = \frac{l_{ext_{max}}}{1 + e_p} \quad (7.45)$$

The volume can then be found by Equation 7.46

$$V = (l_{ext_{max}} - l_{ext_{min}}) \cdot A \quad (7.46)$$

Therefore the total volume is 118000 cm^3 . In order to move these pistons an hydraulic pump is used¹⁷ that is in the market and is able to move 270 cm^3/rev at 1450 RPM using a power of 177000 kW . The flow rate can be found by using Equation 7.47.

$$Q = [RPM] \cdot [cm^3/rev] \quad (7.47)$$

This turns out to be equal to 391500 cm^3/min . The time needed to move the lift platform up and down is found by Equation 7.48

$$t = \frac{V}{flowrate} \quad (7.48)$$

Plugging in the numbers the time required to move the platform up or done turns out to be equal to 18 seconds.

7.10. Taxi Cart

The taxi cart allows to transfer the grid from the Stewart platform and then allows to move the aircraft from the lift platform to the gate, therefore is a crucial element of the system. In the next subsections are described the general characteristics of the cart, the power requirements and the transfer system to move the aircraft on top.

¹⁷URL: <http://downloads.hawe.com/7/9/D7960E-en.pdf> [Accessed 14 June 2019]

7.10.1. Cart General Characteristics

The taxi cart has a rectangular shape that has the same width and length as the grid. Furthermore, it has 4 pairs of wheels, one at each extremity. The size of these wheels and configuration is similar to current aircraft's wheels, however shock absorbers and equipment needed to deploy is not present. This is because these wheels would not sustain substantial impacts and will be statically attached to the cart. Current wheels used on the A321 main landing gear have a dimension of 1270X455R22¹⁸, or in other words, 1270 millimetres in diameter, 455 millimetres in nominal section width, radial tire with 22 inches in rim size. By using current tires, costs can be decreased since the tires do not have to be specifically design for this application. The taxi cart is powered by a motor and a battery pack which have been designed in the next subsection. Furthermore, each taxi cart is able to communicate with ATC and other taxi carts. It is equipped with a Collision Avoidance System that enables them to avoid and/or stop in case of obstacles, and is able to be operated autonomously, more details will be given in chapter 9.

7.10.2. Cart Performance Sizing

The taxi cart requires a certain amount of power in order to perform the taxi procedures. The required power for the taxi cart was calculated using numerical integration similar to the method used previously. First of all, an acceleration profile and maximum acceleration are determined. A trapezoidal acceleration profile is used because this results in a smoother ride for the passengers since the force is gradually build up. The gradient of the acceleration was determined to be $0.1m/s^3$. In other words the acceleration increases $0.1m/s^2$ every second. the maximum acceleration was set on $0.05G$ which is equal to $0.49m/s^2$. The final taxi velocity is set to be $30km/h$ [47]. Finally, the mass had to be determined. This mass is the combined mass of the aircraft, the grid and the taxi platform. The aircraft's MTOW is $97000kg$, the mass of the grid was assumed to be $5000kg$ before and the mass of the taxi cart is assumed to be $15000kg$. This results in a total mass of $117000kg$.

For the numerical integration, the procedure was split up three parts. One with increasing acceleration, one with constant acceleration and one with decreasing acceleration. The following equations were used to calculate the velocity and power every instance.

$$V = V_{-1} + a \cdot dt \quad (7.49)$$

$$P = V \cdot (F_{friction} + m \cdot a) \quad (7.50)$$

Here the friction force was calculated multiplying the normal force with the friction coefficient which is 0.015 for tyres [23]. The acceleration depends on the part. The velocity, acceleration and power required were plotted versus time as can be seen in Figure 7.24.

The maximum power required during this procedure can be found to be $533kW$ Clearly, the decreasing acceleration at the end lowers the power requirement for the cart. More research could be performed in the future to see whether it is better to limit the power and calculate the according acceleration at a certain velocity. This could lower the power requirement significantly but might increase the time required to accelerate the cart.

Now that the power requirement is known, the motor of the taxi cart can be sized. For this, the same approach as Equation 7.8.1 can be used. A 4 pole motor is selected, furthermore the frequency of the grid and the shear stress on the rotor remain the same. This results in a rotor mass of $690kg$ in order to meet the $533kW$ requirement. In order to have a voltage requirement to size the battery, an existing motor was selected. This motor is the ABB NXR355MH4 that delivers $550kW$ at a voltage of $690V$ ¹⁹.

The final step is to size the battery of the taxi cart. This battery should be able to deliver a certain amount of energy and have a maximum power output. The battery should be able to deliver up to $570KW$ since the motor has an efficiency of approximately 0.965²⁰. The battery is made of Lithium-Ion cells of the model Samsung INR18650-15M²¹ that will be linked in series and parallel in order to meet the requirements. When cells are paired in series, the voltage is the sum of all the separate voltages but the current remains constant. When

¹⁸URL:https://www.bridgestone.com/products/speciality_tires/aircraft/products/applications/pdf/tire_applications.pdf [Accessed 18 June 2019]

¹⁹URL:https://library.e.abb.com/public/3e32bd0135a5443694abd2c64ffba74b/ABB_General_purpose_motors_catalog_LR.pdf?x-sign=jNRELDYSrO0ah9hAAobVtEqBsBwjAVXs4/jbgtGVK3Hss/u+V7NI70vvyUL8VaLr [Accessed 18 June 2019]

²⁰URL:https://library.e.abb.com/public/3e32bd0135a5443694abd2c64ffba74b/ABB_General_purpose_motors_catalog_LR.pdf?x-sign=jNRELDYSrO0ah9hAAobVtEqBsBwjAVXs4/jbgtGVK3Hss/u+V7NI70vvyUL8VaLr [Accessed 18 June 2019]

²¹URL:<https://www.batteryspace.com/prod-specs/9720.pdf> [Accessed 18 June 2019]

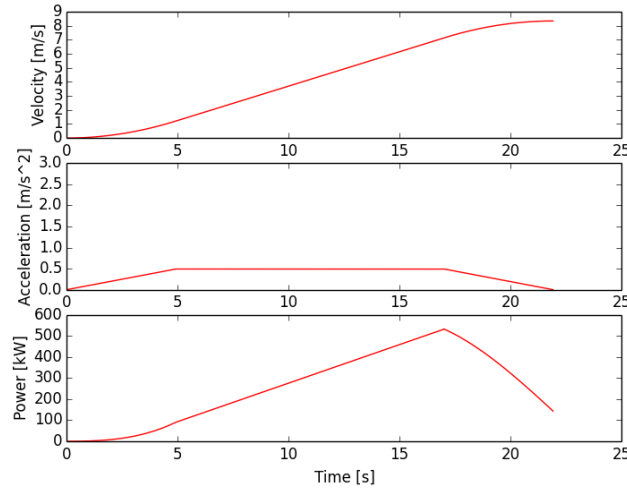


Figure 7.23: Velocity, acceleration and power required vs. time during the acceleration of a taxiing aircraft.

cells are paired in parallel on the other hand, The voltage remains the same, but the current is the sum of all the currents. First of all, the number of cells in series required for the voltage requirement is determined. This can be done by using the following equation.

$$N_{series} = \frac{V_{req}}{V_{cell}} \quad (7.51)$$

V_{req} is simply 690V and the cell that is selected can deliver 3.6V. This means that the batteries consists of series of 192 cells. The number of parallel series has to be determined for two separate requirements. Once for the required power and once for the required energy. The maximum number of parallel series of the two cases should be taken. In order to be able to size the battery pack for a required power output, the maximum discharge current of the cell should be known. For the selected cell this is 23A. Connecting cells in series does not affect the current, thus the maximum discharge current of each series is 23A. Combined with $P = V \cdot I$ the following equation can be found to calculate how many series should be coupled in parallel in order to meet the power requirement.

$$N_{rows} = \frac{P_{req}}{V_{series} \cdot I_{cell}} \quad (7.52)$$

The power requirement of 570kW and the voltage of 690V combined with the discharge current of 23A requires that at least 36 series should be linked in parallel in order to meet the power requirement.

In order to size the battery for the energy, it should first be known how much energy is required from the battery. In order to do this, a reference taxi procedure has to be set. it is decided that one such taxi procedure takes 20 minutes and that the taxi cart has to accelerate 5 times from 0 to 30km/h within this 20 minutes. The energy consumption during the acceleration process was found by numerical integration of the required power over time. The time required time to perform the 5 acceleration is then subtracted from the 20 minutes. The remaining time is multiplied by the required power to maintain a velocity of 30km/h which is the final value of the power required during the acceleration process. Combining these energies results in an energy requirement of 192MJ or 53kWh per taxi procedure. It was decided that the taxi cart should be able to perform 6 of these procedures before being recharged. This is the same as travelling 3 times from the gate to the runway and back.

Each cell has a discharge capacity of 1.5Ah. The discharge capacity of multiple cells in series is equal to the discharge capacity of one cell. This means that each series of 192 cells provides 1035Wh of the required 318000Wh. If the battery consists of 309 parallel series, it is capable of providing the taxi cart with enough energy. Since the energy requirement needs more parallel series than the power requirement, the energy requirement is limiting and thus the battery pack exists of of 309 parallel series that each consists of 192 cells. In total, almost 60000 cells are required for each battery pack and each cell has a mass of 45g. This results

in a total battery mass of approximately 2700kg. Figure 7.24 shows the electrical block diagram of the taxi cart including all the sensors and communication equipment that is required. Since the battery requires DC current and the grid provides AC current, a converter has to be used in order to charge the batteries.

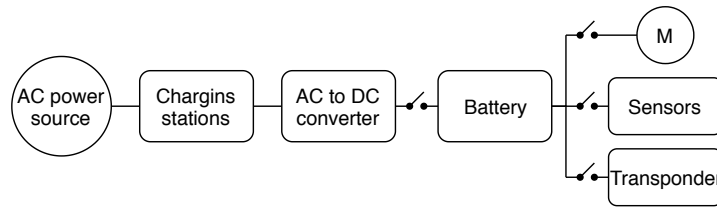


Figure 7.24: Electrical block diagram of the taxi platform

The cells have a charging time of 150 minutes. Since battery pack is able to perform 6 taxi procedures before the battery needs to be recharged, this charging time can be distributed over 3 ramp operations which is more than sufficient time. In case they would need to be recharged quicker, they can be quick charged within 40 minutes. Nonetheless, this is not optimal for the battery lifetime and should be avoided if possible.

7.10.3. Transfer System

Transfer Rails

The lateral movements are executed using a system similar to the one used on steel roller coaster. The wheel system is shown in Figure 7.25. The wheel system slides on top a circular cross-section. There are four wheel systems, one at each extremity of the cart. Each wheel system is composed of three pairs of wheels. Each pair of wheels has a different function: the first wheels on top of the rail are responsible for carrying the platform, the second types are mounted next to the rail and prevent the platform from falling off the track, the third type of wheels are there to reduce vibrations. When designing the wheels there are four elements to design for: low rolling resistance, high load endurance, smooth ride performance, and high durability to keep maintenance cost low.

The wheels are made of polyurethane which is a relatively soft material, reducing the vibrations and providing a smooth ride²². The wheels have a diameter of 0.3 meters and a circumference 0.942 meters or 0.00094 kilometres using the equation below:

$$circumference = 2\pi radius \quad (7.53)$$

The maximum velocity achieved is relative low, the maximum velocity is 10 km/h. The revolutions per minute of the wheels are therefore:

$$RPM = \left(\frac{velocity}{circumference} \right) / 60 \quad (7.54)$$

This translates into 91 RPM. The size of the roller coaster rails can be found by using [53]:

$$\tau = \frac{\frac{4}{3} V (R_o^3 - R_i^3)}{\pi (R_o^4 - R_i^4) (R_o - R_i)} \quad (7.55)$$

where τ is the ultimate shear stress of AISI 1090 Carbon Steel²³ and is equal to 696 MPa, while R_o and R_i are the outer and inner radius of the rail, V is the shear force applied on top due to the weight of the aircraft and grid and is approximately 1000 kN. The radius and thickness are unknown, however by running an optimisation script on Python that by trial-and-error optimise the two variables to find the best compromise between weight and occupied space, the radius and thickness are found and are 0.1 metres and 5 millimetres respectively.



Figure 7.25: Wheel system for lateral movements on the rail.

²²URL: <https://www.coaster101.com/2011/10/24/coasters-101-wheel-design/> [Accessed 5 June 2019]

²³URL: <https://www.azom.com/article.aspx?ArticleID=6560> [Accessed 18 May 2019]

Once the aircraft has shifted laterally, it needs to be fixed in position. This locking mechanism make use of the circular bar on which the roller-coaster's wheels slide. Once it reaches the desired position, it locks to the circular bar by lowering a set of pins that interlocks into holes in the circular bar. A representation is shown in Figure 7.26.

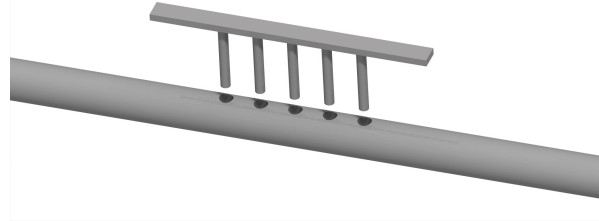


Figure 7.26: Lateral locking mechanism.

There are 4 set of 5 holes on the roller-coaster's bar of the take-off and landing platform and on the lift platform. The holes have a diameter of 4 centimetres. The pins penetrate the rod from side to side providing stability in lateral and longitudinal direction.

Transfer Belt

When the aircraft needs to get on and off, the Stewart platform is moved all the way to one side, thanks to the lateral movement system. Next, the transfer rail of the taxi cart and of the Stewart platform interlock. Then, the aircraft that is attached to the grid is transported on top of the taxi-cart, on top of the lift platform via a conveyor chain installed on the taxi cart. This conveyor chain is extended from the platform such that it can lock in between the aircraft's grid and the top of the Stewart platform. The aircraft moves onto the taxi-cart, sliding on the transfer rail. The load is supported by the rails at all times. This conveyor chain can use the motor and batteries of the taxi cart. A visualisation of the mechanism is shown in Figure 7.27.

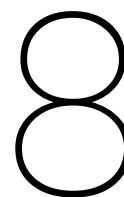


Figure 7.27: Conveyor chain for transferring the aircraft on the lift platform.

7.10.4. Verification and Validation

The power and battery sizing is verified by changing the input variables of the algorithms and checking the outcomes both halfway and at the end. In order to verify the power, first the masses were changed. As expected, this increases the power required to meet the requirements on velocity and acceleration. If the maximum acceleration is increased, the time required to reach the end velocity decreases and the power required increases. If the end velocity is increased on the other hand, the both the time required and the maximum power increase. In order to verify the battery sizing, input variables such as the voltage of a single cell, the voltage required, the maximum discharge current, required energy and required power were changed. It is checked how each of these parameters influences the battery pack. Increasing the energy required for example, increases the size of the battery pack since more parallel series are required. Each of these parameters changed the outcome of the battery pack as expected.

In order to validate the performance of the taxi cart, its required power was compared to the power required for electric taxiing based on literature. It was found that for a maximum taxi velocity of 10 m/s , 1.96 W/kg of electric power is required for taxiing [72]. For example, if the aircraft has a mass of $100 \cdot 10^3\text{ kg}$, it would require 200 kW of electrical power for taxiing. The total mass during taxiing is the MTOW of the aircraft and the mass of the taxi cart, this has a combined mass of 117000 kg . The power required for the taxi procedure according to the simulation is 533 kW . This is more than double the power that is found based on literature, but it is in the same order of magnitude.



REMALS Performance

In order to evaluate how REMALS performs on noise and fuel reduction, the flight profile for take-off and landing has been determined and is presented in section 8.1. Next, the noise reduction is elaborated on in section 8.2, followed by section 8.3 which describes the fuel reduction of the A321REMALS. Finally, the capacity changes of the airport in general are explained in section 8.4.

8.1. Flight Profile for Take-Off and Landing

The determination of the flight profile is closely related to one of the driving requirements of the system as stated in section 3.2:

NCL-Sh18: The system shall provide for a reduction of noise pollution of 7 ± 3 SEL dB in comparison to the current production of noise during the takeoff and landing procedure at Schiphol airport.

In order to fulfil this requirement, the procedure for taking off and landing has to be reconsidered. As explained in subsection 8.2.2, the noise metric used in this analysis (SEL: sound exposure level) does take both intensity as well as duration of the sound into account. Therefore, it is assumed that noise will be reduced if the system is capable of shortening the time of procedure (either to climb or to descend) while not exceeding the maximum peak noise that is currently generated.

The general idea to shorten the procedure, is to launch and approach with higher speeds than conventional aircraft. Since the runway distance is fixed at 3,300 m (section 3.1), this means that the system will have to be able to provide for a higher acceleration and deceleration to reach higher top speeds. The following subsections explain how the take-off (subsection 8.1.1) and landing (subsection 8.1.2) procedure are defined. Amongst the outputs of these sections are a height profile, velocity profile and thrust profile of the A321REMALS compared with the conventional A321NEO.

8.1.1. Take-Off Procedure

In order to reduce the production of noise during take-off, the concept is launched at significant higher speeds than conventional aircraft to climb faster to a certain altitude. As a result, it is expected that the duration of the sound is shortened, thus decreasing the sound exposure level for the procedure.

As a reference altitude, FL100 is chosen. This is in accordance with similar studies concerning the production of aircraft noise by a ground based powered system [27]. Below, the profile for both the conventional A321NEO and the concept are elaborated on.

Take-Off Procedure for the Conventional A321NEO

The current flight profile during take-off for the conventional A321NEO is based on the Aircraft Performance Summary Table provided by the Base of Aircraft Data (BADA)¹. The performance summary tables for take-off can be found in Appendix 15.2. It has to be noted that the Aircraft Performance Summary tables for the Airbus A321-131 are used, instead the A321NEO. The reason for this is that data for the A321NEO was not available.

¹URL: <https://badaext.eurocontrol.fr/> [retrieved on May 16, 2019]

The main difference between the A321-131 and the A321NEO is the weight of the aircraft and the type of engines used. The maximum take-off weight of the A321-131 equals 89,000 kg, whereas the maximum take-off weight of the A321NEO equals 97,000 kg. The Aircraft Performance Summary Tables provide climb data for low mass, medium mass and high mass. Since the mass of the aircraft used as a reference during this project (A321NEO) is higher than the A321-131, the data for high mass procedures is used, in order to resemble the actual flight profile of an A321NEO as much as possible.

Concerning the engine type, the A321-131 is equipped with two V2530-A5 engines, whereas the A321NEO uses two CFM LEAP 1A32/33 engines. With regards to maximum thrust, the CFM LEAP 1A32/33 is capable of providing a maximum thrust of 143 kN [26]. According to the Aircraft Performance Summary Tables, the maximum thrust for high mass climb is 143,301 N, which is reasonably close to 143 kN. Therefore, it is assumed that the performance of the engines is comparable. However, it has to be taken into account that parameters such as fuel flow are engine-specific. As a result, the absolute values for fuel flow are not representative for the actual A321NEO. However, the relative values for fuel flow differences between the conventional aircraft and the concept can be compared, since they are both based on the same assumptions.

In order to find the complete flight profile based on the data from the tables, first the data was converted to SI-units. Next, based on linear interpolation between the data points for each height (based on a time step of 0.1 s), the total height profile is obtained, as well as the velocity and thrust provided by the engines at each time instant. A graphical representation of these outputs is given in Figure 8.1, Figure 8.2, Figure 8.5 and Figure 8.6.

The increase in height and horizontal distance at each time instant is calculated using the rate of climb based on interpolation, the true airspeed and the theorem of Pythagoras, see Equation 8.1 and Equation 8.2.

$$dH = ROC \cdot dt \quad (8.1) \quad dX = \sqrt{V_{TAS}^2 - ROC^2} \cdot dt \quad (8.2)$$

In order to find the noise produced, the thrust setting has to be converted to a N1-setting, expressed in percentage of the maximum rotational speeds of the low pressure rotor (measured in rotations per minute, rpm) [26]. However, the relation between thrust provided (in Newtons) and the rotational speed of the low pressure rotor is not linear for jet engines: a 1 % change in RPM causes a 3.5 % change in thrust [36].

$$100 \cdot 0.965^x \% \text{ thrust} = 100 - x \% \text{ RPM}$$

This can be considered a rough assumption, but since actual data on the engine setting is lacking, this relation is used to relate the provided thrust to a preliminary N1-setting. The percentage change in thrust is defined as the thrust at a certain time instant divided by the maximum thrust provided by one engine (Equation 8.3). According to the Aircraft Performance Summary Tables, the maximum thrust is applied at sea level and equals 143,301 N. This corresponds with the engine data as provided by the manufacturer [26].

The relation between the change in thrust and the resulting change in RPM is summarised in Equation 8.4.

$$\%T = \frac{T \sim f(t)}{T_{max}} \cdot 100\% \quad (8.3) \quad 0.965^x = \frac{T \sim f(t)}{T_{max}} \Rightarrow x = \frac{\log \frac{T \sim f(t)}{\log T_{max}}}{\log 0.965} \quad (8.4)$$

Finally, it has to be noted that the Aircraft Performance Summary Tables do not account for a change in aircraft mass. However, due to the burning of fuel, this is not the case in reality. By linearly interpolating the fuel flow as function of the height, the amount of fuel (in [kg]) burned for each time step (0.1 s) can be found. When summing these values, it was found that a total mass of approximately 650 kg fuel is burned. When comparing this to the total mass of the aircraft (83,000 kg), it can be noted that the mass of the fuel used consists of less than 1% of the total aircraft mass. Therefore, it is assumed that during take-off the change of mass of the aircraft due to the burning of fuel is negligible, both for the A321NEO as for the A321REMAALS.

Take-Off Procedure for the A321REMAALS

For the A321REMAALS, the take-off trajectory looks different than for a conventional A321NEO. In order to shorten the procedure to decrease noise production, the aircraft is being sped up to high speeds in order to increase kinetic energy of the A321REMAALS. Next, kinetic energy is converted into potential energy using the energy height principle up until to the point where the velocity is optimal to climb, which is shown in Equation 8.5. From that moment on, the velocity profile of the conventional A321 is followed.

$$H + \frac{V^2}{2 \cdot g} = \text{constant} \Rightarrow 0 + \frac{V_{TO}^2}{2 \cdot g} = H + \frac{V_{opt}^2}{2 \cdot g} \quad (8.5)$$

During the first phase of the climb, the aircraft follows a circular trajectory, where the radius is calculated using Equation 8.6 and based on a maximum allowable acceleration of 1.4 g, which is based on interviews with experts in the field, including ir. P. C. Roling. In addition, the flight path angle is determined using Equation 8.7, where s equals the distance covered by the aircraft (based on the true airspeed at each time step).

$$R = \frac{V_{TAS}^2}{1.4 \cdot g} \quad (8.6) \quad \gamma = \frac{s}{R} \quad (8.7)$$

When using the energy height principle, it is assumed that the velocity only decreases due to the fact that kinetic energy is converted into potential energy. Thus, a decrease of velocity due to forces working in the opposite direction of the velocity will have to be countered by applying thrust from the moment of detaching. Both a drag force and a component of the aircraft weight are working along the body axis of the aircraft and will have to be countered by applying thrust, which is assumed to work in the same direction as the velocity. The total thrust is calculated according to Equation 8.8, where the drag coefficient is determined using Equation 8.9.

$$\begin{aligned} T &= 0.5 \cdot (D + \sin(\gamma) \cdot W_{alc,TO}) \\ &= 0.5 \cdot \left(C_D \cdot \frac{1}{2} \cdot \rho \cdot V_{TAS}^2 \cdot S + \sin(\gamma) \cdot W_{alc,TO} \right) \quad (8.8) \end{aligned} \quad C_D = C_{D0} + \frac{C_L^2}{\pi \cdot A \cdot e} \quad (8.9)$$

As can be seen in Equation 8.9, the drag coefficient is a function of lift coefficient. The lift coefficient is determined according to Equation 8.10, where a maximum load factor n of 1.4 is used. Furthermore, the density is calculated using the International Standard Atmosphere at every time step for the corresponding height.

$$L = n \cdot W_{alc,TO} \quad C_L = \frac{2 \cdot n \cdot W_{alc,TO}}{\rho \cdot V_{TAS}^2 \cdot S} \quad (8.10)$$

However, if the above equations would be used to determine the flight profile during take-off, one will encounter the problem that the flight path angle will increase up to almost 40 degrees. This is due to the fact that the true airspeed decreases, thus decreasing the radius of the turn (Equation 8.6). As a result, the flight path angle keeps increasing every time step (Equation 8.7) and the thrust will overshoot the maximum thrust available (143 kN per engine), due to the weight component of the aircraft which is dependent on the flight path angle.

Therefore, based on the maximum thrust available, a limit has to be posed on the flight path angle. If according to Equation 8.8, the thrust exceeds 143 kN, the flight path angle is adjusted to a maximum value for which Equation 8.11 holds.

$$T_{max} = 0.5 \cdot (D + \sin(\gamma) \cdot W_{alc,TO}) \Rightarrow \gamma = \arcsin\left(\frac{2T_{max} - D}{W_{alc,TO}}\right) \quad (8.11)$$

The above relation holds for the moment until the velocity has decreased until the optimal velocity to climb has been reached (based on interpolation of the velocity as provided by BADA as function of height). From then on, the aircraft follows the velocity profile of the conventional A321NEO, which is assumed optimal for that type of aircraft at a certain height. Similarly, from the moment the velocity profile of the conventional A321NEO is followed, the thrust provided by the engines is based on interpolation of the data provided by BADA.

Table 8.1: Parameters used for calculation of the flight profile during take-off for the A321NEO and A321REMALS.

| Input parameters | Quantity | Unit |
|----------------------|----------|-------|
| S | 122.4 | m^2 |
| A | 10.47 | [-] |
| e | 0.9244 | [-] |
| C_{d0} | 0.033 | [-] |
| T_{max} | 143,301 | N |
| $N1_{max}$ | 3856 | rpm |
| $W_{alc,TO, REMALS}$ | 97,000 | kg |
| $V_{TO, REMALS}$ | 145 | m/s |

| Output parameter | Quantity | Unit |
|-------------------------|----------|------|
| $time_{TO, A321NEO}$ | 335 | s |
| $time_{TO, A321REMALS}$ | 279 | s |

The optimal take-off speed in term of noise reduction has been determined to be 145 m/s (subsection 8.2.4). In combination with the data as provided in Table 8.1, a graphical representation of the take-off procedure is obtained and shown in Figure 8.1 to Figure 8.6. It can be seen that due to the adjusted take-off procedure, the time to reach FL100 is reduced significantly for the REMALS with respect to the A321NEO. Use of the energy height principle (converting kinetic energy to potential energy) is also clearly visible, especially in Figure 8.2. First, velocity decreases while height is increased, up to the point where the velocity is optimal to climb. From that point onward, the same velocity profile as the conventional aircraft is followed. In order to follow this height and velocity profile, it can be seen that the A321REMALS will have to provide maximum thrust for a longer time than the A321NEO. In Figure 8.4, it can be seen that the flight path angle is restricted to approximately 12 degrees, because of the maximum amount of thrust that can be applied (Equation 8.11).

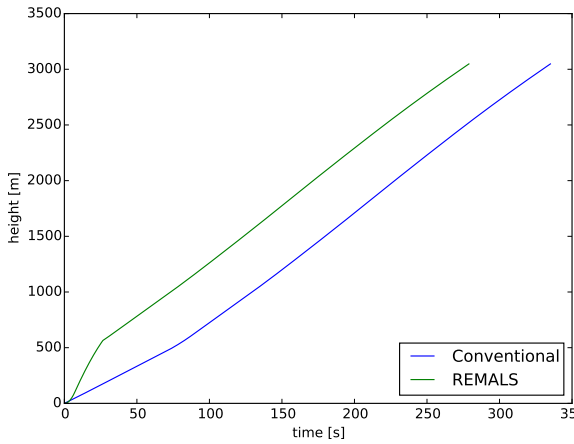


Figure 8.1: Height vs. time during take-off.

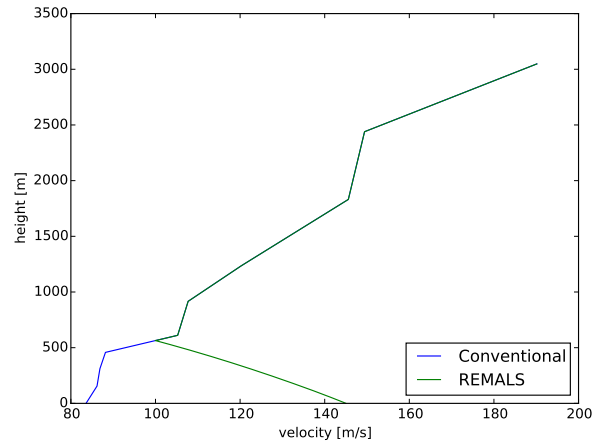


Figure 8.2: Height vs. velocity during take-off.

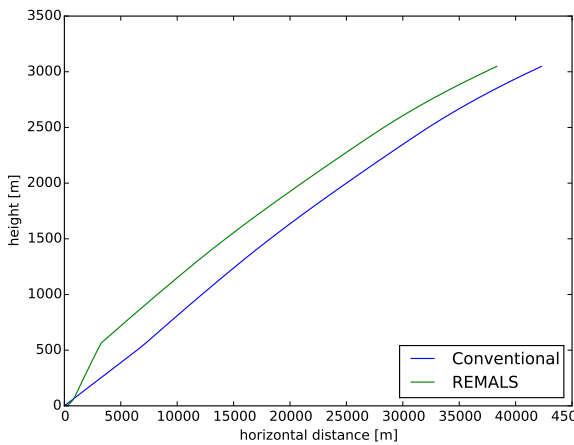


Figure 8.3: Height vs. horizontal distance covered during take-off.

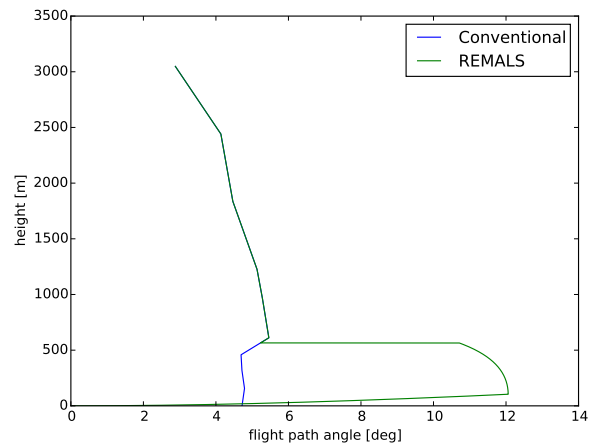


Figure 8.4: Height vs. flight path angle during take-off.

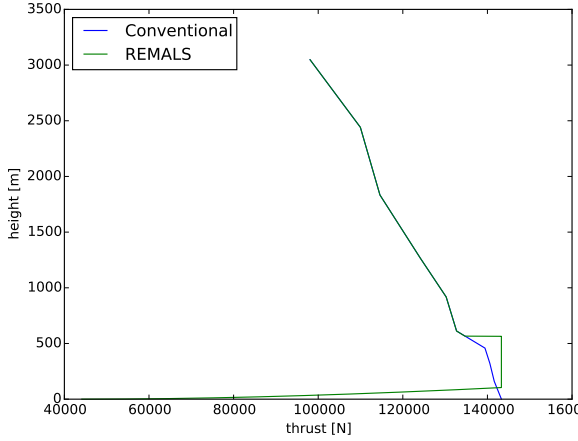


Figure 8.5: Height vs. thrust during take-off.

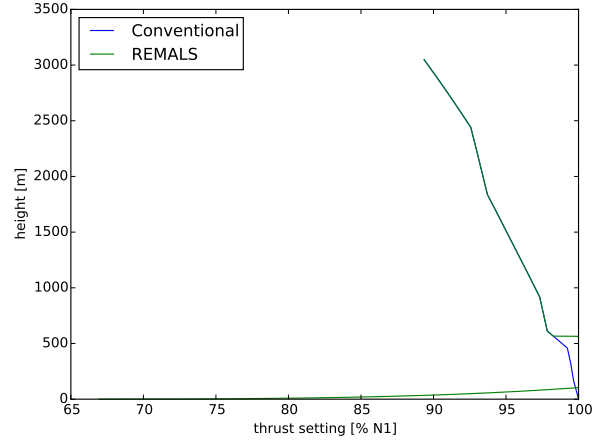


Figure 8.6: Height vs. thrust setting during take-off.

8.1.2. Landing Procedure

As explained in subsection 8.2.1, airframe noise is dominant during landing. The main sources of airframe noise are the deployment of the landing gear and high lift devices [19]. As a consequence, it is assumed that noise will begin to play a role when the aircraft switches to approach configuration. According to the Aircraft Performance Summary Table, this is done at FL20 (Appendix 15.2). Therefore, the landing trajectory is determined from FL20 onwards, for both the conventional A321NEO aircraft and the REMALS.

Landing Procedure for the Conventional A321NEO

Similar as for the take-off trajectory, the landing trajectory is determined based on linear interpolation of the Aircraft Performance Summary Tables provided by the Base of Aircraft Data. Data for the high mass descent is used, after having been converted to SI-units. This results in the height, velocity, distance and thrust profile as shown in Figure 8.7 to Figure 8.10. In order to convert the thrust provided by the engines (in Newtons) to a N1-setting, the same relation was used as described under subsection 8.1.1 (Equation 8.4).

Landing Procedure for the REMALS

In order to simulate the optimal landing procedure for the concept, the maximum approach speed is determined based on power constraints and equals 110 m/s (subsection 7.8.1). Assuming a descent at constant indicated airspeed and idle thrust, Equation 8.12 to determine the descent angle needed to maintain equilibrium between the drag force and the weight component working in the direction of descent.

$$\begin{aligned}
 W_x - D &= 0 \\
 \sin(\gamma) \cdot W_{alc,L} &= C_D \cdot \frac{1}{2} \cdot \rho \cdot V_{TAS}^2 \cdot S \\
 \gamma &= \arcsin\left(\frac{C_D \cdot \frac{1}{2} \cdot \rho \cdot V_{TAS}^2 \cdot S}{W_{alc,L}}\right)
 \end{aligned} \tag{8.12}$$

Similar as for the take-off procedure, the drag coefficient is based on the drag polar (Equation 8.9). With respect to the lift coefficient, this is based on Equation 8.13. Note that it has been taken into account that $W = L_y$, by accounting for the fact that the lift vector is not parallel to the weight vector (due to the descent angle). This has been taken care of by inserting a cosine.

$$C_L = \frac{2 \cdot W_{alc,L}}{\rho \cdot V_{TAS}^2 \cdot S \cdot \cos(\gamma)} \tag{8.13}$$

Table 8.2: Parameters used for calculation of the flight profile during landing for the A321NEO and A321REMALS.

| Input parameters | Quantity | Unit |
|------------------|----------|-------|
| S | 122.4 | m^2 |
| A | 10.47 | [-] |
| e | 0.9244 | [-] |
| C_{d0} | 0.033 | [-] |
| T_{max} | 143,301 | N |
| $N1_{max}$ | 3856 | rpm |
| $W_{a/c,L}$ | 79,200 | kg |
| V_L | 109.5 | m/s |

| Output parameter | Quantity | Unit |
|-----------------------------|----------|------|
| $time_{landing,A321NEO}$ | 145 | s |
| $time_{landing,A321REMALS}$ | 105 | s |

Combining Equation 8.12, Equation 8.9 and Equation 8.13 and the values as presented in Table 8.2, results in a descent angle of 3.8 deg. This corresponds to the maximum flight path angle that can be obtained in clean configuration when looking at the L/D ratio. For commercial aircraft, this is estimated to be approximately 15. According to Equation 8.14, this corresponds to a maximum obtainable angle of 3.8 deg. Thus, approaching with a constant airspeed of 109.5 m/s and idle thrust results in a height, velocity and thrust profile as presented in Figure 8.7 to Figure 8.10. It is assumed that idle thrust corresponds to a 45% N1-setting².

Note that it has not been taken into account that just before landing, the aircraft will have to pitch up and potentially will have to apply extra thrust to flare horizontally over the runway. Further studies will have to show the effect of this manoeuvre on the total flight profile.

$$\gamma_{max} = \arctan\left(\frac{1}{15}\right) \tag{8.14}$$

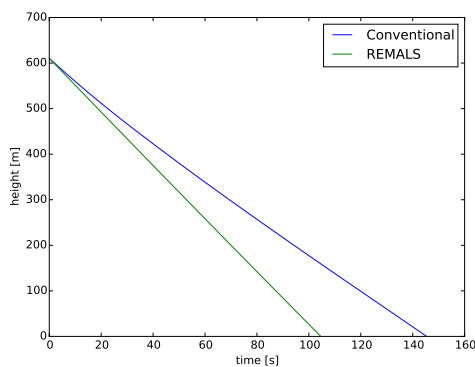


Figure 8.7: Height vs. time during landing.

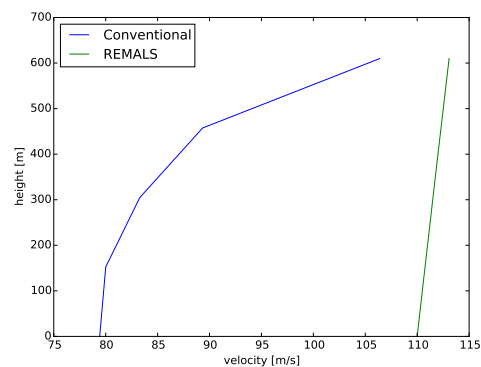


Figure 8.8: Height vs. velocity during landing.

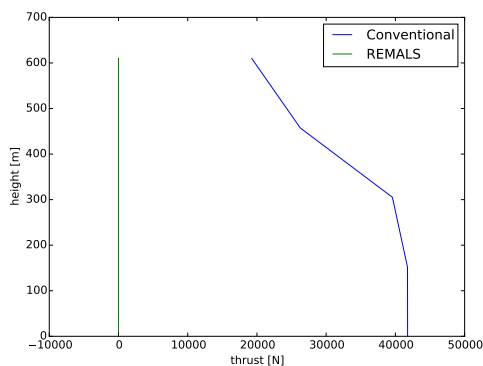


Figure 8.9: Height vs. thrust during landing.

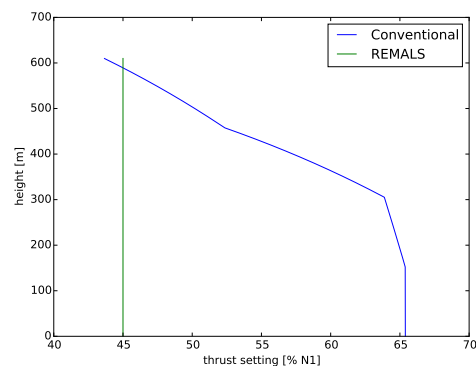


Figure 8.10: Height vs. thrust setting during landing.

²URL: <https://www.pprune.org/tech-log/514926-a320-thrust-idle.html> [retrieved on June 12 2019]

8.1.3. Verification and Validation

Several unit tests have been performed in order to check whether the program produces the right and expected results. First of all, in order to check whether interpolation of the BADA files is done correctly, a hand calculation has been performed. As can be seen in Appendix 15.2 in Table 3, the values for FL50 are not reported in the table. However, for FL40 and FL60, the true airspeed equals 232.55 kts and 281.98 kts respectively. According to Equation 8.15, the true airspeed at FL50 should be 257.27 kts, equal to 132.4 m/s. For the interpolated data, the value closest to FL50 (1524 m) is 1523.55 m at which the true airspeed equals 132.5 m/s, which is within a 0.1 % margin with respect to 132.4 m/s. This was done for several variables, including thrust and rate of climb. Similar results were obtained and thus, the interpolation of the data from the Aircraft Performance Summary Tables is assumed to be correct and verified for both take-off and landing.

$$\begin{aligned}
 V_{FL50} &= \frac{V_{FL60} - V_{FL40}}{2} + V_{FL40} \\
 &= \frac{281.98 - 232.55}{2} + 232.55 \\
 &= 257.27
 \end{aligned}
 \tag{8.15}$$

Next, the program that computes the trajectory for the A321REMALS is verified. The main difference between the take-off and landing trajectory for the different aircraft is that the A321REMALS estimates drag performance, based on theoretical relations, while the A321NEO has real data on which this is based. Therefore, the drag polar for the A321REMALS during take-off is plotted and shown in Figure 8.11 and Figure 8.12 [71]. When comparing this to a drag polar of A320, it can be seen that for each C_D value, the C_L -values are approximately 0.1 higher than for the drag polar of the A321REMALS. However, the general shapes of the drag polars coincide. In addition, the earlier mentioned difference of 0.1 is assumed to be negligible when the goal is to verify the program, since the theoretical drag polar is based on a slightly different aircraft (A320).

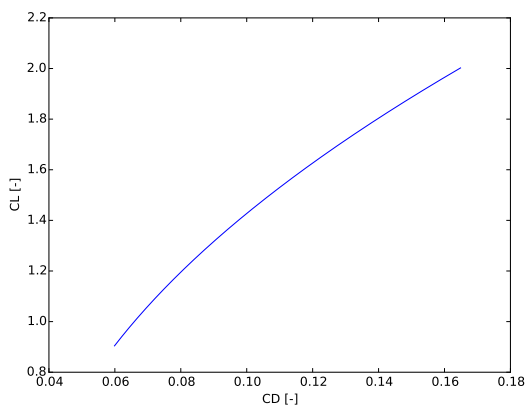


Figure 8.11: Drag polar of REMALS.

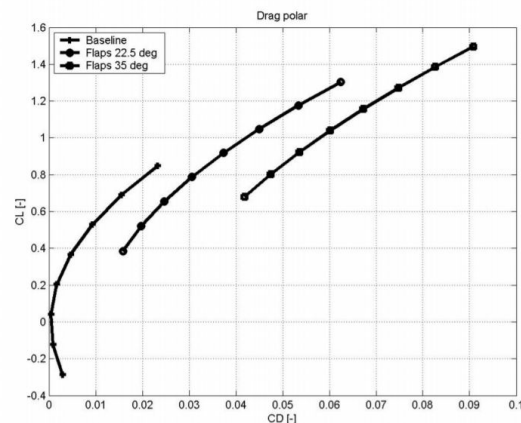


Figure 8.12: Drag polar of A320 [71].

Concerning validation of the program, this has been done by comparing the time the A321NEO takes to reach FL100 and descend from FL20 according to the program with actual flight data from Flightradar. ³ It appeared that an Airbus A321 (VK8405) took approximately 5 minutes to reach FL 100 (300 seconds). As stated in Table 8.1, according to the program, the plane takes 335.1 seconds to reach FL100. This is considered to be close enough to 300 seconds in order to validate the program. With respect to landing, an Airbus A321 (VK8405) takes approximately 200 seconds, while the program generates a landing time of 145 seconds. This is more off than for take-off, however, for landing more uncertainty is present. The reason for this is that during an actual landing, the aircraft descends to a certain flight level and remains on that level for a certain amount of time, while in the calculation it is assumed that a constant rate of descent is used. Therefore, the actual landing time in comparison with the calculated landing time turns out higher.

³URL: <https://www.flightradar24.com/> [Cited: 22th June, 2019]

8.2. Noise Reduction

As stated in section 8.1, one of the driving requirements of the system to be designed for is to reduce the noise produced by 7 ± 3 SEL dB. In order to fully understand how to reduce aircraft noise with the system, first some comments are made on aircraft noise in general [23]. Next, noise reduction in the context of the project is elaborated on.

8.2.1. Aircraft Noise in General

When talking about aircraft noise, a distinction is made between engine noise and airframe noise.

With regards to engine noise, it has to be noted that each component of the engine, i.e. the fan, combustion core, turbine and exhaust jet, produces noise [19]. One of the main parameters concerning the production of noise is the bypass ratio: the ratio of mass flow that bypasses the engine core without undergoing combustion to the mass flow that passes through the engine core and is combusted. As a result, turbofan engines create much less noise in comparison with turbojet engines. For one engine type, the amount of noise produced is also dependent on the actual engine settings, especially the relative fan rotational speed [19].

The other main source of aircraft noise is the noise generated by the airframe. This is due to the flow of air around the outer surface of the plane, and thus, is mainly dependent on the deployment of high-lift devices (flap setting) and landing gear [19].

When comparing the noise breakdown for a typical take-off and landing procedure as shown in Figure 8.13 [19], it can be seen that engine noise during take-off is way more significant than airframe noise. Therefore, it is safe to assume that airframe noise is negligible during take-off [19]. However, during approach, airframe noise is more significant. Note that the sound level in which this breakdown is presented, is not elaborated on further in the report, but is merely to show the typical significance of each component.

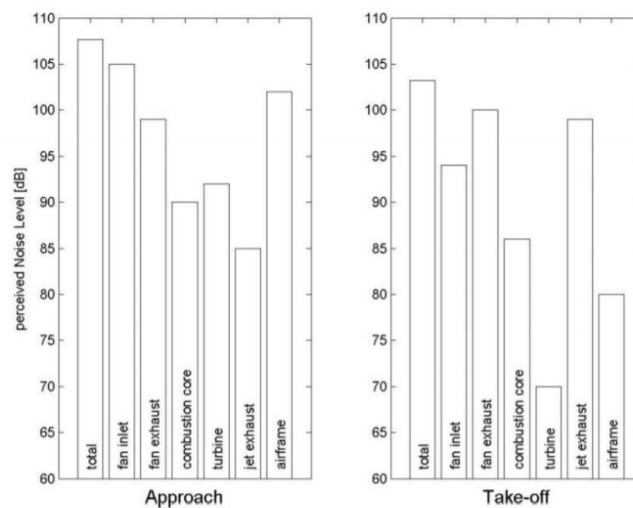


Figure 8.13: Typical noise breakdown for landing and take-off procedures in terms of engine and airframe noise [19].

8.2.2. Measuring Aircraft Noise

Concerning the measurement of aircraft noise, the reader for the course AE4431 Aircraft Noise and Emissions by prof. dr. D.G. Simons [19] was consulted. When measuring noise, one has to realise that noise is a sound wave propagating through a medium. Therefore, as the wave propagates, regions of compressed and expanded air will arise. As a result, a measure for the strength of a sound wave is given by the effective sound pressure. When converting the effective sound pressure [N/m^2] to decibels, the sound pressure level (SPL) is obtained. However, for the human ear, not only the sound pressure level is of importance, but also the frequency. Therefore, the obtained SPL values are often weighted according to a function which results in higher decibels for higher frequencies, since these are perceived by humans as more annoying. As a result, the overall A-weighted sound pressure level L_A in units dBA is obtained.

For non-stationary sound sources, one can imagine that the effect of the duration of noise has to be taken into account. For example, two events may have the same maximum A-weighted sound pressure level

($L_{A_{max}}$), but one event may be perceived as more annoying due to a longer duration. Therefore, it makes sense to include the duration of the event too. As a result, another quantity is introduced to measure noise: the 'sound exposure level' SEL [dBA], which is an integration of the A-weighted sound pressure level over time and is widely used in the field of aircraft noise. The integration time is chosen in such a way that the value of $L_A(t)$ is not 10 dBA below the maximum measured value $L_{A_{max}}$. This is visually explained in Figure 8.14 [20].

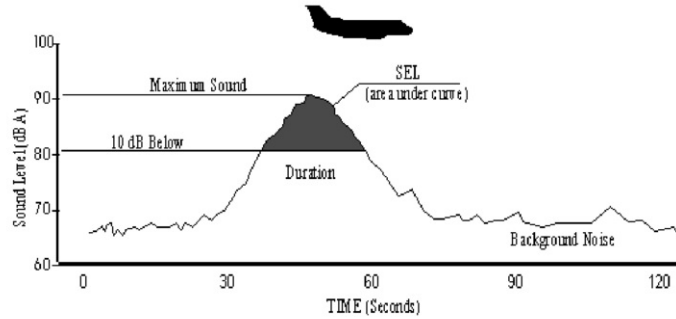


Figure 8.14: Determining the sound exposure level explained [20].

8.2.3. Noise Calculations

Based on the flight profile for take-off and landing as presented in section 8.1, the sound exposure level is determined using the "Nederlands Rekenvoorschrift" as set by NLR [73]. This calculation uses the thrust setting and distance of the aircraft to a measuring point to find noise levels. Besides, it uses a distribution of all aircraft in a limited number of categories. All aircraft in one category are assumed to have the same performance characteristics with respect to noise.

The calculation which transforms a height profile to noise levels itself has not been performed by the project team, but has been obtained by the help of master student Davey Hooymeijer. The same program was used with which he gained results for his master thesis, which resulted in noise levels for each time step for every 500 m from the runway. This was done for 30 km and 11 km for take-off and landing respectively. Using numerical integration with the midpoint rule over time, the sound exposure level for each 500 m point was found.

It has to be noted that the "Nederlands Rekenvoorschrift" does not account for deployment of landing gear and flap setting. However, during landing, especially the deployment of landing gear is an important source for airframe noise for conventional aircraft [19]. Therefore, the noise produced by the deployment of the landing gear has been estimated using Equation 8.16 [19] and added for each timestep at each measuring point for the A321NEO. It can be seen that Equation 8.16 consists of different subequations, listed in Equation 8.17 to Equation 8.24. In Equation 8.17, constants K and a are used which correspond to $3.414 \cdot 10^{-4}$ and 6 respectively.

Note that Equation 8.16 produces the sound on the intensity scale, thus in Watt/m^2 . In order to convert intensity to sound pressure level, Equation 8.24 is used.

For the A321REMALS, the deployment of the harpoons have not been taking into account concerning noise production. This is due to the fact that the empirical relations as stated below are not available for three simple beams. In addition, it is expected that the noise produced by the harpoons is negligible in comparison with a conventional landing gear.

$$I = \frac{P \cdot D(\theta_d, \phi) \cdot F(S)}{4\pi r^2 \cdot (1 - M \cos(\theta_d))^4} \quad (8.16)$$

$$P = K \cdot M^a \cdot G(\rho_\infty \cdot c^3 \cdot b^2) \quad (8.17) \quad D(\theta, \phi) = \frac{3}{2} \cdot \sin(\theta_d)^2 \quad (8.18)$$

$$F(S) = 0.0577 \cdot S^2 (0.25 \cdot S^2 + 1)^{-1.5} \quad (8.19) \quad \theta_d = \frac{1}{2} \pi \pm \arccos\left(\frac{\text{height}}{\text{distance}}\right) \quad (8.20)$$

$$S = \frac{f \cdot L(1 - M \cos(\theta_d))}{M \cdot c} \quad (8.21) \quad L = d \quad (8.22)$$

$$G = n \left(\frac{d}{b} \right)^2 \quad (8.23)$$

$$SPL = 10 \log \left(\frac{I \cdot \rho_{\infty} \cdot c}{p_{e0}^2} \right) \quad (8.24)$$

| Input parameter | Quantity | Unit |
|-----------------|----------|------|
| b | 35.8 | m |
| d | 0.27 | m |
| n | 4 | [-] |

Table 8.3: Parameters used for calculation of noise produced by conventional landing gear

8.2.4. Sensitivity Analysis

When doing preliminary calculations, soon it was found out that a reduction of 7 ± 3 SEL dB along the entire trajectory was not feasible. The further away the aircraft from the runway, the less the difference in noise production between the A321NEO and A321REMALS became. Therefore, it is decided to look at the top 3 zip code areas from which most complaints originated in 2018. The areas are listed in Table 8.4, including their distance to the runway from which they experience the most noise nuisance [9]. In order to contribute to a diminishing of nuisance, it has been decided that a reduction of 7 ± 3 SEL dB for at least 7.8 km from the runway will have to be fulfilled by REMALS.

For take-off, the main input parameter is the take-off speed. Figure 8.15 shows the influence of take-off speed on the noise production for each measuring point, where 0m is the point of lift-off for both aircraft. It can be seen that for a speed of 145 m/s, the 7 ± 3 SEL dB reduction is fulfilled till at least 7.8 km. Therefore, a take-off speed of 145 m/s has been used. This results in the final noise production as presented in Figure 8.16.

Table 8.4: Top 3 zip code areas from which most complaints concerning aircraft noise originated in 2018 [9].

| Zip Code Area | Runway Cluster | Distance [km] |
|-----------------|-------------------|---------------|
| 1187 Amstelveen | Aalsmeerbaan | 4.6 |
| 1054 Amsterdam | Buitenveldertbaan | 7.8 |
| 1188 Amstelveen | Buitenveldertbaan | 6.3 |

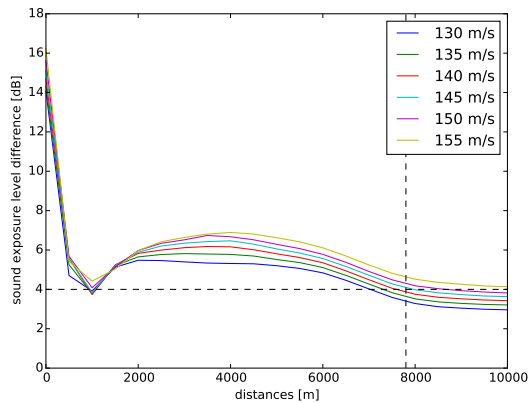


Figure 8.15: Differences in sound exposure level for different take-off speeds with respect to the conventional A321NEO.

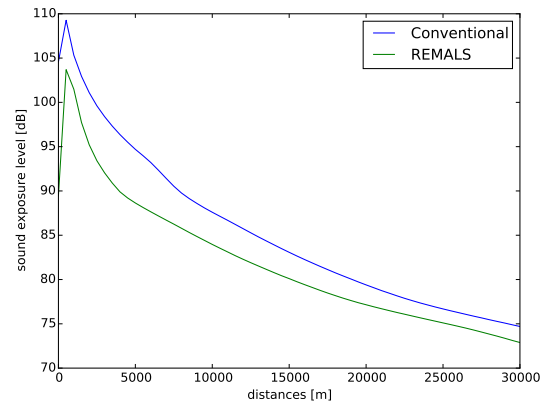


Figure 8.16: Sound exposure level for REMALS with a take-off speed of 145 m/s with respect to conventional A321NEO.

Similarly for landing, the main input parameter is the approach speed. As stated before, the approach speed is fixed at 110 m/s due to a power constraint subsection 7.8.1. The resulting noise production with respect to conventional A321NEO is shown in Figure 8.17, where 0m is the point of touchdown for both aircraft. In Figure 8.18, the influence of a higher and lower approach speed is shown. Note that the constraint on a minimum of 4 SEL dB reduction of at least 7.8 km away is easily met with an approach speed of 110 m/s.

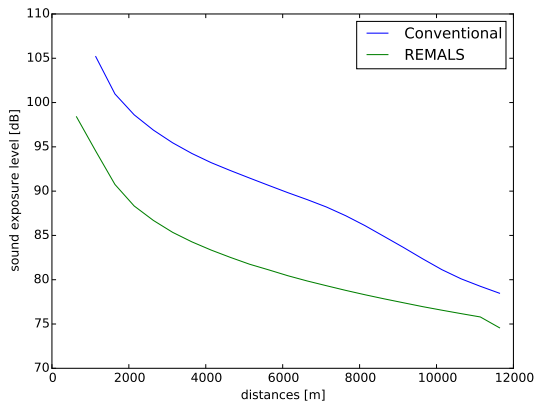


Figure 8.17: Sound exposure level for REMALS with an approach speed of 110 m/s with respect to conventional A321NEO.

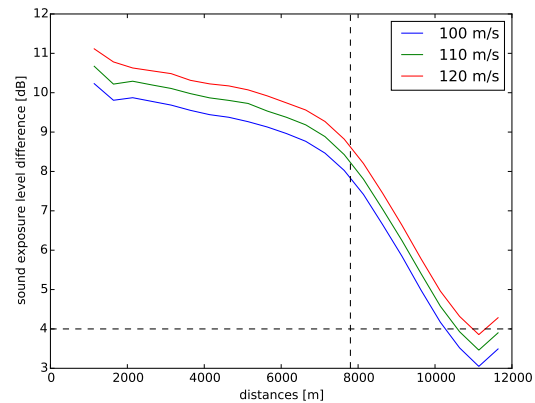


Figure 8.18: Differences in sound exposure level for different approach speeds with respect to the conventional A321NEO.

8.2.5. Verification and Validation

The main part of the program that needs verification is the numerical integration part. Due to the large files generated by the model based on the Netherlands Rekenvoorschrift, verifying the numerical integration is of great importance to be able to present correct results. This was done by creating a list of y-values for the known function $y = -x^2 + 10$, corresponding with a list of t-values from -4.0 to 4.0 with a timestep of 0.1 s (similar as for the actual program). Integrating from -2 to 2 and removing the part of the graph that is under the limit, resulted in a numerical integration value of 10.66. Using Equation 8.25, the exact same value was found, thus, the program can be considered verified.

$$\begin{aligned}
 F &= \int_{-2}^2 -x^2 + 10 dx - (2 - -2) \cdot (-2^2 + 10) \\
 &= \left[-\frac{1}{3}x^3 + 10x \right]_{-2}^2 - 24 \\
 &= -\frac{1}{3} \cdot 8 + 20 - \left(-\frac{1}{3} \cdot (-8) - 20 \right) \\
 &= 10.667
 \end{aligned} \tag{8.25}$$

With regards to validation of the program, this was done by consultation of expert in the field dr. ir. M. Snellen. According to her opinion, the resulting values of the program made perfect sense and were in the same order of magnitude as what one would have expected based on previous studies.

8.3. Fuel Savings

To ensure that the fuel reduction gives the desired results, the requirement for fuel consumption has been divided into a absolute and a relative requirement. Driving requirement NCL-Alc09u1 states that the modification of the aircraft and the different take-off and landing procedures shall decrease the absolute fuel consumption of the entire flight mission with at least 5% for all flights shorter than 1,5 hour. Requirement NCL-Alc09u2 states that the modification of the aircraft and the different take-off and landing procedures shall decrease the total fuel consumption of the entire flight mission per passenger per kilometer with at least 5% for a 1,5 hour flight with 84,7% occupancy. The entire flight mission, as visualised in fig:fuelfractions, is defined from the point the aircraft departs from the gate to the point it arrives at the gate of the airport of destination.

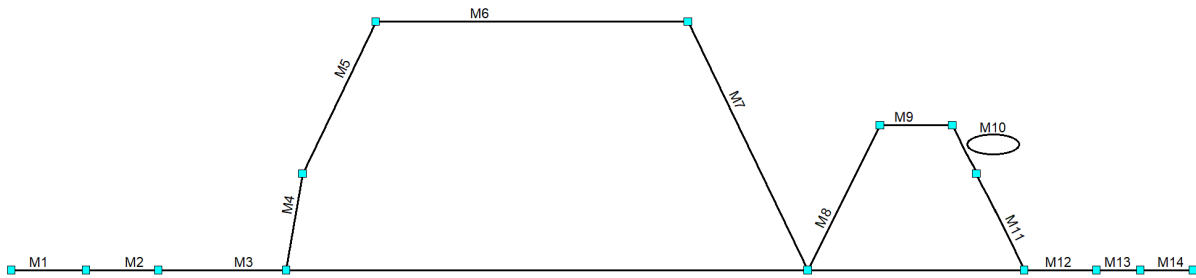


Figure 8.19: Sections of total flight mission

All submission (flight phases) are indicated with the letter M. Submission M1 to M7 and M12 to M14 represents normal flight procedure. Schiphol is located at sea level and the cruise altitude is assumed to be 10.6 km on average⁴. CS-25 states that, after an aborted landing, the aircraft should be able to climb from sea level to 3048 m and thereafter allowing 45 minutes cruise (for max. range) and 20 minutes loiter [2]. M8 to M11 shows the submissions to comply with the CS-25 regulations. The weight of the aircraft after a submission is given with W (W_1 is the aircraft's weight after M1 has finished). Note that, for example, a fuel fraction M_{ff} of $\frac{W_6}{W_5}$ represents the weight reduction ratio of M6.

Subsection 8.3.1 starts this section by evaluating the main causes of the fuel reduction. Then, subsection 8.3.2 analyses the fuel consumption of the A321REMALS and the A321NEO at all flight phases analytically. The subsection concludes with an overview of all fuel weight fractions of the A321REMALS with respect to the conventional aircraft. A flight with maximum range at maximum payload is used as reference flight. Next, subsection 8.3.3 describes how the fuel savings results in more fuel savings, also known as the snowball effect. Subsequently, the fuel savings are expressed in an absolute and relative way. Subsection 8.3.4 and subsection 8.3.5 present these methods and verify whether NCL-Alc09u1 and NCL-Alc09u2 are met. All the results are justified and verified in subsection 8.3.6 and subsection 8.3.8 respectively based on actual flight data. The chapter closes with a conclusion and a recommendation in subsection 8.3.9.

8.3.1. Causes Fuel Reduction

The fuel is reduced due to the different take-off, landing and ground movement procedures and the lower operational empty weight of the aircraft. For submissions M1 to M4 and M12 and M14, less fuel is needed due to the different ground operations. Submissions M5 to M11 uses less fuel due to the reduction in aircraft weight.

weight reduction

The main cause of the fuel reduction is the reduction in the aircraft operational empty weight. As described in chapter 6, the landing gear with a mass of 3804 kg is removed and a connection mechanism with a mass of 1704 kg is added to the aircraft. This gives a new OEW of the A321 REMALS of 49922 kg, a reduction of 4.0% with respect to the A321NEO. The weight of the aircraft at a certain point in flight consists of the operational empty, the payload and the fuel weight, as shown in Equation 8.26. Where W is the aircraft weight at a certain point in flight.

$$W(t) = OEW + M_{PL} + M_f(t) \quad (8.26)$$

To make an estimation of the fuel reduction, this equation needs to be used to calculate the weight reduction at a certain point in flight. Three important things need to be noted here. Firstly, the mass of the payload is not constant for every flight, but depends on the airlines choices. Secondly, the amount of fuel taken on board depends on the distance of the flight destination, and thus differs for every flight. Lastly, due to the consumption of fuel, the aircraft weight changes during flight as well. Therefore, different payloads, initial fuel masses and the consumption of fuel along the flight all need to be taken into account to make an estimation of fuel reduction. In short, the change in weight (and thus the changed fuel consumption) of the A321REMALS depends on the flight profile (the payload and range) and the position in flight. This effect will be taken into account when analysing the flight phases in the next section. The weight reduction ratio of the A321REMALS with respect to the A321NEO at a certain point in flight for a certain flight profile will be given by $\phi W(t)$, as described in Equation 8.27

⁴URL: <https://contentzone.eurocontrol.int/aircraftperformance/details.aspx?ICAO=A321&ICAOFilter=a321> [Accessed 19 June 2019]

$$\phi W(t) = \frac{W_{REMAALS}(t)}{W_{a321}(t)} = \frac{OE W_{REMAALS} + M_{Payload} + M_{fuel} - M_{fuel_{consumed}}(t)}{OE W_{A321} + M_{Payload} + M_{fuel} - M_{fuel_{consumed}}(t)} \quad (8.27)$$

subsection 8.3.2 will express this weight reduction in terms of fuel savings for each flight submission.

Ground Operations

Fuel is saved by powering the aircraft as much as possible by the ground based system. For all ground movement submissions, the aircraft operations are set. Hence, the fuel flow at these missions can be calculated using thrust specific constants.

8.3.2. Fuel Consumption per flight phase

This section presents an in-depth analysis of the fuel consumption at all flight phases, as visualised in Figure 8.19. Fuel consumption is estimated either by statistical data on fuel fractions or by calculations based on free-body diagrams and thrust specific constants. For these calculations, an aircraft with MTOW at M2 (begin of take-off) is assumed. An overview of each submission, the fuel fractions and the consumed fuel (in case M2 = MTOW) is given in Table 8.5.

M1: Taxi-out

The average Taxi-out time estimated by airbus is 12 minutes for an average domestic flight. Airbus estimated a fuel consumption of 162 kg for this flight procedure [8]. With the ground based system, no fuel is used by the aircraft.

M2: Engine start and warm-up

As the average engines start and warm-up, fuel consumption is estimated by Airbus at 108 kg. Since the engines do not change per design, this value will be equal for the conventional aircraft and A321 REMALS.

M3: Take-off

At take-off, part of the energy gets provided by the ground based system. However, the aircraft reaches higher velocities on the runway. The fuel used during take-off is given in Equation 8.28.

$$M_{fuel} = c_t T t \quad (8.28)$$

This calculation can be done for the conventional and ground-based powered take-offs. For the A321REMAALS take-off at MTOW, $T = 87$ kN and $t = 22$ s whereas for the conventional aircraft, $T = 137$ kN and $t = 32$ s⁵. C_t , the thrust specific fuel consumption, for both aircraft is equal to 12 g/kN/s. This results in $M_{fuel} = 22.9$ kg and $M_{fuel} = 52.6$ kg for the A321REMAALS and the conventional aircraft respectively.

M4: Initial Climb (0 - 603 m)

The initial climb is defined from the moment of take-off until the height that all extra kinetic energy is converted into potential energy and the aircraft starts optimum climb procedure. This happens at 603 meters. The mass-fuel fraction from climb to cruise for medium range aircraft is 0.980[44]. Correcting for a distance of 603 meters gives a mass fuel fraction of 0.9988 for the 603 meter climb. However, the ground base system puts additional energy into the aircraft. This amount of energy is given in Equation 8.29.

$$E_k = \frac{1}{2} W(t) (V_{end}^2) \quad (8.29)$$

The take-off speed for the A321 REMALS is 146 m/s. The average take-off speed of a conventional aircraft is 83 m/s⁶. Using the MTOW of the conventional aircraft and the A321REMAALS gives an energy difference of 702 MJ.

$$M_{fuel} = E_k \rho_{ke} \mu_0 \quad (8.30)$$

The overall energy efficiency for a high bypass ratio engine jet at a take-off speed of 73 m/s is around 0.5[1]. With a kerosene density at sea level of 0.785 kg/l, the saved fuel mass during the initial climb is calculated using Equation 8.30 and is found to be 30 kg. This 30 kg is subtracted from the fuel fraction of the A321REMAALS. This will result in a fuel fraction of 0.9988 and 0.9991 for the A321NEO and the A321REMAALS aircraft, respectively.

⁵URL: <http://krepelka.com/fsweb/learningcenter/aircraft/flightnotesairbusa321.htm> [Accessed 12 June 2019]

⁶URL: <http://krepelka.com/fsweb/learningcenter/aircraft/flightnotesairbusa321.htm> [Accessed 12 June 2019]

M5: Climb (603 m - cruise)

The rate of climb for steady climb is given by equation Equation 8.31.

$$RC_s = \frac{P_a - P_r}{W} \quad \text{where } p_a = TV \quad \text{and } p_r = DV \quad (8.31)$$

Where RC_s equals the rate of climb and the extra increment in true airspeed. Reducing the aircraft's weight W makes it possible to reduce thrust while keeping the same rate of climb. The actual thrust reduction depends on the drag of the aircraft. Therefore, an estimation of the drag in relation to the thrust needs to be made.

The average rate of climb for the A321NEO is around 9 m/s at a flight speed of 149 m/s⁷. using Equation 8.31, $T - D$ is calculated. With a max thrust setting of 286 kN and a take-off weight of 97000 kg, D/T is calculated to be 0.227. With the relation D/T known, $(T - D)$ can be expressed in terms of T , as shown in Equation 8.32.

$$(T - D) = T - \frac{D}{T}T = 0.773T \quad (8.32)$$

With this primary estimation, it can be concluded that, if the aircraft weight at a certain point along the climb is reduced by $\phi W(t)$, the thrust can be reduced by $0.773\phi W(t)$.

The mass-fuel fraction from climb to cruise for medium range aircraft is 0.980[44]. Correcting for a distance of 10 km (603 meter to cruise) gives a mass fuel fraction of 0.9811 for the remaining climb for the conventional aircraft. The fuel fraction of the A321REMALS depends on the weight reduction, which depends on the flight mission and flight phase. subsection 8.3.4 elaborates on this.

M6: Cruise 1 (variable range)

To optimise the aircraft's range, it is necessary to optimise the specific range, given in Equation 8.33.

$$\left(\frac{V}{\dot{m}}\right)_{max} \quad \text{where } V = \sqrt{\frac{W}{S} \frac{2}{\rho} \frac{1}{C_{L_{opt}}}} \quad \text{and } \dot{m} = c_t T \quad \text{with } T = D = \frac{C_D}{C_L} W \quad (8.33)$$

Combining the above equations and finding the maxima gives Equation 8.34.

$$(V/\dot{m})_{max} = \frac{1}{c_t} \sqrt{\frac{1}{W} \frac{1}{S} \frac{2}{\rho} \left(\frac{C_L}{C_D^2}\right)_{max}} \quad (8.34)$$

Where the optimal lift and drag coefficient for maximum range are given by Equation 8.35

$$C_{L_{opt}} = \sqrt{\frac{C_{D_0} \pi A e}{3}} \quad \text{and} \quad C_{D_{opt}} = \frac{4}{3} C_{d_0} \quad (8.35)$$

To calculate how weight reduction influences the fuel consumption during cruise, the fuel flow for optimum cruise speed at optimal lift- and drag-coefficients needs to be expressed in terms of the aircraft weight. Equation 8.36 combines Equation 8.35 and Equation 8.34 to express the fuel flow during cruise at optimal range conditions.

$$\dot{m} = \frac{4Wc_t}{\sqrt{\frac{3\pi A e}{C_{D_0}}}} \quad (8.36)$$

The dimensions of the A321REMALS do not change and the thrust-specific fuel consumption will not change either. Therefore, using Equation 8.36, it is valid to assume that, when the aircraft weight W changes with $\phi W(t)$, the fuel consumption will decrease with the same ratio.

The fuel fraction of different flight ranges can be calculated using Breguet's range equation, given in Equation 8.37. In this equation, the aircraft's velocity can be calculated using Equation 8.34, $C_j = 12$ g/kNs, $g = 9.81$ and $\frac{L}{D} = \frac{C_{L_{opt}}}{C_{D_{opt}}}$

Using this equation, combined with a certain flight mission (a combination of payload and range), the fuel fraction of the conventional aircraft and the A321REMALS can be calculated. This will be done for different flight mission in subsection 8.3.4 and subsection 8.3.5.

⁷URL: <https://contentzone.eurocontrol.int/aircraftperformance/details.aspx?ICAO=A321&ICAOFilter=a321> [Accessed 19 June 2019]

$$\frac{W_4}{W_5} = e^{\frac{V_{opt}}{g \cdot C_j} \cdot \left(\frac{L}{D}\right)_{cruise}} \quad (8.37)$$

M7: Descent 1 (Cruise - 0 m)

The mass-fuel fraction from cruise to landing altitude for medium range aircraft is 0.990[44]. The same fuel savings for descent is assumed as for climb. Therefore, the A321REMALS is $0.773\phi W(t)$ times more efficient during descent. The fuel fraction of the A321REMALS depends on the flight mission and the phase in flight.

M8: Climb 2 (0 - 3048 m)

The mass-fuel fraction from climb to cruise for medium range aircraft is 0.980[44]. Correcting for the height of 3048m gives a fuel fraction of 0.9939 for the conventional aircraft. Using Equation 8.31, the $0.773\phi W(t)$ difference ratio in fuel consumption is valid again. Therefore, the fuel fraction of the A321REMALS depends on the flight mission and the phase in flight.

M9: Cruise (45 Minutes)

The weight fraction for the conventional aircraft for a 45 minutes flight can be calculated using Equation 8.38. The same values can be used as in Equation 8.37. However, now the time t is known and equal to 2700 s.

$$\frac{W_8}{W_9} = e^{\frac{1}{g \cdot C_j} \cdot \left(\frac{L}{D}\right)_{cruise} \cdot t} \quad (8.38)$$

This gives a fuel fraction of 0.9663 for the conventional aircraft. The fuel fraction for the A321REMALS again depends on the flight mission and the phase in flight.

M10: Loiter (20 Minutes)

To optimise the aircraft's endurance, it is necessary to generate enough lift to stay up, with the least amount of fuel used. In short, Equation 8.39 needs to be optimised.

$$\left(\frac{L}{\dot{m}}\right)_{max} = \left(\frac{W}{\dot{m}}\right)_{max} \quad \text{where} \quad W = D = \frac{C_L}{C_D} = D \frac{C_L}{C_D} \quad \text{and} \quad \dot{m} = c_t T \quad (8.39)$$

The maxima with the corresponding optimal lift- and drag-coefficient for maximal endurance are given in Equation 8.40.

$$(W/\dot{m})_{max} = \frac{\left(\frac{C_L}{C_D}\right)}{c_t} \quad \text{where} \quad C_{L_{opt}} = \sqrt{C_{D_0} \pi A e} \quad \text{and} \quad C_{D_{opt}} = 2C_{D_0} \quad (8.40)$$

Finding the fuel flow, for a certain weight at maximum endurance lift- and drag-coefficient, gives Equation 8.41.

$$\dot{m} = \frac{\sqrt{\frac{\pi A e}{C_{D_0}}}}{4W c_t} \quad (8.41)$$

The dimensions of the A321REMALS are the same as the A321REMALS and the thrust-specific fuel consumption will not change either. Therefore, using Equation 8.41, it is valid to assume that, when the aircraft weight W changes with $\phi W(t)$, the fuel consumption will decrease with the same ratio.

The fuel fraction of different loiter times can be calculated using Breguet's loiter equation, given in Equation 8.42. C_j and g are similar to the value's used in Equation 8.37. The optimum $L/D = C_{L_{opt}}/C_{D_{opt}}$ given in Equation 8.40. The endurance is 1200 seconds.

$$\frac{W_9}{W_{10}} = e^{\frac{E}{g \cdot C_j} \cdot \left(\frac{L}{D}\right)_{cruise}} \quad (8.42)$$

This gives a fuel fraction of 0.9869 for the conventional aircraft. The fuel fraction for the A321REMALS again depends on the flight mission and the phase in flight. It will be calculated in subsection 8.3.4.

M11: descent 2 (3048 - 0 m)

The mass-fuel fraction from cruise to landing altitude for medium range aircraft is 0.990[44]. Correcting for the height of 3048m gives a fuel fraction (W_{11}/W_{10}) of 0.9970 for the conventional aircraft. The same fuel savings for descent is assumed as for climb. Therefore, the A321REMALS is $0.773\phi W(t)$ times more efficient during descent. The fuel fraction of the A321REMALS depends on the flight mission and the phase in flight.

M12, M13: Landing and engine shut down

The mass-fuel fraction for landing and engine shut-down of medium range aircraft is 0.997 and 0.990, respectively [44]. No significant changes are expected in this flight phase. Therefore, $W_{11}/W_{12} = 0.997$ and $W_{13}/W_{12} = 0.999$ for both the A321REMALS as for the conventional aircraft.

M14: Taxi-in

The average taxi-in time is almost half of the taxi-out time, and is estimated by Bureau of Transportation Statistics to be around 6.9 minutes [61]. Linearly interpolating this with the taxi-out fuel consumption gives a fuel consumption of 93 kg. However, the same distance needs to be covered during this time. The actual fuel consumption for taxi-in will thus be somewhere between 93 kg and 162 kg. Therefore, the average is taken and a fuel consumption of 127.5 kg is assumed.

Overview of all fuel fractions

An overview of all submissions, their mass fuel fractions and their absolute fuel consumption for the A321NEO and A321REMALS are given in Table 8.5.

Table 8.5: All submission with corresponding fuel weight fraction and absolute fuel consumption, MTOW assumed for A321NEO

| Flight Phase | Mission | A321NEO | | A321REMALS | |
|--------------|---------------------------|--------------|------------|------------------------------|------------|
| | | M_{ff} | M_f [Kg] | M_{ff} | M_f [Kg] |
| M1 | Taxi-out | 0.9983 | 162 | 1.0000 | 0 |
| M2 | Engine start | 0.9989 | 108 | 0.9989 | 108 |
| M3 | Take-off | 0.9995 | 52.6 | 0.9998 | 22.9 |
| M4 | Initial Climb (0 - 603 m) | 0.9988 | 116 | 0.9991 | 87 |
| M5 | Climb (603 m - cruise) | 0.9811 | 1830 | Depends on $\phi W(t)$ | |
| M6 | Cruise | Depends on R | | Depends on R and $\phi W(t)$ | |
| M7 | descent (Cruise - 0 m) | 0.9900 | 939 | Depends on $\phi W(t)$ | |
| M8 | Climb (0 - 3048 m) | 0.9939 | 567 | Depends on $\phi W(t)$ | |
| M9 | Cruise (45 Minutes) | 0.9663 | 3110 | Depends on $\phi W(t)$ | |
| M10 | Loiter (20 Minutes) | 0.9869 | 1169 | Depends on $\phi W(t)$ | |
| M11 | descent (3048 - 0 m) | 0.9970 | 264 | Depends on $\phi W(t)$ | |
| M12 | Landing | 0.9970 | 263 | 0.9970 | 264 |
| M13 | Engine shut down | 0.9990 | 88 | 0.9990 | 88 |
| M14 | Taxi-in | 0.9985 | 127.5 | 1.0000 | 0 |

8.3.3. Iteration of Fuel Weight

As stated before, the fuel consumption will decrease due to the reduction of the operating empty weight. This means that the total fuel that needs to be boarded to reach the same distance will decrease. This then reduces the aircraft's weight again, reducing the fuel consumption even more. This effect must be taken into account when calculating the fuel saving. Equation 8.27 thus results in Equation 8.43, where ΔM_{fuel} is the difference in fuel consumption between the A321NEO and A321REMALS.

$$\phi W(t) = \frac{W_{REMALS}(t)}{W_{A321}(t)} = \frac{OEW_{REMALS} + M_{Payload} + (M_{fuel} - \Delta M_{fuel}) - M_{fuel_{consumed}}(t)}{OEW_{A321} + M_{Payload} + M_{fuel} - M_{fuel_{consumed}}(t)} \quad (8.43)$$

8.3.4. Absolute Fuel Savings

For submissions M5 to M11, the fuel fraction of the A321REMALS depends on the weight reduction $\phi W(t)$. This ratio is dependant upon loaded fuel (which depends on the planned range), payload and the position in flight. These variables, together with a possible range of values, are summarised in Table 8.6.

Table 8.6: Possible combinations of payload and fuel mass

| Variable | Symbol | unit | Range | Max. 44,978 |
|--------------------------------------|--------------------------|------|--------------|-------------|
| Payload mass | $M_{Payload}$ | [kg] | 0-23,578 | |
| Initial fuel mass (Depends on range) | M_{fuel} | [kg] | 8,874-25,790 | |
| Fuel consumed (function of time) | $M_{fuel_{consumed}}(t)$ | [-] | 0-1 | |

The weight ratio $\phi W(t)$ can be calculated for all possible combinations of payload, range (which translates into fuel mass) and flight positions from the above table. subsection 8.3.2 showed that for climb and descent, the fuel savings are related to the weight reduction with a ratio of 0.773. For cruise and loiter, the ratio is demonstrated to be around 1. The mass fuel fractions for the A321REMALS can now be calculated for all different combinations of payload and range at all flight phases for climb and descent, and for cruise and loiter using Equation 8.44 and Equation 8.45, respectively.

$$M_{ff_{REMALS}} = M_{ff_{A321}} + (1 - M_{ff_{A321}}) \cdot 0.773 \left(\frac{OEW_{REMALS} + M_{Payload} + (M_{fuel} - \Delta M_{fuel}) - M_{fuel_{consumed}}(t)}{OEW_{A321} + M_{Payload} + M_{fuel} - M_{fuel_{consumed}}(t)} \right) \quad (8.44)$$

$$M_{ff_{REMALS}} = M_{ff_{A321}} + (1 - M_{ff_{A321}}) \cdot \left(\frac{OEW_{REMALS} + M_{Payload} + (M_{fuel} - \Delta M_{fuel}) - M_{fuel_{consumed}}(t)}{OEW_{A321} + M_{Payload} + M_{fuel} - M_{fuel_{consumed}}(t)} \right) \quad (8.45)$$

With all the fuel fractions known, the absolute fuel reduction percentage for a given flight mission can be calculated using Equation 8.46. Results are plotted in Figure 8.20. Note that, since further distances can be reached with the same amount of fuel, the weight limitations line of the A321REMALS will be shifted slightly towards the right of the A321NEO line that is plotted in this figure.

$$M_{fuel_{saved}} = 1 - \frac{M_{fuel_{A321REMALS}}}{M_{fuel_{A321NEO}}} \quad (8.46)$$

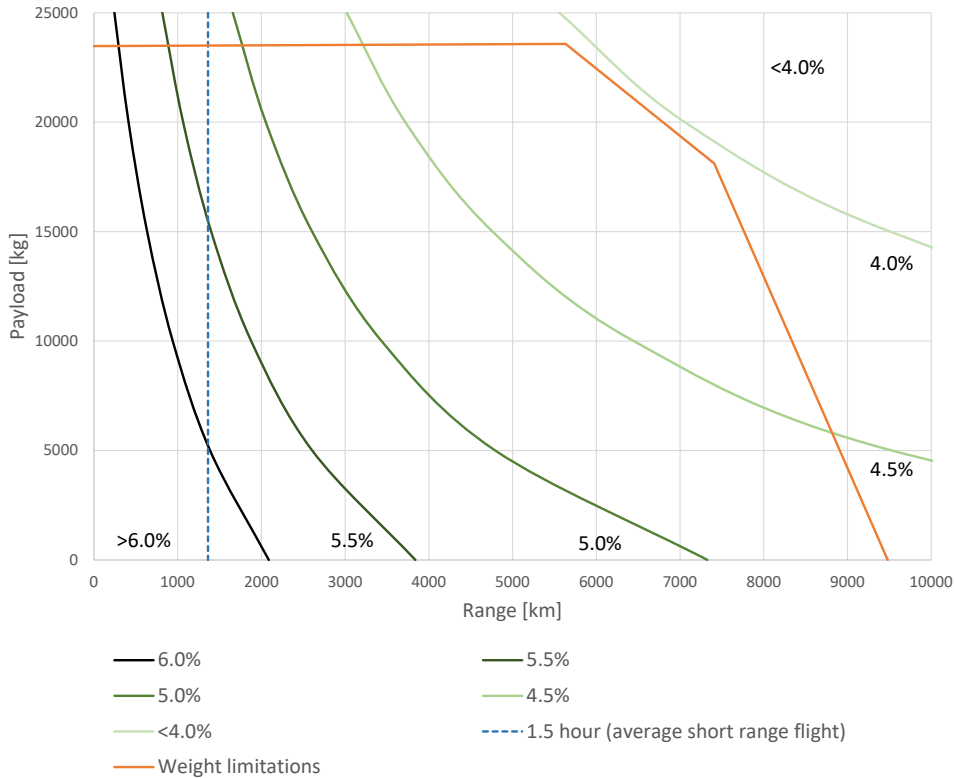


Figure 8.20: Fuel reduction for different flight missions

8.3.5. Relative Fuel savings

NCL-Alc09u2 states that the modification of the aircraft and the different take-off and landing procedures shall decrease the total fuel consumption per passenger per kilometer with at least 5% for a 1,5 hour flight with 84,7% occupancy. The requirement is initiated to examine the fuel consumption from a different perspective. The occupancy is based on the average occupancy rate of Schiphol Airport [57], the capacity of 240 seats[3] for both aircraft, and the average passenger and luggage weight of 77 and 15 kg, respectively [65]. The consumed fuel per kilogram per kilometer can be calculated with Equation 8.47.

$$\frac{M_{fuel}}{M_{payload} \cdot R} \quad \text{where} \quad M_{payload} = Capacity \cdot occupancyrate \cdot (M_{human} + M_{luggage})_{ave} \quad (8.47)$$

For both the A321NEO and the A321REMALS, the capacity stays the same. Furthermore, occupancy rate and the average human and luggage weight are assumed to be equal as well. Therefore, for a certain range, R , the relative fuel savings is linearly related to the reduction in fuel consumption. Results for the reference flight from requirement NCL-Alc09u2 can be found in Figure 8.21.

8.3.6. Justification

Main contributors to the fuel reduction is the aircraft weight reduction and the different take-off and landing procedures. Both contributors can be found in Figure 8.20.

The influence of the different take-off and landing procedures creates the major difference in fuel savings between short and long range flights. This difference is so huge because jet engine performance is optimised for flight conditions, but most aircraft spend considerable time on the ground taxiing from the terminal, out to the runway and back. This leads to a waste of precious time and an inefficient use of fuel. Due to more complex airport congestion, and increasing airport size, this taxi time has increased over the years and is predicted to keep increasing over the coming decades [61]. This will increase the overall fuel efficiency of the A321REMALS compared to the A321NEO even more. This effect is for the short range flights larger than long range flights, increasing the fuel savings difference between the different ranges even more.

The influence of the weight reduction can be seen in Figure 8.20 by the fact that the fuel savings decreases less per km for long range flights than for short range flights. In Figure 8.21 this effect can be seen by the % fuel reduction line approaching a constant values when the range goes to infinity.

As a general rule of thumb, it can be assumed that a reduction in fuel consumption of about 0.8 % results from each 1% reduction in weight [14]. The operational empty weight of the A321REMALS is 4.0% lower than the A321NEO. Hence, in the case where the different take-off and landing procedures were not implemented, the fuel should have been reduced by 3.2%. This value approximately matches with the horizontal asymptote of the relative fuel reduction line in Figure 8.21. This conclusion, combined with the different take-off and landing procedures, makes the findings for fuel savings highly reasonable.

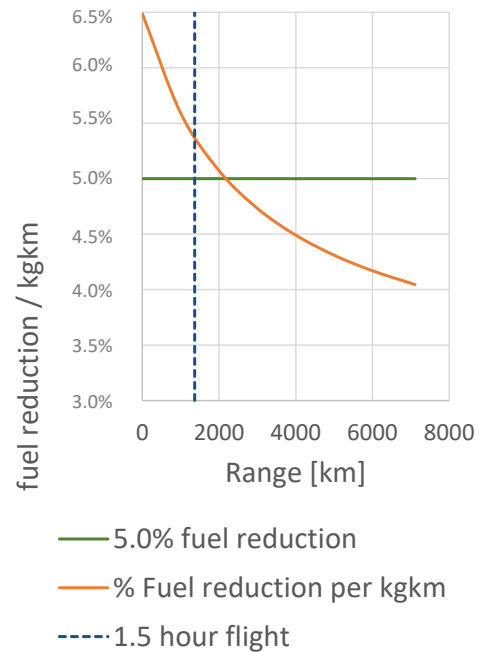


Figure 8.21: Fuel reduction per passenger per kilometer for a payload weight of 18702 kg

8.3.7. Sensitivity Analysis

An important input value for the fuel calculations is the thrust-specific constant, C_t . Therefore, a study have been done to determine how sensitive the final outcome is to the value of this constant. Results are shown in Figure 8.22. The fuel reduction decreases with the increment of the thrust-specific constant. The higher this constant, the less thrust can be provided with a certain amount of fuel. It therefore makes sense that, if less thrust can be provided with the same amount of fuel, the fuel savings due to the weight reduction during flight will become more dominant than the fuel savings due to the ground based power ground movements. Since the fuel savings of the cruise mission is relatively lower than that of the ground movements, the line will go down. It can be concluded that the fuel requirements are still met for a small deviation in the thrust-specific constant.

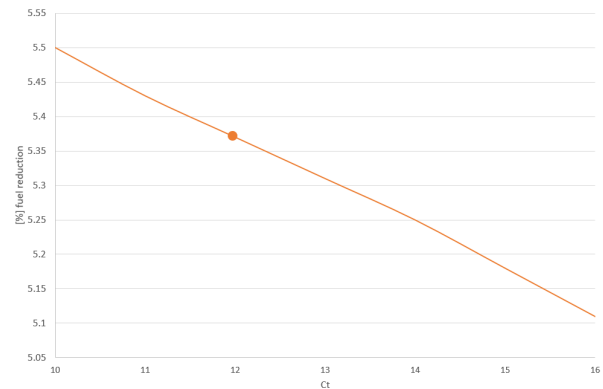


Figure 8.22: Sensitivity analysis for the thrust-specific constant.

8.3.8. Verification and Validation

This section verifies whether the obtained data is correct and validates that the outcome is applicable for the REMALS system. The total fuel consumption of the A321NEO are verified using the BADA files provided in the appendix. It should be noted that some deviations in fuel consumption of the A321NEO does not affect the final conclusion regarding the reduction in fuel consumption of the A321REMALS compared to the A321NEO. This reduction is already justified to be reasonable in subsection 8.3.6.

Climb and descent (FL20-FL350)

The rate of climb is multiplied by the fuel flow for all flight levels between FL20 and FL350, as shown in Equation 8.48. (Note that the rate of climb is plotted negatively for descent.) Values are taken from Table 3 and Table 4 for climb and descent, respectively.

$$\sum_{i=FL20}^{FL350} V_y |i \cdot \dot{m} |i \quad (8.48)$$

This results in a fuel consumption of 2090 kg for climb, which is 12% off the values calculated in this chapter. For descent, this results in a fuel consumption of 138 kg , which is 550% off. It can be concluded that the fuel consumption for climb is relatively correct. However, for descent, the 0.9900 fuel fraction found in [44] is too low. A sensitivity analysis has been done which concludes that the outcome of the update in descent fuel consumption is negligible.

Cruise

The fuel flow for a flight at FL350 according to BADA is 52.54 kg/m , as can be found in Table 5. The reference flight of 1,5 hours thus uses around 4728 kg of fuel for cruise. With Equation 8.45, it is calculated that this flight uses 4583 kg of fuel, a factor 3% off. This is assumed to be a reasonable deviation.

Validation

As described in subsection 3.1.3, a 1,5 hour flight is the average flight time for short-haul flights. Furthermore, all ground based systems run on renewable energy. Therefore, the fuel reduction of the aircraft is truly representative of the overall fuel consumption of the REMALS system; it can thus be concluded that the fuel requirements are valid for REMALS.

8.3.9. Conclusion Fuel Consumption and Recommendations

All flights with the A321REMALS will have at least 4.06% fuel reduction. Flights shorter then 3% hours will have at least 4.6% fuel reduction. 5% fuel reduction for 3 hour flights is only met if a payload of 14050 kg is boarded onto the aircraft, relative to a aircraft occupancy of 64%. For short range flights with an average flight time (1,5 hour), a fuel reduction of at least 5.2% will be reached. Therefore, it can be concluded that NCL-ALC09u1 is met.

For A321REMALS flights with average occupancy rate (84.7%), 5% relative fuel savings is met for flights shorter than 2 hour and 24 minutes. 1,5 hour flights with average occupancy will reach a 5.4% relative fuel reduction. Therefore, NCL-ALC09u2 is also met.

Recommendations

It is clear that great fuel savings can be achieved with REMALS. Moreover, REMALS is definitely not finished yet. The fuel efficiency of the A321REMALS might be improved even more by down-scaling the aircraft to a greater extent. chapter 15 elaborates on this and gives an profound overview of all recommended focus areas to improve fuel efficiency of the A321REMALS even more. Equation 8.49 provide a preliminary method to calculate the % fuel savings from every further kg reduction of the A321REMALS. It should be noted that this calculation is only accurate for small changes in weight (in order of 5% OEW).

$$[\%]fuel_{saved} = 0.001165695 \cdot M \quad (8.49)$$

8.4. Capacity

There are multiple elements that influence the capacity of the airport. There is the time required for take-off, landing and moving all the carts back. These operations will limit the capacity of the REMALS system. Furthermore, there is the lift that moves the grid to the top of the Stewart platform. Each runway should have enough lifts such that they do not limit the capacity of the system. Finally, the pistons of the Stewart platform needs accumulators since there are no pumps that can deliver the required flow rate. These accumulators need to be charged and should not limit the capacity of the airport.

Cart capacity

The carts are accelerated and decelerated in the linear part of the runway at a non-constant velocity. When the base structure reaches a velocity of approximately 26 *m/s* after deceleration, the ground system travels through a buffer zone of 330 metres (10% contingency margin of runway length) and slows down before the corner to turn away from the runway. From here of on, it travels at a velocity of 13*m/s*. At this point the base structure curves and travels away from the runway for 150 metres out of the ILS protection area until a complete stop. Once it comes to a complete stop the grid, with or without aircraft depending on whether a take-off or landing has been performed, is lowered down by the lift platform. In Table 8.7 the times required to move over each part of the runway are summarised. As mentioned before, the time required for the linear acceleration/deceleration is explained in 7.8.1. Furthermore the time to travel the remaining two distances was calculated by dividing the distances by their respective velocities. As was explained before, the buffer zone is covered at a velocity of 26*m/s* while moving out of the ILS safety zone happens at 13*m/s*. Clearly the landing procedures are the limiting part since the landing takes the most time at almost 65s per procedure. This means that 15s can be saved per landing to move all the carts back in order to meet the capacity of one landing per 80s on average.

Table 8.7: Time needed for take-offs/landings

| | Take-off [s] | Landing [s] |
|--|--------------|-------------|
| Linear Acceleration/Deceleration | 37.1 | 40.9 |
| Buffer zone at end of runway | 12.7 | 12.7 |
| Curved part out of ILS protection area | 11.5 | 11.5 |
| Total | 61.3 | 65.1 |

The time required to move the carts back is not constant with the amount of carts. The more carts are moved back, the more time it will take. The carts are linked together before they move back and only the first one will be propelled, the rest of the carts is pulled along. The time and power required for this movement was calculated with a python program. The track was divided such that acceleration and deceleration fits within the length. As the drag force makes the deceleration faster this took up slightly less time. The force that the motor delivers is constant, and as the acceleration reached decreases with the amount of carts, the power usage goes down with an increasing amount of carts.

Table 8.8: Time required to move a certain amount of carts back.

| Number of carts | Time [s] |
|-----------------|----------|
| 1 | 35.4 |
| 2 | 48.6 |
| 3 | 58.6 |
| 4 | 67 |
| 5 | 74.3 |
| 6 | 80.8 |
| 7 | 86.7 |
| 8 | 92.2 |

The time required to move 1 to 8 carts back can be found in Table 8.8. By combining these values with the 65s that is required per landing, an optimal number of carts can be found by calculating the average time per take-off. The lowest amount of carts required that has an average capacity higher than one landing per 80s is 5. When 5 carts are being used a landing can be performed every 80s on average. Furthermore, each take-off would take 76s on average.

Lift capacity

There are multiple operations that need to be performed in order transport the grid from the Stewart platform. First of all the platform should move laterally all the way to the side. Once the platform has moved all the way to the side, the grid has to slide on top of the taxi platform. It is assumed that this will happen in one smooth motion and thus the grid will cover this distance at a constant velocity. Since the taxi platform has the same size as the grid (12m) and the grid has to move from the centre of the rails (30m), the total distance that the grid has to cover is 21m. It is assumed that it travels at a constant velocity of 5km/h and thus the time required for this movement is 15s. The same movement, but in opposite direction will take the same amount of time.

The next step in the procedure is to move the lift up and down. As explained before both moving up and down will take 18s each. Finally, the taxi carts will have to drive on and off the lift platform. It is assumed that one such movement takes approximately 5s.

When the system has performed a take-off, the base structure continues with an empty grid on top. This grid has to be slid off the base structure, connected to the taxi cart and lowered. This taxi cart can transport the grid to the runway that is used for landings where grids are required. Afterwards, a new aircraft is lifted up and then moved laterally on the base structure.

When the system has performed a landing, the base structure brings the aircraft to the 'drop-off' location. Here the aircraft slides off the base structure on top of the taxi-cart and is then lowered to ground level. A new taxi cart with an empty grid that comes from the take-off runway will then move on top of the lift platform and then slide it on the base structure, similarly to the take-off.

Every action that needs to be performed to operate the lift is listed in Table 8.9 in chronological order for both a landing and a take-off procedure together with the required time for each action. This results in a total time required of 76s for both situations. Since this is longer than both the 61s and 65s that are required for a take-off and landing procedure, respectively, two lifts are required at each end of the runway to match the capacity. This results in 4 lifts per runway in total. These lifts can be installed in series on the same track.

Table 8.9: Time needed by the lift during take-off and landing

| Take-off | | Landing | |
|-----------------------------|-----------|-----------------------------|-----------|
| Phase | Time [s] | Phase | Time [s] |
| 1. Grid moves laterally | 15 | 1. Aircraft moves laterally | 15 |
| 2. Lift grid down | 18 | 2. Lift aircraft down | 18 |
| 3. Taxi cart drives off | 5 | 3. Taxi cart drives off | 5 |
| 4. New taxi cart drives on | 5 | 4. New taxi cart drives on | 5 |
| 5. Lift aircraft up | 18 | 5. Lift grid up | 18 |
| 6. Aircraft moves laterally | 15 | 6. Grid moves laterally | 15 |
| Total | 76 | Total | 76 |

In case of a take-off, the first lift will lift up an empty taxi cart such that the empty grid from the previous take-off can be removed. By the time that this has happened the second lift will already have lifted an aircraft such that the base structure can simply move next to the second lift and the aircraft can be slid on top of the base structure in order to perform its next take-off. Furthermore, the taxi cart from lift one that has an empty grid on top of it now moves to the landing runway and the taxi cart from lift two without the grid can simply line up at lift one.

In case of a landing, the first lift will lift up an empty taxi cart that connects to the grid on which the aircraft landed. Next, the base structure will move to the next lift where a new grid will be installed on top of the base structure. A taxi cart that arrives from the take-off runway and thus has a grid connected to it can line up at lift two. The carts that have installed a grid on top of the base structure can line up at lift one without a grid such that the arriving aircraft can be installed on top of it. The taxi carts from lift one that now have an aircraft on top drive the aircraft to the gate. Once the aircraft is ready for departure, the taxi cart drives the aircraft towards the take-off runway where it can start its cycle over again.

Having two lifts on each side of the runway has other advantages as well. For example, if one of the lifts is broken or is under maintenance, the runway can still be used at a slightly lower capacity.

Accumulator pump capacity

The accumulators that are used for the Stewart platform need to be charged for every take-off and landing. Since the pumps that are required to do this are relatively big, it is decided that there will be pump stations behind the lifts where the base structures line up after and before they perform a take-off or landing. Here they are standing still for a relatively long time, hence it is a good opportunity to connect them to a pump station that charges the accumulators. Each base structure is standing still for approximately the time it takes for 3 base structures to perform a take-off or landing when 5 base structures are used in a row. This is due to the fact that the base structure is being used once per cycle of 5 take-offs or landings and that it spends approximately the same time at the lifts. This means that the accumulators have to be charged within the time it takes to perform 3 take-offs or landings. Since the take-off procedure requires less time, the pump stations will be sized for take-offs as this will be the limiting factor. Note that this does not mean that each cart standing still for this amount of time continuously, so some base structures will begin being charged after they performed their take-off and continued being charged after they have been moved back to the other side of the runway.

In order to pump this amount of oil within the time limit at a pressure of 300 bar, very strong pumps would have to be used. A pump was found that has a flow rate of $270\text{cm}^3/\text{rev}$ at 1450RPM at such a high pressure⁸. this results in a flow rate of $391500\text{l}/\text{min}$ or $0.3915\text{m}^3/\text{min}$. If four of these pumps are installed in parallel, they can charge the accumulators in 2.43min or 146s which is significantly less than the 183s it takes to perform 3 take-offs.

This means that each base structure should be charged by 4 pumps when it is standing still. This means that there will be 4 pump stations, each with 4 pumps, behind the lifts at each side of the runway. Only 4 stations are required since the final cart that arrives will move back immediately. In Total each runway will have 32 pumps.

Taxi cart capacity

In the midterm it had been determined that the system would require 200 taxi cart in order to operate [23]. This includes 10% contingency and is based on the fact that each aircraft that is on the ground will require a taxi cart in order to be supported.

⁸URL: <https://www.hawe.com/products/product-search-by-category/hydraulic-pump/axial-piston-pump/v30e/> [Accessed 19 June 2019]

9

Operations and Functioning of REMALS

This chapter presents the operations and functioning of the REMALS. First, the operations and logistics are described in section 9.1 followed by the synchronisation instruments in section 9.2. Then, it is explained how the system communicates with its environment in section 9.3. Finally, the hardware and data handling diagrams are presented in subsection 9.3.2 and 9.3.3 respectively.

9.1. Operation and Logistics Description

This section mainly presents the general ground operations that the aircraft undergoes, including the landing and take-off phases. Subsection 9.1.1 gives an overview of the ground operations while subsection 9.1.2 elaborates on the new lay-out of Schiphol airport.

9.1.1. General Description of the Operations

In order to get a clearer picture of the ground operations of the REMALS concept, an operations diagram was created in Figure 9.1 and is described in this section.

Landing phase (in yellow in Figure 9.1)

When an aircraft approaches the airport for a landing, the grid which is mounted on top of the base structure will synchronise its velocity, lateral position and attitude with the aircraft. This is done by making use of multiple different LIDAR sensors which are presented in section 9.2. Once the aircraft is within proximity of the grid, the harpoons will lock. If the harpoons do not lock correctly, the aircraft can perform a go-around. This is explained in more detail in chapter 10. If the harpoons are locked, the ground system can then start braking by using the linear induction motors such that the energy can be recovered and stored in the flywheels.

From landing to taxi (in orange in Figure 9.1)

Next, the base structure will drive approximately 150 meters before reaching the lift located outside the sensitive zone. The lift platform is placed there for two reasons: first, there should be no obstructing objects within 150 meters next to the runway¹ accordingly to ICAO. Secondly, multiple base structures could line up behind the lift, without obstructing the runway, and all move back to the other side of the runway at once in order to perform their next take-off or landing. The 150 meters away from the runway at the end of each runway are presented in blue in Figure 9.2. This means that the time that is lost by moving the base structure back is only lost once per cycle of multiple take-offs or landings instead of every take-off or landing. In case the lift can not deal with the capacity of the runway, multiple lifts can be installed in series on the same extension or multiple extensions can be built in parallel, each with its own lift. This will be explained in more detail in section 8.4.

There, the grid to which the aircraft is connected will slide on top of a taxi cart and lowered by the lift. Once the taxi cart is lowered, air traffic control will instruct the taxi cart to which gate it should move. The taxi cart will then move autonomously to the gate by using GPS. The taxi carts are equipped with a communication system that can communicate with both the air traffic control and other taxi carts that are within proximity.

¹URL: <https://www.icao.int/NACC/Documents/Meetings/2014/GREPECASF1/GREPECASF1-2-3.pdf>

This way they can detect errors and avoid collisions. Furthermore, the taxi carts are equipped with a collision avoidance system in order to prevent collisions with other objects on the ground.

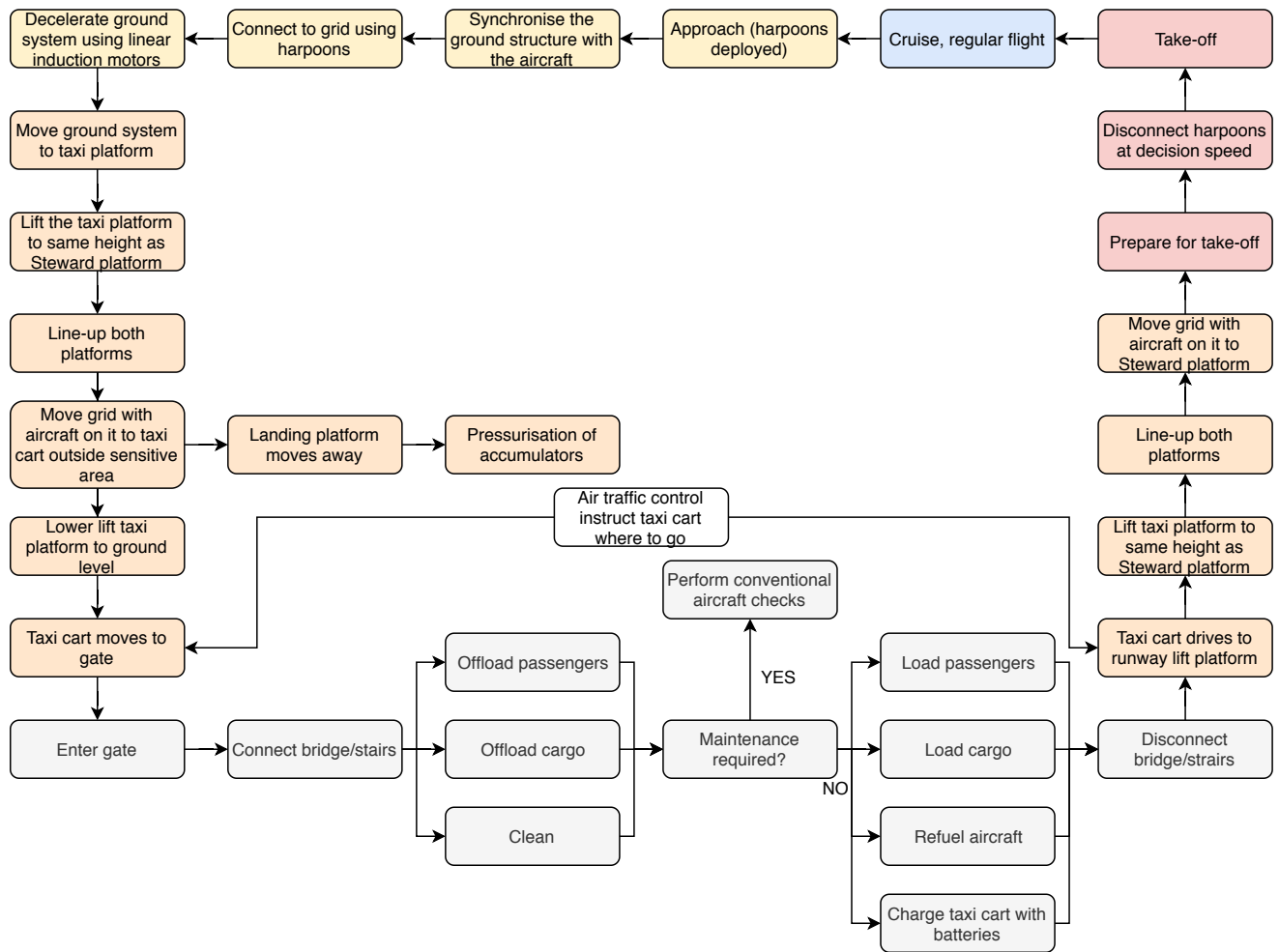


Figure 9.1: Operations diagram of the REMALS.

Ground operations (in grey in Figure 9.1)

Once the aircraft has arrived at its gate, ramp operations will be performed as usual (loading/unloading of cargo and passengers) such that it can be turnaround in the same amount of time as conventional aircraft. If maintenance on the aircraft is needed, it will be directed to the conventional maintenance area. In this maintenance area, all the spare parts for the aircraft as well as for the taxi cart are present. Since there is some space between the fuselage and the grid due to the height of the harpoons, machines and workers can simply be lifted on top of the grid with a special lift and perform operations as usual. Since the grid consist of many holes, a floor can quickly be installed on top of the grid to cover the holes. This way, an accident in which people or machinery equipment gets stuck in the grid or falls from the platform can be prevented. Next to the normal ramp operations, the batteries of the taxi cart will be charged at the gate. Once the aircraft is ready for departure, air traffic control will order the taxi cart to drive autonomously to the take-off runway.

From taxi to take-off (in orange in Figure 9.1)

Upon arrival at the take-off runway, the taxi cart will be lifted by the scissor lift. The grid to which the aircraft is connected will then be mounted from the taxi cart to the base structure. Once the previous base structure is moving outside of the sensitive area the next cart can start moving towards the runway from outside the safety zone.

Take-off phase (in red in Figure 9.1)

When the base structure with the aircraft on top is in position on the runway, it will start acceleration up to the decision speed. The decision speed is calculated to be 122 m/s as is calculated with a similar Python program as in subsection 7.8.1, which takes into account that the aircraft accelerates and decelerates within the length of the runway. Once the decision speed has been reached, the harpoons will close and the aircraft is not constrained in z-direction and is able to take-off in case of an emergency. However the zero-lift angle of attack in which the aircraft is mounted, restrains the aircraft from taking off. The aircraft is further accelerated to the take-off speed where the aircraft detaches from the grid by deploying the flaps. Then the base structure decelerates and moves outside of the sensitive zone such that the next take-off can take place.

Emergency Procedures

Unfortunately there will be situations where the aircraft with no landing gear will have to perform a landing without the aid of the ground-based system, this is called belly landing. This may be due to a malfunction of the ground-based system or due to the fact that there are no airport in range equipped with the ground-based system when the aircraft needs it.

When possible, in case of emergency an aircraft shall always do a belly landing over a hard surface like a runway, even if it is not equipped with the ground-based system. The landing on the grass, specially next to the runways, shall be avoided because it is an uneven surface which result in an uneven absorption of kinetic energy and therefore higher damages on the aircraft. Moreover, the grass next to the runway is often interrupted by taxiways which would further hinder the landing.

In case of a belly landing on the runway, emergency procedures in order to reduce risk to a minimum shall be performed. These actions are aimed at reducing the aircraft damage, reducing the deceleration forces, reducing friction spark hazard, reducing fuel spill hazard. The International Civil Aviation Organisation (ICAO) has performed various studies on the topic and its latest manual [62] does not recommend foaming the runway because its effectiveness has not fully been substantiated by real evidence. From the data available it appears that applying a foam carpet on the runway does not show significant reduction in aircraft damage or fire hazard of fuel vapours in the atmosphere over the foam. Moreover, tests conducted by ICAO have shown that aluminium alloys metal produce no friction sparks capable of igniting aircraft fuel vapours on either dry or foam-covered runways. Finally, foam laying operations uses primary firefighting vehicles and foam that could be better to extinguish the fire from the aircraft. The optimal approach is therefore to spray the aircraft with foam once it comes to a complete stop. The foam used shall be a 'protein' foam (fluorine-free) that is not as efficient as conventional synthetic foams but is more sustainable².

Additionally, to be able to have a safe landing in the situation where the aircraft has to divert to an airport without ground based take-off and landing system, emergency landing carts shall be implemented on those airports to ensure a smooth landing. These emergency carts can also be present at the airports with a ground based take-off and landing system to safely landing during a power outage.

9.1.2. Airport Lay-Out

In order to reduce costs, the airport shall be modified as little as possible and all current operations shall not be disrupted by the installation of the new system. Hence, it is important that the runway can still be used by a conventional aircraft. The rails of the REMALS system is the limit since a smooth surface is required for conventional aircraft to take-off from and land on. It was decided to dig the rails into the ground such that they can be covered by lids that are strong enough to carry the weight of the conventional aircraft. These lids can be opened up by pistons such that the rails can be used by the base structure. Each rail will be covered up by multiple lids that are not very long such that they can easily be lifted by the pistons. Each lid is equipped with a sensor to verify whether the lid is in the correct position. Having a lid that is still closed when the ground system is being used could be disastrous as it could be hit by the wheels of the base structure. On the other hand having a lid that is still open when a conventional aircraft is using the runway might be equally disastrous as the wheels could get stuck in the trench.

Furthermore, in most of the cases not all carts will be used at the same. Hence, they need to be stored on a separate location on the airport's perimeter. This area is shown in Figure 9.2 by the yellow areas and was chosen because it does not interfere with on-ground navigation and landing instrumentation, or taxiways. Using a virtual ruler on Google Maps, the available place for storing is approximately equal to 16 km^2 . The area al-

²URL:https://www.faa.gov/airports/airport_safety/certalerts/media/part-139-cert-alert-19-01-AFFE.pdf [Accessed 03 June 2019]

located to the charging stations is on the airport's perimeter, hence it does not have to occupy neighbouring land and disrupt the life of residents around the airport.

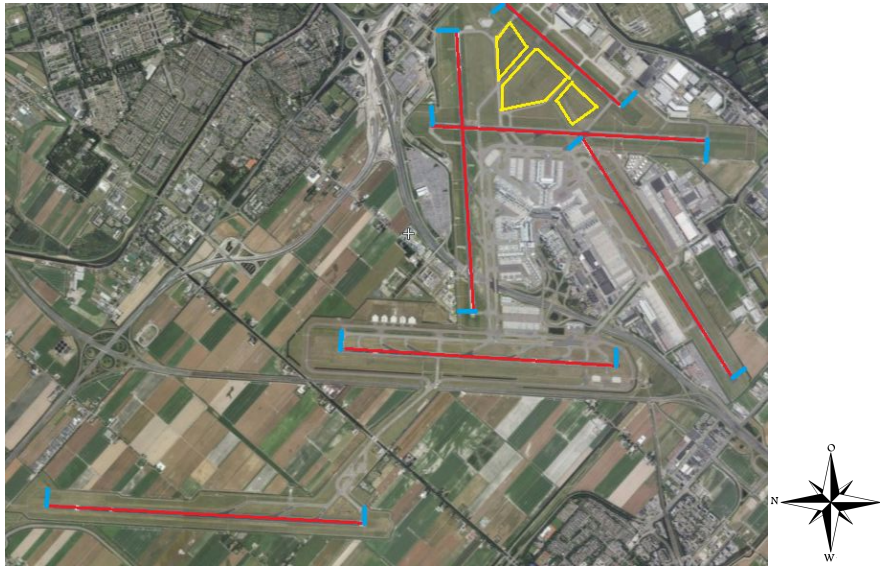


Figure 9.2: New airport layout of Schiphol with the runways marked in red, the storage space marked in yellow, the loop addition marked in blue.

9.2. Synchronisation Instruments

In order to land safely on the ground based vehicle, sensors and tracking systems are needed to provide the required accuracy and a good synchronisation between the ground vehicle and the aircraft. The primary instruments needed to execute a successfully synchronised REMALS landing are ADS-B, LiDAR, photon LiDAR, and a radar sensor.

9.2.1. Instruments

In order to determine the precise position of the aircraft a Light Detection and Ranging (LiDAR) system is placed on the ground vehicle³. It uses the principle of laser pointing where a light energy is sent which hits an object and returns back to the sensor. The time it takes for the emitted light to return to the sensor provides information on the distance between the sensor and the obstacles. LiDAR can therefore only be of use when the objects are in close proximity of the system and can be seen closely. LiDAR technology is widely used today especially in mapping of the Earth but also on autonomous vehicle to avoid collision with obstacles⁴. LiDAR technology is proven to work with high accuracy in highly dynamic environments like the driving of autonomous cars. Therefore LiDAR is deemed appropriate for the use in the REMALS as a system that takes care of the fine synchronisation.

The RE05 3D LiDAR scanner⁵ and OPAL-P1000 3D LiDAR scanner⁶ are specifically used. The RE05 3D LiDAR scanner is a lightweight scanner that can adapt its scanning behaviour rapidly. It can allow to scan a full area of 360°, which is useful for an aircraft that moves freely in space, but it can also focus on a specific wanted region in space. The RE05 3D LiDAR scanner can target an object up to 160 meters in distance with an elevation field of 70° and has a range accuracy of ± 50 mm. The maximum sample rate of this LiDAR scanner is 30kHz. This range is small and therefore the OPAL-P1000 is also used even though it has a smaller field of view of just 45°. The OPAL-P1000 has a range of up to 1000 meters and can start more accurate speed synchronisation earlier on.

As LiDAR's detection range and accuracy are affected by bad weather conditions, a photon LiDAR using time tagging of individual photons shall be used as backup during bad weather conditions. During fog and

³URL:<https://gisgeography.com/lidar-light-detection-and-ranging/> [Accessed 3 June 2019]

⁴URL:<http://lidarradar.com/apps/100-applications-or-uses-of-lidar-technology> [Accessed 3 June 2019]

⁵URL:<http://www.ocularrobotics.com/products/lidar/re05/> [Accessed 3 June 2019]

⁶URL:<http://www.neptectechnologies.com/wp-content/uploads/2019/04/OPAL-P-Series-Panoramic-FOV-88-00202-001-REV-A.pdf> [Accessed 3 June 2019]

rain conditions, the capabilities of the LiDAR sensor are limited and the distinction between an object and fog becomes difficult. Hence, a technique able to see through dense fog and rain has to be implemented. For this, a photon LiDAR system⁷ that can be used on aircraft and helicopters in landing, take-off and low level flight during dense fog conditions is utilised. Photon LiDAR technique is based on ultra-fast measurements using a single photon avalanche diode camera where the unwanted weather condition (for example the fog) is computationally removed. It produces a picture and depth map from this where the fog is absent and only the obstacle remains. Photon LiDAR can actually 'see' through fog and can detect objects that can not be seen with the naked eye. One disadvantage of this system is that it has a lower acquisition time which limits the immediate movement of the ground vehicle. Hence, this technology is used in combination with the RE05 3D LiDAR scanner and is only active during bad weather conditions.

Close to the harpoons located on the aircraft, a radar sensor like⁸ is placed to determine exactly when the harpoons can be opened. This sensor is linked to the harpoon mechanism in the aircraft and gives a signal to the harpoons to open when needed. The radar sensor is reliable, small, designed for extreme environments, and fast.

The synchronisation sensors are placed on top of the Stewart platform in both the front and the back. The lateral sides can not be used as the grid needs to be able to slide of the platform.

9.2.2. Procedure

The conventional landing procedure regarding the pilot's actions is not heavily impacted by the synchronisation requirement. Manual landings are preferred over autolandings as they are generally less stressful and higher quality landings with a lower workload. The aircraft approaches the REMALS runway in a similar way a conventional aircraft would. In low visibility conditions the existing highly redundant autoland system using ILS should provide enough precision to effectively approach the REMALS runway [4]. The ground vehicle will adjust its position and orientation to match the aircraft's. The ground vehicle is made aware of the aircraft's coarse approach details by use of automatic dependent surveillance-broadcast equipment (ADS-B) which will be present on all aircraft from January 2020 onwards⁹. ADS-B is used to send the aircraft's exact location to the air traffic control tower and this information can be forwarded to the relevant ground vehicle. Once the aircraft is in close enough range the ground system will use the LiDAR system to accurately synchronise with the aircraft in more detail regarding the speed and orientation. First the OPAL-P1000 is used and when the aircraft is close enough the RE05 is activated. If the vision is worse than minimally needed for the use of LiDAR, photon LiDAR shall be used. Weather conditions are known from the Automated Weather Observing System (AWOS)¹⁰ already located at the airport. This source will send the weather conditions to the ground vehicle which will then be able to determine which sensor to use. Once the aircraft is close enough to the ground vehicle the radar sensors placed on the aircraft decide when it is time to deploy the harpoon. The ground vehicle checks whether the aircraft is connected and then starts the deceleration procedure. The procedure is synchronisation represented in Figure 9.5.

9.3. Communications within the REMALS

The take-off and landing phases are preferably performed and controlled by the pilots in the aircraft. However, this will not always be the case especially when the weather conditions are bad and the visibility is low. In this case, the auto-land will be activated. Furthermore, the ground vehicle performs every steps automatically, meaning that no physical contact from humans is done with it. Hence, a good understanding on the communications, the flow of data through the system and how the components of the data handling system are interrelated is required.

9.3.1. Communication Flow Diagram

A first general overview of the data flow is provided by the communication flow diagram in Figure 9.3. It presents the interactions between the main components of the system: the aircraft, the pilots, the air traffic control tower, the ground control, the ground based vehicle and the weather radar. The arrows show the information that goes out and in of the systems. Communication within the ground vehicle itself is presented in more detail (in orange) as it is an important part of the design: communication is made between the

⁷URL:<http://web.media.mit.edu/~guysat/fog/> [Accessed 3 June 2019]

⁸URL:<https://www.baumer.com/us/en/product-overview/distance-measurement/radar-sensors/c/291> [Accessed 3 June 2019]

⁹URL:<https://www.govinfo.gov/content/pkg/FR-2010-05-28/pdf/2010-12645.pdf> [Accessed 3 June 2019]

¹⁰URL: [https://www.skybrary.aero/index.php/Automated_Weather_Observing_System_\(AWOS\)](https://www.skybrary.aero/index.php/Automated_Weather_Observing_System_(AWOS)) [Accessed 12 June 2019]

processing units, the navigation systems, the propulsion part and the synchronisation components. More details about these components are given in subsection 9.3.2.

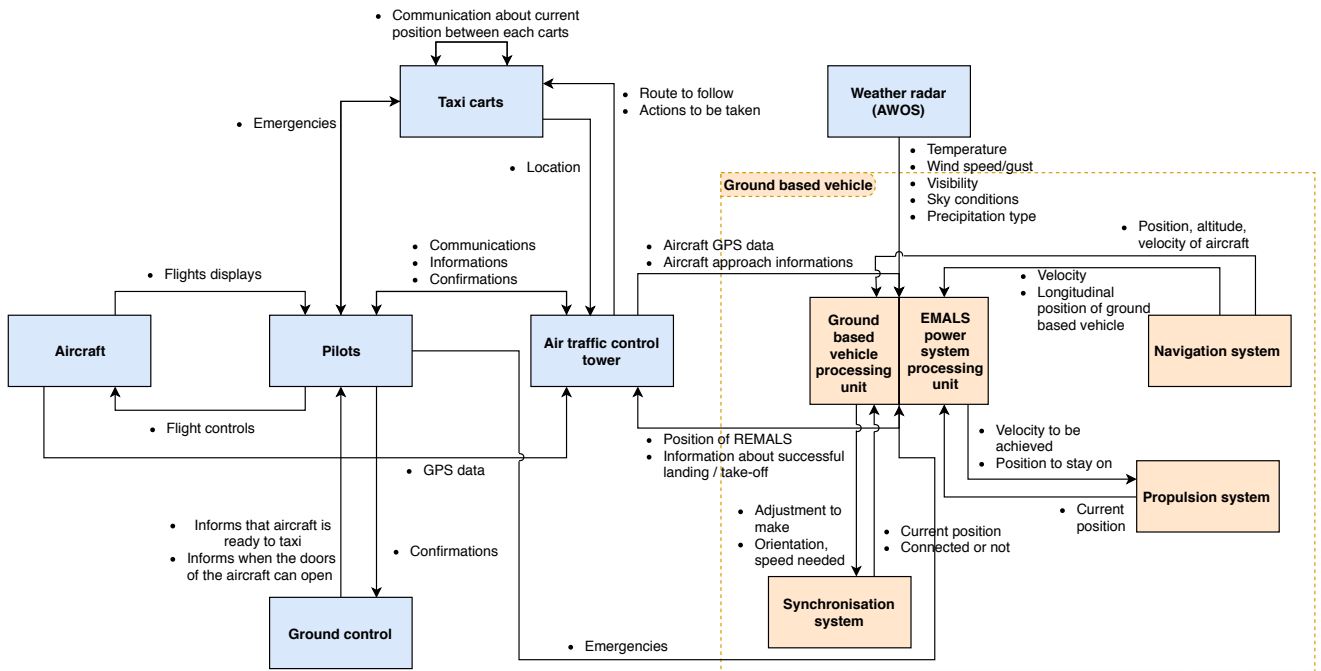


Figure 9.3: Communication flow diagram of the REMALS concept.

9.3.2. Hardware and Software Diagram

A second overview can be done with a Hardware and Software diagram in order to get an insight on the interactions between the hardware and software components. The diagram is constructed and shown in Figure 9.4. The most important components of the ground vehicle and the aircraft leading to a proper functioning of the system are presented in the coloured blocks. The grey boxes are the processing units of each structure: aircraft, EMALS system and the vehicle itself. They process the inputs and "give" instructions as output. The blue boxes refer to the navigation which contains all the sensors and measurement units to calculate the position of the aircraft and the ground vehicle. Then, the green boxes represent the controls of the aircraft which are output of the aircraft's processing unit. Next, the yellow boxes comprise the tools enabling the synchronisation of the platform with the aircraft, which are outputs of the ground vehicle's processing unit. Finally, the orange boxes are for the power/propulsion components of the EMALS system which powers the ground vehicle. Other components as batteries, radio or flight controllers are presented in white. Important information about the hardware components are also included in the boxes. Furthermore, the arrows represent the actual interactions between the hardware components.

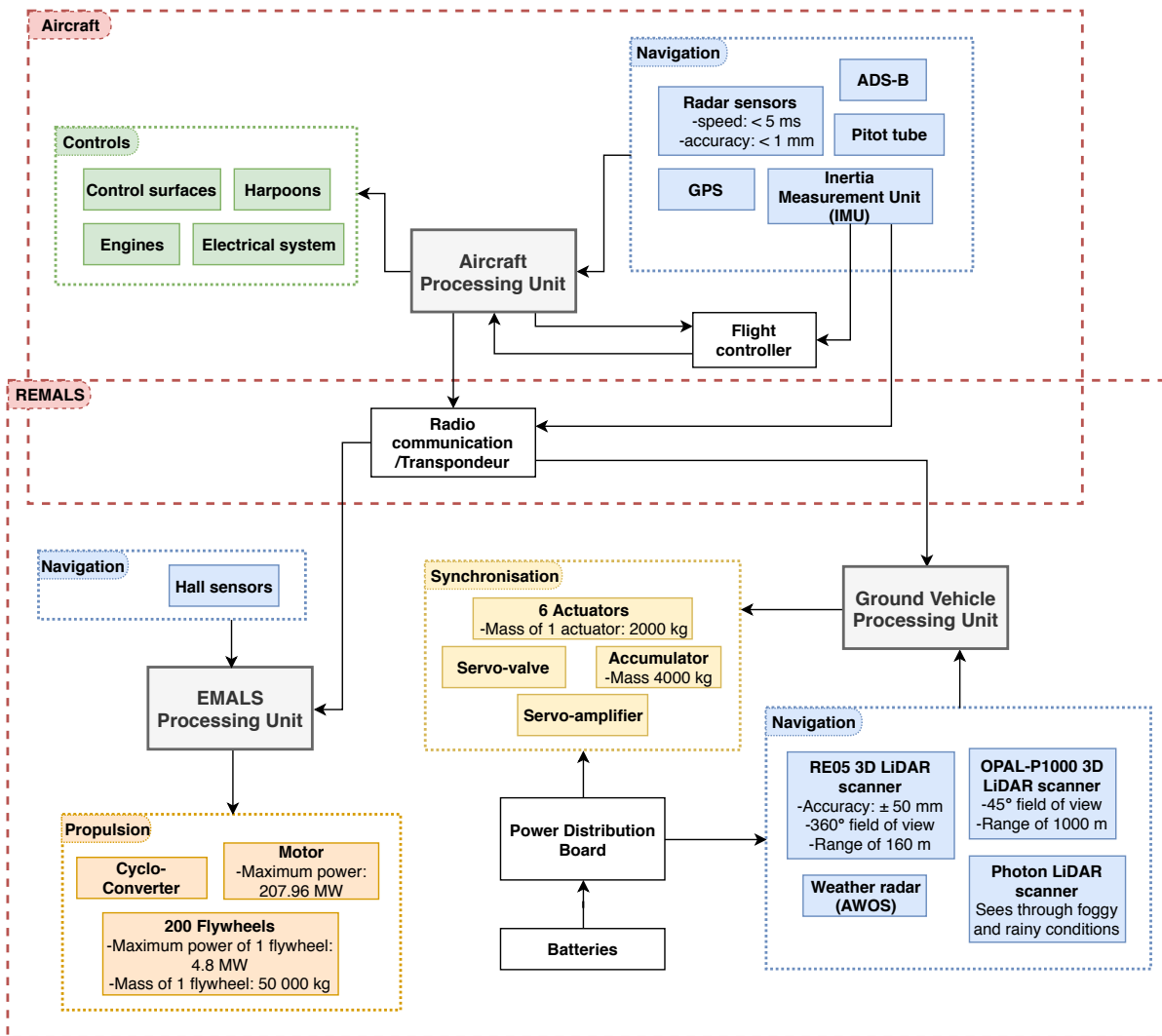


Figure 9.4: Hardware and software diagram of the REMALS concept.

9.3.3. Data Handling Block Diagram

Once the software and hardware components have been established, another interesting aspect is to understand how the data exactly flows within the system. This is represented in Figure 9.5. The main inputs of the REMALS system are the sensors located on the ground vehicle and the aircraft.

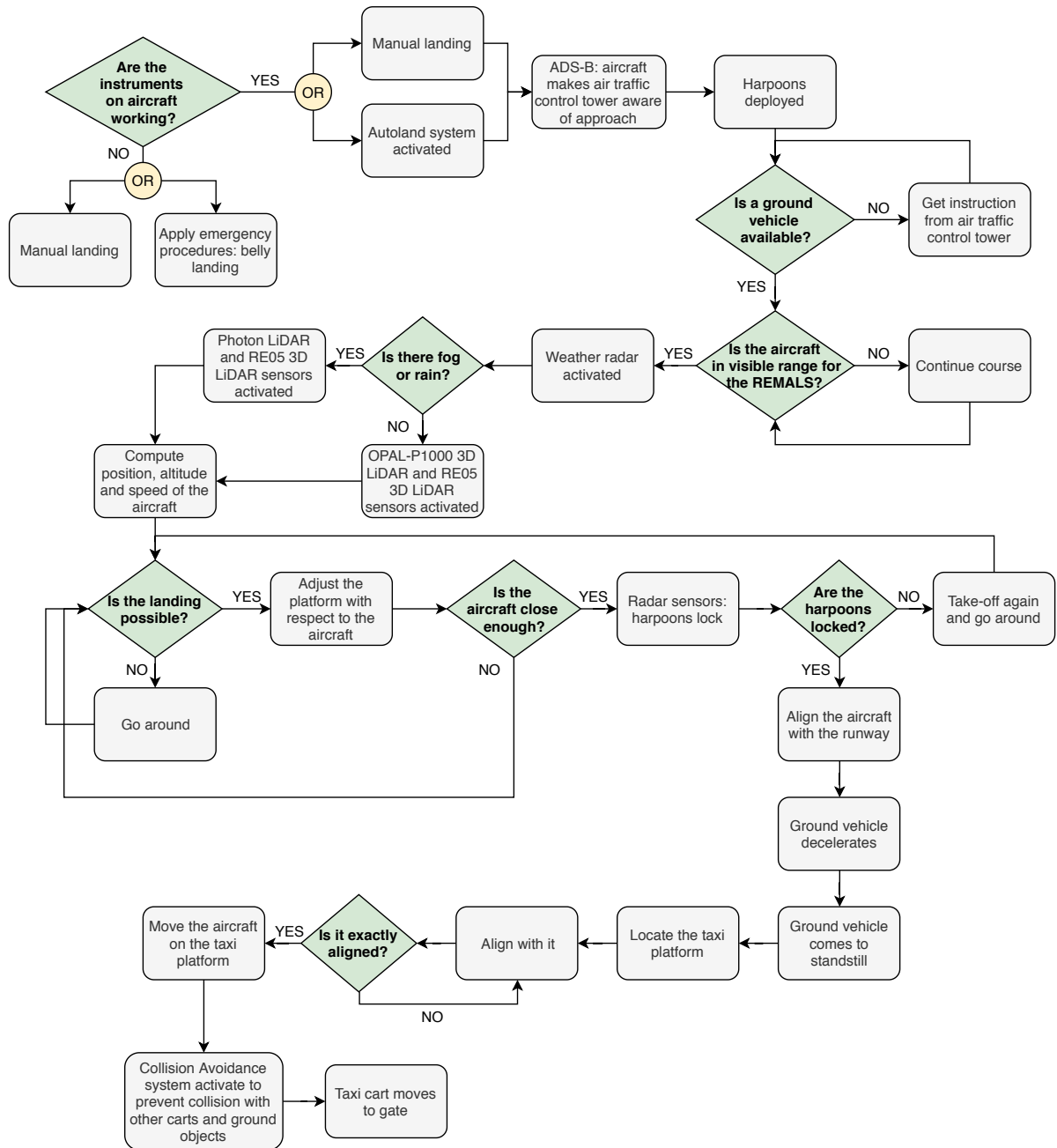


Figure 9.5: Data handling block diagram of the REMALS concept.

10

Risk

It is of utmost importance to identify the risks associated with the REMALS to ensure that a safe and economically feasible solution is developed. Risks in the REMALS are different from risks in conventional take-off and landing procedures. The REMALS introduces additional functions as described in section 3.3 that need to be completed to ensure a successful take-off and landing. Risk identification and management has been an integral part of the design process. Risks have been proactively monitored and handled in the entire design process. The first step in the risk management process, risk identification, is discussed in section 10.1. The next steps, risk assessment and risk analysis, yielded risk maps which are presented in section 10.2. Thereafter, risk mitigation is discussed in section 10.3. Then, the risk assessment is concluded and briefly summarised in section 10.4. Finally, reliability, availability, maintainability and safety (RAMS) characteristics are presented in section 10.5.

10.1. Risk Identification

The technical risk assessment was started by identifying risks. The risk identification process was approached by looking at the risks of not fulfilling the functions of the total system. The functions were linked to the different components of the system as mentioned in section 5.1. The method that was used to find modes of failure and risks is called failure mode effect and criticality analysis (FMECA). FMECA links the functional analysis to the design solution or the components. The failure modes are linked to the components and converted into risks [75]. From this, one can identify the subsystems that are most important for the functioning of the product [18]. The motivation to use FMECA can be found in section 10.5. A drawback of FMECA is that it does not consider combinations of component failure or multiple components failing at the same time.

The components that are assessed with their respective identifiers are presented in Table 10.1. To keep a clear overview in which part of the system a risk is present, a reference is incorporated in the identifier. The identifiers include an RL, RA or RR which refers to risks related to the load carrying structure, the aircraft or the remaining risks respectively.

Table 10.1: Risk identifier categories.

| Risk ID | Description | Risk ID | Description |
|---------|-------------------------|---------|-------------------------|
| RL1-XX | Grid platform | RA3-XX | Landing |
| RL2-XX | Stewart platform | RR1-XX | EMALS |
| RL3-XX | Rotation platform | RR2-XX | Power |
| RL4-XX | Lateral movement system | RR3-XX | Taxi cart |
| RL5-XX | Base structure | RR4-XX | Runway station |
| RL6-XX | Rails and wheels | RR5-XX | Synchronisation sensors |
| RA1-XX | Connection mechanism | RR6-XX | Software |
| RA2-XX | Take-off | RR7-XX | Weather |

The risks for the load carrying structure, the aircraft and the remaining risks are presented in Table 10.2, Table 10.3 and Table 10.4 respectively.

Now all the individual risks are identified, also combinations of the risks should be considered. This is done separately as the FMECA does not account for having multiple risks at the same time. This is mainly

Table 10.2: List of identified risks related to the load carrying ground system.

| Risk ID | Event |
|---------|---|
| RL1-01 | Grid platform is not available for landing of an aircraft. |
| RL1-02 | Grid is damaged by impact loads |
| RL1-03 | People fall through grid during ground operations. |
| RL1-04 | Objects fall off the platform as the platform is higher than ground level. |
| RL2-01 | The failure of an actuator. |
| RL2-02 | Platform is in singular position. |
| RL2-03 | Platform exerts too high forces and damps the aircraft abruptly. |
| RL2-04 | Aircraft is damaged by the platform. |
| RL2-05 | Accumulator unit rupture. |
| RL3-01 | Stewart platform does not have correct orientation for take-off or landing procedure. |
| RL3-02 | Slewing bearing fails. |
| RL4-01 | Lateral movement system is unable to move laterally. |
| RL4-02 | Lateral movement system is not properly aligned with the aircraft. |
| RL5-01 | Base structure failure due to fatigue. |
| RL6-01 | Failure of wheels of base structure occurs. |
| RL6-02 | Vibrations introduced by metal wheels. |
| RL6-03 | Rails system is not covered by lid when desired. |

Table 10.3: List of identified risks related to the aircraft.

| Risk ID | Event |
|---------|--|
| RA1-01 | Aircraft does not disconnect from the grid when desired. |
| RA1-02 | Connection mechanism is damaged by impacts on grid |
| RA1-03 | Connection mechanism is unable to actively connect to grid. |
| RA2-01 | Engine failure during take-off. |
| RA2-02 | Landing gear does not deploy. |
| RA2-03 | Base structure is not out of safe zone before take-off of next aircraft. |
| RA2-04 | Landing gear does not retract. |
| RA2-05 | Take-off with one engine inoperative. |
| RA2-06 | Landing gear is structurally damaged. |
| RA3-01 | Aircraft is directed to take-off runway instead of landing runway. |
| RA3-02 | Divert to different airport without the ground based powered landing system. |
| RA3-03 | Aircraft can not prepare for landing. |
| RA3-04 | Landing with one engine inoperative. |
| RA3-05 | Aircraft is unable to perform go-around. |
| RA3-06 | Aircraft introduces too large forces in the ground system. |
| RA3-07 | Ground system is thought to be properly synchronised with the aircraft whilst it is not. |
| RA3-08 | Ground system is not properly synchronised with the aircraft. |
| RA3-09 | No landing system is ready to be used. |

relevant for risks with a relatively low impact and high likelihood. These risks by themselves are not significant but in combination they can present higher risks [60]. Also some risks might increase the probability of other risks to occur. Some of the most critical risk combinations that are identified are discussed below.

The risk that the landing system is not ready or the grid platform is not available (RA3-09 or RL1-01) in combination with an aircraft unable to perform a go-around (RA3-05) is a serious risk. Also the risk of the aircraft not being properly synchronised with the ground system (RA3-07 or RA3-08) in combination with large impact forces (RA3-06) can result in dangerous situations.

The risk of the sensor not being able to determine the position of the aircraft in adverse weather conditions (RR5-01) can cause the risk of the aircraft not being properly synchronised with the ground system (RA3-07 or RA3-08). Also the risk of excessive heats in the EMALS (RR1-05) might result in a power outage (RR2-01) if a short circuit occurs.

10.2. Risk Maps

For all identified risks as in section 10.1 both the event impact and the likelihood of the event happening are estimated. The impacts and likelihoods are scaled according to Table 10.5 which is a derived scale from the

Table 10.4: List of identified risks related to the remaining categories.

| Risk ID | Event |
|---------|--|
| RR1-01 | Failure of a EMALS section. |
| RR1-02 | Aircraft cannot be decelerated sufficiently. |
| RR1-03 | The EMALS is not able to operate in adverse weather conditions. |
| RR1-04 | Aircraft is accelerated/decelerated too fast. |
| RR1-05 | Excessive heats are generated in the EMALS because of the significant power usage. |
| RR1-06 | Magnetic interference with the aircraft. |
| RR2-01 | Power outage occurs and no acceleration / deceleration force can be created. |
| RR2-02 | Power system that provides power to base structure is not functioning. |
| RR3-01 | Miscommunication between control tower and taxi cart. |
| RR3-02 | Autonomous system of taxi cart is uncontrollable with aircraft connected. |
| RR3-03 | Autonomous system of taxi cart is uncontrollable without aircraft being attached. |
| RR3-04 | Tire failure of taxi cart. |
| RR4-01 | Scissor lift is inoperative. |
| RR4-02 | Pump station is not functioning. |
| RR4-03 | Ground system is not properly aligned with the scissor lift. |
| RR5-01 | Sensor (lidar) is not able to accurately determine the position of the aircraft in adverse weather conditions. |
| RR6-01 | Processing unit crashes. |
| RR6-02 | The system is hacked. |
| RR7-01 | The system is adversely affected in adverse weather conditions. |

Sofia risk matrix from NASA ¹. Using the impacts and likelihoods estimated for every identified risk, the risks are mapped. The probability of occurrence is shown on the vertical axes whilst the impact is shown in the horizontal axes. The colours are linked to the severity of the risk. The red colours indicate high risks, yellow indicates medium risks and green represents low risks.

Table 10.5: Scaling of risks used in the risk maps.

| | Event Impact | Likelihood |
|---|--|----------------|
| 1 | Minimal or no impact | Not likely |
| 2 | Moderate reduction; same approach retained | Low likelihood |
| 3 | Moderate reduction, but workaround available | Likely |
| 4 | Major reduction; workaround available | Highly likely |
| 5 | Unacceptable; no alternatives exist | Near certain |

The risk map for the load carrying ground system can be found in Table 10.6. This risk map contains the risks from Table 10.2. There are 7 medium risks identified before mitigation. The highest risks are related to the control of the Stewart platform and the control of the lateral movement system. These components have to be controlled properly in order not to do damage to the aircraft or the payload inside.

Table 10.6: Risk map for load carrying ground system.

| Likelihood \ Impact | Impact | | | | |
|---------------------|--------|--------|------------------------|--|---|
| | 1 | 2 | 3 | 4 | 5 |
| 5 | | | | | |
| 4 | | | | | |
| 3 | | | RL3-02, RL6-02, RL6-03 | RL2-03, RL4-02 | |
| 2 | | RL1-04 | RL1-03 | RL1-01, RL2-01 | |
| 1 | | | RL2-02, RL3-01 | RL1-02, RL2-04, RL2-05, RL4-01, RL5-01, RL6-01 | |

The risk map of the risks related to the aircraft can be found in Table 10.7. This risk map contains the risks from Table 10.3. There are 4 high and 5 medium risks identified before mitigation. The high risks are related to synchronisation of the ground system with the aircraft and the communication between the two of them. Furthermore, the high risks are related to the loads the aircraft introduces in to the load carrying structure and the availability of the system.

¹URL: https://www.nasa.gov/sites/default/files/thumbnails/image/sae_graphic4_lg2.jpg [Accessed 16 June 2019]

Table 10.7: Risk map for aircraft categories.

| Likelihood \ Impact | Impact | | | | |
|---------------------|--------|----------------|--------|------------------------|----------------|
| | 1 | 2 | 3 | 4 | 5 |
| 5 | | | | | |
| 4 | | | | | RA3-07, RA3-08 |
| 3 | | | RA1-02 | RA1-01, RA1-03 | RA3-06, RA3-09 |
| 2 | RA2-05 | RA2-01, RA2-06 | RA2-03 | RA2-02 | |
| 1 | | RA2-04 | RA3-04 | RA3-01, RA3-03, RA3-05 | RA3-02 |

The risk map for the remaining categories can be found in Table 10.8. This risk map contains the risks from Table 10.4. There are 2 high and 9 medium risks identified before mitigation. These risks are mainly related to the communication between different components of the system.

Table 10.8: Risk map for remaining categories.

| Likelihood \ Impact | Impact | | | | |
|---------------------|--------|--------|--|--------------------------------|--------------------------------|
| | 1 | 2 | 3 | 4 | 5 |
| 5 | | | | | |
| 4 | | | | RR1-05, RR3-01 | |
| 3 | | | | RR5-01 | |
| 2 | | | RR1-01, RR1-03, RR4-01, RR4-02, RR7-01 | RR1-02, RR1-04, RR3-03, RR4-03 | RR2-01, RR2-02, RR3-02, RR6-02 |
| 1 | | RR1-06 | RR3-04 | RR6-01 | |

10.3. Risk Mitigation

After the risks have been identified, the mitigation of medium and high risks should be considered. High risks are unacceptable and should therefore be mitigated. Medium risks should be mitigated where possible. Risk mitigation is of primary importance in the design process as the design is not able to function within the safety requirements if no risk mitigation is done. The mitigation strategies on how the medium and high risks are mitigated is presented in Table 10.9. The risk maps that follow after the risks are mitigated are presented in Table 10.10, Table 10.11, and Table 10.12. The mitigation of the risks combinations is done by mitigating the risks individually. If the risks are less likely to occur, the likelihood of the combination of those risks is also reduced.

10.4. Risk Assessment Conclusion

Evaluating the mitigated risk maps, a general risk evaluation is made for the REMALS. According to NASA ³, risk can be linked to technical performance, cost resources, and schedule time. The Technology Readiness Levels (TRL) of the components of the REMALS is included in the general risk evaluation and can mainly be linked to all components of risk. Technology Readiness Levels of the different components are estimated according to [58]. The TRL indicates the readiness of the technology, it is used to evaluate the current technology's status. A technology that has a low TRL needs a lot of development, analysis, testing, and certification before it can be implemented in an aerospace system. The TRL of the components that make up the REMALS is estimated to be relatively high, however they haven't ever been shown to work in the way they are integrated in the REMALS. Thus, the TRL of the REMALS is estimated to be 4.

For a complex system with high safety requirements and medium TRL, as is the REMALS, it can be a time-consuming process to finish testing and certification of the product. The components of the system already exist, however certifying and developing the combination of them together can add some risk. Thus, schedule risks are medium.

As the market is constantly changing and one can not predict what is going to happen with for instance fuel prices, energy prices or emission taxes it is tough to guarantee the economical feasibility of REMALS in

²URL: <https://www.mromagazine.com/2010/09/13/why-do-turntable-bearings-fail/> Accessed 20 June 2019

³URL: <https://www.nasa.gov/evm/tutorial> [Accessed 23 June 2019]

Table 10.9: Risk mitigation overview.

| Risk ID | Move-ment | Mitigation strategy |
|---------|-----------|---|
| RL1-01 | ↓ | There should be proper planning regarding the allocation of grid platforms. Backup grid platforms with charged accumulators should be available at all times. |
| RL2-01 | ← | Design a different configuration with more than 6 actuators. This way the system is redundant and maximum forces can possibly be reduced. Control system however will be more complicated as the system is overconstrained, but in theory it is possible. |
| RL2-03 | ↓ | Accelerometers should be installed on the platform to monitor the maximum deceleration of the aircraft. |
| RL3-02 | ↓ | Slewing rings need a heavy-duty pressure grease that should be reapplied every 100 hours is the bearing is used intermittently ² . |
| RL4-02 | ↓ | Sufficient sensors that monitor aircraft position and lateral movement platform shall be installed to ensure correct synchronisation. |
| RL6-02 | ↓ | Implement dampers on the base structure and perform a vibration analysis. |
| RA1-01 | ↓ | Disconnect the connection mechanism right before the decision speed and add sensor to check whether connection is connected or not. |
| RA1-02 | ← | Perform frequent checks on the connection mechanism and perform maintenance if required. |
| RA1-03 | ↓ | Implement a passive mechanical system that opens the harpoon connection once required forces is exerted on the landing gear strut by the grid. Additionally an active backup system can hydraulically control the connection mechanism if desired. |
| RA2-02 | ↓ | Gravitation forces are used to deploy the landing gear. |
| RA3-02 | ← | Place emergency cart on nearby airport without the system, or perform a belly landing in case of emergency. |
| RA3-06 | ↓ | Further investigate the most critical impact loads and apply conservative safety factor for the design. |
| RA3-07 | ↓ | LiDAR sensors attached to the aircraft communicate to the pilot whether or not the platform is in the right position. |
| RA3-08 | ✓ | Enough sensors should be installed to have a fully redundant system that is able to accurately determine the position and movement of the aircraft during approach. |
| RA3-09 | ✓ | Backup ground system should be available at all times. If not, the aircraft should loiter for a short period of time until the next ground system is ready. |
| RR1-02 | ← | Implement backup mechanical braking system. |
| RR1-04 | ↓ | Install accelerometers on the platform to monitor the accelerations. |
| RR1-05 | ✓ | Cooling system using liquid nitrogen is implemented in the EMALS together with a fire extinguishing system. |
| RR2-01 | ✓ | Implement backup braking system to decelerate the aircraft safely. Backup generators are installed that supply maximum power required for landing procedure. |
| RR2-02 | ✓ | Implement small battery to provide power to control instrument, lateral movement system and valves of the Stewart platform. |
| RR3-01 | ↓ | Taxi cart can also communicate by itself with other taxi carts. Add LiDAR sensors and a collision avoiding system to monitor surroundings of taxi cart. |
| RR3-02 | ✓ | Pilot can take over the controls of the taxi cart and safely manoeuvre around the airport and air traffic control is able to shut down cart if necessary. |
| RR3-03 | ✓ | Air traffic control is able to shut down every taxi cart. |
| RR4-03 | ↓ | Add sensor that monitors alignment of grid platform with the scissor lift. |
| RR5-01 | ↓ | Additional photon LiDARs are installed to operate in adverse weather conditions. |
| RR6-02 | ✓ | Never have standalone software, have a protection IT team at standby. |

the long term. However, with the right financial analysts at work and a proper market analysis this cost risk can be mitigated substantially. Thus, cost risks are medium.

Performance risks can be linked to the mitigated risk maps in section 10.3. The main risks that remain after risk mitigation are related to the forces the aircraft introduces in the ground system, the synchronisa-

Table 10.10: Mitigated risk map for load carrying ground system.

| Likelihood \ Impact | Impact | | | | |
|---------------------|--------|----------------|--------------------------------|--|---|
| | 1 | 2 | 3 | 4 | 5 |
| 5 | | | | | |
| 4 | | | | | |
| 3 | | | | | |
| 2 | | RL1-04, RL2-01 | RL1-03 | | |
| 1 | | | RL2-02, RL3-01, RL3-02, RL6-02 | RL1-01, RL1-02, RL2-03, RL2-04, RL2-05, RL4-01, RL4-02, RL5-01, RL6-01, RL6-03 | |

Table 10.11: Mitigated risk map for aircraft categories.

| Likelihood \ Impact | Impact | | | | |
|---------------------|--------|------------------------|--------|--|----------------|
| | 1 | 2 | 3 | 4 | 5 |
| 5 | | | | | |
| 4 | | | | | |
| 3 | RA1-02 | | | | |
| 2 | | RA2-01, RA2-03, RA2-05 | RA2-06 | RA3-08 | |
| 1 | | RA2-04 | RA3-04 | RA1-01, RA1-03, RA2-02, RA3-01, RA3-02, RA3-03, RA3-05, RA3-09 | RA3-06, RA3-07 |

Table 10.12: Mitigated risk map for remaining categories.

| Likelihood \ Impact | Impact | | | | |
|---------------------|--------|--------|--|--|---|
| | 1 | 2 | 3 | 4 | 5 |
| 5 | | | | | |
| 4 | | | | | |
| 3 | | | | | |
| 2 | | | RR1-01, RR1-02, RR1-03, RR1-05, RR4-01, RR4-02, RR7-01 | | |
| 1 | | RR1-06 | RR2-01, RR3-02, RR3-03, RR3-04 | RR1-04, RR2-02, RR3-01, RR4-03, RR5-01, RR6-01, RR6-02 | |

tion communication between the aircraft and the ground vehicle, and the synchronisation accuracy. At this point in time these risks have not been properly mitigated as it is unknown what the precise synchronisation requirements are. The exact same story counts for the forces introduced to the system during non-nominal conditions. The team believes that with more research on pre-landing aircraft disturbances and accurate modelling of these disturbances, the synchronisation requirements can be set in a proper way. Once the correct requirements are set, it is possible, in theory, to upscale the system to the requirements and develop a safe and operational system with low performance risk.

10.5. RAMS

In this section the reliability, availability, maintainability, and safety (RAMS) characteristics are presented. Implementation of RAMS methodology in the design process is crucial. It is important to develop a reliable, available, maintainable, and safe system. The system should be ready to be used at the required times and the system should not curtail safety characteristics of a conventional aircraft.

As a first step RAMS requirements should be developed [75]. RAMS requirements state the performance the system should have regarding the RAMS characteristics. RAMS requirements can be linked to hardware as well as software. The RAMS performance is linked to the components that constitute the whole system that ensures a safe take-off and landing. The RAMS performance requirements of the REMALS should be similar to conventional aircraft landing systems. It is not necessary to exceed these requirements by far as this might be costly and limit the economical feasibility. The RAMS requirements can be linked to the requirements regarding reliability, availability, maintainability, and safety set in section 3.2.

As there was no statistical RAMS data available on subsystem level or component level of the REMALS, a failure mode, effects and criticality analysis (FMECA) was done [75]. Had there been statistical data available

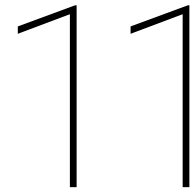
on RAMS, the team would have performed a (dynamic) fault tree analysis (FTA) or event tree analysis (ETA).

The reliability of the system should not be lower than that of conventional aircraft. Reliability is related to the chance that the system fulfils its function without failing for a specified amount of time [74]. An unreliable system has a high probability of failure and this would impact the capacity, the safety and the economical feasibility in a negative way. Reliability can be linked to the components' probability of failure. The system's probability of failure has been reduced by applying safety factors and making the system redundant by for instance installing more sensors than necessary.

The system should have the same availability as a conventional take-off and landing. Availability is related to the extent to which the system is functioning properly when it is needed at an unknown point in time [59]. Conventional landings can not take place if crosswinds are too high. The REMALS is able to land aircraft with a high yaw angle as aircraft do not need to de-crab and can land with higher crosswinds. In that aspect the REMALS is more available than conventional methods according to requirement NCL-Fun-T012. Furthermore, the availability of the runway to conventional aircraft shall not be negatively impacted by the REMALS as stated in requirement NCL-Sh116-Sys01. The availability is closely linked to the maintainability, as a system that requires a lot of maintenance might have a lower availability. The availability of the system has been increased by always having a backup ground vehicle available, having backup power generators, and minimising impact on conventional aircraft.

Maintainability is related to whether the system can be inspected, repaired, or preventive maintenance can be performed if necessary. If REMALS needs a lot of maintenance on the ground system located on the runway this impacts the availability of the runway to all aircraft. The REMALS components are all repairable, however the system can not be inspected at all desired times because maintenance could impact the capacity of the whole airport. As the REMALS should not decrease the capacity of the airport (requirement NCL-Sh101) maintenance of the components should be carefully planned. The maintainability of the system has been increased by making the system such that components can be detached for inspection without drastically affecting availability of the complete system.

Safety is related to human life and potential fatalities. The safety critical functions identified and redundancy philosophy applied to increase safety have been discussed in section 10.4 and section 10.3 respectively. Safety has been increased by performing risk mitigation and applying a redundancy philosophy. The safety critical functions identified are mainly related to the synchronisation of the REMALS at landing and the loads that the aircraft introduces to the system. Further analysis on the synchronisation requirements and impact loads of the aircraft upon landing is necessary to ensure a safe system.



Sustainability

This chapter elaborates on how sustainability influences the design and how the design aims at achieving the Sustainability Development Goals (SDGs). Sustainability is not simply another separate factor to take into account but needs to be deeply embedded in the design of the system. When designing each element of the system the team follows the principles of the Value Sensitive Design (VSD) [17]. The VSD offers an approach that accounts for values throughout the design-phase of a system. The values chosen by the team are the values embedded in the chosen relevant SDGs. The potential impact of new designs like the one proposed in this report urges design teams for the need of implementing the VSD as a strategy to deal with these impacts. Therefore, a strategic approach is taken to tackle sustainability in a responsible and comprehensive way such that it involves many fields and covers very interlinked and complex areas. Sustainability is more a different way of thinking and decision making that allows to deliver an all-round design which take on sustainability from many different perspectives. The next two sections discuss the sustainability influence on the design, and how the design contributes towards SDGs and sustainability. An useful way to cover the most crucial fields of sustainability was already discussed in the project plan [22]. In short, the SDGs set by the United Nations ¹ and the triple bottom line theory [48] are used to involve all aspects of sustainability. In section 11.1 the urgency to work towards a more sustainable society and fight climate change is explained and the design choices of the team driven by sustainability are discussed. In section 11.2 it is discussed how this specific design works towards complying with the SDGs.

11.1. Sustainability Influence on the Design

The need for a more sustainable society is self-evident. Aviation is one of the most polluting industry and is growing at a constant rate [25]. The European Union is taking actions to curb this problem. The main tool used so far is the EU Emissions Trading System (ETS) ². This system sets a maximum quantity of emissions for the aviation industry, each airline receives a fixe number of pollution permits for free and for every tonne of CO_2 emitted they must surrender one permit. In case an airline needs more permits, they can be bought. In this way, the European Union try to deter the most contaminating industries from polluting more than they are allowed to. However, current prices of a tonne of CO_2 are around €25 which is relatively low considering all the impacts associated with greenhouse gases. Greenhouse gasses trap heat inside Earth causing the Earth to heath up resulting in loss of biodiversity, ocean acidification, extreme weather, drought sea, level rises and famine. Moreover the noise produced and NO_x gases emitted by aircraft are not taken into account and not priced for. More action is needed by all the stakeholders involved, drastic and revolutionary measures need to be taken. In order to steer the aviation industry into a more sustainable future, the team has made sustainability the first priority in the design. Therefore, throughout the design the team's choices have been deeply influenced by sustainability. For instance when deciding upon which material to use for the construction of the system, the team opted for metals like steel and aluminium because at the end of their lifetime they can be recycled. In fact, steel is the most recycled material in the world ³. Moreover, the team designed to

¹URL: www.sustainabledevelopment.un.org [Accessed 20 June 2019]

²URL:<https://carbonmarketwatch.org/2019/02/19/better-pricing-of-aviation-emissions-in-the-eu-is-needed-and-the-netherlands-is-championing-it/> [Accessed 20 June 2019]

³URL:<https://www.prnewswire.com/news-releases/celebrating-steel-the-most-recycled-material-on-earth-on-america-recycles-day-nov-15-2012-179561881.html> [Accessed 21 June 2019]

have autonomous electric taxi carts, in this way the aircraft can taxi electrically to the gate following the optimal route from runway to gate thanks to complex algorithms. Furthermore, it has been decided during the design process to integrate the ground-based system on current airports such that conventional and non-conventional aircraft can use the same runways and same ramp operations infrastructures. Another example of how sustainability influenced the design is to put the focus on retrofitting current aircraft instead of completely redesigning and rebuilding a new aircraft for the system. Finally, the ground-based system is going to need massive amount of power. Hence, the team has determined that the energy shall come from renewable sources of energy. If the electricity would be provided by fossil fuels it would simply invalidate the purpose of this design. The most practicable option would then be to get the energy from a green energy supplier that can provide clean and reliable energy throughout the year.

11.2. Design Towards Achieving SDGs

The proposed design works towards achieving some of SDGs in many different ways. For each relevant SDG it is explained how this design fulfil the goals. An overview of all the SDGs in the triple bottom line theory framework is shown in Figure 11.1. The environmental, social and economical SDGs together cooperate towards achieving crucial milestones in the field of sustainability.

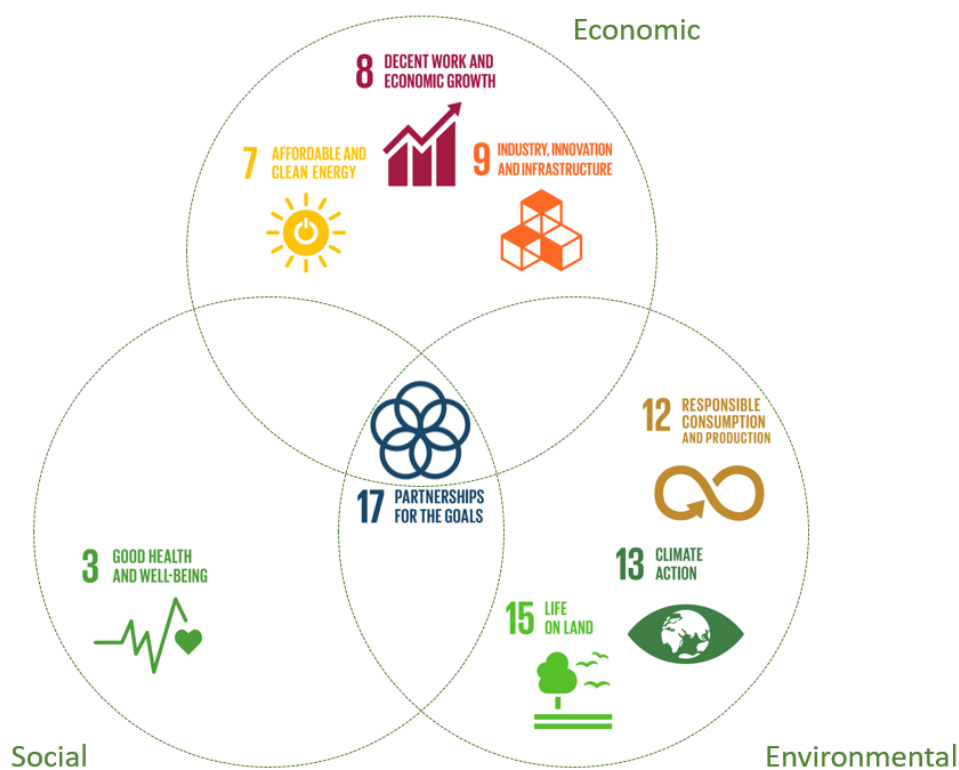


Figure 11.1: Overview of the relevant social, environmental and social SDGs goals

SDG 3: Good health and well-being

This SDG 3 is one of the most important. Requirement NCL-Sh118 is a driving requirement related to noise reduction which is strictly related to this goal. Hence it is extremely important to reduce noise to comply with this driving requirement. The more silent departures and approaches will have a beneficial effect on Schipol's residents. Due to lower noise levels their quality of sleep will improve and the medical cost due noise-related issues will decrease. This overall will increase the residents well-being and happiness. Preliminary calculations have proved that a reduction of 4 dB SEL for take-off in the top three zip code areas where complaints usually come from is achievable as explained in subsection 8.2.4.

SDG 7: Affordable and clean energy

Renewable energies are implemented in the design of the system. The energy is bought from a green energy contracts that get the energy needed from renewable energies like solar and wind energies. As of now, extract-

ing energy from renewable resource is already more profitable both economically and for the environment than using fossil resources⁴. In the future, photo-voltaic and windmill technologies will be enhanced and renewable energies will get even more affordable and efficient.

SDG 8: Decent work and economic growth

More silent departures and approaches will make grow economically the area around Schiphol. The house prices will increase and positive societal effects on the communities can be expected. Not only the communities near the airport will be benefited, the entire city of Amsterdam will gain from it. The economic development of the airport will translate into more tourism and trade for the city. In addition, new jobs will be created in the airport and in the relevant construction and maintenance industries that will take care of the ground-based system. Even though some jobs will be lost, probably the same amount or more will be created.

SDG 9: Industry, innovation and infrastructure

If this design will actually be implemented in future airports, the project has the potential of radically disrupting the aviation sector, completely changing the future aircraft designs. However, from every disruptive technology, new companies and new industries and companies will be created to produce all the machinery and equipment needed. To be implemented, it shall be economically attractive for current industries. This particular project is at the ideal intersection between innovation and current practices, because it radically changes the industries however it is built upon current infrastructure and procedures.

SDG 12: Responsible consumption and production

This goal is sufficiently satisfied. Not only the material shall be environmentally-friendly during production but the whole life cycle of the product shall be analysed such that it can be recycled at the end of life and contributing in creating a circular economy. Most of the structures are made out of metals this means they can be recycled at the end of life. Moreover all the parts necessary for the construction will be made as much as possible from scrap metal and recycled material in order to reuse already available products and reduce the environmental impact. Finally, the ground-based system is made such that it is compatible with current ramp operations equipments, reducing the need to build additional infrastructures.

SDG 13: Climate action

This SDG is another very important goal. NCL-Alc09 is another driving requirement and is strictly related to this goal. Therefore it is crucial to adhere to it by reducing greenhouse gases and fuel consumption. Preliminary calculations have proved that a fuel reduction of 4-5 %, depending on the flight range and payload, is possible. This calculation would translate into a reduction of 1094 kg of fuel. Every kg of fuel burned produce 3.16 kg of CO_2 [25] hence 3457 kg of CO_2 would be saved from the environment. Not only CO_2 emissions would decrease but also the emissions of nocive gases and particulate matter like sulfur dioxide and nitrogen oxides. In fact, currently more people die from plane exhaust gases than from plane crashes.⁵

SDG 15: Life on land

As a result of decreasing noise and nocive gas emissions near the airport biodiversity will increase which is not particularly good for air traffic operations. However, this potential problem can be curbed with specific countermeasures as trained eagles or special radar to deter birds and animals to trespass the airport perimeter.

⁴URL: <https://www.forbes.com/sites/energyinnovation/2018/12/03/plunging-prices-mean-building-new-renewable-energy-is-cheaper-than-running-existing-coal/#65476d7531f3> [Accessed 22 June 2019]

⁵URL:<https://news.nationalgeographic.com/news/2010/10/101005-planes-pollution-deaths-science-environment/> [Accessed 20 June 2019]

12

System Verification & Validation

This chapter presents the verification and validation of the total system. Throughout the report, verification and validation has been performed for all components separately. However, it still has to be checked if the components together, forming the full system, work and if they comply with the system requirements. Does everything match together? Does the design solution meet the requirements set by the stakeholders? These questions are answered by means of a requirement compliance matrix in section 12.1. Then the sensitivity analysis provided in section 12.2 analyses the robustness of the REMALS as a solution of the problem of ground based powered take-off and landing. Finally, in section 12.3 a brief validation is conducted to investigate if the product accomplishes the intended purpose based on stakeholder expectations.

12.1. Requirement Compliance Matrix

Every requirement is verified in order to check whether it has been met. The results are summarised in the form of compliance matrices. First, the stakeholder requirements are checked (see Table 12.1) followed by the system requirements (Table 12.3 and Table 12.4). In the first column of the compliance matrices, the identifier of the requirement can be found. The requirements themselves can be found in section 3.2. Next, the second column shows whether the requirement has been met or not or whether it has not been checked yet using a letter and a colour scheme. If it contains a C. and it is green, the requirement is met. If it contains a N.C. and it is red, the requirement is not met. If the requirement has not been checked yet, the method that should be used to verify the requirement is shown and it is given the colour blue. Requirements can be verified in four ways: inspection, analysis, demonstration or by tests. However, in this case, mainly test, demonstration or analysis can be used as the product is not produced yet, hence inspection becomes difficult. The third column shows the value that had to be attained while the last column shows the value that was actually found. When these columns are not applicable, they say N.A. for not applicable. When the actual value still has to be determined the fourth column says T.B.D. Finally after the compliance matrices, a rationale is given for each requirement which explains why it has (not) been met or why the verification method is applicable.

Stakeholder Requirements

First, the stakeholder requirements are verified. These are requirements that are set by the stakeholders of the system. Their compliance can be found in Table 12.1 while the rationale is summarised in Table 12.2.

Table 12.1: Compliance matrix of the stakeholder requirements.

| Identifier | Comply/ Method | Goal | Actual value |
|-------------------------|-------------------|---------------|-----------------|
| Schiphol Airport | | | |
| NCL-Shl01 | C. | 80s | 80s |
| NCL-Shl06 | N.C. | N.A. | N.A. |
| NCL-Shl07 | N.C. | N.A. | N.A. |
| NCL-Shl09 | Demonstration | N.A. | N.A. |
| NCL-Shl10 | Test | 35 years | T.B.D |
| NCL-Shl14 | C. | N.A. | N.A. |
| NCL-Shl15 | C. | N.A. | N.A. |
| NCL-Shl16 | C. | N.A. | N.A. |
| NCL-Shl17 | C. | N.A. | N.A. |
| NCL-Shl18 | C. | 7 ± 3 SEL dBA | 4 SEL dBA |
| NCL-Shl19 | C. | €650 million | €626 million |
| NCL-Shl20 | Analysis | €50 million | T.B.D |
| NCL-Shl21 | C. | €25 million | €15.4 million |
| Airline company | | | |
| NCL-Alc01 | C. | N.A. | N.A. |
| NCL-Alc03 | Analysis | 10% | T.B.D |
| NCL-Alc04 | Demonstration | 1.5 years | T.B.D |
| NCL-Alc06 | C. | 244 seats | 244 seats |
| NCL-Alc09u1 | C. | 5% | 5.2% |
| NCL-Alc09u2 | C. | 5% | 5.4% |
| NCL-Alc10 | Demonstration | N.A. | N.A. |
| NCL-Alc11 | Demonstration | 6 months | T.B.D |
| Passengers | | | |
| NCL-Pax01 | C. | N.A. | N.A. |
| NCL-Pax02 | Analysis | 120% | T.B.D |
| Airbus | | | |
| NCL-Amf02 | Demonstration | N.A. | N.A. |
| NCL-Amf03 | Analysis | N.A. | N.A. |
| Project team | | | |
| NCL-Pjt01 | C. | 10 weeks | 10 weeks |

Table 12.2: Stakeholder requirement verification.

| Identifier | Rationale |
|------------|--|
| NCL-Shl01 | At the moment, Schiphol uses maximum 3 runways at the same time. Each of these runways is able to perform one take-off or landing every 80s. The number of base structures per runway has been determined such that the system is able to function at this maximum capacity. |
| NCL-Shl02 | From analysis in the cost breakdown structure, the one time investment cost is expected to be €626 · 10 ⁶ . This fits within the maximum budget of €650 · 10 ⁶ for the one time investment cost. Thus the requirement has successfully been verified by means of analysis. |
| NCL-Shl03 | The implementation costs were not determined in the cost breakdown structure as a separate cost from the one time investment cost and thus no estimate is found. Further analysis in the cost breakdown structure should be done in order to separate these costs. |
| NCL-Shl04 | From analysis in the cost breakdown structure, the annual fixed costs are expected to be €15.4 · 10 ⁶ . This fits within the maximum budget of €25 · 10 ⁶ for the one time investment cost. Thus the requirement has successfully been verified by means of analysis. |

| | |
|-------------|--|
| NCL-Shl06 | Each runway will be equipped with the system. Even if the runways are adapted one by one and only a maximum of 3 runways are used simultaneously, it will limit the selection of runways depending on the direction of the wind. Furthermore, there might be aircraft that require the longest runway which would not be possible if it is under construction. |
| NCL-Shl07 | The ground system will be powered by its own grid, so this would not disturb the electrical grid of Schiphol. Nonetheless, the taxi cart will be charged at the gate thus they will use the electrical grid from the airport. |
| NCL-Shl09 | Once a prototype has been built, multiple test flights can be performed in order to estimate the rate of successful take-offs and landings. When the system is operational, this success rate can be determined more accurately by monitoring the take-offs and landings. This method is called demonstration. |
| NCL-Shl10 | The lifetime of the system mainly depends on its fatigue strength. This can be tested in special environments where the cycles are represented in a much shorter time. These kind of tests should be performed in order to find the life time of the system. |
| NCL-Shl14 | The ground system will be implemented on every runway of the airport. Conventional aircraft will still be able to use these runways as well. |
| NCL-Shl15 | As mentioned before, conventional aircraft will still be able to use the runways. Furthermore, since the aircraft will use the taxi cart for the remaining ground operations, the procedures will be similar to the current procedures and thus not limit the operations of conventional aircraft. |
| NCL-Shl16 | Because of the lids, the runways can switch from a conventional runway to the REMALS system and the other way around very quickly. This way a conventional aircraft can use the runway at any moment. |
| NCL-Shl17 | There are no factors that vary with time thus the system can be used at any moment independent on the time. |
| NCL-Shl18 | From analysis, it follows that the minimum noise reduction in areas where a lot of complains come from is 4 SEL dBA. This fits just within the requirement of 7 ± 3 SEL dBA. Nonetheless, there are areas near Schiphol where the noise reduction is much higher. |
| NCL-Shl19 | From analysis in the cost breakdown structure, the one time investment cost is expected to be $\text{€}626 \cdot 10^6$. This fits within the maximum budget of $\text{€}650 \cdot 10^6$ for the one time investment cost. Thus the requirement has successfully been verified by means of analysis. |
| NCL-Shl20 | The implementation costs were not determined in the cost breakdown structure as a separate cost from the one time investment cost and thus no estimate is found. Further analysis in the cost breakdown structure should be done in order to separate these costs. |
| NCL-Shl21 | From analysis in the cost breakdown structure, the annual fixed costs are expected to be $\text{€}15.4 \cdot 10^6$. This fits within the maximum budget of $\text{€}25 \cdot 10^6$ for the one time investment cost. Thus the requirement has successfully been verified by means of analysis. |
| NCL-Alc01 | The system has been designed for flights with a flight time up to 3 hours. The aircraft on which the design is based is the A321NEO which is used for these kind of missions. This fits the profile of a short to medium range flight. |
| NCL-Alc03 | In order to determine the cost of the modified aircraft, an analysis should be performed using the economical models of the manufacturer. These models can be adapted such that all the changes made to the aircraft are included in the cost estimation of the aircraft. |
| NCL-Alc04 | The delivery time of an aircraft can be verified using demonstration. Once the first orders are placed by airline companies, it can simply be checked how long it takes for the manufacturer to deliver the aircraft. |
| NCL-Alc06 | The aircraft is a modified A321NEO that was changed as little as possible. As a result, the cabin did not change and thus still has the same capacity as the original A321NEO which has a maximum capacity of 244 seats. |
| NCL-Alc09u1 | From analysis on the fuel consumption on the modified A321NEO, it follows that a total of 5.2% of fuel can be saved on the reference flight. This is more than the 5% required and thus this requirement is verified by means of analysis. |
| NCL-Alc09u2 | From analysis on the fuel consumption on the modified A321NEO, it follows that a total of 5.4% of fuel can be saved on the reference flight. This is more than the 5% required and thus this requirement is verified by means of analysis. |
| NCL-Alc10 | Once a modified version of the A321NEO has been built, it can be verified whether the required maintenance time is more than the maintenance time for the conventional A321NEO by demonstration. This demonstration will simply include a full maintenance operation on the aircraft after which the times can be compared. |
| NCL-Alc11 | Once training starts on modified version of the A321NEO, the required time for retraining can be verified by means of demonstration. It has to be checked whether the retraining progress takes longer than 6 months or not. If it does not, the requirement is verified. |

| | |
|-----------|---|
| NCL-Pax01 | Limits were set for passenger comfort during the design of the system based on accelerations and maximum climb angles. At no time during the mission, these limits are crossed. This ensures a comfortable flight for the passengers. |
| NCL-Pax02 | Analysis can be performed if airline companies adapt their economical models that determine the ticket prices. These models should include the additional cost of the aircraft launch, but also the cost savings due to fuel savings. |
| NCL-Amf02 | When the modified aircraft is being manufactured, it should be tried to do it in existing factories. If this is possible, the requirement is successfully verified by demonstration. If it is not possible, the requirement is not met. |
| NCL-Amf03 | When the necessary equipment is known to produce the aircraft, the cost can be found of all the equipment and added together. If the total cost is below the budget of the manufacturer, the requirement is met and verified by analysis. |
| NCL-Pjt01 | The final design has been developed as an Design Synthesis Exercise which is a group project for third year bachelor aerospace students at Delft University of Technology. The duration of this project is 10 weeks. |

System Requirements

Next, the system requirements are verified. These are requirements that are derived from the stakeholder requirements, but are more technical. Their compliance can be found in Table 12.3 and Table 12.4 while the rationale can be found in Table 12.5.

Table 12.3: Compliance matrix of the system requirements set 1.

| Identifier | Comply/ Method | Goal | Actual Value |
|-------------------------|----------------|---------------------------|--------------------------|
| Schiphol Airport | | | |
| NCL-Shl01-Sys03 | C. | 756 | 2160 |
| NCL-Shl01-Sys04 | C. | 830 | 2270 |
| NCL-Shl07-Sys01 | C. | 250 · 10 ⁶ kWh | 80 · 10 ⁶ kWh |
| NCL-Shl09-Sys01 | C. | N.A. | N.A. |
| NCL-Shl10-Sys01 | Test | 35 years | T.B.D. |
| NCL-Shl14-Sys01 | C. | 3300m | 3300m |
| NCL-Shl16-Sys01 | C. | N.A. | N.A. |
| NCL-Shl16-Sys02 | N.C. | N.A. | N.A. |
| NCL-Shl17-Sys02 | C. | N.A. | N.A. |
| NCL-Shl17-Sys03 | Demonstration | 9Bft | T.B.D. |
| NCL-Shl19-Sys01 | C. | €650 million | €626 million |
| NCL-Shl20-Sys01 | Analysis | €50 million | T.B.D. |
| NCL-Shl21-Sys01 | C. | €25 million | €15.4 million |
| Passengers | | | |
| NCL-Pax01-Sys01 | C. | N.A. | N.A. |
| NCL-Pax01-Sys02 | C. | N.A. | N.A. |
| Airline company | | | |
| NCL-Alc01-Sys03 | C. | N.A. | N.A. |
| NCL-Alc03-Sys01 | Analysis | 10% | T.B.D. |
| NCL-Alc04-Sys01 | Demonstration | 1.5 years | T.B.D. |
| NCL-Alc04-Sys03 | Demonstration | 2 years | T.B.D. |
| NCL-Alc06-Sys01 | C. | N.A. | N.A. |
| NCL-Alc06-Sys02 | C. | N.A. | N.A. |
| NCL-Alc10-Sys01 | Demonstration | N.A. | N.A. |
| NCL-Alc10-Sys02 | Test | N.A. | N.A. |

Table 12.4: Compliance matrix of the system requirements set 2.

| Identifier | Comply/ Method | Goal | Actual value |
|------------------------------|----------------|----------|--------------|
| Ground take-off | | | |
| NCL-Fun-TO4 | C. | N.A. | N.A. |
| NCL-Fun-TO8 | C. | N.A. | N.A. |
| NCL-Fun-TO9 | C. | 80s | 61.3s |
| NCL-Fun-TO11 | C. | 1G | 0G |
| NCL-Fun-TO12 | Demonstration | N.A. | N.A. |
| NCL-Fun-TO13 | C. | 3300m | 2967m |
| NCL-Fun-TO14 | C. | N.A. | N.A. |
| NCL-Fun-TO15 | C. | N.A. | N.A. |
| NCL-Fun-TO16 | C. | 1G | 0.682G |
| Ground landing system | | | |
| NCL-Fun-LA2 | C. | 0.4G | 0.395G |
| NCL-Fun-LA4 | C. | 3300m | 2970m |
| NCL-Fun-LA6 | C. | 100s | 64.9s |
| NCL-Fun-LA7 | C. | N.A. | N.A. |
| NCL-Fun-LA9 | C. | N.A. | N.A. |
| NCL-Fun-LA10 | Demonstration | N.A. | N.A. |
| Aircraft system | | | |
| NCL-Fun-AC1 | C. | N.A. | N.A. |
| NCL-Fun-AC6 | C. | N.A. | N.A. |
| NCL-Fun-AC8 | Demonstration | N.A. | N.A. |
| NCL-Fun-AC9 | C. | N.A. | N.A. |
| NCL-Fun-AC10 | Analysis | 3.2% | T.B.D. |
| NCL-Fun-AC12 | Test | 20 years | T.B.D. |
| NCL-Fun-AC13 | C. | N.A. | N.A. |
| NCL-Fun-AC14 | Analysis | 1.2% | T.B.D. |
| NCL-Fun-AC15 | Test | N.A. | N.A. |

Table 12.5: System requirements verification.

| Identifier | Rationale |
|-----------------|---|
| NCL-Shl01-Sys03 | Each landing with the system takes 80s. Since 3 runways can be used simultaneously, 756 arrivals will take 20160s or 5.6 hours. This fits easily within the required 24 hours. If two runways are used for landing during the whole day, 2160 landings can be performed. |
| NCL-Shl01-Sys04 | Each take-off with the system takes 76s. Since 3 runways can be used simultaneously, 830 departures will take 21027s or 5.8 hours. This fits easily within the required 24 hours. The system can also handle both the requirements for arrivals and departures at the same time as 756 landings and 830 take-offs can be performed in 11.4 hours. If two runways are used for take-off during the whole day, 2270 take-offs can be performed. |
| NCL-Shl07-Sys01 | From analysis it follows that operating the system would require $80 \cdot 10^6 kWh$ annually in order to operate the system. This is significantly below the $250 \cdot 10^6 kWh$ requirement, thus the requirement is verified by analysis. |
| NCL-Shl09-Sys01 | The decision speed is set at $116m/s$. If the pilot decides to abort the take-off before this velocity has been reached there is still enough distance to safely decelerate the ground system. |
| NCL-Shl10-Sys01 | All the non-replaceable parts of the system should be tested for fatigue. The fatigue life of these parts can be determined in special test setups that imitate the loading cycles at a higher frequency. If these tests are successful, the requirement is verified by means of tests. |
| NCL-Shl14-Sys01 | The system has been designed in such a way that it requires a runway of $3300m$ including 10% contingency. Since the shortest runway on schiphol has a length of $3300m$, no runways will need to be elongated. |
| NCL-Shl16-Sys01 | Because the rails are dug into the ground and can be covered with lids, a conventional aircraft can use the runway at any moment. When a conventional aircraft need to use the runway, the covers will close the trenches of the rails in order to have a smooth runway. Once the REMALS system needs to use the runway again the covers will simply open up again. |
| NCL-Shl16-Sys02 | The system requires additional space at both ends of the runway in order to be outside of the safety zone and to locate the lifts and the pump stations. Furthermore, the flywheels and the hanger for the taxi carts need to be located on the aircraft perimeter, but this could be at a location that is not used currently. |
| NCL-Shl17-Sys02 | In order to mitigate the risk of a power cut, back-up generators that are powerful enough to power the system will be installed at the airport. Furthermore, the flywheels will also contain some energy when a power failure happens. This energy can still be used as well. |
| NCL-Shl17-Sys03 | Once the system and aircraft have been build, a demonstration landing can be performed during a storm of type 9 on the scale of Beaufort. If this landing is successful, this requirement is verified by demonstration. |
| NCL-Shl19-Sys01 | From analysis in the cost breakdown structure, the total costs to construct the ground based system, the power supply chain and the control strategy system at Schiphol airport is expected to be $\text{€}626 \cdot 10^6$. This fits within the maximum budget of $\text{€}650 \cdot 10^6$ for the one time investment cost. Thus the requirement has successfully been verified by means of analysis. |
| NCL-Shl20-Sys01 | The total costs to incorporate the ground based system, the power supply chain and the control strategy system into the work environment at Schiphol airport were not determined in the cost breakdown structure as a separate cost from the one time investment cost and thus no estimate is found. Further analysis in the cost breakdown structure should be done in order to separate these costs. |
| NCL-Shl21-Sys01 | From analysis in the cost breakdown structure, the costs to maintain the ground based system, the power supply chain and the control strategy system at Schiphol airport are expected to be $\text{€}15.4 \cdot 10^6$. This fits within the maximum budget of $\text{€}25 \cdot 10^6$ for the one time investment cost. Thus the requirement has successfully been verified by means of analysis. |
| NCL-Pax01-Sys01 | The damping distance of the stewart platform is based on the damping distance of conventional aircraft. This means that the shock during landing impact will be equally big as the shock during landing impact with a conventional aircraft. |
| NCL-Pax01-Sys02 | No changes were made to the cabin of the aircraft. This means that the seat configuration can still be anything that is possible for a conventional aircraft and is thus not limited by the system. |
| NCL-Alc01-Sys03 | The reference aircraft used in the design is an A321NEO where the landing gear has been replaced by harpoons. |
| NCL-Alc03-Sys01 | The manufacturer should adapt its economical models that estimate the design cost of an aircraft. If the models predict the design cost of the required changes does not increase the purchase price of the aircraft more than 10%, the requirement is verified by analysis. |

| | |
|-----------------|--|
| NCL-Alc04-Sys01 | Once production of the aircraft has started, the time required to produce an aircraft can simply be measured and checked whether it is within the limit of 1.5 years. If it does, the requirement is verified by demonstration. |
| NCL-Alc04-Sys03 | When the system is being implemented, the time required to complete it can simply be measured. If it is within the time requirement of 2 years, the requirement is successfully verified by demonstration, otherwise the requirement is not met. |
| NCL-Alc06-Sys01 | The Fuselage and cabin of the A321NEO were kept the same for the modified version. This means that the cross-section of the fuselage will not have changed either. |
| NCL-Alc06-Sys02 | The cargo bays and cabin of the modified A321NEO are the same as for the conventional A321NEO. Thus, the cabin volume for cargo did not change either. |
| NCL-Alc10-Sys01 | once a prototype of the aircraft has been built, the time required to access each modified part can be measured. If it does not require more time than before, the requirement is verified by demonstration. |
| NCL-Alc10-Sys02 | The lifetime of the materials used in the design can be tested in a special test environment that imitates the loading cycles at a higher frequency. If the lifetime is at least equally long as the lifetime of current materials, the requirement is verified by means of a test. |
| NCL-Fun-TO4 | The aircraft connects to the EMALS system via harpoons that are located at the current landing gear positions that connect to a grid on top of the base structure. |
| NCL-Fun-TO5 | During acceleration for take-off, a maximum acceleration of $6.69m/s^2$ by analysis. This corresponds to an acceleration of 0.682G which is significantly less than the limit of 1G |
| NCL-Fun-TO8 | By retracting the harpoons from the grid, the aircraft can decouple from the base structure. The system has been designed in such a way that the harpoons can retract even if there is a failure. When enough force is applied on the harpoons, they disconnect from the grid. This way, when the aircraft rotates during take-off, the lift of the aircraft increases which will release the harpoons. |
| NCL-Fun-TO9 | The REMALS system that was used for the first take-off first has to leave the safety zone before the next REMALS system can perform a take-off. This adds additional time and means that every take-off procedure takes 61.3s. The average time between two consecutive take-offs is higher since all the base structures have to be moved back after 5 take-offs. This results in an average interval between two consecutive take-offs of 76s. |
| NCL-Fun-TO11 | The system does not accelerate the aircraft in vertical direction at all. The aircraft only experiences 1G due to gravity, but it does not get accelerated vertically by the system. |
| NCL-Fun-TO12 | When a prototype of the aircraft and system have been built a demonstration flight can be done in the worst flight conditions that current aircraft are allowed to fly in. If the aircraft and system are able to perform the take-off successfully, the requirement is verified by means of demonstration. |
| NCL-Fun-TO13 | From analysis it follows that in case the pilot decides to abort the take-off at the decision speed of $116m/s$ the system can perform the deceleration and acceleration within $2967m$. |
| NCL-Fun-TO14 | The taxi cart that is used to transport the aircraft within the airport perimeter is not restricted by tracks or rails. This way it can reach any location that is accessible to a conventional aircraft. |
| NCL-Fun-TO15 | The pilot is able to abort the take-off in case something goes wrong if the aircraft has not exceeded the decision speed of $116m/s$ yet. |
| NCL-Fun-LA2 | The maximum deceleration that passengers experience during landing was found to be $3.87m/s^2$. This corresponds to a deceleration of 0.395G which is just below the limit of 0.4G. |
| NCL-Fun-LA4 | From analysis it follows that the system requires $2970m$ to perform a landing which includes accelerating the system, connecting the aircraft and decelerating the system. $2970m$ is 10% less than the limit of $3300m$. This is to include a safety margin. |
| NCL-Fun-LA6 | The total time required to perform a landing is 64.9s. This includes reaching the save zone and thus the required interval between two consecutive landings is also 64.9s. This is significantly less than the maximum interval of 100s set by the requirement. The average interval between two consecutive landings due to the base structures moving back is 80s which is still significantly below the requirement of 100s. |
| NCL-Fun-LA7 | When the aircraft approaches the runway, it will deploy harpoons at the locations of the current landing gear. These harpoons can connect to a grid that is attached to the EMALS system. |
| NCL-Fun-LA9 | The system uses multiple LIDAR systems to synchronise with the aircraft including some systems that can also be used in bad weather conditions. |
| NCL-Fun-LA10 | When a prototype of the aircraft and system have been built a demonstration flight can be done in the worst flight conditions that current aircraft are allowed to fly in. If the aircraft and system are able to perform the landing successfully, the requirement is verified by means of demonstration. |
| NCL-Fun-AC1 | The flaps and slats of the A321NEO were not removed in the modified version that can be used with the system. This means that the modified aircraft will still be able to change into climb configuration. |

| | |
|--------------|---|
| NCL-Fun-AC6 | The taxi cart does not block the bridge that is currently used to board the aircraft. This system can still be used to connect to the gate. Furthermore all the remaining ramp operations such as fuelling the aircraft will be performed in a similar way but with the use of a lift. |
| NCL-Fun-AC8 | Demonstrations will be used in order to show compliance with the CS-25. If the system passes the certification, the demonstration is successful. Nonetheless, there are parts from the CS-25 regulations that will need to be revised as they assume that the aircraft has a conventional landing gear. |
| NCL-Fun-AC9 | The loads that are applied by the ground system are similar to the loads for which the landing gear is currently designed. Since the harpoons are located on the same locations as the landing gear of the conventional landing gear, the aircraft structure is able to withstand the applied loads by the ground system. |
| NCL-Fun-AC10 | Further analysis should be performed on the gradient of climb in landing configuration. The gradient of climb can be found from a landing simulation at maximum thrust. |
| NCL-Fun-AC12 | The lifetime of the aircraft can be tested in a special test environment that imitates the loading cycles at a higher frequency once a prototype has been built. If the lifetime is equal or longer than 20 years, the requirement is verified by means of a test. |
| NCL-Fun-AC13 | The aircraft will be able to deploy the harpoons in a similar fashion as the landing gear is currently deployed. This makes the aircraft suitable for attaching to the ground system for landing. |
| NCL-Fun-AC14 | Similar analysis as for requirement NCL-Fun-AC10 should be done in order to find the gradient of climb with an engine inoperative from simulations. |
| NCL-Fun-AC15 | A prototype of the modified aircraft equipped with sensors such as accelerometers should perform an emergency landing without the system. If the data indicates that the passengers would have survived the landing, the test verifies the requirement. |

12.2. Sensitivity Analysis

In order to test the robustness of the REMALS as a solution for the problem of ground based powered take-off and landing, a sensitivity analysis was performed. A technical sensitivity analysis evaluates the degree of compliance with requirements of the final design by looking at the sensitivity of the design to a change of system parameters, while a design sensitivity analysis one studies what structural modifications are needed and whether they are possible when design parameters change slightly [76].

12.2.1. Technical Sensitivity Analysis

In this section, it is evaluated how the performance of REMALS with respect to the three driving requirements (concerning fuel reduction, noise reduction and capacity as stated in subsection 3.2.1) changes when its mass changes. It is analysed how an increase and decrease of 5 % of the OEW of the aircraft and of the mass of the ground system influences the capability of REMALS to meet with the driving requirements, while keeping all other system parameters the same (power e.g.). The results are summarised in Table 12.6, where situation 1, 2 and 3 corresponds with the current mass of the system, an increase of 5 % and a decrease of 5 % respectively.

Table 12.6: Sensitivity of key parameters when the system is subject to a mass change

| | Units | Situation 1 | Situation 2 | Situation 3 |
|------------------------------------|-------|-------------|-------------|-------------|
| Mass characteristics | | | | |
| OEW | [kg] | 52022 | 54623 | 49421 |
| Mass ground system | [kg] | 128000. | 134400. | 121600. |
| Noise reduction | | | | |
| Take-off speed | [m/s] | 145 | 143 | 147 |
| Approach speed | [m/s] | 109.5 | 109 | 110 |
| Fuel reduction | | | | |
| Fuel reduction | [%] | 5.37% | 5.27% | 5.470% |
| Capacity | | | | |
| Runway time during take-off | [s] | 37.1 | 37.6 | 36.5 |
| Runway time during landing | [s] | 40.9 | 41.2 | 40.6 |
| Total time for landing | [s] | 80 | 80.4 | 79.7 |

As can be seen in Table 12.6, changing the aircraft or combined ground based system weight has minor influences on the take off and approach speed. While keeping the force that the motor delivers within a $\pm 1kN$ margin, the maximum velocity change is $2m/s$. For noise reduction, it is expected that reducing the take-off speed with $2 m/s$, the requirement of noise reduction of 7 ± 3 SEL dB within a radius of 7.8 km from Schiphol airport is still being fulfilled, as can be seen in Figure 8.15. With respect to landing, changing the approach speed with $0.5 m/s$ will not have any significant influence at all on fulfilling the requirement, since this requirement was already easily met (Figure 8.18).

For fuel reduction, in case the operational empty weight increases, the relative weight reduction becomes less. Therefore, less fuel is saved in comparison to the A321NEO. This is again done for flights of average short range flight time and average occupancy. This concludes that the requirements are still met for a small deviation in operational empty weight.

The additional time required for the linear acceleration and deceleration during a landing procedure, which is the limiting procedure for capacity, increases only by $0.5s$. Since the time spend in the buffer zone and the ILS safety zone do not change, the total time required for a landing increases from 65.1 to $65.6s$. Combined with the time required to move the carts back, the average time required per landing increases to $80.4s$ per landing which does not drastically change the capacity. The average time per landing should not exceed $80s$, but the $0.4s$ are negligible.

12.2.2. Design Sensitivity Analysis

The REMALS is designed specifically for Schiphol airport, however it can be implemented at any airport as long as the power can be provided. REMALS imposes high requirements on power and can not be implemented on an airport if the power can not be delivered. All international airports in Europe could in theory implement REMALS. As REMALS needs many users to become economically feasible it shall be implemented on big airports and on busy routes. As REMALS can, in theory, be implemented on all relevant airports the solution is insensitive to changing this system parameter.

The REMALS is designed for an A321, however it can be up-scaled and the system can be designed such that it can be used by multiple different aircraft. The grid can be interchanged and the right grid can be installed when necessary or a universal grid can be developed. Furthermore, the base structure and Stewart platform can be up-scaled to make the system compatible with bigger aircraft like the A380.

The REMALS is designed for the impact loads and synchronisation requirements as described in chapter 6 and chapter 7, if however these loads turn out to be higher after further analyses, the REMALS can be up-scaled. By using the N2 chart as in section 5.2 and some iterations, increasing the impact loads or synchronisation requirements will lead to an adjusted, up-scaled, feasible solution.

In a nutshell, changing the system parameters would not drastically impact the feasibility of REMALS. REMALS is found to be a robust solution that can adjust to the needs set by the user.

12.3. System Validation

Once the system is finally designed, it is crucial to validate all the steps and the final results. It is relevant to check if the team has actually developed the right product as the solution for the problem of ground-based powered take-off and landing. The validation is done by experience, analysis or comparison. Since this project is conceptual and exceptionally cutting-edge, there are not many references in literature to compare it with. The only similar projects that have been found are the GABRIEL project and a Design Synthesis Exercise focusing on a similar project. By comparing the outcomes of this project with those two projects, a preliminary validation can be performed. The results on power required by the system, required runway length, reduction in noise, reduction in fuel, costs, forces applied are compared with previous projects and roughly match the results obtained by the team therefore proving a proof of the rightness of the team's work and procedure followed. Additionally the validation of the integration of the different elements is done in Catia. This way it is validated that the dimensions of the different elements do match.

13

Project Design and Development

Further activities need to be executed to implement REMALS successfully. This chapter will give an overview of all steps that need to be taken in order to implement REMALS into the aviation industry. Section 13.1 gives an overview of all steps that need to be taken in the next phases. Section 13.2 presents these activities in a chronological order. In section 13.3, a more in-depth analysis has been made concerning manufacturing of the system. Finally, a cost breakdown structure for the remaining activities is given in section 13.4.

13.1. Project Design and Development Logic

This DSE project demonstrated the feasibility of the concept. However, it also demonstrated that further research into the concept is justified. As a consequence the following activities are identified that should be given attention in the future: technical developments, operational issues and assessment of potential benefits. The activities are summarised in Figure 13.1.

13.1.1. Technical Developments

Further work is needed to develop a navigation and guidance system that ensure a safe and accurate landing on the runway under all weather conditions. The photon Lidar could be an option, however, further research needs to be done and the new set up of sensors and synchronisation instruments needs to be validated by performing model tests and full size flight tests.

The taxi cart shall be designed in further detail, especially the guidance and steering of the cart, and the feasibility of having the cart completely autonomous, simply controlled by ATC. In addition, the possibility to make the taxi cart adjustable while being stable and rigid, shall be explored in the future. In this way, it will be possible to avoid the investment in numerous carts for different types of aircraft. Moreover, power requirements may change if bigger aircraft need to be transported on top. In addition, a supplementary emergency cart shall be designed in detail, in case of a malfunction of the ground-based system or for smaller airports that cannot afford the ground-based system. These emergency carts would have a simple structure as their only function is to provide a landing platform and they would operate under their own power.

The Stewart platform shall be optimised in the future. The attachment positions of the double chambered actuators on the platform relative to the base can be further optimised in future research to obtain a lighter system. Furthermore, more exotic configurations such as the octapod configuration should be considered to develop a more redundant and more reliable system that complies with aerospace industry standards. Lateral touchdown position deviations should be further investigated and researched such that the platform can be sized with statistical evidence. Singularities of this exotic configuration need to be analysed in the future. The concept of damping using actuators should be further investigated. In addition, the energy obtained from this process may be stored in accumulators.

The design of the harpoon system will need further attention. The current design includes a connection between aircraft and the grid by a harpoon system that replaces the aircraft undercarriage. In the post-DSE small scale tests and full scale tests are needed to validate the feasibility of the harpoon system.

There is a lot of space for improvement in the aerodynamic performance of the ground-based system. Further research will have to be done in order to obtain high aerodynamic efficiency at high speeds. This could be done by means of aerodynamic lightweight fairings.

A point of concern which need to be addressed in further research is a mechanism to cover the rails during conventional landing. The rails disrupt the runway and technology needs to be developed to cover the rails quickly between a conventional and non-conventional take-off/landing.

Finally, all the new technologies that have been developed for the ground-based system need to be certified and approved by authorities like EASA or the FAA.

13.1.2. Operational Issues

Several issues in terms of operations will have to be assessed in future developments. Feasibility studies will have to be performed in order to determine whether it is achievable to implement a ground based powered system in other airports across Europe besides Schiphol Airport. Moreover, runway integration is another point of concern which need to be further investigated. The integrated runway would have to be able to accommodate both standard aircraft and modified aircraft, translating in a logistical challenge. Detailed design is needed to show how the concept would look like and how it would integrate with current ramp operations equipment and structures.

In addition, new emergency mitigation procedures will have to be studied. The modified aircraft will not be able to divert to all alternative airports available. Belly landings and ditching might become more common. Hence, more research needs to be done on the impact and likelihood of these events.

Last but not least, all the new operations and procedures will have to be standardise and certified by the regulating authorities.

13.1.3. Assessment of Potential Benefit

All current aircraft could potentially be retrofitted to be able to use the system, or future aircraft on production lines could be modified to make use of the ground based system. A detailed design is needed to understand how the harpoon system can be integrated in current aircraft and future production lines. For future aircraft the landing gear fairing on the fuselage can be deleted, moreover, smaller engines without thrust reversers can be installed instead. By applying these further modifications on future aircraft, even more fuel can possibly be saved.

An in-depth environmental and cost analysis shall be performed in further stages of the design. As mentioned in chapter 11, current prices for CO₂ emissions are very low. A sensitivity analysis will have to be performed to understand the effects of increasing the market value of CO₂ emissions. In addition, as of today, NO_x emission does not have a market value, however in the future it may have a price. Possible effects of this may be a subject of further studies.

Noise calculations have now been performed with respect to the A321NEO. It will have to be investigated upon to what extent noise can be reduced for different types of aircraft. Furthermore, the noise produced by the acceleration and deceleration of the ground-based system is not taken into account and is something that will have to be investigated in the future. Further investigation shall explore the societal effects by calculating the increasing in house prices in the region next to Schipol as a result of more silent departures and approaches. Further investigation shall also quantify the effects of a reduction of awakenings of Schipol's residents and medical care cost due to lower noise levels.

The project focused on the feasibility of launching and recovering an A321NEO type of aircraft. However, further studies should be performed to quantify the applicability and benefit of using this system for larger and heavier aircraft as the reduction in aircraft weight would allow for substantially lower fuel consumption especially for long-haul flights. Once it has been studied whether this system can be applied on other aircraft, it should then be investigated the versatility of the ground-based system. More research is needed to decide whether it is better to use a single system for all the aircraft type or multiple different systems depending on the aircraft type.

13.1.4. End-Of-Life

Once the ground-based system reaches the end of life the system is disassembled and the parts that can be recycled will be recycled. The parts which cannot be recycled will be reused for different purposes and the parts which are non-recyclable and non re-usable are disposed in a sustainable way. The process is visualise in Figure 13.2

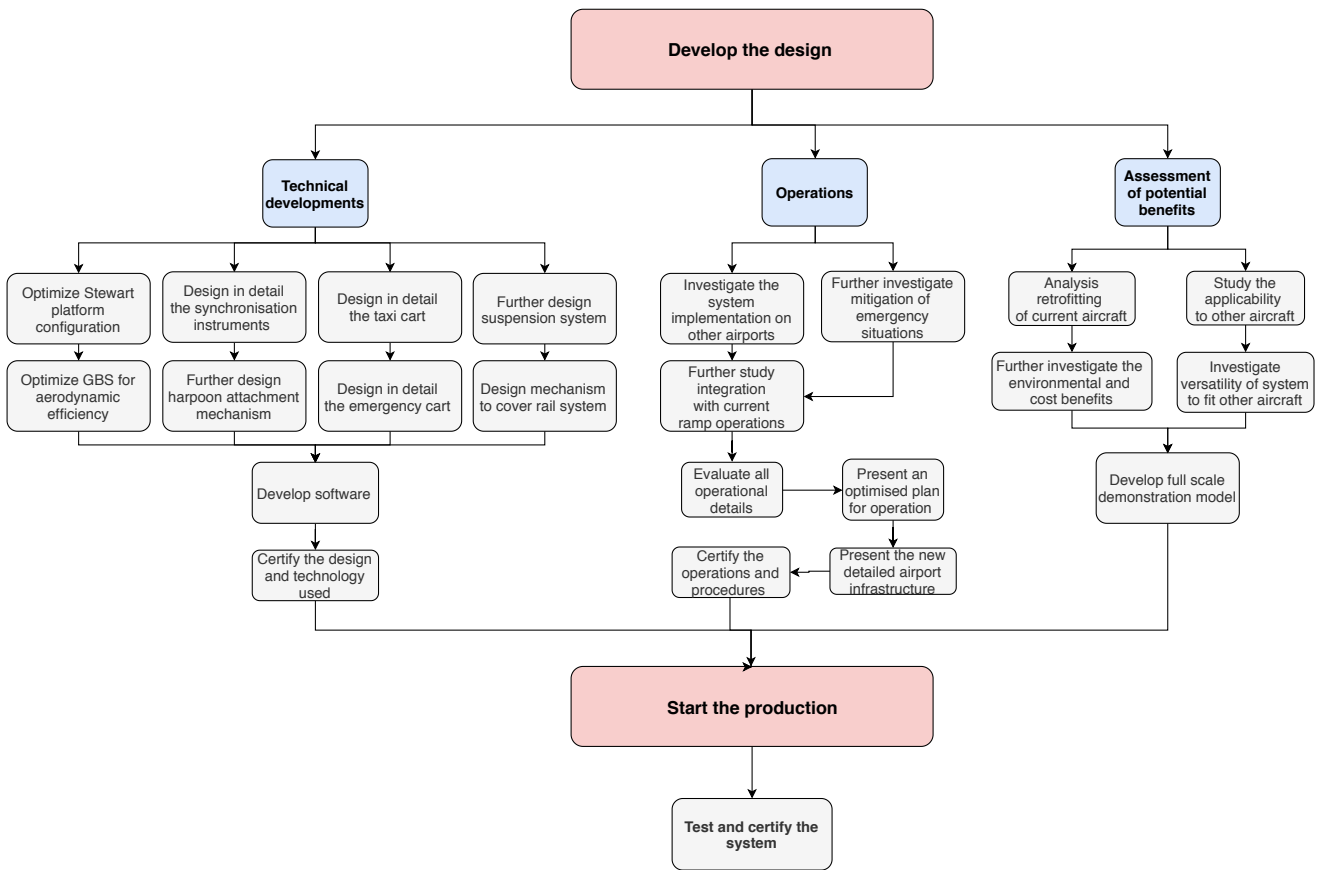


Figure 13.1: Project Development & Design logic diagram.

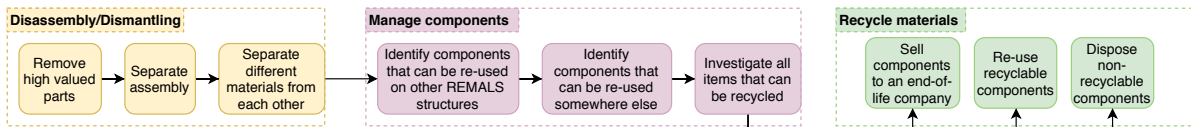


Figure 13.2: End-of-life of the REMALS.

Once all the issues have been resolved, the system can be built, tested and certified as a whole. New concepts in aviation require a long process of certification, therefore to reduced certification time and cost, policy-makers and EASA shall be involved in the development of the project as soon as possible. In this way, the project will run at a faster pace and will benefit by the EASA expertise with respect to safety issues.

13.2. Project Gantt Chart

The post DSE activities are organised such that they can be performed within the 20 years target. This target is based off the GABRIEL project, which is a similar project and a similar timeline is projected for the development. In the next 20 years, further analysis and studies need to be performed, each subsystem need to be built, tested and certified. Moreover, full scale demonstration models and prototypes need to be built along the way to demonstrate the capabilities and to get consent by all the stakeholders involved. Finally, the entire system needs to be built, tested and certified. In order to extract the full potential of this concept, it will have to be built in multiple airports at the same time. In Figure 13.3 the activities that need to be performed are shown in chronological order. Each activity from the Project Development & Design logic diagram (Figure 13.1) is repeated in the Gantt chart in chronological order and expanded upon. For each activity a rough time estimate is given and a list of subtasks provided.



Figure 13.3: Post-DSE project Gantt chart.

13.3. Manufacturing, Assembly and Integration Plan

This section presents the production plan of the REMALS system given in a time ordered outline of the activities required to construct the final product. It starts with manufacturing all the different components which are then assembled and implemented in real life.

Manufacturing

As can be seen from the yellow boxes in Figure 13.4, relatively small parts of the REMALS system are first manufactured, as the beams for the base structure or the different platforms. However, not all parts can be created by the company itself, hence they need to be ordered or bought if they already exist on the market, as electric motors or the hydraulic pumps. Ordering could also start at the same time as manufacturing, as it takes some time to produce them. Once all components are delivered and manufactured, the assembly can start.

Assembly

The assembly plan is presented in Figure 13.4 by the orange boxes. First, a subsub-assembly is performed on smaller parts as creating the wheels and connection for the rotation and lateral movement or assembling the harpoons. These are then used for the sub-assembly where more important parts of the structure are put together as the harpoons on the aircraft or constructing the base structure using the beams. After that, the sub-assemblies components are combined into the final assembly in order to form the final structure. Next, the structure is also coated.

Integration

The integration plan is represented by the red boxes in Figure 13.4. One of the most important steps before implementing the system is the testing of the REMALS in order to prove its safety and good functioning. Once the testings are approved, the implementation of the system can start. The most important physical changes made on the airport are the implementation of the rails in the ground and the power supply of the structure which is located underground. Moreover, lids are added to cover the rails such that the runway can still be used by conventional aircraft. Finally, the lift platforms used for taxi are implemented into ground at the end of each runway. From this, the A321 REMALS is delivered and the system is ready to be used.

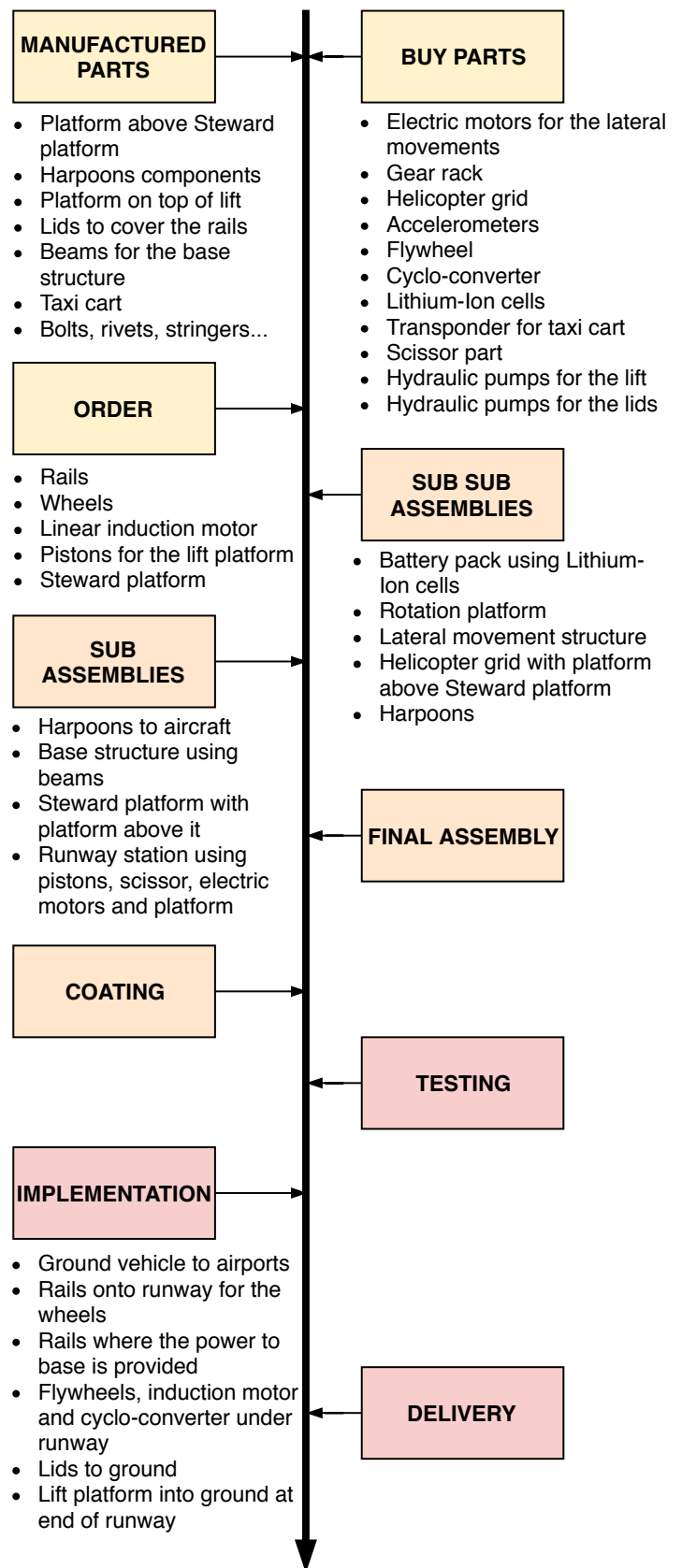


Figure 13.4: Production plan.

13.4. Cost Breakdown Structure

In this section the Cost Breakdown Structure is generated, this is a systems engineering tool that allows for identifying all separate costs. Then the cost of all components of the design are found and a cost estimation is made. The Cost Breakdown Structure is displayed in Figure 13.5 where first complete costs are first divided in Operational Expenses (Opex), costs which have to be paid yearly, and Capital Expenditures (Capex), that are only paid once. This can then be further divided in development, production of the system and implementation on Schiphol.

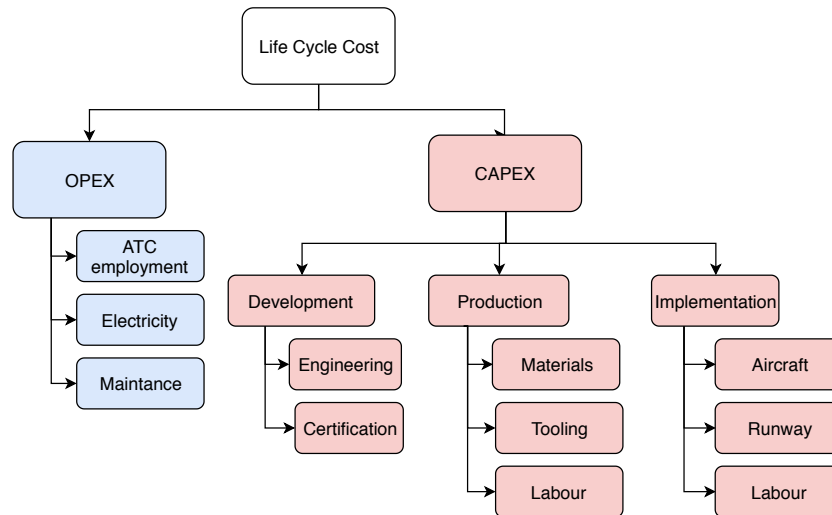


Figure 13.5: Cost breakdown.

13.4.1. CAPEX

The total capital expenditures add up to approximately $\text{€ } 626 \cdot 10^6$. This consists of the following components:

Base structure costs

The base structure is made with approximately 12.3 m^3 of carbon steel. This gives a steel mass of $97 \cdot 10^3 \text{ kg}$. With an average price of $\text{€ } 0.68/\text{kg}$ and a density of carbon steel of 7850 kg m^{-3} , capital spent on metal for the structure will be around $\text{€ } 66 \cdot 10^3$. For steel constructions, typically the raw materials account for 30% of the total cost. Therefore, the structure will cost around $\text{€ } 2.2 \cdot 10^5$ per cart, for a total of $\text{€ } 1.1 \cdot 10^6$.

Rails

The costs of implementing rails is estimated by using the HSL as a reference. This 147 km long railway cost $\text{€ } 7.2 \cdot 10^9$ to build. This means that the cost per km of high speed rails is approximately $\text{€ } 49 \cdot 10^6$. This is also in line with estimates made by the GAO[32]. For 3 runways of 3.3 km each, an estimated cost of $\text{€ } 4.8 \cdot 10^8$.

Linear Induction Motors

The linear induction motors are estimated to cost $\text{€ } 14.2 \cdot 10^6$. For 3 runways of 3.3 km each, this adds to $\text{€ } 140.6 \cdot 10^6$.

Stewart Platform

The cost of the total Stewart platform can be estimated based on expert opinion. Ir. G. Bufalari made an educated guess on the cost of approximately $5 \times 10^6 \text{ €}$ for a full Stewart Platform. This includes the custom made servo valves, custom accumulators, and custom actuators amongst others.

13.4.2. OPEX

Total operating expenditures are found to be approximately $\text{€ } 15.4 \cdot 10^6$ annually.

Power system

Electricity costs €18 cents per kWh before tax, and the electricity bill for first the EMALS, then the lateral movement and finally the taxi cart is calculated. All power values that were previously notated in SI-units are now converted to kWh.

The EMALS yearly electricity use is determined by the amount of energy used, minus the amount of energy the system recovers during braking. The total amount of movements a year is restricted by 500,000 movements that are divided between take-off and landing. The cost can be seen in Equation 13.1.

$$(E_{acc_{to}} + E_{acc_{to}} - E_{acc_{to}} - E_{acc_{to}}) \cdot 250000 \cdot 0.18 = €14.53 \cdot 10^6 \quad (13.1)$$

The taxi carts are used for moving the aircraft from the runway to the gate and back, they have electric motors that are driven by batteries. The taxi cart is designed to perform this manoeuvre three times, and the amount of electricity is calculated with Equation 13.3.

$$E_{taxi} \cdot \frac{500000}{2 \cdot 3} \cdot 0.18 = €769706 \quad (13.2)$$

The lateral movement system should be able to account for crosswinds during landing.

$$E_{lateralmove} \cdot 250000 \cdot 0.18 = €16249 \quad (13.3)$$

Maintenance

Maintenance of the rail and structural system are estimated to be high in the range of maintenance costs of high speed trains. This means the annual maintenance cost is approximately €7.2 · 10⁴ / km of track [13]. This means, for 3 runways of 3.3 km each, annual maintenance costs of approximately €7.13 · 10⁵ have been estimated. Other parts require very little large maintenance. One FTE of employment will suffice for this, costing an estimated €0.1 · 10⁶.

13.4.3. End-of-Life

It is assumed that the decommissioning costs of the system will be negligible compared to the costs to produce the system. It is therefore not taken into account in further calculations regarding return on investment.

13.5. Return on Investment

The return on investment is a measure used to assess economic feasibility of an investment or project and to make different investments comparable. It is defined according to Equation 13.4.

$$ROI = \frac{R - C}{I} \quad (13.4)$$

in which R is revenue, C the recurring costs associated with the project and I the total investment costs.

The annual benefits found in chapter 2 are summed to find the revenue for this equation. The recurring costs are found in the previous section, regarding OPEX. Investment costs are equal to the CAPEX.

Plugging those values in gives a return on investment of 9.31%. In the current contingency margins, if all costs turn out to be 30% higher, and the benefits 20% lower, the ROI will be 3.8%. On the flipside, when costs are 20% lower and benefits 30% higher, it will be 13.9%. Either way, it is in the order of magnitude of Schiphol's current return on equity of 7.2%.

14

Conclusion

Aviation is growing with 4.7% a year, even though aircraft have a significant CO_2 emission and the noise produced by aircraft has an impact on the quality of life of the people surrounding the airport. To facilitate this growth, a change is necessary in the aviation industry. Hence the main goal of this report was to explore the feasibility of a concept that makes take-off and landing an aircraft without a landing gear possible. The selected concept was designed in details and each main subsystem was engineered and sized. This resulted in a final design that allows for at least 4 SEL dB reduction in a radius of 7.8 km around the airport and a reduction in fuel used between 5-6% in short flights, while keeping the current airport capacity at Schiphol.

This achievement is obtained in the following way, a ground based structure is designed which assist the aircraft during take-off and landing procedures. Due to the addition of a ground based system, the landing gear can be removed from the aircraft. The aircraft is then transported over the airport on a taxi cart, with an electrical motor. During taxiing the engines of the aircraft are turned of. This combination of factors resulted in the 5.2% fuel reduction for the average short flight.

The linear induction motor that is used to propel the ground based system can obtain higher accelerations than the jet engines of the aircraft. This is due to the fact that the jet engines are optimised for cruise and only just facilitate the thrust setting required for take-off. As higher accelerations can be obtained by a ground based system, the take-off and landing procedures are optimised such that a noise reduction of 4 SEL dBa is realised in the area where most noise complaints come from.

To implement this system a ground based structure was designed that moves on rails, the rails are 30 m apart to limit the impact in of the runway for conventional aircraft. On the rails a steel truss structure is put with an actuator system on top that can accurately line up with the approaching aircraft using LIDAR sensors. The aircraft than connects to the ground based system by deploying harpoons which lock in the grid that forms the top part of the ground vehicle. During take-off the harpoons are closed, and the flaps are deployed.

The design satisfies the main requirements for capacity, cost, noise and fuel reduction. This confirms that the design is feasible and it is profitable to develop the system in more detail. The main parameters of the designed system can be seen in Table 14.1. As not all requirement can be checked at this stage, because actual real life tests are necessary, this is recommended.

Table 14.1: Main design parameters of the ground based system.

| Noise | Fuel | M _{GBS} | P _{grid} | Implementation Cost | Yearly cost | V _{to} | V _{land} | # Carts |
|-------------|------|------------------|-------------------|----------------------|------------------------|-----------------|-------------------|---------|
| ≥ 4 SEL dBa | > 5% | 128,000 [kg] | 200 MW | €626·10 ⁶ | €15.4 ·10 ⁶ | 145 [m/s] | 109.5 [m/s] | 5 |

This is an important development for the aviation industry as it contributes to 2-3% of the global annual CO_2 emissions. By implementing the designed system, more growth will be allowed in the aviation industry while complying with the limitations on the amount of movements that are allowed per airport based on fuel and noise emissions, set by the United Nations. This ground based system would also be beneficial for airline companies, as after 15 years of purchasing, noise and fuel tax as well as kerosene cost will be saved.

15

Recommendations

In this chapter, the team takes a step back to reflect on the relevance of the research conducted. This chapter presents further recommendations on both the REMALS design in section 15.1 and the implementation of the system in section 15.2.

15.1. Design Recommendations

The REMALS components and procedures that should be analysed in more detail are discussed in this section. The main points of focus that should be considered are the aircraft, the power supply, the landing requirements, the runway length, and the grid.

Aircraft Modifications

As described in section 8.3, the fuel reduction heavily depends on the weight reduction of the aircraft. The current weight reduction is sufficient to comply with the requirements set. However, A321REMALS is not in its final design stage and the performance can be improved. Implementation of REMALS makes some existing systems over designed or unnecessary. The team realises this and advises to have a closer look at three aircraft elements that could be downsized significantly to improve flight performance even more. They are visualised in Figure 15.1.



Figure 15.1: Recommended focus areas for improving A321REMALS flight performance

First of all, the rudder should be investigated. The asymmetric thrust during take-off due to engine failure is the critical flight condition for the rudder sizing [55]. If take-off is performed using the system, the moment

due to asymmetric thrust will be cancelled by the platform, thereby potentially reducing the rudder size. Furthermore, as landing and take-off speeds are higher than for conventional aircraft, the effect of the rudder on the motion of the aircraft is greater. Therefore, the rudder can be downsized.

Secondly, the thrust reversers should be looked at. As the aircraft is mainly decelerated using the ground system, the aircraft might not be required to provide additional drag forces using the thrust reversers. Therefore these system could be removed from the aircraft and significantly reduce the weight of the aircraft. This should be further investigated to see whether or not this is possible and how much weight is reduced.

Lastly, a recommendation is to resize the high lift devices. Since the take-off speed of the system is significantly increased compared to conventional aircraft, the high lift devices can possibly be reduced in size. This follows from the fact that possibly already sufficient lift is generated by the wing without the high lift devices deployed. Since the landing speed is also increased it might be possible to eliminate the high lift devices from the aircraft and reduce the aircraft's weight. The most critical phase should be identified and the lift devices sized accordingly.

For future aircraft produced it is also relevant to investigate the snowball effect to lighten the entire aircraft.

Power supply

The maximum power required for the system is currently determined by summing up two take-offs and one landing, as they have to be delivered at the same moment in time. However in practise this will almost never occur, the flight tower could schedule the flights such that the total maximum power required out is more evenly spread out over the 80 second per procedure time. In this way the flywheels can be sized down and the grid power can be lowered. The energy consumption of the system will stay the same and time and maximum power per procedure does not change. Additionally, it could be considered to limit the power required to a maximum at the cost of reducing the acceleration force of the ground system. It should be further investigated how this affects the performance and energy consumption of the system.

Landing Requirements

To be able to accurately determine the required lateral movement of the system, the landing of conventional aircraft should accurately be monitored. This includes both the lateral landing position, the aircraft attitude and the lateral velocities of the aircraft during final approach. From this data, a probability distribution could be developed that can be used to determine the required lateral movement, attitude and velocity of the system. Once these parameters are known, the system can be optimised to comply with these specific synchronisation requirements.

The impact loads also need to be accurately determined based on the specific landing procedure of the REMALS. As the aircraft is not required to de-crab and therefore the side forces exerted on the connection mechanism reduce compared to a conventional landing. Also the platform does have the same orientation as the aircraft and therefore a single wheel landing is less likely to occur. Taking these aspects into account the new critical impact loads should be further investigated.

Stewart Platform

The configuration of the Stewart platform could be modified to create a system that is not affected by single points of failure. In the current configuration, a failure of an actuator, results in an unsafe situation. This could be eliminated when a octapod configuration is chosen that contains eight actuators. Another advantage that might follow from this new configuration is that the maximum forces in the actuators possibly reduce.

Runway Length

The runway length can be increased to increase take-off velocity with the same force. Longer runway length gives you more time to accelerate, thus a higher take-off velocity can be achieved. If the take-off velocity is a fixed parameter, increasing the runway length causes the motor to deliver less force and thus the maximum power decreases. However, as the total procedure time increases, the total energy consumption increases as well, while the maximum required power decreases. For further research it may be more beneficial to implement this system only on longer runway as then the decrease in noise becomes bigger.

Grid

Once the actual impact loads are determined, a more in depth structural analysis should be performed on the grid. This includes a more in depth analysis on the load path that introduces the loads into the Stewart platform, and a fatigue analysis. From this a more detailed sizing could be done and a accurate mass estimation can be obtained.

Noise Production Ground Based System

The noise produced by the ground based system has not been analysed by the REMALS team. It is assumed to be nearly neglectable with the noise produced by an aircraft. Main reason for this that the noise produced by the ground based system would be very local. However, the local noise might effect the noise levels closer to the airport, increase the noise level in those areas.

15.2. System Recommendations

Apart from these technical aspects, there are also a several recommendations on a bigger scale that need to be investigated in order to assure a successful launch of concept.

Airports

The system only works if the REMALS system can be implemented on big scale airports. Currently the design is investigated for Schiphol, but sufficiently many big airports have to agree to this concept in order for it to work in the first place. The aircraft needs to be able to use this system for take-off and landing for a wider range of missions. Therefore it needs to be investigated: on how many airports it is necessary in order to be feasible, if it is technically possible on these airports, and if the airport organisations are willing to cooperate in the project.

Passengers

Several other market analysis have to be performed for the stakeholders. The comfort feeling of passengers could be investigated. People are afraid of flying, and it could be that this new system decreases comfort. This has to be investigated in order to predict customer behaviour.

Airlines

The airlines have to perform market analysis for this new concept. An extensive analysis of the most efficient ratio of conventional or REMALS aircraft, during the transition period and in the long term, is needed. There could be an optional length of flight to use this for, and therefore an optimisation analysis should be done.

Aircraft types

This project has investigated the effects on the A321NEO aircraft. However, in order to implement this system widely on airports, it would be efficient to use it for different types of aircraft. In order to achieve this goal, it could be investigated how the grid can be used for different configurations of landing gear, and how the massbalance of other types change with their designed harpoon system.

Appendix A - Work Distribution

| Work package | Who worked on it | Who wrote in the report |
|--|--|---|
| Preface | Olga | Olga |
| Executive Summary | Everyone | Everyone |
| Introduction | Stefano | Stefano |
| Market Analysis -Current Market -Prediction of Future Market -Cost Budget | Lucia Lucia Lucia (Only fuel), Merijn | Lucia Lucia Lucia (Only fuel), Merijn |
| Requirements, Functional Analysis -Context of the Design -Stakeholder and System Requirements -Functional Analysis | Maartje Maartje, Joost, Marie, Roy Mitchel, Roy | Maartje Marie, Maartje Mitchel |
| Concept Generation -Concept Overview -Trade-Off Summary -Winning Concept | Everyone Roy, Marie, Mitchel Roy, Marie, Mitchel | Marie Marie Marie |
| Design Process Set-Up -Configuration, Component and System Identification -N2 Chart -Budget Breakdown | Everyone Roy, Olga, Maartje Merijn | Mitchel Roy Merijn |
| Aircraft Design -Connection Mechanism -Weight and Balance | Olga, Marie Olga, Marie | Olga, Marie Olga, Marie |
| Ground System Analysis -Grid -Grid to Platform Connection -Stewart Platform -Rotation Platform -Lateral Movement Structure -Base Structure -Rails and Wheels Structure -Power -Power (Flywheel, subsection 7.8.3) -Electrical block diagrams -Runway Station -Taxi Cart | Roy, Mitchel, Marie Stefano, Jan Roy, Mitchel, Marie Roy, Mitchel Stefano, Jan Joost, Merijn Merijn Lucia Jan Lucia Stefano, Jan Stefano, Jan | Roy, Mitchel Stefano, Jan Roy, Mitchel Roy, Mitchel Stefano, Jan Merijn Merijn Lucia Jan Lucia Stefano, Jan Stefano, Jan |
| REMALS Performance -Flight Profile for Take-Off and Landing -Noise Reduction -Fuel Savings -Capacity | Maartje Maartje Joost Lucia, Stefano, Jan | Maartje Maartje Joost Lucia, Stefano, Jan |

Table 1: Work distribution.

| Work package | Who worked on it | Who wrote in the report |
|---|---|--|
| Operations and Functioning of REMALS -Operation and Logistics Description -Synchronisation Instruments -Communications Within the REMALS | Stefano, Jan, Lucia Mitchel, Marie Marie, Lucia | Stefano, Jan, Marie (diagram) Mitchel, Marie Marie |
| Risk -Risk Identification -Risk Maps -Risk Mitigation -Risk Assessment Conclusion -RAMS | Roy, Mitchel Roy, Mitchel Roy, Mitchel Roy, Mitchel Roy, Mitchel | Roy, Mitchel Roy, Mitchel Roy, Mitchel Roy, Mitchel Roy, Mitchel |
| Sustainability | Stefano | Stefano |
| System Verification and Validation -Requirement Compliance Matrix -Sensitivity Analysis -System Validation | Jan Mitchel, Maartje Stefano, Roy, Mitchel | Jan Mitchel, Maartje Stefano, Roy, Mitchel |
| Project Design and Development -Project Design and Development Logic -Project Gantt Chart -Manufacturing, Assembly and Integration Plan -Cost Breakdown Structure -Return on Investment | Stefano, Jan Stefano Marie Merijn, Lucia Merijn, Lucia | Stefano Stefano Marie Merijn, Lucia Merijn |
| Conclusion | Lucia, Stefano | Lucia, Stefano |
| Recommendations | Roy, Olga, Joost, Mitchel | Roy, Olga, Joost |
| CATIA visualisations -Figure 1 -Figure 6.2 -Figure 6.4 -Figure 7.1 -Figure 7.2 -Figure 7.3 -Figure 7.8 -Figure 7.25 -Figure 7.26 -Figure 15.1 | Joost Olga Olga Joost Olga Joost Joost Joost Joost Joost | n.a. n.a. n.a. n.a. n.a. n.a. n.a. n.a. n.a. n.a. |

Table 2: Work distribution.

Appendix B - BADA files

Table 3: Aircraft performance data provided by Base of Aircraft Data for high mass climb (83,000 kg) of A321-131.

| FL [-] | V_{TAS} [kt] | Thrust [N] | Drag [N] | Fuel flow [kg/min] | Rate of climb [fpm] | Flight path angle [deg] |
|------------------|--------------------------------|----------------------|--------------------|------------------------------|-------------------------------|-----------------------------------|
| 0 | 162.5 | 143301 | 74188 | 113.24 | 1266 | 4.72 |
| 5 | 167.50 | 141659 | 71347 | 112.72 | 1325 | 4.79 |
| 10 | 168.75 | 140705 | 71352 | 112.02 | 1315 | 4.72 |
| 15 | 171.40 | 139448 | 70547 | 111.35 | 1326 | 4.69 |
| 20 | 204.57 | 132720 | 51304 | 111.44 | 1842 | 5.46 |
| 30 | 209.32 | 130295 | 50928 | 109.79 | 1832 | 5.31 |
| 40 | 232.55 | 124916 | 47147 | 108.39 | 1970 | 5.14 |
| 60 | 281.98 | 114621 | 45129 | 105.26 | 2073 | 4.47 |
| 100 | 369.70 | 98059 | 50479 | 98.36 | 1749 | 2.88 |
| 140 | 392.10 | 89540 | 50378 | 90.74 | 1494 | 2.32 |
| 180 | 416.27 | 81040 | 50292 | 83.35 | 1215 | 1.78 |
| 220 | 442.33 | 72803 | 50281 | 76.33 | 920 | 1.27 |
| 260 | 470.40 | 64988 | 50907 | 69.74 | 594 | 0.77 |
| 310 | 477.44 | 56724 | 49652 | 61.03 | 417 | 0.54 |
| 350 | 469.71 | 50254 | 49363 | 53.64 | 52 | 0.07 |

Table 4: Aircraft performance data provided by Base of Aircraft Data for high mass descent (83,000 kg) of A321-131

| FL [-] | V_{TAS} [kt] | Thrust [N] | Drag [N] | Fuel flow [kg/min] | Rate of climb [fpm] | Flight path angle [deg] |
|------------------|--------------------------------|----------------------|--------------------|------------------------------|-------------------------------|-----------------------------------|
| 0 | 154.39 | 41762 | 85591 | 42.54 | 765 | -3.00 |
| 5 | 155.52 | 41748 | 85599 | 42.27 | 771 | -3.00 |
| 10 | 161.91 | 39566 | 83524 | 41.16 | 802 | -3.00 |
| 15 | 173.67 | 26238 | 70402 | 33.26 | 860 | -3.00 |
| 20 | 206.86 | 19239 | 64047 | 29.64 | 1024 | -3.00 |
| 40 | 241.13 | -446 | 46193 | 13.23 | 1220 | -3.07 |
| 80 | 290.45 | -1120 | 45150 | 11.73 | 1412 | -2.95 |
| 120 | 368.71 | -5441 | 49014 | 10.12 | 1992 | -3.29 |
| 160 | 391.39 | -5688 | 48946 | 9.49 | 2075 | -3.24 |
| 200 | 415.88 | -5504 | 48903 | 9.06 | 2141 | -3.15 |
| 240 | 442.32 | -4627 | 48962 | 8.82 | 2182 | -3.02 |
| 280 | 470.82 | -3024 | 49769 | 8.82 | 2218 | -2.90 |
| 310 | 477.44 | -1196 | 49652 | 9.06 | 2999 | -3.87 |
| 330 | 473.59 | 20 | 49019 | 9.25 | 2862 | -3.73 |
| 350 | 469.71 | 1070 | 49363 | 9.42 | 2793 | -3.67 |

Table 5: Aircraft performance data provided by Base of Aircraft Data for high mass cruise (83,000 kg) of A321-131

| FL [-] | V_{TAS} [kt] | Thrust [N] | Drag [N] | Fuel flow [kg/min] | Rate of climb [fpm] | Flight path angle [deg] |
|------------------|--------------------------------|----------------------|--------------------|------------------------------|-------------------------------|-----------------------------------|
| 350 | 469.71 | 49363 | 49363 | 52.54 | 0 | 0 |

Bibliography

- [1] El-Sayed A.F. Performance Parameters of Jet Engines. *Fundamentals of Aircraft and Rocket Propulsion*. Springer, London, 2016.
- [2] European Union Aviation Safety Agency. Certification Specifications and Acceptable Means of Compliance for Large Aeroplanes, November 2018.
- [3] AIRBUS. A321: AIRCRAFT CHARACTERISTICS AIRPORT AND MAINTENANCE PLANNING, Feb 2019.
- [4] Flight Operations Support Line Assistance Airbus. GETTING TO GRIPS WITH CATEGORY II AND III OPERATIONS, October 2001.
- [5] *Capacity declaration Amsterdam Airport Schiphol: Summer 2019*. Airport Coordination Netherlands, 1.0 edition, September 2018.
- [6] Johnson, A.P. "High Speed Linear Induction Motor Efficiency Optimization". Master's thesis, Massachusetts Institute of Technology, Buffalo, June 2005.
- [7] Rajawat, A.S. "Linear induction motors and its applications". Master's thesis, Rajasthan technical university, Kota, August 2009.
- [8] Maurice Bellont. Getting to grips with Fuel Economy. *AIRBUS, Flight Operations Support Line Assistance*, 2004.
- [9] *Jaarrapportage 2018*. Bewoners Aanspreekpunt Schiphol, 2019.
- [10] M. et al. Bos. Take-Off and Landing Using Ground Based Power: Project Plan, May 2019.
- [11] Heerens, N., C. " Landing gear design in an automated design environment", 2014.
- [12] F.C. Campbell, editor. *Elements of Metallurgy and Engineering Alloys*. ASM International, 2008.
- [13] Javier Campos, Gines de Rus, and I-naki Barron. The cost of building and operating a new high speed rail line. *BBVA Foundation*, 2007.
- [14] Barney L. Capehart. Encyclopedia of Energy Engineering and Technology. *CRC Press*, 2007.
- [15] Davide Castelvechi. Flywheels: Spinning into control. *Science News*, 171(20):312, May 2007.
- [16] Stewart, D. A Platform with Six Degrees of Freedom. *Aircraft Engineering*, 38(4):30–35, 1966.
- [17] Van den Hoven, J. *Value Sensitive Design and Responsible Innovation*, pages 75–83. 04 2013. ISBN 9781119966364. doi: 10.1002/9781118551424.ch4.
- [18] UNITED STATES OF AMERICA DEPARTMENT OF DEFENSE. *PROCEDURES FOR PERFORMING A FAILURE MODE, EFFECTS AND CRITICALITY ANALYSIS*. 1977.
- [19] Simons, D.G. *Aircraft Noise and Emissions*. Delft University of Technology, January 2019.
- [20] Grubb, T.G., Delaney, D.K. and Bowerman, W.W. Investigating potential effects of heli-skiing on golden eagles in the wasatch mountains, utah. January 2007.
- [21] EEA EASA and EUROCONTROL. "European aviation environmental report 2019",.
- [22] Bos, M. et al. Take-off and landing using ground based power: Baseline. Technical report, Delft University of Technology, 2019.
- [23] Bos, M. et al. Take-off and landing using ground based power: Midterm draft. Technical report, Delft University of Technology, 2019.
- [24] Burghouwt, G., Boonekamp, T., Suau-Sanchez, P., Volta, N., Pagliari, R., et al. "The impact of airport capacity constraints on air fares",.
- [25] EASA EUROCONTROL, European Environmental Agency. European Aviation Environmental Report . 2019.
- [26] *Type-Certificate Data Sheet No. E.110*. European Union Aviation Safety Agency, 2019.
- [27] Adamo, F and Majka, A. *Airport and fly-over noise of the GABRIEL concept*. CIRA Centre Italiano Ricerche Aerospaziali, November 2013.
- [28] Oliviero , F "AE3211-I Systems Engineering and Aerospace Design: Lecture 5: Requirement Analysis and Design Principles for A/C Stability and Control (Part 2)", 2019.
- [29] Oliviero, F "AE3211-I Systems Engineering and Aerospace Design: Lecture 3: WeightBalance in AC design", 2019.

- [30] Oliviero, F. "AE3211-I Systems Engineering and Aerospace Design: Lecture 4: Requirement Analysis and Design Principles for A/C Stability and Control (Part 1)", 2019.
- [31] Association for the Advancement of Cost Engineering. Cost estimate classification system – as applied in engineering, procurement, and construction for the process industries tcm framework: 7.3 – cost estimating and budgeting, 2005.
- [32] GAO. High speed passenger rail future development will depend on addressing financial and other challenges and establishing a clear federal role, March 2009.
- [33] Schiphol group. "Facts and figures 2017",.
- [34] Hamzehbahmani, H. "MODELING AND SIMULATING OF SINGLE SIDE SHORT STATOR LINEAR INDUCTION MOTOR WITH THE END EFFECT",.
- [35] Polinder, H. Electric system: Power from main shaft to utility grid. PowerPoint.
- [36] Hurt, H.H. Aerodynamics for naval aviators. Technical report, University of Southern California, 1965.
- [37] Guan, Q., Che, X., Li, J., Liu, J., Huang, Y.,. "WIND TUNNEL TEST STUDY OF AEROSTATIC DRAG SHIELDING FACTOR OF A TRUSS BRIDGE SECTION ". *The Eighth Asia-Pacific Conference on Wind Engineering, India*, page 9, December 2013.
- [38] "International Air Transport Association (IATA) ". fact-sheet-fuel. november 2018.
- [39] Dhole, J., Kulkarni, N, Borse, J.
- [40] Roskam, J. "*Airplane Design Part IV: Layout of Landing Gear and Systems*". Design, Analysis and Research Corporation, 2000.
- [41] Sun, J., Hoekstra, J.M., Ellerbroek, J.,. "Aircraft Drag Polar Estimation Based on a Stochastic Hierarchical Mode". *SID, Control and Simulation, Faculty of Aerospace Engineering Delft University of Technology, the Netherlands*, 2018.
- [42] A. Malwitz J. T. Wilkerson, M. Z. Jacobson.
- [43] M. Z. Jacobson J. T. Wilkerson. Analysis of emission data from global commercial aviation: 2004 and 2006. *Atmos. Chem. Phys.*, 10: 6391–6408,, 2010.
- [44] Vos, R., Melkert, J.A. and Zandbergen, B.T.C. "Aerospace Design and Systems Engineering Elements I – AE1222-II, A/C Preliminary Sizing ", 2017.
- [45] L.R. Jenkinson and P Simpkin. *Civil Jet Aircraft Design*. American Institute of Aeronautics - Astronautics, January 2000.
- [46] Andrew P. Johnson. High speed linear induction motor efficiency optimization. Master's thesis, Massachusetts Institute of Technology, June 2005.
- [47] Reynolds, T.G. Jordan, R., Ishutkina, M. A. A statistical learning approach to the modeling of aircraft taxi-time. Technical report, MIT Lincoln Laboratory, 2010.
- [48] Wilson, J.P. The Triple Bottom Line. *International Journal of Retail Distribution Management*, 43(4-5):432–447, 2015.
- [49] R. Cadoux K. Jones. Ercd report 0904, metrics for aircraft noise. *Environmental Research and Consultancy Department*, 2009.
- [50] R. Heyder M. Brehmer K. Mädler, A. Zoll. Rail materials - alternatives and limits. *Deutsche Bahn AG, DB Systemtechnik, Brandenburg-Kirchmöser, Germany*, page 9.
- [51] Jenkinson, L., Simpkin, P., and Rhodes, D. Aircraft data file. *Butterworth-Heinemann, Civil jet aircraft design*, 2001.
- [52] T.H.G. Megson. *Aircraft Structures for Engineering Students*. Elsevier, 6th edition.
- [53] T.H.G. Megson. *Aircraft Structures for Engineering Students - Fifth Edition*. Elsevier, Kidlington, Oxford, United Kingdom, 2013.
- [54] Currey, N.S. "*Aircraft Landing Gear Design: Principles and Practises*". American Institute of Aeronautics and Astronautics, 1988.
- [55] Al-Shamma, O. An educational rudder sizing algorithm for utilization in aircraft design software. *International Journal of Applied Engineering Research*, 2018.
- [56] Balci, O. Verification, Validation, and Testing Techniques.
- [57] Huibregtse, O. and Zijlstra, T. Luchtvaartfeiten. Technical report, Ministerie van Infrastructuur en Waterstaat, 2018.
- [58] Australian Government Department of Defence. *Technical Risk Assessment Handbook*. 2010.
- [59] Department of Defense United States of America. *Department of Defense GUIDE FOR ACHIEVING RELIABILITY, AVAILABILITY, AND MAINTAINABILITY*. 2005.
- [60] Headquarters Department of the Army. *Risk Management*. 2014.
- [61] U.S. Department of Transportation. Sitting on the Runway: Current Aircraft Taxi Times Now Exceed Pre-9/11 Experience. *Bureau of Transportation Statistics*, May, 2008.

- [62] International Civil Aviation Organization. *Airport Services Manual Part 1: Rescue and Fire Fighting*. 1990.
- [63] A., Brice, C., Dougal, R., Pettus, R., Patterson, D., Monti.
- [64] V.A. PROFILLIDIS. *Railway Management and Engineering*. Ashgate Publishing Limited, 4th edition edition, 2014.
- [65] Civil Aviation Advisory Publication. Standard passenger and baggage weights. Technical report, Civil Aviation Safety Authority, 1990.
- [66] Doyle, M.R., Samuel, D.J., Conway, T., Klimowski, R.R. "Electromagnetic Aircraft Launch System - EMALS ". *TRANSACTIONS ON MAGNETICS*, Volume 31(1):528–533, January 1995.
- [67] Koekebakker, S. Model based control of a flight simulator motion system. Technical report, Delft University of Technology, 2001.
- [68] Thomas, L., Saaty. Decision making with the analytic hierarchy process. *Int. J. Services Sciences*, 1(1):83–98, 2008.
- [69] Schiphol. Facts and figures 2017, April 2018.
- [70] Schiphol. Airport charges and conditions 2019, April 2019.
- [71] Melin, T. Using internet interactions in developing vortex lattice software conceptual design. Master's thesis, Kungliga Tekniska Hogskolan, 2003.
- [72] Edzard V.M. van Baaren. The feasibility of a fully electric aircraft towing system. Master's thesis, Delft University of Technology, May 2019.
- [73] van der Wal, H. M. M., Vogel, P., and F. J. M. Wubben. *Voorschrift voor de berekening van de L_{den} and L_{night} in dB(A) ten gevolge van vliegerkeer van en naar de luchthaven Schiphol*. National Aerospace Laboratory NLR, 2001.
- [74] Rijkswaterstaat Ministerie van Infrastructuur en Waterstaat. *Handreiking prestatiegestuurde risicoanalyses (PRA)*. 2018.
- [75] Rijkswaterstaat Ministerie van Infrastructuur en Waterstaat. *Leidraad RAMS, Sturen op prestaties van systemen*. 2018.
- [76] A. Saltelli W. Becker. *Design for sensitivity analysis, in Chapman and Hall "Handbook of Design of Experiments"*. 2014.